BULLETIN OF RUSSIAN STATE MEDICAL UNIVERSITY

BIOMEDICAL JOURNAL OF PIROGOV RUSSIAN NATIONAL RESEARCH MEDICAL UNIVERSITY

SUBMISSION http://vestnikrgmu.ru/login?lang=en
CORRESPONDENCE editor@vestnikrgmu.ru
COLLABORATION manager@vestnikrgmu.ru
ADDRESS ul. Ostrovityanova, d. 1, Moscow, Russia, 117997

Indexed in Scopus. CiteScore 2023: 0,8

Indexed in WoS. JCR 2021: 0.5

Five-year h-index is 10

SCImago Journal & Country Rank 2020: 0.14

Listed in HAC 31.01.2020 (№ 507)

Open access to archive

Issue DOI: 10.24075/brsmu.2024-05
The mass media registration certificate № 012769 issued on July 29, 1994
Founder and publisher is Pirogov Russian National Research Medical University (Moscow, Russia)

Approved for print 31.10.2024
Circulation: 100 copies. Printed by Print.Formula
www.print-formula.ru

ВЕСТНИК РОССИЙСКОГО ГОСУДАРСТВЕННОГО МЕДИЦИНСКОГО УНИВЕРСИТЕТА

НАУЧНЫЙ МЕДИЦИНСКИЙ ЖУРНАЛ РНИМУ ИМ. Н. И. ПИРОГОВА

ГЛАВНЫЙ РЕДАКТОР Денис Ребриков, д. б. н., профессор

ЗАМЕСТИТЕЛЬ ГЛАВНОГО РЕДАКТОРА Александр Эттингер, д. м. н., профессор

РЕДАКТОРЫ Валентина Гейдебрехт, к. б. н.; Надежда Тихомирова

ТЕХНИЧЕСКИЙ РЕДАКТОР Евгений Лукьянов

ПЕРЕВОДЧИКИ Надежда Тихомирова, Вячеслав Витюк

ДИЗАЙН И ВЕРСТКА Марины Дорониной

ПОДАЧА РУКОПИСЕЙ http://vestnikrgmu.ru/login
ПЕРЕПИСКА С РЕДАКЦИЕЙ editor@vestnikrgmu.ru
СОТРУДНИЧЕСТВО manager@vestnikrgmu.ru
АДРЕС РЕДАКЦИИ ул. Островитянова, д. 1, г. Москва, 117997

Журнал включен в Scopus. CiteScore 2023: 0,8 — Журнал включен в WoS. JCR 2021: 0,5 — Индекс Хирша (h⁵) журнала по оценке Google Scholar: 10

SCImago Journal & Country Rank 2020: 0,14 — Журнал включен в Перечень 31.01.2020 (№ 507) — Здесь находится открытый архив журнала

DOI выпуска: 10.24075/vrgmu.2024-05
Свидетельство о регистрации средства массовой информации № 012769 от 29 июля 1994 г.
Учредитель и издатель — Российский национальный исследовательский медицинский университет имени Н. И. Пирогова (Москва, Россия)

Подписано в печать 31.10.2024
Тираж 100 экз. Отпечатано в типографии Print.Formula
www.print-formula.ru

BULLETIN OF RSMU **5, 2024**
ВЕСТНИК РГМУ

Contents
Содержание

GUT DYSBIOSIS AND COLORECTAL CANCER: FROM ONCOGENESIS HYPOTHESES TO NON-INVASIVE DIAGNOSTICS

Glazunova EV, Kurnosov AS, Zlobovskaya OA✉

Centre for Strategic Planning and Management of Biomedical Health Risks of the Federal Medical Biological Agency, Moscow, Russia

Colorectal cancer (CRC) is one of the most prevalent malignant neoplasms that occupies the leading position in terms of cancer mortality. The main problem of CRC is that the disease is diagnosed at the advanced stages (about 50% of cases identified are stage III and IV CRC), which results in high mortality. Dysbiotic gut microbiota alterations represent one of the key risk factors of CRC. Three hypotheses of CRC emergence were formulated in order to explain the relationship between dysbiosis and carcinogenesis: “alpha-bug”, keystone pathogen, and driver–passenger hypotheses. The driver–passenger model is the most promising, it divides bacteria into “drivers” of cancer triggering inflammation and cell damage and the passenger bacteria modeling tumor microenvironment, accelerating tumor growth, and exacerbating dysbiosis. Drivers and passengers can be markers of various carcinogenesis stages. Colonoscopy involving examination of the surface of the rectum and colon is the most effective method to detect CRC, including the early stage disease. However, the wide use of this procedure is limited by the fact that it is associated with discomfort for patients and the risk of possible sequelae. Non-invasive microbiota assessment based on the driver–passenger model can become a safe and affordable alternative to the invasive diagnostics during preventive screening, since it makes it possible to improve survival rate due to involvement of a larger number of patients.

Keywords: colorectal cancer, inflammatory bowel diseases, microbiota, microbiome, diagnostics, carcinogenesis hypotheses, personalized medicine, non-invasive studies, survival

Author contribution: Glazunova EV — literature review, data acquisition, manuscript writing; Kurnosov AS — manuscript editing; Zlobovskaya OA — manuscript concept, manuscript editing.

✉ **Correspondence should be addressed:** Olga A. Zlobovskaya
Pogodinskaya, 10, str. 1, Moscow, 119121, Russia; OZlobovskaya@cspfmba.ru

Received: 15.10.2024 **Accepted:** 25.10.2024 **Published online:** 30.10.2024

DOI: 10.24075/brsmu.2024.046

ДИСБИОЗ КИШЕЧНИКА И КОЛОРЕКТАЛЬНЫЙ РАК: ОТ ГИПОТЕЗ ОНКОГЕНЕЗА К НЕИНВАЗИВНОЙ ДИАГНОСТИКЕ

Е. В. Глазунова, А. С. Курносов, О. А. Злобовская ✉

Центр стратегического планирования и управления медико-биологическими рисками здоровью Федерального медико-биологического агентства, Москва, Россия

Колоректальный рак (КРР) — одно из самых распространенных злокачественных новообразований, занимающее лидирующие позиции по смертности от рака. Основная проблема КРР — диагностика заболевания на поздних стадиях (около 50% случаев выявляют на III и IV стадиях), что приводит к высокой летальности. Одним из ключевых факторов риска КРР являются дисбиотические нарушения кишечной микробиоты. С целью объяснить взаимосвязь дисбиоза и канцерогенеза были сформулированы три гипотезы возникновения КРР: «Alpha-bug», «Keystone pathogen hypothesis» и «Driver-Passenger». Модель «Driver-Passenger» наиболее перспективна и разделяет бактерии на «драйверы» рака, запускающие воспаление и повреждение клеток, и «бактерии-пассажиры», моделирующие микроокружение опухоли, усиливающие ее рост и усугубляющие дисбиоз. Драйверы и пассажиры могут выступать маркерами различных стадий онкогенеза. Колоноскопия поверхности прямой и ободочной кишки — наиболее эффективный метод для обнаружения КРР, в том числе на ранних стадиях заболевания. Однако повсеместное применение данной процедуры ограничивается связанным с ней дискомфортом для пациентов и риском возможных последствий. Неинвазивное исследование микробиоты на основе модели «Driver-Passenger» может стать безопасной и доступной альтернативой инвазивной диагностике в ходе профилактического скрининга, позволяя повысить выживаемость за счет вовлечения большего числа пациентов.

Ключевые слова: колоректальный рак, воспалительные заболевания кишечника, микробиота, микробиом, диагностика, гипотезы канцерогенеза, персонализированная медицина, неинвазивные исследования, выживаемость

Вклад авторов: Е. В. Глазунова — анализ литературы, сбор данных, написание рукописи; А. С. Курносов — редактирование рукописи; О. А. Злобовская — идея рукописи, редактирование рукописи.

✉ **Для корреспонденции:** Ольга Анатольевна Злобовская
ул. Погодинская, д. 10, с. 1, г. Москва, Россия, 119121; OZlobovskaya@cspfmba.ru

Статья получена: 15.10.2024 **Статья принята к печати:** 25.10.2024 **Опубликована онлайн:** 30.10.2024

DOI: 10.24075/vrgmu.2024.046

CRC Statistics

Colorectal cancer (CRC) is a malignant neoplasm of various parts of the colon or rectum and one of the most common types of pathological tumor processes (10% of all cancer cases) [1]. CRC ranks second or third among the most frequent causes of cancer deaths: about 1.1–2 million new cases (600–935 thousand deaths per year) [2].

Given the trends, the forecast for detecting new CRC cases in Western countries by 2030 is 2.2 million people, and by 2040, about 1.6 million deaths annually will occur among 3.2 million patients [1, 3]. The highest mortality is recorded in Eastern Europe. Among adults under 50, there is a tendency towards an increase in CRC cases, especially rectal and colon cancer, and subsequent deaths [3, 4], which, along with the overall dynamics, is causing concern.

The dynamics of CRC incidence in the Russian Federation corresponds to the global trend. For the period 2011–2021, the average annual increase in the detection of colon and rectal cancer is 2.14% and 1.47%, respectively [5]. In 2021, cancer of various parts of the intestine accounted for a total of 12.2% of all malignant neoplasms [4]. This trend can be explained not only by a true increase in incidence but also, probably, by improved screening quality [1].

Along with an annual increase in CRC cases among young people by 1–2.4%, there is a steady decrease in morbidity and mortality among people aged ≥65 years, which is associated with increased participation of the risk group in regular preventive screening and once again confirms the need to develop new strategies for early diagnosis and prevention [3, 4].

The prognosis for the course and outcome of the disease depends on the diagnosed stage. Approximately 50% of CRC detection cases occur collectively at stages III and IV of the disease, leading to high mortality in the first year after detection [1,4]. Early tumor diagnosis (at stages 0, I, or II) is accompanied by 80% survival over five years, which decreases to 10% with later diagnosis [6].

Most CRC cases are sporadic, and only 20–30% are caused by hereditary syndromes [3]. The prevalence of sporadic cancer cases over hereditary ones indirectly confirms the dominance of various environmental factors as the main cause of the onset and development of carcinogenesis [2].

Risk Factors

The emergence and development of CRC is a multifactorial and multi-stage process, representing a complex interaction of environment, lifestyle, genetic, epigenetic, and other factors [2]. Among other risk factors, age, Western diet (especially consumption of large amounts of red meat), smoking, alcohol abuse, obesity, diabetes, and inflammatory bowel diseases (IBD) are highlighted [3]. Dysbiotic disturbances in the microbiota are also considered a key risk factor for CRC. Every year, the global scientific community publishes new data confirming the pathogenic and carcinogenic effects of dysbiotic microbial communities [2, 3, 6–10].

Dysbiosis stimulates the emergence and development of a cascade of various inflammatory reactions in the intestine, up to IBD, which, along with the direct impact of pathogenic and opportunistic microorganisms, is recognized as one of the main causes of CRC [2, 6]. Patients diagnosed with IBD have a higher risk of developing CRC: the probability of development is 8.3–20% [11].

Thus, a comprehensive approach to studying intestinal oncogenesis involves analyzing the three-way interaction between the intestinal microbiota, the mucosal immune system, and colonic epithelial cells [7, 8].

CRC Hypotheses and Microbiota

To approach understanding the potential mechanism of carcinogenesis influenced by the microbiota, as well as the development of dysbiotic disturbances in this process, three models were successively proposed: "Alpha-bug", "Keystone pathogen hypothesis", and "Driver-Passenger".

"Alpha-bug" Model

This model was based on a hypothesis that emerged as a result of studies on the enterotoxigenic subtype of Bacteroides fragilis (ETBF) and was proposed by Sears CL and Pardoll DM [7]. According to this model, bacteria possessing unique virulence factors not only directly trigger chronic inflammation and carcinogenesis and negatively affect the immune system but also contribute to dysbiosis by displacing commensal bacteria with anti-tumor effects. Such bacteria were called "alpha-bugs".

In the process of developing the "Alpha-bug" model, various researchers supplemented it with the following taxa: *Escherichia coli* pks+, *Enterococcus faecalis*, *Fusobacterium spp*., *Streptococcus gallolyticus* subsp. *gallolyticus* (*S. bovis* biotype I) [2].

"Keystone pathogen hypothesis" Model

In their model, Hajishengallis G and co-authors point out several shortcomings of the "Alpha-bug" hypothesis: focusing only on individual toxigenic species, excluding the influence of commensals from consideration (i.e., lack of a comprehensive approach), analyzing oncogenesis starting from the dysbiotic stage. Their proposed model suggests considering "keystone" bacteria whose impact on the host organism is disproportionate to their numbers. These "keystone" minor bacteria affect homeostasis, microbiota composition, initiate inflammatory processes, and dysbiosis. The hypothesis complements the list of organisms included in the "Alpha-bug" model with the following species: *B. thetaiotaomicron*, *Citrobacter rodentium*, *Klebsiella pneumoniae*, *Methanobrevibacter smithii*, *Porphyromonas gingivalis*, *Proteus mirabilis* [10].

"Driver-Passenger" Model

The "Driver-Passenger" model, also proposed by Tjalsma H and colleagues, expands and unifies the first two concepts, viewing carcinogenesis as a complex process induced by driver bacteria and progressing under the influence of passenger bacteria. Drivers cause inflammation and epithelial cell damage, contributing to the onset of CRC, and create a favorable environment for the development of opportunistic and commensal passengers. Passengers are better adapted to the tumor microenvironment, promote further progression of carcinogenesis, can suppress the growth of drivers, and exacerbate dysbiotic disturbances in the microbiota [12].

The functional role of driver bacteria shows significant similarities with the characteristics of alpha-bugs and "keystone" bacteria, which expectedly suggests common candidates. Researchers propose the following bacteria: *B. thetaiotaomicron*, *Bifidobacterium bifidum*, *E. coli* (филотип B2 и pks+), *E. faecalis*, *Eubacterium rectale*, ETBF, *P. endodontalis*, *Ruminococcus gnavus*; *Citrobacter spp*., *Morganella spp*., *Salmonella spp*., *Shigella spp*.; *Enterobacteriaceae*, *Porphyromonadaceae*, *Pseudomonadaceae*, *Ruminococcaceae*.

Taxa such as Clostridium septicum, P. *gingivalis*, S. gallolyticus *subsp*. gallolyticus, *Proteus spp*., *Fusobacterium spp*., and other *E. coli* pathotypes can be singled out into a separate "driver-passenger" subgroup, as they combine properties of both groups. For example, *Fusobacterium spp*. have a high affinity for intestinal epithelial cells, especially tumor cells. *F. nucleatum* can form biofilms between itself and other species, such as *C. difficile, Candida albicans*, *E. faecalis*, *P. gingivalis*, *Streptococcus spp*. [3].

The group associated with late stages of carcinogenesis and functioning as passengers includes: Akkermansia muciniphila, *Prevotella intermedia*, *Parvimonas micra*, *Peptostreptococcus anaerobius*, *P. stomatis*, *Saccharomyces cerevisiae*; *Aspergillus spp*., *Lactobacillus spp*., *Clostridium spp.*, *Collinsella spp*., *Klebsiella spp*., *Mucor spp*., *Peptostreptococcus spp.*, *Prevotella spp*., *Roseburia spp.*, *Staphylococcus spp.*, *Streptococcus spp*., *Veillonella spp*.; *Streptococcaceae*. Both drivers and passengers show proven associations with certain stages and mechanisms of carcinogenesis, with elevated levels of various interleukins and Th17-mediated immune response, with some CRC subtypes, and with the mutational status of tumor and adenoma cells [3, 13].

Currently, the "Driver-Passenger" model is a comprehensive concept that most closely reflects the dynamic, functional, and temporal interactions within the microbial community at various stages of CRC, compared to other hypotheses. The limitations of this model lie in the heterogeneity and multifunctionality of the microbiota, whose composition and quantity vary depending on many factors, and currently do not take into account the influence of commensal archaeal species and parasitic infections [12].

Further research will help clarify microbiome-associated mechanisms of CRC development and progression to create a more universal model of oncogenesis.

Dysbiotic Disturbances of the Archaeome

Archaea are minor commensal representatives of the microbiome that metabolize various compounds produced during the anaerobic decomposition of organic substances by intestinal bacteria. Throughout oncogenesis, archaeome dysbiosis is observed: depletion of the methanogenic component and an increase in the abundance of halophilic species [14]. The role of archaea requires further study in the context of the "Driver-Passenger" hypothesis.

Parasitic Infection as a CRC Driver

Common parasitic invasions of the gastrointestinal tract include: amebiasis (*Entamoeba histolytica*), ascariasis (Ascaris *lumbricoides*), balantidiasis (*Balantidium coli*), blastocystosis (*Blastocystis spp*.), cryptosporidiosis (*Cryptosporidium sp*.), giardiasis (*Giardia lamblia*), strongyloidiasis (*Strongyloides sp.*), trichocephalosis (*Trichuris trichiura*), cystoisosporiasis (*Cystoisospora belli*), cyclosporiasis (*Cyclospora cayetanensis*), schistosomiasis (*Schistosoma sp.*), enterobiasis (*Enterobius vermicularis*). Some of these are classified as normobiota, but the vast majority of these organisms have been proven to influence the development of inflammation and dysbiosis. They secrete toxic metabolites, alter pH, compete for resources, initiate immune responses, increase intestinal wall permeability, and affect the balance between symbionts and pathogens (even after therapy). Thus, they can function as drivers, which requires further analysis [15].

CRC Diagnostics

Given CRC statistics, developing new strategies for early diagnosis and prevention is becoming an increasingly urgent task in modern medicine.

Physical examination, diagnostic imaging, endoscopic examination, biopsy analysis, and fecal occult blood testing are the main methods for diagnosing and detecting CRC. Currently, colonoscopy is the best method for early CRC detection [1]. However, the invasiveness of this procedure limits its widespread use.

In the context of the presented data, the state of the intestinal microbiota can be considered as an alternative diagnostic and prognostic marker for CRC. Microbiota analysis can help in making a decision about the need for colonoscopy, as well as in determining the stage of the disease, the possibility of unfavorable development, outcome and metastasis formation [7, 9].

CONCLUSION

Non-invasive intestinal microbiota examination based on the "Driver-Passenger" model is a convenient and safe preventive method of primary diagnosis, increasing the likelihood of a positive outcome in case of detecting dysbiotic disturbances and identifying CRC through this screening. Its widespread use in medical practice can help reduce morbidity and mortality by increasing the flow of people willing to undergo screening. The development of such non-invasive diagnostic methods is a relevant socially significant direction.

References

1. World Health Organization. 2024. World Health Organization. Available from: https://www.who.int/
2. Yu YN, Fang JY. Gut Microbiota and Colorectal Cancer. Gastrointest Tumors. 2015; 2 (1): 26–32.
3. Cheng Y, Ling Z, Li L. The Intestinal Microbiota and Colorectal Cancer. Front Immunol. 2020; 11: 615056.
4. Bakulin IG, Zharkov AV, Zhuravleva MS, Serkova MYu. Colorectal cancer screening: current status and future prospects. Profil Meditsina. 2023; 26 (12): 12.
5. Zlokachestvennye novoobrazovanija v Rossii v 2023 godu (zabolevaemost' i smertnost'). M.: MNIOI im. P. A. Gercena — filial FGBU «NMIC radiologii» Minzdrava Rossii, 2024; 276 p. Dostupno po ssylke: https://oncology-association.ru/wp-content/uploads/2024/08/zis-2023-elektronnaya-versiya.pdf. Russian.
6. Saus E, Iraola-Guzmán S, Willis JR, Brunet-Vega A, Gabaldón T. Microbiome and colorectal cancer: Roles in carcinogenesis and clinical potential. Mol Aspects Med. 2019; 69: 93–106.
7. Sears CL, Pardoll DM. Perspective: Alpha-Bugs, Their Microbial Partners, and the Link to Colon Cancer. J Infect Dis. 2011; 203 (3): 306–11.
8. Yadav D, Sainatham C, Filippov E, Kanagala SG, Ishaq SM, Jayakrishnan T. Gut Microbiome–Colorectal Cancer Relationship. Microorganisms. 2024; 12 (3): 484.
9. Wang Z, Dan W, Zhang N, Fang J, Yang Y. Colorectal cancer and gut microbiota studies in China. Gut Microbes. 2023; 15 (1): 2236364.
10. Hajishengallis G, Darveau RP, Curtis MA. The keystone-pathogen hypothesis. Nat Rev Microbiol. 2012; 10 (10): 717–25.
11. Eaden JA. The risk of colorectal cancer in ulcerative colitis: a meta-analysis. Gut. 2001; 48 (4): 526–35.
12. Tjalsma H, Boleij A, Marchesi JR, Dutilh BE. A bacterial driver–passenger model for colorectal cancer: beyond the usual suspects. Nat Rev Microbiol. 2012; 10 (8): 575–82.
13. Li J, Zhang A hua, Wu F fang, Wang X jun. Alterations in the Gut Microbiota and Their Metabolites in Colorectal Cancer: Recent Progress and Future Prospects. Front Oncol. 2022; 12: 841552.
14. Coker OO, Wu WKK, Wong SH, Sung JJY, Yu J. Altered Gut Archaea Composition and Interaction With Bacteria Are Associated With Colorectal Cancer. Gastroenterology. 2020; 159 (4): 1459-1470.e5.
15. Abdel Hamed EF, Mostafa NE, Farag SM, Ibrahim MN, Ibrahim BH, Rashed HE, et al. Human protozoa infection and dysplasia in ulcerative colitis: a neglected aspect in a prominent disease. Parasitol Res. 2023; 122 (11): 2709–18.

Литература

1. World Health Organization. 2024. World Health Organization. Available from: https://www.who.int/
2. Yu YN, Fang JY. Gut Microbiota and Colorectal Cancer. Gastrointest Tumors. 2015; 2 (1): 26–32.
3. Cheng Y, Ling Z, Li L. The Intestinal Microbiota and Colorectal Cancer. Front Immunol. 2020; 11: 615056.
4. Bakulin IG, Zharkov AV, Zhuravleva MS, Serkova MYu. Colorectal cancer screening: current status and future prospects. Profil Meditsina. 2023; 26 (12): 12.
5. Злокачественные новообразования в России в 2023 году (заболеваемость и смертность). М.: МНИОИ им. П. А. Герцена — филиал ФГБУ «НМИЦ радиологии» Минздрава России, 2024; 276 р. Доступно по ссылке: https://oncology-association.ru/wp-content/uploads/2024/08/zis-2023-elektronnaya-versiya.pdf.
6. Saus E, Iraola-Guzmán S, Willis JR, Brunet-Vega A, Gabaldón T. Microbiome and colorectal cancer: Roles in carcinogenesis and clinical potential. Mol Aspects Med. 2019; 69: 93–106.
7. Sears CL, Pardoll DM. Perspective: Alpha-Bugs, Their Microbial Partners, and the Link to Colon Cancer. J Infect Dis. 2011; 203 (3): 306–11.
8. Yadav D, Sainatham C, Filippov E, Kanagala SG, Ishaq SM, Jayakrishnan T. Gut Microbiome–Colorectal Cancer Relationship. Microorganisms. 2024; 12 (3): 484.
9. Wang Z, Dan W, Zhang N, Fang J, Yang Y. Colorectal cancer and gut microbiota studies in China. Gut Microbes. 2023; 15 (1): 2236364.
10. Hajishengallis G, Darveau RP, Curtis MA. The keystone-pathogen hypothesis. Nat Rev Microbiol. 2012; 10 (10): 717–25.
11. Eaden JA. The risk of colorectal cancer in ulcerative colitis: a meta-analysis. Gut. 2001; 48 (4): 526–35.
12. Tjalsma H, Boleij A, Marchesi JR, Dutilh BE. A bacterial driver–passenger model for colorectal cancer: beyond the usual suspects. Nat Rev Microbiol. 2012; 10 (8): 575–82.
13. Li J, Zhang A hua, Wu F fang, Wang X jun. Alterations in the Gut Microbiota and Their Metabolites in Colorectal Cancer: Recent Progress and Future Prospects. Front Oncol. 2022; 12: 841552.
14. Coker OO, Wu WKK, Wong SH, Sung JJY, Yu J. Altered Gut Archaea Composition and Interaction With Bacteria Are Associated With Colorectal Cancer. Gastroenterology. 2020; 159 (4): 1459-1470.e5.
15. Abdel Hamed EF, Mostafa NE, Farag SM, Ibrahim MN, Ibrahim BH, Rashed HE, et al. Human protozoa infection and dysplasia in ulcerative colitis: a neglected aspect in a prominent disease. Parasitol Res. 2023; 122 (11): 2709–18.

METHOD FOR QUANTITATIVE ASSESMENT OF GUT MICROBIOTA: A COMPARATIVE ANALYSIS OF 16S NGS AND qPCR

Zlobovskaya OA[1] ✉, Kurnosov AS[1], Sheptulina AF[2], Glazunova EV[1]

[1] Centre for Strategic Planning and Management of Biomedical Health Risks of the Federal Medical Biological Agency, Moscow, Russia

[2] National Medical Research Center for Therapy and Preventive Medicine of the Ministry of Healthcare of the Russian Federation, Moscow, Russia

Recently, considerable commercialization of services for quantification of gut microbiota aimed to diagnose dysbiosis, the microbial imbalance, is observed. In the context of growing interest to the personalized approaches in medicine and preventive therapy, the diagnosis of dysbiosis is becoming increasingly important. The results of such screening are used to adjust guidelines on correction of the diet, lifestyle modification, or, where necessary, drug therapy prescription. Such assessment requires a reliable and accurate method for evaluation of microbiota, since validity of further recommendations and therapeutic interventions depends on the quality of the data obtained. The paper reports the main aspects of the two approaches used for microbiota quantification: 16S rRNA next-generation sequencing (16S NGS) and real-time PCR (qPCR). The strengths (from our perspective) and weaknesses of the approaches are also provided.

Keywords: 16S NGS, real-time PCR, metagenomic analysis, quantitative analysis, microbiome, personalized medicine

Author contribution: Zlobovskaya OA — concept, literature review, manuscript writing; Kurnosov AS, Sheptulina AF, Glazunova EV — manuscript editing.

✉ **Correspondence should be addressed:** Olga A. Zlobovskaya
Pogodinskaya, 10, str. 1, Moscow, 119121, Russia; OZlobovskaya@cspfmba.ru

Received: 15.10.2024 **Accepted:** 25.10.2024 **Published online:** 30.10.2024

DOI: 10.24075/brsmu.2024.047

ВЫБОР МЕТОДА КОЛИЧЕСТВЕННОЙ ОЦЕНКИ МИКРОБИОТЫ КИШЕЧНИКА: СРАВНИТЕЛЬНЫЙ АНАЛИЗ 16S NGS И ПЦР-РВ

О. А. Злобовская[1] ✉, А. С. Курносов[1], А. Ф. Шептулина[2], Е. В. Глазунова[1]

[1] Центр стратегического планирования и управления медико-биологическими рисками здоровью Федерального медико-биологического агентства, Москва, Россия

[2] Национальный медицинский исследовательский центр терапии и профилактической медицины Министерства здравоохранения Российской Федерации, Москва, Россия

В последнее время наблюдается значительная коммерциализация услуг по количественной оценке микробиоты кишечника с целью диагностики дисбиоза — нарушения микробного баланса. В условиях растущего интереса к персонализированным подходам в медицине и профилактической терапии диагностика дисбиоза приобретает все большее значение. Результаты подобного скрининга используют для рекомендаций по корректировке питания, изменению образа жизни или, при необходимости, назначения медикаментозного лечения. Для подобной оценки необходим надежный и точный метод оценки микробиоты, поскольку от качества полученных данных зависит корректность последующих рекомендаций и терапевтических вмешательств. В статье рассмотрены основные аспекты двух подходов, применяемых для количественной оценки микробиоты, — высокопроизводительного секвенирования гена 16S рРНК (16S NGS) и ПЦР в реальном времени (ПЦР-РВ), а также представлены их сильные, на наш взгляд, и слабые стороны.

Ключевые слова: 16S NGS, ПЦР-РВ, метагеномный анализ, количественный анализ, микробиом, персонализированная медицина

Вклад авторов: О. А. Злобовская — идея, анализ литературы, написание рукописи; А. С. Курносов, А. Ф. Шептулина, Е. В. Глазунова — редактирование рукописи.

✉ **Для корреспонденции:** Ольга Анатольевна Злобовская
ул. Погодинская, д. 10, с. 1, г. Москва, 119121, Россия; OZlobovskaya@cspfmba.ru

Статья получена: 15.10.2024 **Статья принята к печати:** 25.10.2024 **Опубликована онлайн:** 30.10.2024

DOI: 10.24075/vrgmu.2024.047

16S NGS: Broad Capabilities and Significant Limitations

The 16S NGS method has become an essential tool for studying the microbiota. Its main advantage is the ability to simultaneously sequence multiple samples and detect a wide range of microorganisms. Comprehensive assessment of the taxonomic composition of microbial communities and their diversity makes 16S NGS indispensable for fundamental research. However, despite its benefits, this method has several significant limitations that can lead to distorted quantitative results.

Uneven amplification (dependence on primers)

Universal primers are used to amplify the variable regions of the 16S rRNA gene. They exhibit different affinities for the DNA of various taxa, resulting in unequal amplification efficiency during library preparation [1]. As a result, the microbiota structure data can be skewed, with some taxa being overestimated, while others are underestimated or entirely missed.

Uneven amplification (dependence on taxonomic composition)

The most abundant taxa gain a significant advantage during the early stages of amplification [2], thus reducing the likelihood of accurately detecting rare taxa (up to 10% of the total community). Since each sample has a unique microbiota composition, it is impossible to apply a systematic correction for all samples, even when using the same protocols [3, 4].

Low sensitivity

On average, between 5,000 and 50,000 reads are obtained per sample when using the 16S NGS method. However, according to Poisson distribution, quantitative assessment of a taxon can only be considered statistically reliable when there are at least 100 reads for that taxon in the sample [5]. This limits the ability to reliably quantify taxa that make up less than 0.2–2% of the total reads (depending on the total number of reads). Increasing the number of reads per sample is not

always effective, as the amplification of dominant taxa occurs in the early stages, leading to a significant underrepresentation or even loss of minor taxa. Consequently, the taxonomic diversity saturation curve reaches a plateau at 20,000–50,000 reads, meaning that further increasing the number of reads will not improve data representativeness. This is especially important for minor opportunistic microorganisms that may have clinical significance at low concentrations but are often either undetected or inaccurately quantified. Additionally, there is no consensus among researchers on whether it is more accurate to compare samples with different numbers of reads or to introduce bias by unifying the number of reads [6, 7].

Reduced specificity

When analyzing short regions (V1-V3, V3-V4, V6, etc.), the high degree of conservation in the 16S region often prevents taxonomic resolution at the species level, and sometimes even at the genus level [1, 8]. Using the full-length 16S gene increases the resolution of sequencing but is only available on such platforms as ONT, PacBio, and LoopSeq. A significant drawback of these platforms is their higher error rate compared to short-read platforms like Illumina.

Limitations of relative quantification of taxa

The 16S NGS method evaluates only the relative abundance of taxa, not their absolute quantity. This means that an increase in the relative abundance of one taxon, for example, due to dietary changes, will automatically reduce the proportion of other taxa in the analysis. Simultaneous changes in multiple taxa in either direction makes the reconstruction of the true dynamics of the community impossible [4–6].

Impact of 16S rRNA gene copy number

Each microbial species has a unique number of 16S rRNA gene copies, which is rarely considered during analysis, particularly when identifying sequences to the genus or family level. Even when using specialized plugins for QIIME 2, biases usually persist. One reason is that in cases where the copy number data for a specific taxonomic group is absent from the rrnDB database, the algorithm automatically assigns a copy number of one.

Uneven phylogenetic resolution

Different regions of the 16S rRNA gene have varying levels of phylogenetic resolution [1, 8–10]. This leads to inconsistent classification accuracy, complicating the comparison of data across different studies.

Differences in sequencing platforms and data processing methods

The choice of sequencing platforms and library preparation methods can lead to significant variations in results [1, 11, 12]. As mentioned above, this makes it more challenging to compare data across various studies.

Dependence on databases

Different databases (RDP, SILVA, Greengenes, etc.) can yield different quantitative assessments for the same sample [1, 13]. Additionally, databases are updated every few years, which means that newly introduced taxa may be missing.

qPCR: Specialized Tasks, High Accuracy

Unlike NGS, specific DNA fragments are amplified in real-time PCR (qPCR). This results in several advantages.

High sensitivity and a broad quantitative range

qPCR enables the detection and quantification of even a few target copies in a reaction with high precision. This is especially important when studying rare clinically significant taxa, which may be missed by 16S NGS. Additionally, qPCR can reliably quantify up to 10^7–10^8 target copies in a reaction.

High specificity

Oligonucleotides are designed to distinguish even closely related microorganisms with high accuracy.

Improved Precision

Unlike 16S NGS, the absence of simultaneous amplification of hundreds of different targets leads to a more reliable individual assessment of a specific taxon abundance.

Fast and simple interpretation

Unlike 16S NGS, qPCR does not require complex bioinformatics methods for data interpretation. This makes it more accessible and convenient for clinical research and diagnostics, where speed and accuracy are critical.

High reproducibility

qPCR provides higher reproducibility compared to 16S NGS due to the simplicity of the method and data analysis. This is particularly important for clinical diagnostics and long-term studies, and also facilitates data comparison between different studies and laboratories.

Absolute quantification

qPCR allows for both relative and absolute quantification of taxa. Thus qPCR enables analysis of microbiota dynamics under different conditions, unlike the relative approach of NGS.

Reduced dependency on sample quality

qPCR analysis is less dependent on the initial quality of the sample (e.g., quantity, presence of PCR inhibitors) compared to the 16S NGS method, where these factors significantly impact the library preparation stage.

Nevertheless, the qPCR method also has certain limitations. However, unlike NGS, many of potential issues can be minimized if addressed properly.

Selection of target microorganisms

Preselected genetic targets are amplified in qPCR, which requires prior knowledge of the microbiota key representatives in the given study.

Target region selection

The most commonly studied region for the majority of bacteria is the 16S rRNA gene, making it the typical target for qPCR

assay development. However, this is a highly conserved genomic region, so for some taxonomic units at the species level (and occasionally at the genus level, e.g., *Oscillibacter*/*Dysosmobacter*), it may not be possible to develop specific systems that amplify 16S region. For some microorganisms, whole-genome data are available, allowing the selection of another region for detection. However, these organisms are in the minority, so the chosen target may be nonspecific, or the system may fail to amplify all members of the given taxonomic group.

Limitation on the number of taxa

High qPCR specificity limits the number of taxa that can be analyzed simultaneously. For accurate quantitative assessment, it is recommended to combine no more than two targets (if they exhibit a broad range and are consistently present in most samples) or three targets (for rare taxa) in a single tube. Moreover, due to the limited number of taxa analyzed in this method, qPCR does not provide information on the structure of the entire microbial community or its diversity, which may also hold clinical significance.

Biases related to gene copy number

This issue can arise if the system is designed to detect a taxonomic group at a higher level (e.g., family), where different genera/species within the group possess significantly varying numbers of 16S rRNA gene copies.

Need for data standardization

Converting the data obtained through qPCR into absolute values requires the use of calibration standards. For maximum accuracy, it is essential to pre-assess the standards using droplet digital PCR. In addition, the sensitivity and linear range of oligonucleotide systems should preferably be tested not on model samples (e.g., plasmid or amplicon titration) but on the genomic DNA of the corresponding taxon, ideally against a background of fecal DNA in clinically relevant quantities.

CONCLUSION

A comparison of the 16S NGS and qPCR methods shows that NGS is better suited for studying the overall composition and diversity of the microbiota. However, its use for quantitative assessment is limited by several factors that currently lack practical solutions. Meanwhile, qPCR offers more accurate and reliable quantitative assessment, making it the preferred method for studies where high precision is required, and the target markers are well-defined.

References

1. Abellan-Schneyder I, Matchado MS, Reitmeier S, Sommer A, Sewald Z, Baumbach J, et al. Primer, Pipelines, Parameters: Issues in 16S rRNA Gene Sequencing. Tringe SG, editor. mSphere. 2021; 6 (1): e01202–20.
2. Gonzalez JM, Portillo MC, Belda-Ferre P, Mira A. Amplification by PCR Artificially Reduces the Proportion of the Rare Biosphere in Microbial Communities. Gilbert JA, editor. PLoS ONE. 2012; 7 (1): e29973.
3. Boers SA, Jansen R, Hays JP. Understanding and overcoming the pitfalls and biases of next-generation sequencing (NGS) methods for use in the routine clinical microbiological diagnostic laboratory. Eur J Clin Microbiol Infect Dis. 2019; 38 (6): 1059–70.
4. Vaginal Microbiome Consortium (additional members), Brooks JP, Edwards DJ, Harwich MD, Rivera MC, Fettweis JM, et al. The truth about metagenomics: quantifying and counteracting bias in 16S rRNA studies. BMC Microbiol. 2015; 15 (1): 66.
5. Barlow JT, Bogatyrev SR, Ismagilov RF. A quantitative sequencing framework for absolute abundance measurements of mucosal and lumenal microbial communities. Nat Commun. 2020; 11 (1): 2590.
6. Vandeputte D, Kathagen G, D'hoe K, Vieira-Silva S, Valles-Colomer M, Sabino J, et al. Quantitative microbiome profiling links gut community variation to microbial load. Nature. 2017; 551 (7681): 507–11.
7. Nearing JT, Douglas GM, Hayes MG, MacDonald J, Desai DK, Allward N, et al. Microbiome differential abundance methods produce different results across 38 datasets. Nat Commun. 2022; 13 (1): 342.
8. Johnson JS, Spakowicz DJ, Hong BY, Petersen LM, Demkowicz P, Chen L, et al. Evaluation of 16S rRNA gene sequencing for species and strain-level microbiome analysis. Nat Commun. 2019; 10 (1): 5029.
9. Rintala A, Pietilä S, Munukka E, Eerola E, Pursiheimo JP, Laiho A, et al. Gut Microbiota Analysis Results Are Highly Dependent on the 16S rRNA Gene Target Region, Whereas the Impact of DNA Extraction Is Minor. J Biomol Tech JBT. 2017; 28 (1): 19–30.
10. Kameoka S, Motooka D, Watanabe S, Kubo R, Jung N, Midorikawa Y, et al. Benchmark of 16S rRNA gene amplicon sequencing using Japanese gut microbiome data from the V1–V2 and V3–V4 primer sets. BMC Genomics. 2021; 22 (1): 527.
11. Tremblay J, Singh K, Fern A, Kirton ES, He S, Woyke T, et al. Primer and platform effects on 16S rRNA tag sequencing. Front Microbiol. 2015; 6.
12. Chuang HH, Huang CG, Chou SH, Li HY, Lee CC, Lee LA. Comparative analysis of gut microbiota in children with obstructive sleep apnea: assessing the efficacy of 16S rRNA gene sequencing in metabolic function prediction based on weight status. Front Endocrinol. 2024; 15: 1344152.
13. Ceccarani C, Severgnini M. A comparison between Greengenes, SILVA, RDP, and NCBI reference databases in four published microbiota datasets. 2023 [cited 2024 Oct 4]. Available from: http://biorxiv.org/lookup/doi/10.1101/2023.04.12.535864.

Литература

1. Abellan-Schneyder I, Matchado MS, Reitmeier S, Sommer A, Sewald Z, Baumbach J, et al. Primer, Pipelines, Parameters: Issues in 16S rRNA Gene Sequencing. Tringe SG, editor. mSphere. 2021; 6 (1): e01202–20.
2. Gonzalez JM, Portillo MC, Belda-Ferre P, Mira A. Amplification by PCR Artificially Reduces the Proportion of the Rare Biosphere in Microbial Communities. Gilbert JA, editor. PLoS ONE. 2012; 7 (1): e29973.
3. Boers SA, Jansen R, Hays JP. Understanding and overcoming the pitfalls and biases of next-generation sequencing (NGS) methods for use in the routine clinical microbiological diagnostic laboratory. Eur J Clin Microbiol Infect Dis. 2019; 38 (6): 1059–70.
4. Vaginal Microbiome Consortium (additional members), Brooks JP, Edwards DJ, Harwich MD, Rivera MC, Fettweis JM, et al. The truth about metagenomics: quantifying and counteracting bias in 16S rRNA studies. BMC Microbiol. 2015; 15 (1): 66.

5. Barlow JT, Bogatyrev SR, Ismagilov RF. A quantitative sequencing framework for absolute abundance measurements of mucosal and lumenal microbial communities. Nat Commun. 2020; 11 (1): 2590.
6. Vandeputte D, Kathagen G, D'hoe K, Vieira-Silva S, Valles-Colomer M, Sabino J, et al. Quantitative microbiome profiling links gut community variation to microbial load. Nature. 2017; 551 (7681): 507–11.
7. Nearing JT, Douglas GM, Hayes MG, MacDonald J, Desai DK, Allward N, et al. Microbiome differential abundance methods produce different results across 38 datasets. Nat Commun. 2022; 13 (1): 342.
8. Johnson JS, Spakowicz DJ, Hong BY, Petersen LM, Demkowicz P, Chen L, et al. Evaluation of 16S rRNA gene sequencing for species and strain-level microbiome analysis. Nat Commun. 2019; 10 (1): 5029.
9. Rintala A, Pietilä S, Munukka E, Eerola E, Pursiheimo JP, Laiho A, et al. Gut Microbiota Analysis Results Are Highly Dependent on the 16S rRNA Gene Target Region, Whereas the Impact of DNA Extraction Is Minor. J Biomol Tech JBT. 2017; 28 (1): 19–30.
10. Kameoka S, Motooka D, Watanabe S, Kubo R, Jung N, Midorikawa Y, et al. Benchmark of 16S rRNA gene amplicon sequencing using Japanese gut microbiome data from the V1–V2 and V3–V4 primer sets. BMC Genomics. 2021; 22 (1): 527.
11. Tremblay J, Singh K, Fern A, Kirton ES, He S, Woyke T, et al. Primer and platform effects on 16S rRNA tag sequencing. Front Microbiol. 2015; 6.
12. Chuang HH, Huang CG, Chou SH, Li HY, Lee CC, Lee LA. Comparative analysis of gut microbiota in children with obstructive sleep apnea: assessing the efficacy of 16S rRNA gene sequencing in metabolic function prediction based on weight status. Front Endocrinol. 2024; 15: 1344152.
13. Ceccarani C, Severgnini M. A comparison between Greengenes, SILVA, RDP, and NCBI reference databases in four published microbiota datasets. 2023 [cited 2024 Oct 4]. Available from: http://biorxiv.org/lookup/doi/10.1101/2023.04.12.535864.

PRODUCTION AND BIOLOGICAL ACTIVITY OF THE EXOGENOUS mRNA ENCODING HUMAN MxA PROTEIN

Plotnikova MA[1], Bobkov DE[1,2], Klotchenko SA[1]✉

[1] Smorodintsev Research Institute of Influenza of the Ministry of Health of the Russian Federation, St. Petersburg, Russia

[2] Institute of Cytology, Russian Academy of Science, St. Petersburg, Russia

Human MxA protein induced by type I and III interferons is an important innate immunity mediator, it shows antiviral activity against a broad spectrum of RNA and DNA viruses. According to the latest data, the MxA protein overexpression increases chemotherapy sensitivity and represents one of the favorable prognostic factors in patients with breast cancer. The exogenous mRNA capable of intracellular MxA protein production not only has the potential for treatment of viral respiratory infection, but also can become an important fundamental research tool. The study aimed to construct and produce the exogenous mRNA encoding the functional human cytoplasmic MxA protein by *in vitro* transcription (IVT); to study its translational properties; to assess and identify the patterns of the expression of some interferon system genes in response to introduction of this exogenous mRNA into cells. As a result of the study, the exogenous mRNAs capable of effective translation (up to 20 ng/mL of protein from 100 ng of mRNA per well of the 96-well plate) in the eukaryotic cell systems were successfully constructed and produced by IVT (in the amount of up to 200 μg); diffuse distribution of the MxA protein in the MDCK cells was confirmed; significant changes in the expression of the interferon-stimulated genes, such as OAS1, PKR (EIF2AK2), MDA5, RIG-I, were revealed. Our further research will be focused on assessing the developed exogenous mRNAs' therapeutic potential against influenza A and B viruses, respiratory syncytial virus, and coronavirus SARS-CoV-2.

Keywords: MxA protein, exogenous mRNA, *in vitro* transcription, IFN-stimulated genes

Funding: the study was supported by the Russian Science Foundation, Agreement No. 23-25-00433, project title: "Assessment of antiviral effect of the mRNA encoding human MxA protein" (manager M. A. Plotnikova), https://rscf.ru/project/23-25-00433/

Author contribution: Plotnikova MA — study design, experimental procedure, analysis of the results, statistical processing, manuscript writing; Bobkov DE — confocal microscopy examination; Klotchenko SA — production and characterization of the exogenous mRNA preparations, manuscript editing.

✉ **Correspondence should be addressed:** Sergey A. Klotchenko
Professora Popova, 15/17, St. Petersburg, 197022, Russia; fosfatik@mail.ru

Received: 30.09.2024 **Accepted:** 22.10.2024 **Published online:** 30.10.2024

DOI: 10.24075/brsmu.2024.048

ПОЛУЧЕНИЕ И ОЦЕНКА БИОЛОГИЧЕСКОЙ АКТИВНОСТИ ЭКЗОГЕННОЙ мРНК, КОДИРУЮЩЕЙ БЕЛОК MxA ЧЕЛОВЕКА

М. А. Плотникова[1], Д. Е. Бобков[1,2], С. А. Клотченко[1]✉

[1] Научно-исследовательский институт гриппа имени А. А. Смородинцева Министерства здравоохранения России, Санкт-Петербург, Россия

[2] Институт цитологии Российской академии наук, Санкт-Петербург, Россия

Индуцируемый интерферонами типа I и типа III человеческий белок MxA является важным медиатором врожденного иммунитета и проявляет антивирусную активность в отношении широкого спектра РНК- и ДНК-содержащих вирусов. По последним данным, сверхэкспрессия белка MxA повышает чувствительность к проводимой химиотерапии и является одним из факторов благоприятного прогноза для пациентов с раком молочной железы. Экзогенная мРНК, способная к внутриклеточной продукции белка MxA, не только обладает потенциалом для лечения респираторных вирусных инфекций, но и может стать важным инструментом для фундаментальных исследований. Целью работы было сконструировать и получить методом *in vitro* транскрипции (IVT) экзогенную мРНК, кодирующую функциональный цитоплазматический белок MxA человека; изучить ее трансляционные свойства; оценить и выявить закономерности в экспрессии некоторых генов системы интерферонов в ответ на введение этой экзогенной мРНК в клетки. В результате работы были успешно сконструированы и получены методом IVT экзогенные мРНК (в количествах до 200 мкг), способные к эффективной трансляции (до 20 нг/мл белка со 100 нг мРНК в лунке 96-луночного планшета) в эукариотических клеточных системах; подтверждено диффузное внутриклеточное распределение белка MxA в клетках MDCK; выявлены достоверные изменения экспрессии интерферон-стимулируемых генов, таких как OAS1, PKR (EIF2AK2), MDA5, RIG-I. Наши дальнейшие исследования будут посвящены оценке терапевтического потенциала разработанных экзогенных мРНК в отношении вирусов гриппа A и B, респираторно-синцитиального вируса и коронавируса SARS-CoV-2.

Ключевые слова: белок MxA, экзогенная мРНК, *in vitro* транскрипция, ИФН-стимулируемые гены

Финансирование: исследование выполнено при финансовой поддержке Российского научного фонда, Соглашение № 23-25-00433, название проекта: «Изучение противовирусного действия мРНК, кодирующей MxA белок человека» (руководитель — М. А. Плотникова), https://rscf.ru/project/23-25-00433/

Вклад авторов: М. А. Плотникова — дизайн исследования, проведение экспериментов, анализ результатов, статистическая обработка, написание рукописи; Д. Е. Бобков — исследования с использованием метода конфокальной микроскопии; С. А. Клотченко — получение и характеристика препаратов экзогенных мРНК, редактирование рукописи.

✉ **Для корреспонденции:** Сергей Анатольевич Клотченко
ул. Профессора Попова, 15/17, г. Санкт-Петербург, 197022, Россия; fosfatik@mail.ru

Статья получена: 30.09.2024 **Статья принята к печати:** 22.10.2024 **Опубликована онлайн:** 30.10.2024

DOI: 10.24075/vrgmu.2024.048

The Mx proteins induced by type I and III interferons are the important innate immunity mediators and are involved in protection against various RNA and DNA viruses [1]. These proteins belonging to the large hydrolase enzyme family (GTPases) are homologous to vertebrates [2, 3].

In humans, two different Mx-GTPases referred to as MxA and MxB are encoded on chromosome 21. Both proteins are localized to the cytoplasm and show a characteristic granular staining pattern when detected by the immunofluorescence method [3]. Human MxA is a cytoplasmic protein with

the weight of 78 kDa that is closely linked with the smooth endoplasmic reticulum [1]. MxA has a comparatively wide antiviral spectrum against various types of viruses, regardless of their intracellular replication type. The MxA-sensitive viruses include representatives of the bunyaviruses, orthomyxoviruses, paramyxoviruses, rhabdoviruses, togaviruses, picornaviruses, and hepatitis B virus, a DNA virus with the genomic RNA intermediate [2, 4, 5]. It is interesting that some viruses are inhibited in the cell-type specific manner. This suggests that unknown cellular factors may affect antiviral specificity [6].

In addition to antiviral activity, recent studies defined the role of MxA in various cancer types, specifically breast cancer and prostate carcinoma [1]. Thus, it has been reported that high MxA levels and large amounts of tumor-infiltrating lymphocytes are independent prognostic factors of relapse-free survival in patients with triple-negative breast cancer [7]. It has been also reported that MxA expression by tumor cells more often results in metastasis-free survival after adjuvant chemotherapy [8]. In this regard, it is expected that artificial increase in tumor MxA levels can lead to favorable outcomes in cancer patients and make chemotherapy more effective. All the above suggests that MxA is an extremely promising therapeutic agent.

Since MxA is an intracellular protein, and delivery of proteins of such size into cells remains a major problem, we have proposed a relatively new approach involving the use of the human MxA protein-encoding exogenous mRNA for investigation of the MxA biological properties. This concept has been actively developing in the past decade; it was quite successfully implemented in 2020 when creating the next generation of mRNA vaccines against COVID-19 produced by Pfizer/BioNTech and Moderna. Considerable progress was made in regenerative medicine, where mRNA is used to reprogram somatic cells, as well as in protein replacement therapy used for treatment of genetic disorders.

The study aimed to construct and produce the exogenous mRNA encoding the functional human cytoplasmic MxA protein by IVT; to study its translational properties; to assess and identify the patterns of the expression of some interferon system genes (IFN-stimulated genes) in response to introduction of the exogenous mRNA into cells. In the future we suppose to assess the therapeutic potential of the mRNA construct developed against influenza A and B viruses, respiratory syncytial virus, and coronavirus SARS-CoV-2.

METHODS

Construction of plasmid vectors

The nucleotide insertions encoding human MxA protein were obtained from the total RNA preparations extracted from the A549 cells by RT-PCR using the primers (GAGAGCGGCCGCGCCACCATGGTTGTTT/ ATCTTCTAG ATTAACCGGGGAACTGGGCAAGC) comprising restriction sites for the Not I and Xba I endonucleases. The fragments of appropriate size (2017 bp) were inserted in the pJET1.2 vector system comprising the T7 promoter region by the Not I/Xba I restriction with subsequent sticky-end ligation. To produce the construct with the cap-independent translation, the IRES-element sized 605 bp was amplified in a similar way using the pIRESneo3 plasmid vector as a template; the poly(A) sequences, 5′ and 3′ UTR sized 114, 57, and 110 bp, respectively, were synthesized by Evrogen (Russia). All untranslated cassette components were ligated into the pJET1.2 vector in accordance with the design proposed (see Results).

The colonies obtained by cloning were screened by RT-PCR. The plasmid constructs containing insertions of the expected size were accumulated and purified using the Plasmid Miniprep 2.0 kit (Evrogen; Russia). The sequences of the plasmid constructs developed were confirmed using Sanger sequencing by Evrogen (Russia).

In vitro transcription

Preparations of the exogenous mRNAs (mRNA-MxA-CDS, mRNA-MxA-IRES, mRNA-MxA-UTR, and mRNA-GFP-CDS) were obtained by IVT using the HighYield T7 ARCA mRNA Synthesis Kit (#RNT-102, Jena Bioscience; Germany). A total of 1 μg of the plasmid linearized by the Xba I site was used as a template for RNA synthesis. The synthetic Anti-Reverse Cap Analog (ARCA) added to the reaction mixture to the ratio of ARCA/GTP 4 : 1 was used as a cap. The modified nitrogenous bases, 5-methylcytidine (#NU-1138, 5-Methyl-CTP, m5C, Jena Bioscience; Germany) and pseudouridine (#NU-1139, Pseudo-UTP, Ψ, Jena Bioscience; Germany), were used in the reaction. The reaction was carried out in accordance with the manufacturer's protocol.

After the RNA synthesis, the DNA template was removed by further cleavage with the Turbo DNAse (#AM1345, Thermo Fisher Scientific; USA). The Poly(A) Tailing Enzyme Testkit (#RNT-004, Jena Bioscience; Germany) was used for the non-templated 3' polyadenylation of the transcribed mRNAs. The resulting transcripts were purified using the columns, the RNA Clean & Concentrator kit (#R1017, Zymo Research; USA). The resulting mRNA concentrations were measured with the NanoDrop-1000 spectrophotometer and Qubit 4 fluorometer (Thermo Fisher Scientific; USA).

Agarose gel electrophoresis

The plasmid DNA preparations were analyzed in the 0.8% agarose gel prepared based on the 1× TAE buffer containing up to 0.5 μg/mL of ethidium bromide using the 6× buffer for DNA application.

The mRNA samples were analyzed under denaturing conditions in the 1% agarose gel containing 0.5 μg/mL of ethidium bromide. A total of 500 ng of mRNA sample were mixed with the equal amount of the Gel Loading Buffer II (#AM1344, Invitrogen; USA), heated for 5 min at 80 °C, and applied to the gel.

The electrophoretic separation results were imaged using the Gel Doc EZ Imager (Bio-Rad; USA).

Cell culture maintenance and transfection with the exogenous mRNAs

The following cultures were used in the study for various experiments: the passaged culture of the A549 cells (human lung carcinoma) obtained from the ATCC collection (USA) and the culture of the MDCK FR58 cells (canine kidney cells) obtained from the IRR collection (USA).

The A549 cells were cultured in the F12K growth medium (Gibco; USA) in the presence of the 10% KPC serum (Gibco; USA); the MDCK cells were cultured in the alpha-MEM medium (BioloT; Russia) added KPC serum to 5%. The culture maintenance and all the experiments were implemented without adding antibiotics.

To ensure transfection with the exogenous mRNAs, we used the 24 h 90–100% cell monolayer; the growth medium was replaced with the serum-free medium immediately before

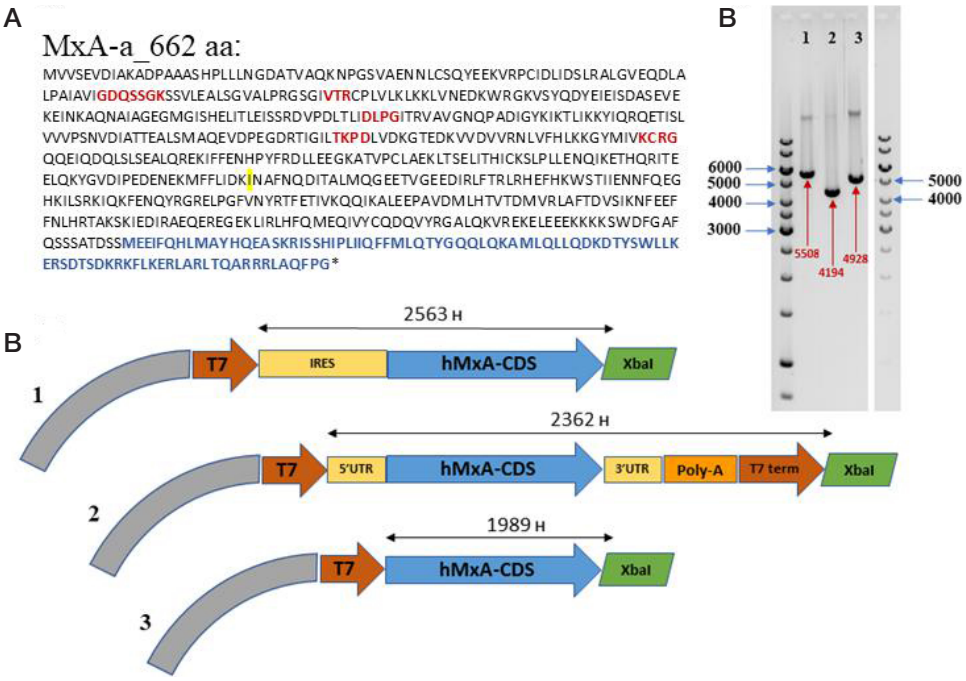

Fig. 1. Structure of the plasmid-based constructs encoding the exogenous human MxA mRNA. **A**. Amino acid sequence of the encoded MxA protein (obtained by sequencing of the constructs developed), the G1–G5 motifs (in the order of occurrence) are highlighted in red, the C-terminal GTPase effector domain — in blue, the V379I variation — in *yellow*. **B**. Scheme of the linearized plasmids designed for mRNA production by IVT. In the schemes, the T7 promoter region for T7 polymerase (and T7 terminator region for the construct #2) is highlighted in brick red, the auxiliary non-coding regulatory elements — in *yellow*, the fragment ensuring the template addition of the poly(A) tail (114 b) — in *orange* (in the second case), the MxA-encoding sequence — in *blue*, the restriction site used for linearization — in *green*. **C**. Electrophoretic separation of the linearized plasmids, the expected product lengths (bp) are highlighted in *red*

adding mRNA. Cells were transfected using the commercially available Lipofectamine MessengerMAX transfection reagent (Thermo Fisher Scientific; USA) in accordance with the manufacturer's instructions. The mRNA complexes were added to the wells of the 96-well plate in a volume of 10 µL, and to the wells of the 12-well plate in a volume of 50 µL. There were 100 ng of mRNA and 0.3 µL of the Lipofectamine MessengerMAX reagent per well of the 96-well plate, 450 ng of RNA and 1 µL of the Lipofectamine MessengerMAX reagent per well of the 12-well plate. Depending on the objectives of the experiment, cells were incubated with the RNA/Lipofectamine complexes for 4–24 h at 37 °C and 5% CO_2.

Confocal miscroscopy

Confocal imaging of the fixed cells was performed 24 h after transfection with the exogenous mRNAs. For that the cell monolayer grown on the glass slides was washed with DPBS, fixed with the 4% paraformaldehyde solution for 10 min, and permeabilized with the 0.1% Triton X-100. Blockage was accomplished using the 1% BSA solution in DPBS. The nuclei were stained with DAPI (AppliChem; USA), and the actin cytoskeleton was stained with phalloidin covalently linked to rhodamine (Thermo Fisher Scientific; USA). The human MxA protein imaging was performed using the primary MxA/Mx1 Antibody labeled with biotin (Novus Biologicals; Germany) with subsequent development using Streptavidin DyLight 633 (Thermo Fisher Scientific; USA). Cell microscopy was performed using the TCS SP8 inverted confocal laser scanning microscope (Leica; Germany).

Enzyme-linked immunosorbent assay (ELISA)

The MxA protein levels were measured using the Human MxA Protein ELISA kit (BioVendor; Czech Republic) in accordance with the manufacturer's instructions. The results were recorded in the dual-wavelength mode (at the primary wavelength of 450 nm and reference wavelength of 655 nm) using the CLARIOstar microplate reader (BMG Labtech; Germany)

Expression level assessment

The IFN-stimulated gene expression levels were assessed by real-time RT-PCR using the previously designed primers [9]. The total RNA preparations were extracted using the TRIzol reagent (Thermo Fisher Scientific; USA) and then treated with DNAse (Biolabmix; Russia). The RT reaction was carried out using the RNAscribe RT kit (Biolabmix; Russia), dT(16) primers and 2 µg of the DNA-free RNA. PCR was conducted using the ready-made BioMaster HS-qPCR (2×) kit (Biolabmix; Russia), to which 1–2 µL of cDNA were added.

Relative gene expression was calculated by the double delta Ct (ΔΔCt) method using GAPDH and ACTB as the normalizing genes. The relative gene expression levels were determined using the inductive formula $R = 2^{-[\Delta\Delta Ct]}$. Calculations were performed using the Microsoft Office Excel 2003/2007 software (USA).

Statistical data processing

Significance of differences was assessed with the GraphPad Prism 6 software tool (GraphPad Software; USA) using the nonparametric Kruskal–Wallis test (to assess significance of differences between three or more independent groups) and the Dunnett's test (for multiple intergroup comparisons). The differences were considered significant at $p < 0.05$.

RESULTS

Functional mRNA production

According to the NCBI database [10], four MxA protein-encoding mRNA transcript variants were identified in humans.

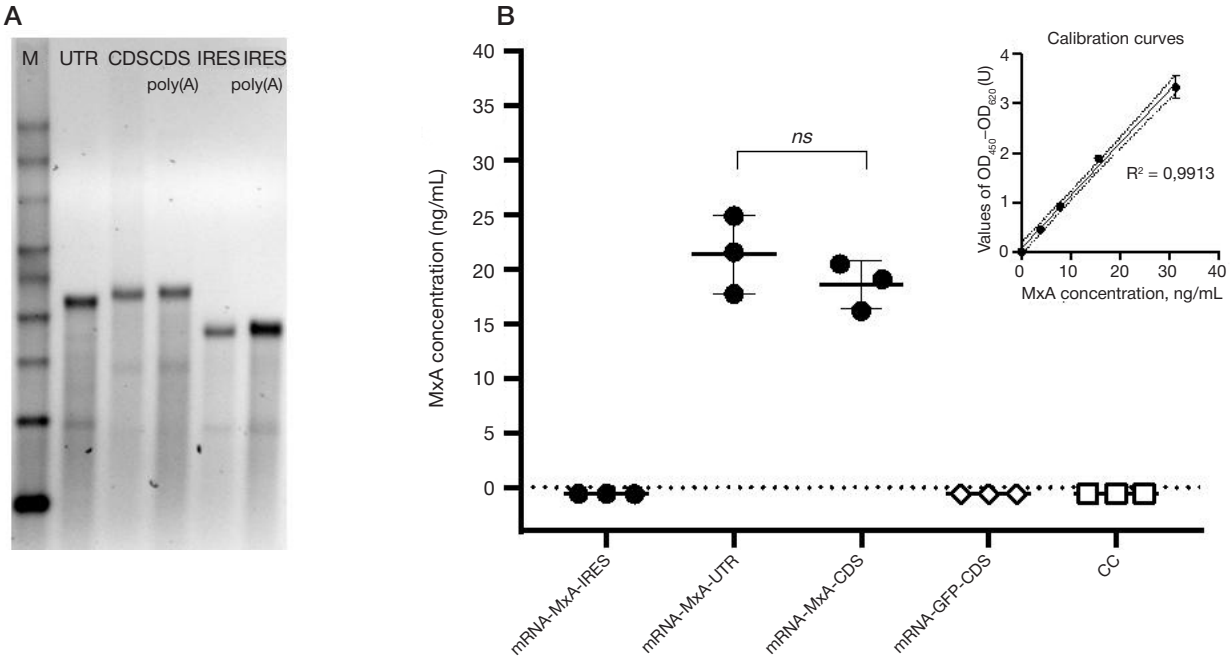

Fig. 2. Human MxA protein-encoding exogenous mRNAs and their translation in the MDCK cells. **A**. Electrophoretic separation of the produced exogenous mRNA products before and after polyadenylation, M — RNA molecular weight marker (#AM1750, Thermo Fisher Scientific; USA), UTR — mRNA-MxA-UTR (initially having the poly(A) tail), CDS and CDS-poly(A) — mRNA-MxA-CDS before and after polyadenylation, IRES and IRES-poly(A) — mRNA-MxA-IRES before and after polyadenylation. **B**. ELISA in the MDCK cells 24 h after transfection with the exogenous mRNAs

Despite the differences in length and 5′ UTR variation, the transcript variants 1, 2 and 3 encode the same MxA protein isoform referred to as isoform a. The transcript variant 4 has an alternative 5′ UTR and does not comprise three exons in the 3′ coding region, which leads to the frameshift, due to which this mRNA encodes the shorter MxA protein isoform (b), also known as varMxA [11]. When designing the constructs encoding mRNA of human MxA gene, primers for specific cloning of the canonical MxA protein form (a) were selected.

The human MxA protein-encoding sequence was obtained from the total RNA preparation (after DNAse treatment) by RT-PCR (Pfu DNA polymerase) using the selected primers. According to the sequencing results (Fig. 1A), the sequence was completely identical to the expected canonical MxA protein form (a), but it had a single reported amino acid variation V379I having no effect on the MxA protein physical and chemical properties [12].

To generate mRNA by the IVT method, three plasmid constructs were proposed (Fig. 1B) comprising the promoter region specific for the phage T7 polymerase as a mandatory component of the cassette. One of the constructs comprised the MxA protein-encoding sequence (mRNA-MxA-CDS) only, while untranslated regions potentially enhancing the effectiveness of translation of the protein encoded by these mRNAs were additionally introduced to the other two. To ensure realization of the cap-independent translation, the second mRNA-MxA-IRES was constructed complemented with the cropped type II IRES element from the encephalomyocarditis virus (EMCV) comprising an A7 bifurcation sequence on the 5′ end [13, 14]. The third mRNA-MxA-UTR comprised additional untranslated regions on the 5′ and 3′ ends, as well as the region ensuring the templated extension of the poly(A) tail during IVT.

All three proposed plasmid constructs were successfully generated and accumulated; the expression cassette sequencing showed that these were completely matched to the expected sequences. Then the plasmids were linearized (the electrophoretic separation results are provided in Fig. 1C) and used as a DNA template for IVT.

The mRNAs we had generated (Fig. 2A) comprised the synthetic cap analog (ARCA), the modified bases pseudouridine (Ψ) and 5-methylcytidine (m5C), which, according to modern literature data, reduce the exogenous transcript immunogenicity [15, 16], as well as the 3’ poly(A) tail. The latter was added in the templated manner (when the cassette was used for mRNA-MxA-UTR) or by conducting a separate polyadenylation reaction (for mRNA-CDS and mRNA-IRES). In addition, we also produced the exogenous mRNA encoding the green fluorescent protein (GFP): mRNA-GFP-CDS containing no untranslated regions, the structure of which was equivalent to that of mRNA-MxA-CDS. The amounts of the resulting MxA protein-encoding mRNAs reached 200 μg, and the concentrations were up to 350 ng/μL.

Assessment of the exogenous mRNA-encoded protein product translation

Translational activity of the exogenous mRNAs produced was assessed by transfection of the MDCK cells. The use of ELISA and the results obtained in a series of experiments showed that mRNA-MxA-IRES was incapable of translation in the studied cell line: when using this mRNA, we failed to detect the MxA protein throughout 36 h after the mRNA introduction into cells. However, the diagnostically significant amounts of human MxA protein were detected in the cell lysates as early as 4 h after transfection of the MDCK cells with two other mRNAs (results not shown).

When using both mRNA-MxA-CDS and mRNA-MxA-UTR, the human MxA protein concentrations were comparable and reached 20 ng/mL 20 h after transfection (Fig. 2B).

Internalization and intracellular localization of human MxA protein encoded by the exogenous mRNAs were studied by confocal microscopy. As shown in Fig. 3, the MxA protein was effectively translated by the MDCK cells 24 h after the mRNA introduction. According to the ELISA results, MxA encoded by both exogenous mRNAs was found exclusively in the cell cytoplasm, it was spread diffusely in the form of the characteristic granules.

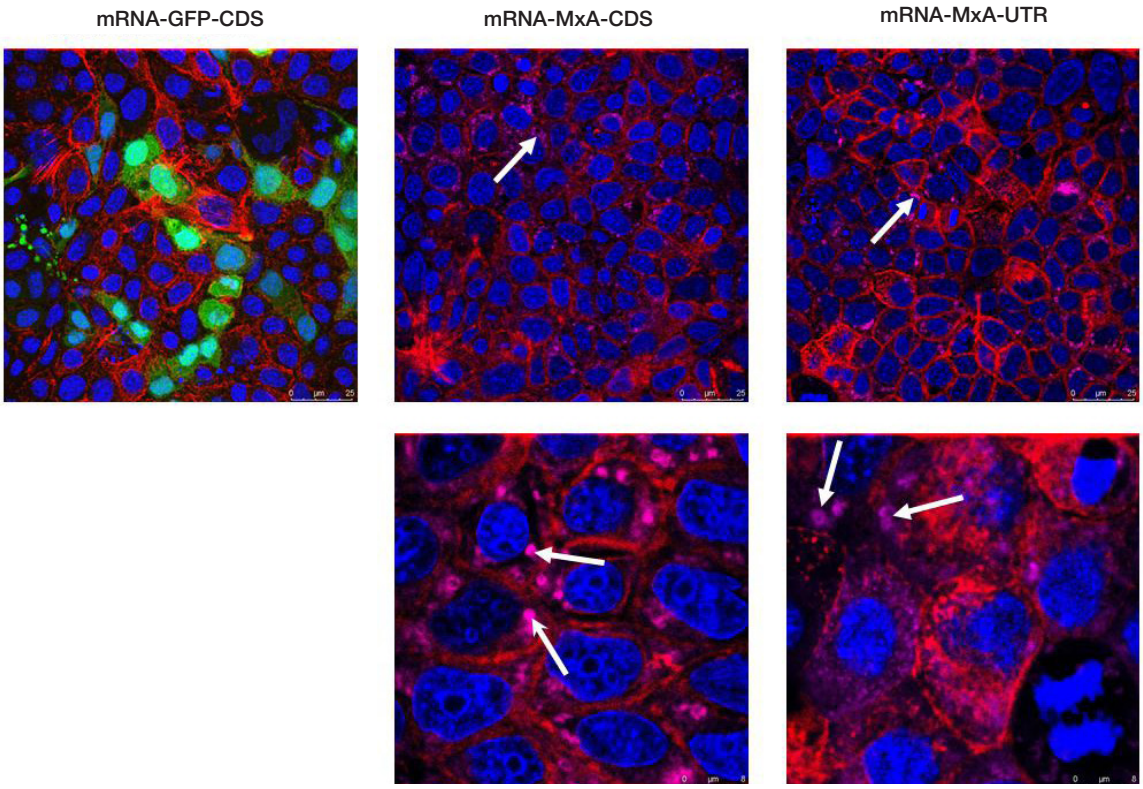

Fig. 3. Confirmation of the MxA production in the MDCK cells by confocal microscopy. Representative images of the MDCK cells (fixed specimens) were obtained 24 h after transfection with the exogenous mRNAs encoding the green fluorescent protein (mRNA-GFP-CDS) and human MxA protein (mRNA-MxA-CDS and mRNA-MxA-UTR), presented from left to right. The cell nuclei are highlighted in *blue* (DAPI, extinction/emission: 358 (UV)/461 nm), the actin cytoskeleton — in *red* (phalloidin: 540/605 nm). MxA is highlighted in *magenta* (620/655 nm); GFP (control cells not transfected with the MxA-encoding mRNA) is highlighted in *green* (488/509 nm). *White* arrows point to the characteristic structures defined as MxA protein

Assessment of the IFN-stimulated gene expression in response to introduction of the exogenous mRNA-MxA-UTR

It is well known that introduction of synthetic exogenous mRNAs can lead to activation of the cytoplasmic RNA sensors and activate the immune response. The MxA protein also can modulate production of the IFN-stimulated genes, as one of the most important effector metabolites of the innate immunity. We assessed specificity of such response 4 h and 24 h after transfection of the A549 cells with mRNA-MxA-UTR using mRNA-GFP-CDS as a non-specific stimulation control (Fig. 4). Thus, 4 h and 24 h after transfection of cells with mRNA-MxA-UTR the detected relative MxA mRNA level was about 6500 times higher compared to the level in the control cells (taken as the unit) (Fig. 4A). It has been also shown that the exogenous mRNA introduction into cells results in the non-specific (not dependent on the exogenous mRNA type) upregulation of OAS1, as well as the cytoplasmic sensor genes MDA5 and RIG-I, which suggests the innate immune response activation. It is interesting that transfection of cells with mRNA-MxA-UTR led to almost 1000-fold decrease in the PKR levels compared to intact cells, while the trend towards a 4-fold increase in activity of this gene was reported for mRNA-GFP-CDS.

DISCUSSION

The protein-encoding exogenous mRNAs represent a promising tool that makes it possible to conduct fundamental research on the patterns of functioning, signaling, and metabolism of proteins in cells and has a huge therapeutic potential. The human MxA protein-encoding mRNA preparations we have constructed and synthesized will be used to assess their antiviral activity against respiratory viruses in the future.

Synthetic mRNAs have the same structure as natural mRNA molecules: 5' cap (more often its structural analog), 5′ and 3′ UTRs flanking the protein-coding region, and poly(A) tail [17, 18].

Of the three proposed mRNAs, we managed to reliably demonstrate stable translation of two constructs, one of which comprised 5′ and 3′ UTRs, and the other one comprised no service regions in addition to the protein-coding part (except for the cap analog and poly(A) tail). Surprisingly, despite the increased effectiveness of the IRES-containing mRNA translation reported in the literature [19], there was no protein synthesis with the mRNA-MxA-IRES we had proposed. In our study, we used the IRES element of EMCV belonging to the Picornaviridae family not using cap during replication. The resulting mRNA construct comprised both cap analog and the IRES element. Presumably, the simultaneous presence pf these two ribosome recognition sites in the close proximity results in blockage of the cap-dependent translation from this transcript.

In the future we nevertheless plan to assess translation of synthetic mRNA-MxA-IRES comprising no cap analog. According to the literature data, despite the fact that the IRES-dependent translation is less effective compared to the cap-dependent translation under normal conditions, the IRES-mediated translation can persist and outperform the translation involving cap under conditions of cellular stress (including heat shock, viral infection, etc.) [20].

It is well known that the 5′ and 3′ UTRs are among key regulators of the mRNA molecule intracellular kinetics. In particular, mRNAs having long 3′ UTRs have a shorter half-life, while mRNAs having short 3′ UTRs are less effectively translated [18]. Comparison of MxA protein levels in the MDCK cells 24 h after transfection with the exogenous mRNAs revealed no

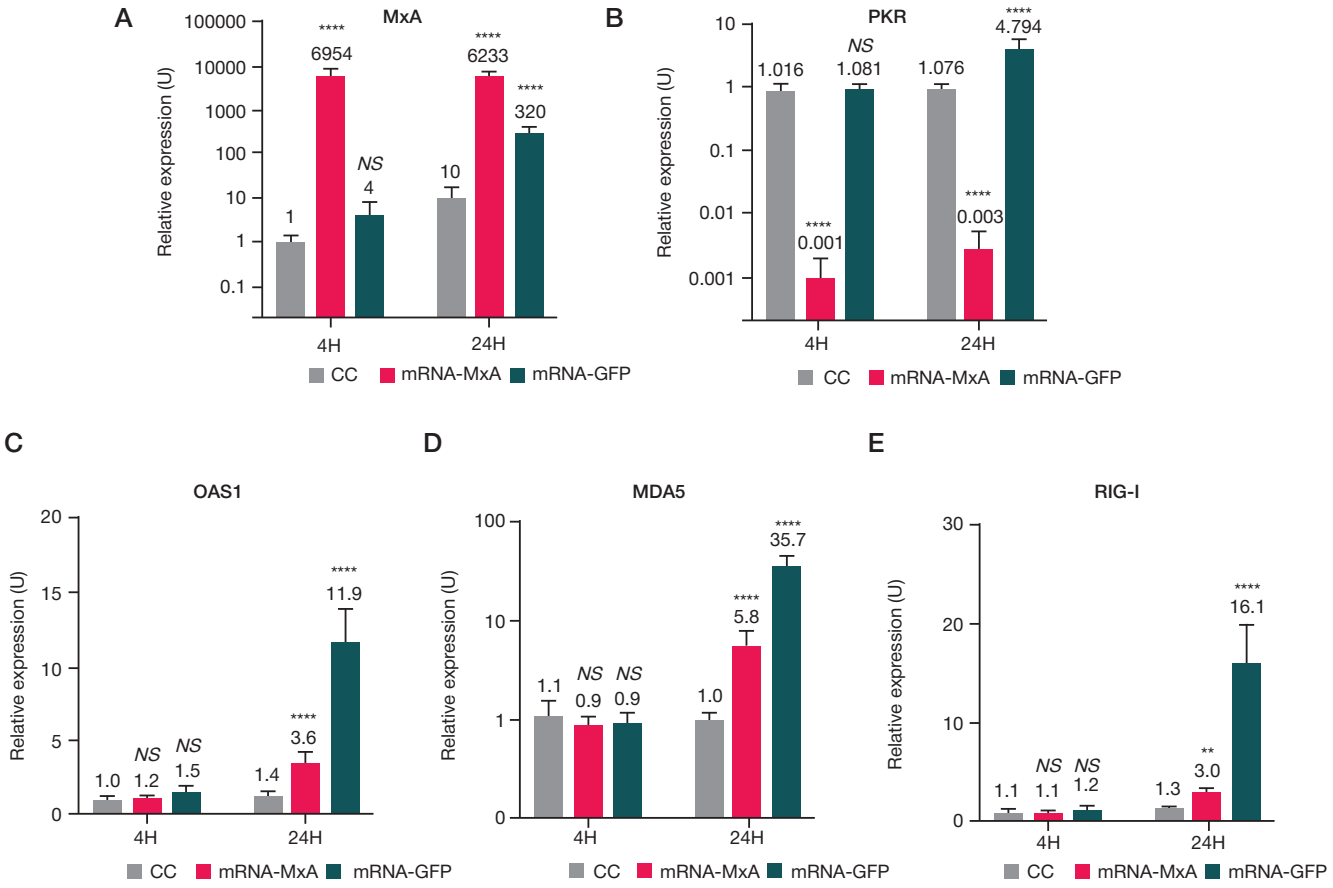

Fig. 4. Expression of the genes MxA, PKR, OAS1, as well as MDA5 and RIG-I in the A549 cells 4 h and 24 h after transfection with mRNA relative to intact cells (CC). The mean expression values (captions on top) for four biological repeats and standard error of the mean as bias are presented as bars. One-way analysis of variance (ANOVA) and the Holm–Sidak test for pairwise comparison of samples were used to calculate statistical significance of the differenced revealed. Significant differences revealed when comparing the appropriate group with the CC at the same time point are marked with *asterisks*: *ns* — $P_{value} < 0.1234$; ** — $P_{value} < 0.0021$; **** — $P_{value} < 0.0001$

advantage in the translation activity resulting from the presence or absence of UTRs in the mRNAs. Both mRNAs capable of translation led to protein production (within 20 ng/mL) 24 h after transfection. Immunofluorescence analysis of the MDCK cells transfected with the exogenous mRNAs showed that these contained the granules, presumably having a ring configuration (visible at maximum magnification), which were diffusely distributed in the cytoplasm. This finding is entirely consistent with the published data on the fact that the MxA homo-oligomerization occurs at physiological salt concentrations in the cell in vivo, and such aggregation prevents degradation and ensures stability of protein with the half-life exceeding 24 h [21]. Our findings suggest that the MxA protein produced will function in the cells like native.

When assessing antiviral potential of the MxA protein translated from the exogenous mRNA, special attention should be paid to the non-specific innate immune response activation resulting from the increased immunogenicity of the mRNA molecule. It is well known that the pattern recognition receptors, such as transmembrane TLR3, 7, 8, 9, and the RIG-I and MDA5 cytoplasmic sensors can recognize foreign nucleic acids and lead to the reciprocal expression of pro-inflammatory cytokines or activation of inflammation [22]. We have shown upregulation of the RIG-I and MDA5 cytoplasmic sensors, as well as the OAS1 IFN-stimulated gene 24 h after transfection of cells with the exogenous mRNAs. The expression patterns of these genes differed in strength and correlated with each other for various exogenous mRNAs. We assume that such alterations result from non-specific immunogenicity of the exogenous mRNA. The GFP-encoding mRNA had the greatest effect on the expression of the studied genes, which can be due to its structure or due to the fact that negative regulation of the expression of these genes associated with the negative feedback loop is possible in case of mRNA-MxA.

It is interesting that transfection of the A549 cells with mRNA-MxA-UTR caused the prolonged (at least up to 24 h) potent specific suppression of PKR at the transcription level as early as after 4 h.

CONCLUSIONS

During the reported study: 1) the MxA protein-encoding mRNAs capable of effective translation in the eukaryotic systems were produced using the plasmid constructs we had designed as a template in the IVT reactions; 2) up to 20 ng/mL of the MxA protein product were accumulated within 24 h after transfection of cells with the exogenous mRNAs; 3) the diffuse intracellular MxA protein distribution in the cells was confirmed; 4) the expression of cytoplasmic sensors and some IFN-stimulated genes in response to introduction of the human MxA protein-encoding exogenous mRNA in the cells was assessed. The authors' further research will be focused on assessing the therapeutic potential of the designed mRNA constructs against influenza A and B viruses, respiratory syncytial virus, and coronavirus SARS-CoV-2. Assessment will primarily involve the cell-based models of infections caused by the above pathogens; if the therapeutic potential is high, we plan to assess antiviral activity of the MxA protein-encoding exogenous mRNAs in the murine model of influenza pneumonia.

References

1. Liao S, Gao S. MxA: a broadly acting effector of interferon-induced human innate immunity. Visualized Cancer Medicine. 2022; 3: 2. Available from: https://doi.org/10.1051/vcm/2022002.
2. Verhelst J, Hulpiau P, Saelens X. Mx proteins: antiviral gatekeepers that restrain the uninvited. Microbiology and Molecular Biology Reviews. 2013; 77 (4): 551–66. Available from: https://doi.org/10.1128/mmbr.00024-13.
3. Haller O, Kochs G. Interferon–induced mx proteins: dynamin–like GTPases with antiviral activity. Traffic. 2002; 3 (10): 710–7. Available from: https://doi.org/10.1034/j.1600-0854.2002.31003.x.
4. Zürcher T, Pavlovic J, Staeheli P. Mechanism of human MxA protein action: variants with changed antiviral properties. The EMBO Journal. 1992; 11 (4): 1657–61. Available from: https://doi.org/10.1002/j.1460-2075.1992.tb05212.x.
5. Johannes L, et al. Antiviral determinants of rat Mx GTPases map to the carboxy-terminal half. Journal of virology. 1997; 71 (12): 9792–5. Available from: https://doi.org/10.1128/jvi.71.12.9792-9795.1997.
6. Jung HE, Oh JE, Lee HK. Cell-penetrating Mx1 enhances anti-viral resistance against mucosal influenza viral infection. Viruses. 2019; 11 (2): 109. Available from: https://doi.org/10.3390/v11020109.
7. Sistigu A, et al. Cancer cell–autonomous contribution of type I interferon signaling to the efficacy of chemotherapy. Nature medicine. 2014; 20 (11): 1301–9. Available from: https://doi.org/10.1038/nm.3708.
8. Kim YA, et al. MxA expression is associated with tumor-infiltrating lymphocytes and is a prognostic factor in triple-negative breast cancer. Breast cancer research and treatment. 2016; 156: 597–606. Available from: https://doi.org/10.1007/s10549-016-3786-z.
9. Klotchenko SA, et al. Comparative analysis of MxA, OAS1, PKR gene expression levels in leukocytes of patients with influenza and coronavirus infection. Medical academic journal. 2023; 23 (3): 65–75. Available from: https://doi.org/10.17816/MAJ623374.
10. Available from: https://www.ncbi.nlm.nih.gov/nuccore/.
11. Noguchi S, et al. MxA transcripts with distinct first exons and modulation of gene expression levels by single-nucleotide polymorphisms in human bronchial epithelial cells. Immunogenetics. 2013; 65: 107–14. Available from: https://doi.org/10.1007/s00251-012-0663-8.
12. Tazi-Ahnini R, et al. Structure and polymorphism of the human gene for the interferon-induced p78 protein (MX1): evidence of association with alopecia areata in the Down syndrome region. Human genetics. 2000; 106: 639–45. Available from: https://doi.org/10.1007/s004390000318.
13. Elroy-Stein O, Fuerst TR, Moss B. Cap-independent translation of mRNA conferred by encephalomyocarditis virus 5'sequence improves the performance of the vaccinia virus/bacteriophage T7 hybrid expression system. Proceedings of the National Academy of Sciences. 1989; 86 16: 6126–30. Available from: https://doi.org/10.1073/pnas.86.16.6126.
14. Bochkov YA, Palmenberg AC. Translational efficiency of EMCV IRES in bicistronic vectors is dependent upon IRES sequence and gene location. Biotechniques. 2006; 41 (3): 283–92. Available from: https://doi.org/10.2144/000112243.
15. Kariko K, Weissman D. Naturally occurring nucleoside modifications suppress the immunostimulatory activity of RNA: implication for therapeutic RNA development. Current Opinion in Drug Discovery and Development. 2007; 10 (5): 523. PMID: 17786850.
16. Karikó K, et al. Incorporation of pseudouridine into mRNA yields superior nonimmunogenic vector with increased translational capacity and biological stability. Molecular therapy. 2008; 16 11: 1833–40. Available from: https://doi.org/10.1038/mt.2008.200.
17. Weissman D. mRNA transcript therapy. Expert review of vaccines. 2015; 14 (2): 265–81. Available from: https://doi.org/10.1586/14760584.2015.973859.
18. von Niessen AGO, et al. Improving mRNA-based therapeutic gene delivery by expression-augmenting 3′ UTRs identified by cellular library screening. Molecular Therapy. 2019; 27 (4): 824–36. Available from: https://doi.org/10.1016/j.ymthe.2018.12.011.
19. Xue S, et al. RNA regulons in Hox 5′ UTRs confer ribosome specificity to gene regulation. Nature. 2015; 517 (7532): 33–38. Available from: https://doi.org/10.1038/nature14010.
20. Koch A, et al. Quantifying the dynamics of IRES and cap translation with single-molecule resolution in live cells. Nature structural & molecular biology. 2020; 27 (12): 1095–104. Available from: https://doi.org/10.1038/s41594-020-0504-7.
21. Haller O, Kochs G. Mx genes: host determinants controlling influenza virus infection and trans-species transmission. Human genetics. 2020; 139 (6): 695–705. Available from: https://doi.org/10.1007/s00439-019-02092-8.
22. Kawai T, Akira S. The role of pattern-recognition receptors in innate immunity: update on Toll-like receptors. Nature immunology. 2010; 11 (5): 373–84. Available from: https://doi.org/10.1038/ni.1863.

Литература

1. Liao S, Gao S. MxA: a broadly acting effector of interferon-induced human innate immunity. Visualized Cancer Medicine. 2022; 3: 2. Available from: https://doi.org/10.1051/vcm/2022002.
2. Verhelst J, Hulpiau P, Saelens X. Mx proteins: antiviral gatekeepers that restrain the uninvited. Microbiology and Molecular Biology Reviews. 2013; 77 (4): 551–66. Available from: https://doi.org/10.1128/mmbr.00024-13.
3. Haller O, Kochs G. Interferon–induced mx proteins: dynamin–like GTPases with antiviral activity. Traffic. 2002; 3 (10): 710–7. Available from: https://doi.org/10.1034/j.1600-0854.2002.31003.x.
4. Zürcher T, Pavlovic J, Staeheli P. Mechanism of human MxA protein action: variants with changed antiviral properties. The EMBO Journal. 1992; 11 (4): 1657–61. Available from: https://doi.org/10.1002/j.1460-2075.1992.tb05212.x.
5. Johannes L, et al. Antiviral determinants of rat Mx GTPases map to the carboxy-terminal half. Journal of virology. 1997; 71 (12): 9792–5. Available from: https://doi.org/10.1128/jvi.71.12.9792-9795.1997.
6. Jung HE, Oh JE, Lee HK. Cell-penetrating Mx1 enhances anti-viral resistance against mucosal influenza viral infection. Viruses. 2019; 11 (2): 109. Available from: https://doi.org/10.3390/v11020109.
7. Sistigu A, et al. Cancer cell–autonomous contribution of type I interferon signaling to the efficacy of chemotherapy. Nature medicine. 2014; 20 (11): 1301–9. Available from: https://doi.org/10.1038/nm.3708.
8. Kim YA, et al. MxA expression is associated with tumor-infiltrating lymphocytes and is a prognostic factor in triple-negative breast cancer. Breast cancer research and treatment. 2016; 156: 597–606. Available from: https://doi.org/10.1007/s10549-016-3786-z.
9. Klotchenko SA, et al. Comparative analysis of MxA, OAS1, PKR gene expression levels in leukocytes of patients with influenza and coronavirus infection. Medical academic journal. 2023; 23 (3): 65–75. Available from: https://doi.org/10.17816/MAJ623374.
10. База данных NCBI, доступно по ссылке: https://www.ncbi.nlm.nih.gov/nuccore/.
11. Noguchi S, et al. MxA transcripts with distinct first exons and modulation of gene expression levels by single-nucleotide polymorphisms in human bronchial epithelial cells. Immunogenetics. 2013; 65: 107–14. Available from: https://doi.org/10.1007/s00251-012-0663-8.
12. Tazi-Ahnini R, et al. Structure and polymorphism of the human gene for the interferon-induced p78 protein (MX1): evidence of association with alopecia areata in the Down syndrome region. Human genetics. 2000; 106: 639–45. Available from: https://doi.org/10.1007/s004390000318.
13. Elroy-Stein O, Fuerst TR, Moss B. Cap-independent translation of mRNA conferred by encephalomyocarditis virus 5'sequence improves the performance of the vaccinia virus/bacteriophage T7 hybrid expression system. Proceedings of the National Academy of Sciences. 1989; 86 16: 6126–30. Available from: https://doi.org/10.1073/pnas.86.16.6126.
14. Bochkov YA, Palmenberg AC. Translational efficiency of EMCV IRES in bicistronic vectors is dependent upon IRES sequence and gene location. Biotechniques. 2006; 41 (3): 283–92. Available from: https://doi.org/10.2144/000112243.

15. Kariko K, Weissman D. Naturally occurring nucleoside modifications suppress the immunostimulatory activity of RNA: implication for therapeutic RNA development. Current Opinion in Drug Discovery and Development. 2007; 10 (5): 523. PMID: 17786850.
16. Karikó K, et al. Incorporation of pseudouridine into mRNA yields superior nonimmunogenic vector with increased translational capacity and biological stability. Molecular therapy. 2008; 16 11: 1833–40. Available from: https://doi.org/10.1038/mt.2008.200.
17. Weissman D. mRNA transcript therapy. Expert review of vaccines. 2015; 14 (2): 265–81. Available from: https://doi.org/10.1586/14760584.2015.973859.
18. von Niessen AGO, et al. Improving mRNA-based therapeutic gene delivery by expression-augmenting 3′ UTRs identified by cellular library screening. Molecular Therapy. 2019; 27 (4): 824–36. Available from: https://doi.org/10.1016/j.ymthe.2018.12.011.
19. Xue S, et al. RNA regulons in Hox 5′ UTRs confer ribosome specificity to gene regulation. Nature. 2015; 517 (7532): 33–38. Available from: https://doi.org/10.1038/nature14010.
20. Koch A, et al. Quantifying the dynamics of IRES and cap translation with single-molecule resolution in live cells. Nature structural & molecular biology. 2020; 27 (12): 1095–104. Available from: https://doi.org/10.1038/s41594-020-0504-7.
21. Haller O, Kochs G. Mx genes: host determinants controlling influenza virus infection and trans-species transmission. Human genetics. 2020; 139 (6): 695–705. Available from: https://doi.org/10.1007/s00439-019-02092-8.
22. Kawai T, Akira S. The role of pattern-recognition receptors in innate immunity: update on Toll-like receptors. Nature immunology. 2010; 11 (5): 373–84. Available from: https://doi.org/10.1038/ni.1863.

CHANGES IN BACTERIAL FITNESS DURING THE *PSEUDOMONAS AERUGINOSA* EXPERIMENTAL ADAPTATION TO COLISTIN

Mayanskiy NA, Brzhozovskaya EA ✉, Skvortsov-Igralov GA, Chausova SV, Chebotar IV

Pirogov Russian National Research Medical University, Moscow, Russia

Pseudomonas aeruginosa, the opportunistic pathogen, occupies one of the leading places in the structure of pathogens causing nosocomial infections, which is due to high adaptive potential and the ability to quickly develop antimicrobial resistance. The study aimed to assess the influence of the *P. aeruginosa* adaptation to colistin on bacterial fitness. A total of nine isolates obtained during the experimental evolution of the *P. aeruginosa* strain (laboratory number 1202) under conditions of increasing colistin concentrations, the growth kinetics of which was compared to that of wild type strain, were included in the study; the whole genome sequencing of all isolates was performed, and the minimum inhibitory concentration of colistin was determined. Growth rate was estimated using the Varioskan LUX multimodal reader (Thermo Scientific, USA) throughout 18 h at 37 °C; optical density (OD) at λ = 600 nm was measured every 15 min. The maximum growth rate (GR_{max}, i.e. the maximum change in OD within 1h) and the time to reach 50% of the maximum OD reported when growing the wild type *Pa_1202_0* strain ($T\_OD_{50\%}$) were considered. Isolates of the clone carrying mutations of the genes *phoQ*, *lptA*, and *prs* showed low fitness values compared to wild type strains. For example, GR_{max} of the isolate *Pa_1202_43* was 0.029 OD/h vs. 0.182 OD/h reported for the original isolate *Pa_1202_0*, and it reached $OD_{50\%}$ 4.6 h later. The growth characteristics of the clone carrying mutations of *lpxL* and *lptB*, as well as the clone carrying mutant *pmrB* were generally comparable with the characteristics of the wild type strain. Thus, the genome modifications observed during the *P. aeruginosa* adaptation to colistin have an ambiguous effect on bacterial fitness.

Keywords: *Pseudomonas aeruginosa*, nosocomial infections, bacterial fitness, colistin, resistance genes

Funding: the study was supported by the Russian Science Foundation grant (project No. 20-15-00235).

Author contribution: Mayanskiy NA — concept, data analysis, manuscript editing; Brzhozovskaya EA — methodology, manuscript preparation and writing; Skvortsov-Igralov GA — formal analysis of experimental data; Chausova SV — data validation; Chebotar IV — methodology, concept, data validation.

✉ **Correspondence should be addressed:** Ekaterina A. Brzhozovskaya
Leninsky prospect, 117/1, Moscow, 119571; emmbf@yandex.ru

Received: 22.08.2024 **Accepted:** 29.09.2024 **Published online:** 19.10.2024

DOI: 10.24075/brsmu.2024.042

ИЗМЕНЕНИЕ БАКТЕРИАЛЬНОГО ФИТНЕСА В ХОДЕ ЭКСПЕРИМЕНТАЛЬНОЙ АДАПТАЦИИ *PSEUDOMONAS AERUGINOSA* К КОЛИСТИНУ

Н. А. Маянский, Е. А. Бржозовская ✉, Г. А. Скворцов-Игралов, С. В. Чаусова, И. В. Чеботарь

Российский национальный исследовательский медицинский университет имени Н. И. Пирогова

Оппортунистический патоген *Pseudomonas aeruginosa* занимает одно из ведущих мест в структуре возбудителей нозокомиальных инфекций, что связано с высоким адаптивным потенциалом и способностью быстро формировать устойчивость к антимикробным препаратам. Целью работы было оценить влияние адаптации *P. aeruginosa* к колистину на бактериальный фитнес. В исследование включили 9 изолятов, полученных в ходе экспериментальной эволюции штамма *P. aeruginosa* (лабораторный номер 1202) в условиях возрастающей концентрации колистина, кинетику роста которых сравнивали с родительским штаммом; у всех изолятов провели полногеномное секвенирование и определили минимальную подавляющую концентрацию колистина. Темпы роста оценивали при помощи многофункционального ридера Varioskan LUX (Thermo Scientific, США) в течение 18 ч при 37 °C, каждые 15 мин измеряя оптическую плотность (ОП) при λ = 600 нм. Учитывали максимальную скорость роста ($СР_{max,}$ т. е. максимальное изменение ОП в течение 1 ч) и время, необходимое для достижения 50% от максимальной ОП, зарегистрированной при росте родительского штамма *Pa_1202_0* (Т_ОП50%). Изоляты клона с мутациями в генах *phoQ*, *lptA* и *prs* отличались низкими показателями фитнеса от родительских штаммов. Например, $СР_{max}$ изолята *Pa_1202_43* составила 0,029 ОП/ч против 0,182 ОП/ч у исходного изолята *Pa_1202_0*, а $ОП_{50\%}$ он достигал на 4,6 ч позже. Ростовые характеристики клона с мутациями в *lpxL* и *lptB*, а также клона, несущего мутированный *pmrB*, в целом были сопоставимы с показателями родительского штамма. Таким образом, модификации генома, наблюдавшиеся в ходе адаптации *P. aeruginosa* к колистину, оказывают неоднозначное влияние на бактериальный фитнес.

Ключевые слова: синегнойная палочка, нозокомиальные инфекции, бактериальный фитнес, колистин, гены резистентности

Финансирование: работа выполнена при поддержке гранта Российского научного фонда (проект № 20-15-00235).

Вклад авторов: Н. А. Маянский — концептуализация, анализ данных, редактирование рукописи; Е. А. Бржозовская — методология, подготовка и написание рукописи; Г. А. Скворцов-Игралов — формальный анализ экспериментальных данных; С. В. Чаусова — валидация данных; И. В Чеботарь — методология, концептуализация, валидация данных.

✉ **Для корреспонденции:** Екатерина Анатольевна Бржозовская
Ленинский проспект, д. 117/1, г. Москва, 119571; emmbf@yandex.ru

Статья получена: 22.08.2024 **Статья принята к печати:** 29.09.2024 **Опубликована онлайн:** 19.10.2024

DOI: 10.24075/vrgmu.2024.042

Pseudomonas aeruginosa is an important opportunistic pathogen, the successful survival of which in clinical settings results from high adaptive potential. Quick adaptation to new ecological loci, antimicrobial drugs, and the immune system effectors allows *P. aeruginosa* to be one of the main causes of nosocomial morbidity [1]. The infections caused by multidrug-resistant *P. aeruginosa* strains are difficult to treat, and only a few antimicrobial drugs remain active against such pathogens. Colistin, the polymyxin antibiotic, is one of the “last chance” antibiotics [2].

The increasing clinical use of colistin inevitably leads to colistin resistance. Resistance to colistin is associated with the structural modification of its target, lipopolysaccharide (LPS), which decreases the antibiotic binding to the bacterial cell wall [3]. LPS modification and colistin resistance in *P. aeruginosa* are usually associated with damage to the

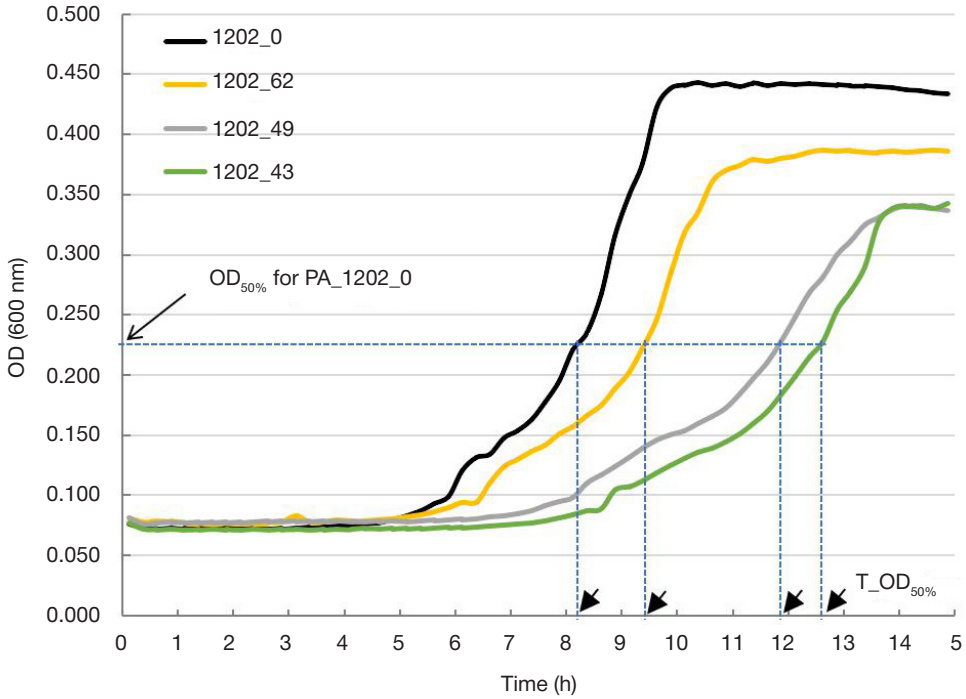

Fig. Growth curves of the wild type *Pa_1202_0* strain and descendants strains of the clone *Pa_phoQ/lptA/prs*. Bacteria were incubated in the 96-well plate at 37 °C, and optical density (OD) at λ = 600 nm was measured every 15 min. The *long open arrow* points to the OD value corresponding to 50% of the maximum OD reported when growing the wild type *Pa_1202_0* strain ($OD_{50\%}$). The *short closed arrows* point to the time needed by the studied isolates to reach $OD_{50\%}$ ($T\_OD_{50\%}$). The isolate characteristics are provided in the Table. Representative results of one of three repetitions of the experiment

PhoP-PhoQ and PmrA-PmrB two-component systems resulting from mutations of appropriate genes, although are not limited to these mechanisms [3, 4]. Mutations that form resistance are advantageous for carriers of mutations in the presence of antibiotic. However, the same mutations can reduce viability of microorganism as a whole, making it uncompetitive in the absence of antibiotic. Mutations that trigger alternative metabolic pathways in the cell and replace missing metabolism links can compensate for biological expenditures associated with resistance [5–7]. In this regard, assessment of bacterial fitness, i.e. viability level that can be inter alia expressed as the bacterial population growth rate changes [8], is an important complement to genetic analysis of the resistance mechanisms.

In the recent study focused on the *P. aeruginosa* experimental adaptation to colistin, we have shown that the genome evolved by alternative routes not only in different strains, but also within the same bacterial strain when developing colistin resistance [9]. Isolates of one experimental *P. aeruginosa* strain obtained at various stages of adaptation to colistin and analyzed by whole genome sequencing were used in this study. Isolates with various mutations were selected for the study, in which the growth kinetics was assessed and compared with that of the parent strain. The study aimed to investigate the relationship between genotypic and phenotypic characteristics in the experimental models, which highlights the importance of genetic background for the development of antimicrobial resistance, makes it possible to gain new knowledge about the mechanisms underlying antibiotic resistance, and outline new ways to overcome drug resistance of bacteria.

METHODS

We studied the *P. aeruginosa* strain (laboratory number 1202, genome deposited in GenBank) isolated from the environment in 2016 that was susceptible to all antibiotics and its *Pa_1202*-descendants isolates obtained during experimental adaptation to colistin, the methodology of which had been earlier discussed in detail [9].

To estimate bacterial fitness, we compared growth rates of the wild type and descendants *Pa_1202* strains obtained in the adaptive experiment. A single colony of the 24-h culture of each isolate was used to prepare a bacterial suspension, which was standardized by optical density to 0.5 McFarland units. A total of 10 mL of the Luria–Bertani broth were inoculated with 10 µL of the resulting suspension, after which 200 µL were collected and transferred to the well of the flat-bottom 96-well plate. The plate was sealed with the transparent film and incubated in the Varioskan LUX multimodal reader (Thermo Scientific, USA) for 18 h at 37 °C; optical density (OD) at λ = 600 nm was measured every 15 min. Growth curves were analyzed using the SkanIt v. 7.0 software tool (Thermo Scientific; USA). Growth rate was estimated based on two indicators: 1) maximum growth rate (GRmax, corresponds to the maximum change in OD within 1h measured in OD/h); 2) time to reach 50% of the maximum OD reported when growing the wild type *Pa_1202_0* strain ($T\_OD_{50\%}$) (Fig). The decrease in GRmax and the increase in $T\_OD_{50\%}$ were considered as the fitness decrease. The experiment was carried out in triplicate.

The minimum inhibitory concentration (MIC) of colistin within the range of 0.25–16 mg/L was determined using the ComASP Colistin 0.25–16 kits (Liofilchem srl.; Italy), while higher MICs (up to 64 mg/L) were estimated by the broth microdilution method. The MIC values were interpreted based on their experimental dynamics, not clinical significance.

The whole genome sequencing was performed using the bacterial DNA extracted from the 24-h cultures of the experimental *Pa_1202* isolates grown from frozen samples (see above) on the Mueller–Hinton agar. The whole genome sequencing and bioinformatics analysis procedure has been earlier discussed in detail [9].

Statistical analysis was performed using the IBM SPSS Statistics v. 27.0 software (USA). The quantitative results are presented in the text and the Table as mean values (standard deviations). The Mann–Whitney U test was used to compare the GR_{max} and $T\_OD_{50\%}$ values; the differences were considered significant at $p < 0.05$.

Table. Phenotype and genotype of the isolates obtained during experimental adaptation to colistin

Isolate	Day	MIC of colistin (mg/L)	GR_{max} (OD/h)	$T\_OD_{50\%}$ (h)	*phoQ*	*pmrB*	*lpxL*	*lptA*	*lptB*	*prs*	*speE*	*hp/PA2117*	*tetC*	*oprH*
			Mean (SD)											
1202_0	0	1	0.182 (0.018)	8.8 (0.1)										
Clone *Pa_phoQ/lptA/prs*														
1202_43	11	32	0.029 (0.001) *	13.4 (0.2) *										
1202_49	13	1	0.038 (0.009) *	12.7 (0.2) *										
1202_62	16	2	0.140 (0.012)	10.0 (0.1) *										
Clone *Pa_phoQ/lpxL/lptB*														
1202_63	16	16	0.285 (0.015) *	8.9 (0.0)										
1202_80	20	2	0.268 (0.059)	9.0 (0.1)										
1202_95	28	16	0.163 (0.016) *	9.2 (0.1)										
Clone *Pa_pmrB*														
1202_37	9	1	0.155 (0.016)	8.9 (0.0)										
1202_44	11	2	0.219 (0.029)	9.0 (0.1)										
1202_88	24	16	0.198 (0.026)	7.9 (0.1) *										

Note: 10 *Pa_1202* isolates were obtained on the specified days of the experiment [9]. We determined the minimum inhibitory concentration (MIC) of colistin and assessed fitness by analysis of the growth curves and measurement of the maximum growth rate (GR_{max}) and the time to reach 50% of the maximum optical density (OD) reported when growing the wild type *Pa_1202_0* strain ($T\_OD_{50\%}$) (see Fig). Genes of the core genome were studied using whole genome sequencing. *Green* cells correspond to the gene sequences identical to *Pa_1202_0*, mutations are highlighted in *red*. Names of the genes involved in lipopolysaccharide synthesis and associated with colistin resistance are highlighted in *orange*; names of the genes of general metabolism not directly associated with colistin resistance are uncolored. SD — standard deviation. * — $p < 0.05$, comparison with *Pa_1202_0*.

RESULTS

Growth rates of the wild type *Pa_1202_0* strain and nine *Pa_1202* isolates representing three earlier described major clonal lineages obtained during experimental adaptation to colistin were assessed [9] (Table). Two clones carried the same mutation of *phoQ* (ins-ATCGCCT-1086), but were distinguished by mutations of other genes. In one case further damage was found in the genes *lptA* (ins-CCGCGC-490) and *prs* (T143→C), the clone was named *Pa_phoQ/lptA/prs*. In another case the *lpxL* (ins-C-335) and *lptB* (ins-GCG-27) genes were altered, the clone was named *Pa_phoQ/lpxL/lptB*. The third clone was characterized by mutation of the gene *pmrB* (T92→G) (the clone was named *Pa_pmrB*) combined with the damaged gene *hp/PA2117* (G326→A).

Isolates of the clone *Pa_phoQ/lptA/prs* showed low fitness compared to the wild type *Pa_1202_0* strain (Fig, Table). For example, GR_{max} of the isolate 1202_43 was 0.029 (0.001) OD/h vs. 0.182 (0.018) OD/h reported for the original *Pa_1202_0* isolate, and it reached $OD_{50\%}$ 4.6 h later.

The growth characteristics of the clones *Pa_ lpxL/lptB* and *Pa_pmrB* were generally comparable with the characteristics of the wild type *Pa_1202_0* strain (Table). Two isolates showed a significant increase in GR_{max} (1202_63) and a significant decrease in $T\_OD_{50\%}$ (1202_88), which suggested better growth rate compared to the wild type strain, despite the 16-fold increase in the colistin MIC (Table). Isolate 1202_95 of the clone *Pa_pmrB* showed a significantly decreased GR_{max}, however, the difference in $T\_OD_{50\%}$ from the original strain was non-significant.

DISCUSSION

In this study we have shown how the *P. aeruginosa* experimental adaptation affects bacterial fitness by assessing growth kinetics of the isolates with various genotypes. It is the most logical choice to explain the differences in fitness between representatives of three studied clones via analysis of the profiles of the genomic alterations typical for each clone. The genomes of isolates of the clone *Pa_phoQ/lptA/prs* comprise alterations of two types: 1) mutations of the genes *phoQ* and *lptA* that directly control biosynthesis of LPS, the main target of polymyxins [10, 11]; 2) mutations of the gene encoding ribose-phosphate pyrophosphokinase (prs) that is not directly associated with the LPS synthesis and controls the nucleotide synthesis and metabolism. PhoP, the component of the PhoPQ regulatory system, is directly involved in the LPS synthesis regulation, and its breakage is considered to be the common cause of colistin resistance [10]. The *lptA* gene product ensures the LPS assembly and outer membrane translocation [11]. In the clone *Pa_phoQ/lptA/prs*, the complex genomic alterations were combined with the most pronounced bacterial fitness decrease.

In the clone *Pa_phoQ/lpxL/lptB*, we found only mutations of the LPS synthesis genes, including the abovementioned *phoQ*, *lpxL* (gene encoding lauroyl acyltransferase ensuring the lipid A biosynthesis), and *lptB* (gene encoding the LptB2FG transporter transferring LPS to the outer membrane) [12, 13].

The *Pa_pmrB* clone combined mutations of the genes encoding the sensor kinase (pmrB) and the hypothetic protein (*hp/PA2117*). The PmrB kinase is a component of the two-component system ensuring regulation of multiple functions, including expression of the LPS operon genes; earlier it had been proven that damage to the *pmrB* gene decreases the *P. aeruginosa* susceptibility to polymyxins [14, 15]. To date, the *hp/PA2117* gene product has not been verified.

CONCLUSIONS

Thus, the genome modifications observed during the *P. aeruginosa* adaptation to colistin have an ambiguous effect on bacterial fitness. It is clear that the combination of mutations of the LPS synthesis genes and genes of general metabolism has the most severe effect on bacterial fitness, as reported for the clone *Pa_phoQ/lptA/prs*. Further study of the interplay between genotype and phenotype via experimental modeling will improve understanding of the mechanisms underlying adaptation of bacteria to environmental factors, including the development of antibiotic resistance, and outline new ways to overcome bacterial resistance to drugs.

References

1. Algammal A, Hetta HF, Mabrok M, Behzadi P. Editorial: Emerging multidrug-resistant bacterial pathogens "superbugs": A rising public health threat. Front Microbiol. 2023; 14: 1135614. DOI: 10.3389/fmicb.2023.1135614. PMID: 36819057; PMCID: PMC9930894.
2. Andrade FF, Silva D, Rodrigues A, Pina-Vaz C. Colistin Update on Its Mechanism of Action and Resistance, Present and Future Challenges. Microorganisms. 2020; 8 (11): 1716. DOI: 10.3390/microorganisms8111716. PMID: 33147701; PMCID: PMC7692639.
3. Shahzad S, Willcox MDP, Rayamajhee B. A Review of Resistance to Polymyxins and Evolving Mobile Colistin Resistance Gene mcr among Pathogens of Clinical Significance. Antibiotics (Basel). 2023; 12 (11): 1597. DOI: 10.3390/antibiotics12111597. PMID: 37998799; PMCID: PMC10668746.
4. Yang B, Liu C, Pan X, Fu W, Fan Z, Jin Y, et al. Identification of Novel PhoP-PhoQ Regulated Genes That Contribute to Polymyxin B Tolerance in Pseudomonas aeruginosa. Microorganisms. 2021; 9 (2): 344. DOI: 10.3390/microorganisms9020344. PMID: 33572426; PMCID: PMC7916210.
5. Chebotar IV, Kuleshov KV. Mezhdu antibiotikorezistentnost'ju i virulentnost'ju: dialektika bakterial'nogo fitnesa. Klinicheskaja mikrobiologija i antimikrobnaja himioterapija. 2024; 26 (1): 59-66. https://doi.org/10.36488/cmac.2024.1.59-66. Russian.
6. Olivares Pacheco J, Alvarez-Ortega C, Alcalde Rico M, Martínez JL. Metabolic Compensation of Fitness Costs Is a General Outcome for Antibiotic-Resistant Pseudomonas aeruginosa Mutants Overexpressing Efflux Pumps. mBio. 2017; 8 (4): e00500-17. DOI: 10.1128/mBio.00500-17. PMID: 28743808; PMCID: PMC5527304.
7. Sendra E, Fernández-Muñoz A, Zamorano L, Oliver A, Horcajada JP, Juan C, Gómez-Zorrilla S. Impact of multidrug resistance on the virulence and fitness of Pseudomonas aeruginosa: a microbiological and clinical perspective. Infection. 2024. DOI: 10.1007/s15010-024-02313-x. Epub ahead of print. PMID:38954392.
8. Shamina OV, Kryzhanovskaja OA, Lazareva AV, Aljabeva NM, Mayanskiy NA. Ustojchivost' karbapenemrezistentnyh shtammov Klebsiella pneumoniae k kolistinu: molekuljarnye mehanizmy i bakterial'nyj fitnes. Vestnik RGMU. 2020; 3: 11–18. DOI: 10.24075/vrgmu.2020.032. Russian.
9. Chebotar I, Savinova T, Bocharova J, Korostin D, Evseev P, Mayanskiy N. Genetic Alternatives for Experimental Adaptation to Colistin in Three Pseudomonas aeruginosa Lineages. Antibiotics. 2024; 13: 452. Available from: https://doi.org/10.3390/antibiotics13050452.
10. Miller AK, Brannon MK, Stevens L, Johansen HK, Selgrade SE, Miller SI, et al. PhoQ mutations promote lipid A modification and polymyxin resistance of Pseudomonas aeruginosa found in colistin-treated cystic fibrosis patients. Antimicrob Agents Chemother. 2011; 55 (12): 5761–9. DOI: 10.1128/AAC.05391-11. Epub 2011 Oct 3. PMID: 21968359; PMCID: PMC3232818.
11. Shapiro AB, Gu RF, Gao N. Dimerization of isolated Pseudomonas aeruginosa lipopolysaccharide transporter component LptA. Biochem Biophys Res Commun. 2014; 450 (4): 1327–32. DOI: 10.1016/j.bbrc.2014.06.138. Epub 2014 Jul 5. PMID: 25003324.
12. Dovala D, Rath CM, Hu Q, Sawyer WS, Shia S, Elling RA, et al. Structure-guided enzymology of the lipid A acyltransferase LpxM reveals a dual activity mechanism. Proc Natl Acad Sci U S A. 2016; 113 (41): E6064-E6071. DOI: 10.1073/pnas.1610746113. Epub 2016 Sep 28. PMID: 27681620; PMCID: PMC5068295.
13. Luo Q, Yang X, Yu S, Shi H, Wang K, Xiao L, et al. Structural basis for lipopolysaccharide extraction by ABC transporter LptB₂FG. Nat Struct Mol Biol. 2017; 24 (5): 469-474. DOI: 10.1038/nsmb.3399.
14. Moskowitz SM, Brannon MK, Dasgupta N, Pier M, Sgambati N, Miller AK, et al. PmrB mutations promote polymyxin resistance of Pseudomonas aeruginosa isolated from colistin-treated cystic fibrosis patients. Antimicrob Agents Chemother. 2012; 56 (2): 1019–30. DOI: 10.1128/AAC.05829-11. Epub 2011 Nov 21. PMID: 22106224; PMCID: PMC3264203.
15. Disney-McKeethen S, Seo S, Mehta H, Ghosh K, Shamoo Y. Experimental evolution of Pseudomonas aeruginosa to colistin in spatially confined microdroplets identifies evolutionary trajectories consistent with adaptation in microaerobic lung environments. mBio. 2023; 14 (6): e0150623. DOI: 10.1128/mbio.01506-23.

Литература

1. Algammal A, Hetta HF, Mabrok M, Behzadi P. Editorial: Emerging multidrug-resistant bacterial pathogens "superbugs": A rising public health threat. Front Microbiol. 2023; 14: 1135614. DOI: 10.3389/fmicb.2023.1135614. PMID: 36819057; PMCID: PMC9930894.
2. Andrade FF, Silva D, Rodrigues A, Pina-Vaz C. Colistin Update on Its Mechanism of Action and Resistance, Present and Future Challenges. Microorganisms. 2020; 8 (11): 1716. DOI: 10.3390/microorganisms8111716. PMID: 33147701; PMCID: PMC7692639.
3. Shahzad S, Willcox MDP, Rayamajhee B. A Review of Resistance to Polymyxins and Evolving Mobile Colistin Resistance Gene mcr among Pathogens of Clinical Significance. Antibiotics (Basel). 2023; 12 (11): 1597. DOI: 10.3390/antibiotics12111597. PMID: 37998799; PMCID: PMC10668746.
4. Yang B, Liu C, Pan X, Fu W, Fan Z, Jin Y, et al. Identification of Novel PhoP-PhoQ Regulated Genes That Contribute to Polymyxin B Tolerance in Pseudomonas aeruginosa. Microorganisms. 2021; 9 (2): 344. DOI: 10.3390/microorganisms9020344. PMID: 33572426; PMCID: PMC7916210.
5. Чеботарь И. В., Кулешов К. В. Между антибиотикорезистентностью и вирулентностью: диалектика бактериального фитнеса. Клиническая микробиология и антимикробная химиотерапия. 2024; 26 (1): 59-66. https://doi.org/10.36488/cmac.2024.1.59-66.
6. Olivares Pacheco J, Alvarez-Ortega C, Alcalde Rico M, Martínez JL. Metabolic Compensation of Fitness Costs Is a General Outcome for Antibiotic-Resistant Pseudomonas aeruginosa Mutants Overexpressing Efflux Pumps. mBio. 2017; 8 (4): e00500-17. DOI: 10.1128/mBio.00500-17. PMID: 28743808; PMCID: PMC5527304.
7. Sendra E, Fernández-Muñoz A, Zamorano L, Oliver A, Horcajada JP, Juan C, Gómez-Zorrilla S. Impact of multidrug resistance on the virulence and fitness of Pseudomonas aeruginosa: a microbiological and clinical perspective. Infection. 2024. DOI: 10.1007/s15010-024-02313-x. Epub ahead of print. PMID:38954392.
8. Шамина О. В., Крыжановская О. А., Лазарева А. В., Алябьева Н. М., Маянский Н. А. Устойчивость карбапенемрезистентных штаммов Klebsiella pneumoniae к колистину: молекулярные механизмы и бактериальный фитнес. Вестник РГМУ. 2020; 3: 11–18. DOI: 10.24075/vrgmu.2020.032.
9. Chebotar I, Savinova T, Bocharova J, Korostin D, Evseev P, Mayanskiy N. Genetic Alternatives for Experimental Adaptation to Colistin in Three Pseudomonas aeruginosa Lineages. Antibiotics. 2024; 13: 452. Available from: https://doi.org/10.3390/antibiotics13050452.
10. Miller AK, Brannon MK, Stevens L, Johansen HK, Selgrade SE, Miller SI, et al. PhoQ mutations promote lipid A modification and polymyxin resistance of Pseudomonas aeruginosa found in colistin-treated cystic fibrosis patients. Antimicrob Agents Chemother. 2011; 55 (12): 5761–9. DOI: 10.1128/AAC.05391-11. Epub 2011 Oct 3. PMID: 21968359; PMCID: PMC3232818.
11. Shapiro AB, Gu RF, Gao N. Dimerization of isolated Pseudomonas aeruginosa lipopolysaccharide transporter component LptA. Biochem Biophys Res Commun. 2014; 450 (4): 1327–32. DOI: 10.1016/j.bbrc.2014.06.138. Epub 2014 Jul 5. PMID: 25003324.
12. Dovala D, Rath CM, Hu Q, Sawyer WS, Shia S, Elling RA, et al. Structure-guided enzymology of the lipid A acyltransferase LpxM reveals a dual activity mechanism. Proc Natl Acad Sci U S A. 2016; 113 (41): E6064-E6071. DOI: 10.1073/pnas.1610746113. Epub 2016 Sep 28. PMID: 27681620; PMCID: PMC5068295.
13. Luo Q, Yang X, Yu S, Shi H, Wang K, Xiao L, et al. Structural basis for lipopolysaccharide extraction by ABC transporter

LptB₂FG. Nat Struct Mol Biol. 2017; 24 (5): 469-474. DOI: 10.1038/nsmb.3399.
14. Moskowitz SM, Brannon MK, Dasgupta N, Pier M, Sgambati N, Miller AK, et al. PmrB mutations promote polymyxin resistance of Pseudomonas aeruginosa isolated from colistin-treated cystic fibrosis patients. Antimicrob Agents Chemother. 2012; 56 (2): 1019–30. DOI: 10.1128/AAC.05829-11. Epub 2011 Nov 21. PMID: 22106224; PMCID: PMC3264203.
15. Disney-McKeethen S, Seo S, Mehta H, Ghosh K, Shamoo Y. Experimental evolution of Pseudomonas aeruginosa to colistin in spatially confined microdroplets identifies evolutionary trajectories consistent with adaptation in microaerobic lung environments. mBio. 2023; 14 (6): e0150623. DOI: 10.1128/mbio.01506-23.

THE CANDIDATE ANTI-TUBERCULOSIS mRNA VACCINE IMMUNOGENICITY AND REACTOGENICITY DEPENDENCY ON THE ANIMAL'S SEX AND THE VACCINE DOSE

Reshetnikov VV[1]✉, Shepelkova GS[2], Rybakova AV[3], Trashkov AP[3], Yeremeev VV[2], Ivanov RA[1]

[1] Sirius University of Science and Technology, Sirius, Russia

[2] Central Tuberculosis Research Institute, Moscow, Russia

[3] National Research Centre "Kurchatov Institute", Moscow, Russia

mRNA vaccines turned out to be highly effective in combating the COVID-19 pandemic and other viral infections. Despite extensive study of mRNA vaccines in the last five years, the issue of safety of their use is still relevant. The study aimed to assess immunogenicity of two anti-tuberculosis mRNA vaccine doses in female and male rats 2 and 4 weeks after vaccination. Hematological and biochemical parameters of blood were determined within the same timeframe. The dose-dependent nature of mRNA vaccine immunogenicity was confirmed in both females and males. Vaccination led to moderate lymphopenia and neutrophilia in male rats, as well as to apparent dose-dependent and sex-related changes in blood biochemistry parameters at various time points. The findings suggest moderate toxicity of the anti-tuberculosis mRNA vaccine and the importance of assessing its toxic effects at various time points in animals of both sexes.

Keywords: mRNA vaccine, tuberculosis, immunogenicity, toxicity

Funding: the study was supported by the Ministry of Science and Higher Education of the Russian Federation (agreement No. 075-10-2021-113, project ID RF----193021X0001).

Acknowledgements: the authors express their gratitude to staff members of the Sirius University of Science and Technology: I. M. Terenin for *in vitro* transcription, O. V. Zaborova for formulation of mRNA into lipid nanoparticles.

Author contribution: Reshetnikov VV — mRNA vaccine preparation, experimental procedure, manuscript writing; Shepelkova GS — experimental procedure, data analysis; Rybakova AV — experimental procedure, data analysis; Trashkov AP — planning the experiment, manuscript editing; Yeremeev VV — planning the experiment, manuscript editing; Ivanov RA — planning the experiment, manuscript editing.

Compliance with ethical standards: the study was approved by the Ethics Committee of the National Research Centre "Kurchatov Institute" (protocol No. 2 dated 31 October 2023) and conducted in accordance with the Order of the Ministry of Health No. 755 and the Guidelines issued by the Office of Laboratory Animal Welfare (A5502-01).

✉ **Correspondence should be addressed:** Vasily V. Reshetnikov
Olimpiysky prospekt, 1, Sochi, 354340, Russia; reshetnikov.vv@talantiuspeh.ru

Received: 16.09.2024 **Accepted:** 04.10.2024 **Published online:** 30.10.2024

DOI: 10.24075/brsmu.2024.045

ЗАВИСИМОСТЬ ИММУНОГЕННОСТИ И РЕАКТОГЕННОСТИ КАНДИДАТНОЙ мРНК-ВАКЦИНЫ ПРОТИВ ТУБЕРКУЛЕЗА ОТ ПОЛА ЖИВОТНЫХ И ДОЗЫ ПРЕПАРАТА

В. В. Решетников[1]✉, Г. С. Шепелькова[2], А. В. Рыбакова[3], А. П. Трашков[3], В. В. Еремеев[2], Р. А. Иванов[1]

[1] Автономная некоммерческая образовательная организация высшего образования «Научно-технологический университет «Сириус», Сириус, Россия

[2] Центральный научно-исследовательский институт туберкулеза, Москва, Россия

[3] Национальный исследовательский центр «Курчатовский институт», Москва, Россия

мРНК-вакцины показали высокую эффективность в борьбе с пандемией COVID-19 и другими вирусными инфекциями. Несмотря на интенсивное изучение мРНК-вакцин в последние пять лет, вопрос о безопасности их применения все еще остается актуальным. Целью работы было оценить иммуногенность противотуберкулезной мРНК вакцины в двух дозах у самок и самцов крыс через 2 и 4 недели после вакцинации. В эти же сроки определяли гематологические и биохимические показатели крови. Подтверждена дозозависимость иммуногенности мРНК вакцин как у самок, так и у самцов. Вакцинация привела к умеренной лимфоцитопении и нейтрофилии у самцов крыс, а также к выраженным дозо- и гендерзависимым изменениям в биохимических параметрах крови в различных временных точках. Полученные результаты свидетельствуют об умеренной токсичности противотуберкулезной мРНК вакцины и важности исследования ее токсических действий в различных временных точках у животных обоих полов.

Ключевые слова: мРНК-вакцина, туберкулез, иммуногенность, токсичность

Финансирование: исследование выполнено при поддержке Министерства науки и высшего образования Российской Федерации (соглашение № 075-10-2021-113, уникальный идентификатор проекта РФ----193021X0001).

Благодарности: авторы выражают благодарность сотрудникам АНО ВО «Университет «Сириус» И. М. Теренину за постановку транскрипции *in vitro*, О. В. Заборовой — за формуляцию мРНК в липидные наночастицы.

Вклад авторов: В. В. Решетников — подготовка мРНК вакцины, планирование эксперимента, написание рукописи; Г. С. Шепелькова — постановка экспериментов, анализ результатов; А. В. Рыбакова — постановка экспериментов, анализ результатов; А. П. Трашков — планирование эксперимента, редактирование рукописи; В. В. Еремеев — планирование эксперимента, редактирование рукописи; Р. А. Иванов — планирование эксперимента, редактирование рукописи.

Соблюдение этических стандартов: исследование одобрено этическим комитетом НИЦ «Курчатовский институт» (протокол № 2 от 31 октября 2023 г.), проведено в соответствии с Приказом Минздрава № 755 и Руководством Управления по охране лабораторных животных А5502-01.

✉ **Для корреспонденции:** Василий Владимирович Решетников
Олимпийский пр-т, д. 1, г. Сочи, 354340, Россия; reshetnikov.vv@talantiuspeh.ru

Статья получена: 16.09.2024 **Статья принята к печати:** 04.10.2024 **Опубликована онлайн:** 30.10.2024

DOI: 10.24075/vrgmu.2024.045

Currently, new mRNA vaccines against various viral and bacterial infections, including tuberculosis, the previously developed live, attenuated, recombinant, and DNA vaccines against which have not shown acceptable effectiveness, are being actively developed [1, 2]. However, there are many gaps in our understanding of the biology of mRNA vaccines delivered using lipid nanoparticles (LNPs). It is well known, that the mRNA-LNPs show broad biodistribution, are found in most tissues [3, 4], cause inflammatory response at the injection site, and can be associated with neuroinflammation [5]. There are plenty of reports that the use of mRNA-based vaccines is sometimes associated with allergy, myocarditis, and pulmonary hemorrhage [6]. In some cases, vaccination with the mRNA-LNPs leads to the delayed transcriptome alterations and moderate CpG island methylation level changes in peripheral blood monocytes [7]. Furthermore, there is insufficient information about the biodistribution and clearance time of mRNA vaccines and antigens encoded by these vaccines [4].

The pre-clinical trials of the RNA-1273 and BNT162b2 vaccines against COVID-19 involving rats showed a moderate decrease in the animals' body weight and the body temperature increase in the first 24 h after vaccination. Pro-inflammatory hematological and biochemical alterations, as well as the cytokine level increase were also revealed [8, 9]. Macroscopic alterations included the increase in the weight of the spleen, liver, and adrenal glands, while microscopic alterations included moderate inflammation at the injection site, in the groin, in the iliac and popliteal lymph nodes, along with the signs of inflammation in the liver and spleen. All alterations were dose-dependent, the majority of indicators were back to normal 2–3 weeks after administration of the last vaccine dose [8, 9]. Clinical trials of the RNA-1273, BNT162b2, and CS-2034 mRNA vaccines [10–12] also showed the dose-dependent, local irritant, and systemic adverse effects, including inflammation at the injection site, fatigue, headache, fever, muscular and joint pain, changes in the hematological and biochemical parameters of blood. The mRNA vaccine adverse effects can be associated with both active substance of the vaccine, the mRNA molecule, and the antigens encoded by this molecule or lipid nanoparticles, in which RNA is encapsulated.

We have previously shown that the mRNA vaccine against tuberculosis we have developed yields adaptive and protective immune responses [13]. However, safety of its use was poorly understood. The study aimed to assess toxic effects of two anti-tuberculosis mRNA vaccine doses based on the hematological and biochemical parameters of blood in male and female rats 2 and 4 weeks after vaccination.

METHODS

Animals

The experiment involved 30 female (126–149 g) and 30 male (154–180 g) SPF Wistar rats aged 8–12 weeks. The tests were performed at the breeding nursery of the National Research Centre "Kurchatov Institute"; the animals were kept under the SPF conditions with the fixed 12.00 : 12.00 h light/dark cycle and ad libitum access to food and water.

Experimental design

Three experimental groups, 10 males and 10 females per group, were formed for the study:

group I: the group administered the MTB-mEp5-1 mRNA vaccine in a dose of 5 μg/animal;

group II: the group administered the MTB-mEp5-1 mRNA vaccine in a dose of 15 μg/animal;

group III: the group administered the phosphate buffered saline (PBS).

The mRNA vaccine or phosphate buffered saline was administered to the experimental animals twice with a 14-day interval: 200 μL intramuscularly into the thigh using a 3-piece insulin syringe with the 26G needle (Fig. 1A). The animals were euthanized using the tiletamine-zolazepam plus xylazine anesthesia in a dose of 15 mg/kg and 6 mg/kg, respectively, with subsequent drainage of blood from the heart cavities and collection of the spleen and inguinal lymph nodes. Five males and five females per group were euthanized on day 16 of the experiment (24 h after administration of the second vaccine dose), other animals were euthanized on day 29 (two weeks after administration of the second vaccine dose). After euthanasia, blood was collected from the heart cavities of all animals for further clinical and biochemical testing. Furthermore, inguinal lymph nodes and the spleen were collected to access the mRNA vaccine immunogenicity.

The mRNA vaccine doses used correspond to the dose of the CVnCoV mRNA vaccine against COVID-19 that is currently undergoing clinical trials [NCT04652102]. MTB-mEp5-1 is a vaccine with the unmodified nucleotide composition (without any uridine analogues). The dose of the CVnCoV mRNA vaccine corresponds to 12 μg. The doses of the tested candidate vaccine we have selected (5 and 15 μg) are similar to the doses used in the clinical trial, but not adjusted to the animal's weight.

MTB-mEp5-1 vaccine

The MTB-mEp5-1 multi-epitope mRNA vaccine matches the 5′-TPL-mEpitope-mRNA1273-3′ vaccine that has been reported before, with minor modifications [13]. During *in vitro* transcription, m7G(3'OMe)pppA(2'OMe)pG (Biolabmix; Russia) at a concentration of 2.4 mm was used as a cap analogue. One more adenine was added to the plasmid DNA sequence after the T7 promoter sequence in order to ensure specific insertion of this cap analogue during the co-transcriptional capping. The MTB-mEp5-1 mRNA sequence is provided in the Appendix 1.

The other previously reported [13] stages of the mRNA vaccine development remained unchanged. mRNA was formulated into lipid nanoparticles using the microfluid cartridge in the NanoAssemblr™ Benchtop system (Precision NanoSystems Inc.; Canada). Particles were concentrated and sterilized using the PES membrane filter with the 0.22 μm pore size. The lipid nanoparticles were stored at +4 °C for no longer than 3 weeks before administration of the vaccine.

Analytical characterization of the particles obtained was performed as previously reported [13]; it included estimation of the particle size, polydispersity index, zeta potential, mRNA encapsulation percentage and integrity. Particle size was within the range of 86–88 nm in all experimental groups, zeta potential was between –3 and –2 mV, polydispersity index did not exceed 0.1. The mRNA encapsulation percentage exceeded 90%, and RNA integrity was above 85% according to the capillary electrophoresis data.

Blood hematology and biochemistry tests

Blood was collected from the heart cavities into the test tubes containing anticoagulant (K3-EDTA) for hematology testing; the DIATRON Abacus Junior 22.5 hematology analyzer was used for testing. Red blood cell counts, hemoglobin levels, hematocrit, white blood cell counts, platelet counts, and white blood cell differential were determined in the whole blood samples.

Blood samples were collected into the separator gel test tubes and centrifuged at 3000 g to obtain serum for further blood biochemistry testing. Serum concentrations of alanine aminotransferase (ALT), aspartate aminotransferase (AST), urea, alkaline phosphatase, total bilirubin, total protein, glucose were determined using the Architect c8000 chemistry analyzer (Abbott; USA).

Determination of the number of IFNγ-producing cells

The protective T-cell immune response level was estimated based on the number of cells extracted from the spleen and inguinal lymph nodes that secreted IFNγ in response to stimulation with the mycobacterial antigens (*M. tuberculosis* sonicate, 10 μg/mL) or ESAT6 recombinant protein at a concentration of 10 μg/mL (the ESAT6 production method was reported earlier [14]) by the ELISPOT method using the Mouse IFNγ ELISpot Set (BD; USA) and AEC Substrate Set (BD; USA) in accordance with the manufacturer's guidelines.

Statistical analysis

All data were tested for normality using the Shapiro–Wilk (W) test. The median and interquartile range (Q_{25}–Q_{75}) were calculated; the intergroup comparisons (post hoc analysis) were carried out using the Tukey`s test. One-way analysis of variance (ANOVA) was used for comprehensive assessment of the data of independent groups at the control points. The results were considered significant at $p < 0.05$. Statistical analysis was performed using the Statistica 6.0 software (StatSoft; USA).

RESULTS

Immunogenicity assessment

We assessed the effects of the vaccine dose on the adaptive immune response formation in female and male rats at two time points. A significant impact of immunization on the levels of IFNγ-producing cells (IPCs) in the spleen and the inguinal lymph node after specific stimulation was revealed (Fig. 1B). However, the number of IPCs in the spleen was significantly higher. Large differences in the IPC number per well depending on the specific stimulation type (ESAT6 protein or *M.tb* sonicate) were also reported for both lymph node cells and cells of the spleen at both time points. It is most likely that these effects are explained by different target antigen concentrations in the formulation used for specific stimulation.

Estimation of the adaptive immune response dynamics showed that the most prominent response was observed on day 29 of the experiment, two weeks after the second vaccination, which is in line with the literature data.

The dose-dependent effects were observed after stimulation with ESAT6: IPC levels in the lymph node cells were higher in group I administered the dose of 5 μg, than in group II on day 16 of the experiment, and on day 29 of the experiment IPC levels in the cells of the spleen were almost twice higher in group II, than in group I. No significant differences in the adaptive immune response levels between males and females were observed ($p > 0.05$).

Thus, our findings suggest that administration of two MTB-mEp5-1 mRNA vaccine doses to rats results in the

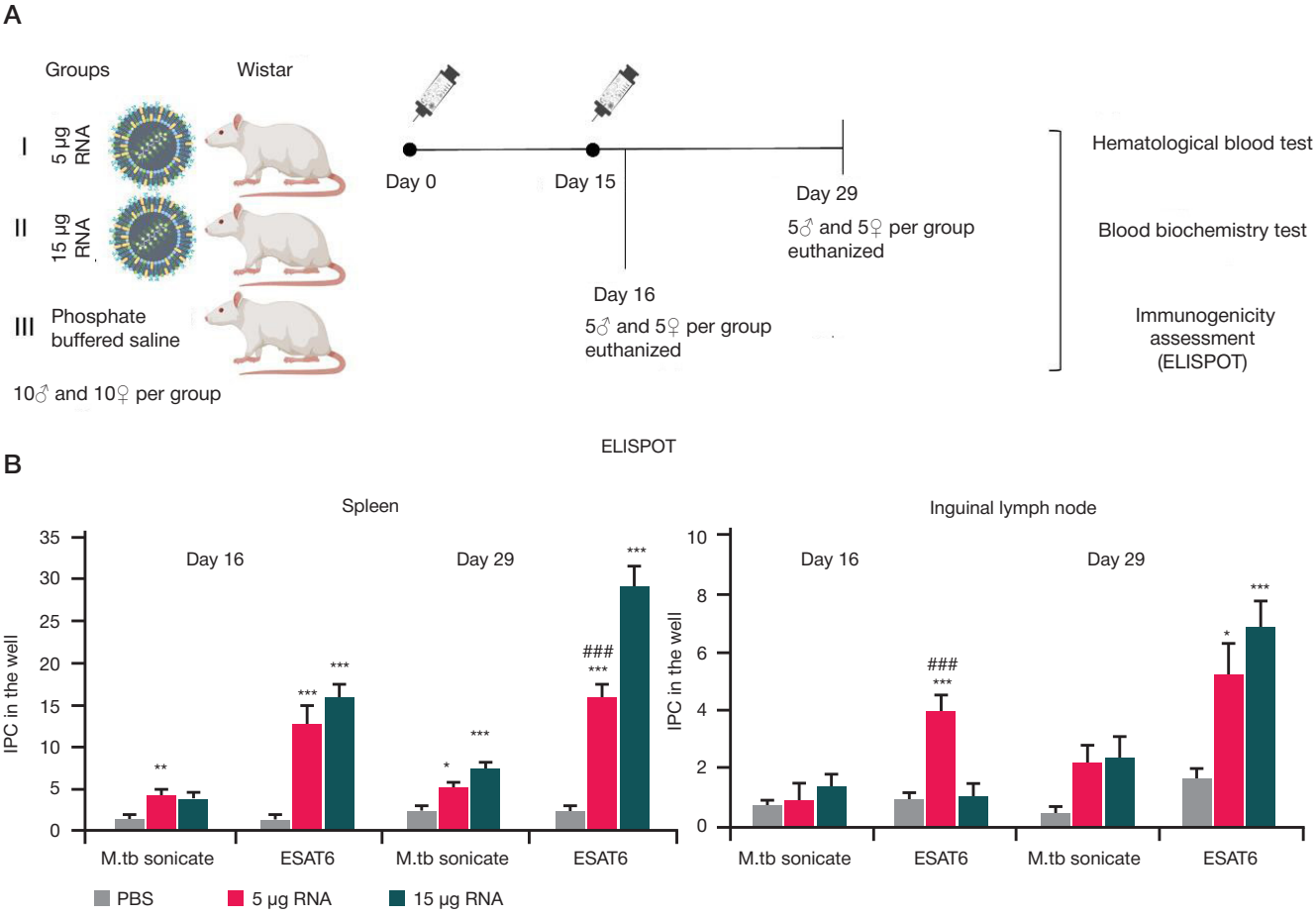

Fig. 1. mRNA vaccine immunogenicity assessment. **A**. Experimental design. **B**. ELISPOT analysis data for cells of the spleen and inguinal lymph nodes. IPC – IFNγ-producing cells. The data are provided as mean ± error of the mean. * — $p < 0.05$; ** — $p < 0.01$; *** — $p < 0.001$ compared to appropriate control group (PBS); ### — $p < 0.001$ compared to the group administered 15 μg of RNA

Table 1. Hematological parameters of blood

Group	Sex		WBC 10^9/L	Neu%	Lym%	Mon%	Eos%	Bas%	RBC 10^{12}/L	HGB g/L	HCT	PLT 10^{12}/L
Day 16 of the study												
Phosphate buffered saline (PBS)	♂	Median	5.86	24.9	67.9	5.9	1.1	0.1	6.3	146	38.4	684
		Q25–Q75	5.74–5.87	24 25.4	67.5–68.9	4.6–6.5	1–1.5	0.1–0.1	6.1–6.4	144–146	38.2–38.4	678–936
	♀	Median	4.06	21.1	72.5	4.6	2	0.1	6.03	137	36.7	1197
		Q25–Q75	3.67–4.45	20.0–21.6	71.7–72.5	3.9–4.6	1.1–2.6	0.00–0.10	5.99–6.33	135–144	36.5–38.9	925–1311
MTB–mEp5-1 5 μg	♂	Median	5.78	33.6	57.6	6.3	1.4	0.2	6	137	36.3	1054
		Q25–Q75	5.55–6.44	29.4–34.5	55.9–63.6	5.7–6.3	1.3–1.4	0.1–0.2	5.9–6.1	136–137	35.9–37.2	987–1079
	♀	MMedian	5.01	32.3	59.5	6.4	1.4	0.1	6.1	138	37.2	990
		Q25–Q75	4.6–5.63	28.4–37.4	54.5–68.0	4.3–6.5	1.2–1.5	0.10–0.20	5.99–6.20	138–139	37.1–38.1	951–1011
MTB-mEp5-1 15 μg	♂	Median	4.69	51.1*	38.8*	7.3	1.5	0.2	5.9	132	35	978
		Q25–Q75	3.67–6.19	48.6–54.9	38–42.4	5.6–8.7	1.3–1.6	0.1–0.2	5.8–6.0	131 134	34.2–35.3	908–985
	♀	Median	3.51	31.1	64	4.6	1.7	0.1	6.07	139	38	867
		Q25–Q75	2.87–4.29	26.4–35.7	56.3–66.6	3.9–4.8	1.6–2.1	0.10–0.10	6.07–6.21	139–145	37.5–38.2	845–906
Day 29 of the study												
Phosphate buffered saline (PBS)	♂	Median	5.7	42.2	51	5.1	1.5	0.1	6.39	143	36.5	780
		Q25–Q75	5.63–6.03	37.3–44.1	48.9–56.5	4.6–5.6	1.2–1.6	0.00–0.10	6.34–6.45	141–147	35.7–36.7	774–850
	♀	Median	3.39	31.3	61.3	5.1	1.7	0.1	6.38	139	36.4	734
		Q25–Q75	3.02–3.44	30.8–32.7	60.7–61.3	4.5–5.3	1.4–2	0.1–0.2	6.16–6.44	139–141	36.2–36.5	696–781
MTB-mEp5-1 5 μg	♂	Median	6.38	25	69.6	4.2	1.2	0.1	6.58	142	37.5	738
		Q25–Q75	6.13–7.56	24.8–25.5	65.2–69.7	4.1–5.3	1.1–1.3	0–0.1	6.45–6.92	142–148	37–40.4	711–796
	♀	Median	4.1	22.9	70.7	4.5	1.4	0.1	6.91	156	39.9	780
		Q25–Q75	3.88–4.71	22.7–25.4	69.5–71.7	4–4.8	1.2–1.6	0.1–0.2	6.76–7.01	151–156	39.3–40.3	737–852
MTB-mEp5-1 15 μg	♂	Median	6.9	26.2	66.1	5	1.1	0.1	6.53	145	36.8	797
		Q25–Q75	6.19–7.41	25.9–27.6	65.5–67.4	4.6–5.8	0.9–1.3	0.1–0.2	6.42–6.66	143–149	36.6–38.1	791–845
	♀	Median	5.05	23.1	72.6	4.2	1	0.1	6.18	135	35.2	834
		Q25–Q75	4.41–6.49	22.1–24.9	69–74.2	1.7–4.6	0.9–1.1	0–0.1	6.15–6.19	135–136	34.9–35.6	782–922

Note: the data are presented as median and interquartile range (Q_{25}–Q_{75}). The data on the absolute lymphocyte and neutrophil counts are not provided, but significance of intergroup differences is the same when comparing absolute values. * — the difference from control values is significant at the selected significance level ($p < 0.05$). WBC (white blood cells) — white blood cell count; Neu% — relative neutrophil count; Lym% — relative lymphocyte count; Mon% — relative monocyte count; Eos% — relative eosinophil count; Bas% — relative basophil count; RBC (red blood cells) — absolute red blood cell count; HGB (hemoglobin) — hemoglobin concentration; HCT — hematocrit; PLT (platelets) — absolute platelet count.

development of adaptive immune response detected at two studied time points, and the response level depends on the dose, not on the animal's sex

Evaluation of hematological and biochemical alterations in blood

We found no significant effect of vaccination on the studied experimental animals' blood parameters. No significant changes were observed in females of all experimental groups at both time points (Table 1). Only males immunized with the MTB-mEp5-1 vaccine dose of 15 μg showed a significant decrease in the median absolute (1.97×10^9/L vs. 3.78×10^9/L in the PBS group) and relative lymphocyte counts (lymphopenia), along with the increase in the median absolute (2.64×10^9/L vs. 0.89×10^9/L in the PBS group) and relative neutrophil counts (neutrophilia) on day 16 of the study. However, these parameters were back to normal two weeks after administration of the second vaccine dose, on day 29 of the experiment.

When performing analysis of the main blood biochemistry indicators, significant blood biochemistry alterations were reported in the experimental animals receiving the test formulation on days 16 and 29 of the study. In female rats, vaccination affected blood levels of ALT, AST, and total protein on day 16 of the experiment (ANOVA: $F(2.12) = 4.03$, $p = 0.046$; $F(2.12) = 8.58$, $p = 0.005$; $F(2.12) = 9.05$, $p = 0.004$, respectively). Females immunized with the MTB-mEp5-1 dose of 15 μg showed a significant increase in blood levels of ALT and AST, along with the decrease in total protein levels. Females immunized with the MTB-mEp5-1 dose of 5 μg showed the increase in AST levels only. At the same time, no such blood biochemistry indicator changes were found in males.

On day 29 of the experiment, in female rats of the experimental groups, alterations of most biochemical parameters were leveled, except for ALT [ANOVA: $F(2.12) = 14.12$, $p = 0.001$], the levels of which were still high in the MTB-mEp5-1 15 μg group. On the contrary, in males, vaccination led to alteration of most blood biochemistry parameters on day 29 of the experiment: ALT ($F(2.12) = 7.65$, $p = 0.007$], AST ($F(2.12) = 8.13$, $p = 0.006$), urea ($F(2.12) = 6.5$, $p = 0.012$], and total protein levels ($F(2.12) = 5.2$, $p = 0.024$]. Our findings showed that the urea, ALT and AST levels were elevated in both experimental groups, regardless of the mRNA vaccine dose. At the same time, the administered mRNA vaccine dose had a great effect on the increase/decrease in total protein levels reported for the experimental groups.

Thus, immunization with the MTB-mEp5-1 mRNA vaccine led to apparent blood biochemistry alterations depending on the animals' sex and the vaccine dose at different time points in female and male rats. At the same time, vaccination with MTB-mEp5-1 had a moderate effect on hematological parameters of blood (Table 2).

Table 2. Biochemical parameters of blood

Group	Sex	Assessed indicators						
		ALT, U/L	AST, U/L	Urea, mM/L	Alkaline phosphatase, U/L	Total bilirubin, μM/L	Total proteing/L	Glucose, mM/L
Day 16 of the study								
Phosphate buffered saline (PBS)	♂	78; 66–80	72; 69–94	4,6; 4,3–5,1	353; 339–362	18,9; 16,6–21,1	59; 58–62	4,9; 4,8–5,0
	♀	73; 71–90	66; 64–73	5,0; 4,8–5,3	382; 350–402	17,1; 15,5–20,3	61; 59–66	4,7; 4,7–5,0
MTB-mEp5-1 5 μg	♂	78; 75–101	82; 70–92	4,8; 4,1–5,2	381; 377–420	18,0; 16,6–19,4	54; 51–59	5,0; 4,9–5,2
	♀	82; 70–96	92*; 65–95	4,4; 4,4–4,7	390; 382–408	18,0; 15,2–18,4	57; 55–59	4,3; 4,1–4,5
MTB-mEp5-1 15 μg	♂	99; 81–114	98; 87–110	4,9; 4,9–4,9	364; 361–400	18,8; 17,2–20,0	53; 51–54	4,6; 4,2–4,8
	♀	104*; 93–110	106*; 101–111	5,1; 4,0–5,2	401; 385–414	18,0; 16,2–18,9	50*; 49–52	4,3; 4,3–4,5
Day 29 of the study								
Phosphate buffered saline (PBS)	♂	73; 69–77	78; 71–80	4,2; 4,2–4,5	370; 364–402	19,5; 17,5–19,5	57; 55–60	5,0; 4,8–5,1
	♀	77; 75–78	83; 75–83	4,8; 4,5–4,9	361; 351–380	18,3; 18,2–19,1	56; 54–57	5,0; 5,0–5,3
MTB-mEp5-1 5 μg	♂	85*; 80–88	96*; 90–97	5,2*; 5,0–5,4	401; 400–414	20,4; 19,2–20,5	55; 53–55	5,1; 4,9–5,5
	♀	82; 82–90	90; 83–101	5,2; 4,4–5,3	388; 383–397	20,1; 19,0–21,0	52; 50–53	4,3; 4,2–4,7
MTB-mEp5-1 15 μg	♂	99*; 92–101	101*; 93–107	5,3*; 5,1–5,6	387; 385–410	20,0; 18,3–20,6	52*; 50–52	5,0; 4,1–5,0
	♀	105*; 96–110	102; 97–114	5,2; 4,8–5,5	415; 402–416	20,9; 19,7–21,1	50; 50–52	4,9; 4,8–5,2

Note: the data are presented as median and interquartile range (Q_{25}–Q_{75}). * — the difference from control values is significant at the selected significance level ($p < 0.05$)

DISCUSSION

Vaccination often leads to side effects of inflammatory genesis that can include pain, redness or swelling at the injection site, as well as to systemic symptoms, such as body temperature increase and altered cellular composition of blood [15]. mRNA vaccines have immunostimulatory properties due to both RNA molecule itself and the lipid nanoparticle components [16]. When entering the cell, RNA can be recognized by intracellular receptors, including toll-like receptors 3 and 7, which results in activation of the innate immunity signaling pathways [16, 17].

We have shown that male rats demonstrate lymphocytopenia and neutrophilia that level out two weeks after the mRNA vaccine administration 24 h after the second injection of the larger vaccine dose. These data are consistent with the data of pre-clinical trials of other mRNA vaccine formulations, such as RNA-1273, BNT162b2 [8 ,9], in which elevated blood cytokine levels, elevated white blood cell, neutrophil, and eosinophil counts, decreased lymphocyte counts were observed in the first 24 h after injection. It is well known that moderate inflammatory response is essential for adaptive immunity formation. The recent study [18] has also shown that the more prominent inflammatory responses to vaccine administration correlate with the development of stronger adaptive immune response. In our study, administration of the elevated vaccine dose (15 μg) resulted in the more prominent adaptive immune response, along with the altered cellular composition of blood.

In contrast to the short-term changes in hematological parameters, biochemistry alterations associated with inflammation were more stable. According to our data, females had elevated ALT levels even two weeks after administration of the second vaccine dose, while males had elevated ALT, AST, urea levels and decreased total protein levels. Alterations of these biochemical parameters can be associated with the liver and kidney function impairment. We conducted histological assessment of the animal's organs (data not shown) and found microscopic signs of inflammation in the liver (dose-dependent progression of the productive vasculitis signs: vessel wall thickening, lymphocyte infiltration, focal accumulation of lymphocytes and macrophages). At the same time, no microscopic signs of inflammation were found in the kidneys.

Blood biochemistry alterations and microscopic alterations in the liver were also reported in the pre-clinical trials of mRNA vaccines conducted by BioNTech and Moderna [8, 9]. In these trials some animals also showed elevated levels of AST, urea, alkaline phosphatase, triglycerides, cholesterol, bilirubin, along with the decreased total protein levels. These changes were accompanied by structural alterations of the liver represented by the increase in organ weight, hepatocyte vacuolation, Kupffer cell hypertrophy, single cell necrosis or hepatocyte degeneration. However, the authors do not specify, when biochemical and histological indicators return to normal after vaccination, in their pre-clinical report.

In the pre-clinical trial of the BNT162b2 mRNA vaccine, the authors assume that hepatocyte vacuolation can be associated with specific accumulation of the ALC-0315 ionizable lipids [9]. Other lipid components, such as SM102, ALC-0159 or PEG2000-DMG, can also be toxic at high doses, however, the much lower doses used in the vaccine are supposed to have no toxic effects [8, 9, 19].

In our studies, we also used lipids ALC-0315, SM-102, which can activate the innate immunity response, as earlier

reported [16]. The use of unmodified uridine in the RNA sequence represents a significant MTB-mEp5-1 vaccine difference from the RNA-1273 and BNT162b2 vaccines. The unmodified uridine is a potent innate immunity stimulator, in contrast to N1-methylpseudouridine used in the RNA-1273 and BNT162b2 vaccines [16, 17].

It is most likely that excessive innate immunity activation due to both unmodified RNA and lipid components can result in the more severe and prolonged inflammation. It should be noted that excessive immune activation capable of causing liver tissue damage can be accompanied by changes in biochemical parameters of blood. However, when using various vaccines, including RNA-1273 and BNT162b2, such extremely rare cases (one per 14 million cases) are associated with autoimmune processes [20].

The differences in the strength of the MTB-mEp5-1 vaccination effect on biochemical parameters of blood in females and males are worth special attention. Our findings show that the differences in biochemical parameters of blood 24 h after the booster mRNA vaccine dose were detected in females only. At the same time, the more pronounced alterations were detected in males two weeks after the second vaccine dose. Such differences can result from the differences in physiological vaccine concentrations related to the animals' weight (the weight of males was 15–20% higher) and other physiological features (sex hormone levels), genetic differences (including X-linked gene expression) [21]. The differences in the sex steroid hormone levels affect the immune cell functioning, which leads to differences in the immune response activity [21]. In particular, the clinical trial results suggest that women show more intense antibody production and more pronounced cellular response after vaccination [21, 22]. Vaccination of women with the mRNA-based and other vaccines results in more frequent side effects, such as body temperature increase, pain, and local inflammation [22, 23]. Thus, the literature data on the gender-specific vaccination effects are consistent with our results showing that the MTB-mEp5-1 administration causes faster changes in biochemical parameters of blood in females. These changes are likely to be associated with the higher female rats' immune system responsiveness to the mRNA vaccine components.

CONCLUSIONS

Our findings suggest high reactogenicity of the unmodified RNA-based MTB-mEp5-1 vaccine. Signs of inflammation in the studied organs and steady changes in the animals' blood biochemistry test parameters provide the basis for the extended study of the tested formulation safety and the mechanisms underlying its specific pharmacological activity.

References

1. Matarazzo L, Bettencourt PJG. mRNA vaccines: a new opportunity for malaria, tuberculosis and HIV. Front Immunol. 2023;14: 1172691.
2. Kazakova A, Zhelnov P, Sidorov R, Rogova A, Vasileva O, et al. DNA and RNA vaccines against tuberculosis: a scoping review of human and animal studies Frontiers in Immunology. 2024; 15.
3. Ndeupen S, Qin Z, Jacobsen S, Bouteau A, Estanbouli H, et al. The mRNA-LNP platform's lipid nanoparticle component used in preclinical vaccine studies is highly inflammatory. iScience. 2021; 24: 103479.
4. Pateev I, Seregina K, Ivanov R, Reshetnikov V. Biodistribution of RNA Vaccines and of Their Products: Evidence from Human and Animal Studies. Biomedicines. 2023; 12.
5. Kirshina AKA, Kolosova E, Imasheva E, Vasileva O, Zaborova O, Terenin I, Muslimov A, Reshetnikov V. Effects of various mRNA-LNP vaccine doses on neuroinflammation in BALB/c mice. RSMU. 2022; 6.
6. van den Ouweland F, Charpentier N, Tureci O, Rizzi R, Mensa FJ, et al. Safety and reactogenicity of the BNT162b2 COVID-19 vaccine: Development, post-marketing surveillance, and real-world data. Hum Vaccin Immunother. 2024; 20: 2315659.
7. Pang APS, Higgins-Chen AT, Comite F, Raica I, Arboleda C, et al. Longitudinal Study of DNA Methylation and Epigenetic Clocks Prior to and Following Test-Confirmed COVID-19 and mRNA Vaccination. Front Genet. 2022; 13: 819749.
8. European Medicines Agency. Moderna Assessment Report COVID-19 Vaccine Moderna. 2021.
9. European Medicines Agency. Assessment report: Comirnaty. 2021.
10. Jin Z, Wu J, Wang Y, Huang T, Zhao K, et al. Safety and immunogenicity of the COVID-19 mRNA vaccine CS-2034: A randomized, double-blind, dose-exploration, placebo-controlled multicenter Phase I clinical trial in healthy Chinese adults. J Infect. 2023; 87: 556–70.
11. Jackson LA, Anderson EJ, Rouphael NG, Roberts PC, Makhene M, et al. An mRNA Vaccine against SARS-CoV-2 - Preliminary Report. N Engl J Med. 2020; 383: 1920–31.
12. Walsh EE, Frenck RW, Jr, Falsey AR, Kitchin N, Absalon J, et al. Safety and Immunogenicity of Two RNA-Based Covid-19 Vaccine Candidates. N Engl J Med. 2020; 383: 2439–50.
13. Reshetnikov V, Terenin I, Shepelkova G, Yeremeev V, Kolmykov S, et al. Untranslated Region Sequences and the Efficacy of mRNA Vaccines against Tuberculosis. Int J Mol Sci. 2024; 25.
14. Vasileva O, Krapivin B, Muslimov A, Kukushkin I, Pateev I, Rybtsov S, et al. Immunogenicity of full-length and multi-epitope mRNA vaccines for M. Tuberculosis as demonstrated by the intensity of T-cell response: a comparative study in mice. Bulletin of RSMU. 2023; 03: 42–48.
15. Teijaro JR, Farber DL. COVID-19 vaccines: modes of immune activation and future challenges. Nat Rev Immunol. 2021; 21: 195–7.
16. Verbeke R, Hogan MJ, Lore K, Pardi N. Innate immune mechanisms of mRNA vaccines. Immunity. 2022; 55: 1993–2005.
17. Muslimov A, Tereshchenko V, Shevyrev D, Rogova A, Lepik K, et al. The Dual Role of the Innate Immune System in the Effectiveness of mRNA Therapeutics. Int J Mol Sci. 2023; 24.
18. Zhuang CL, Lin ZJ, Bi ZF, Qiu LX, Hu FF, et al. Inflammation-related adverse reactions following vaccination potentially indicate a stronger immune response. Emerg Microbes Infect. 2021; 10: 365–75.
19. Kang DD, Hou X, Wang L, Xue Y, Li H, et al. Engineering LNPs with polysarcosine lipids for mRNA delivery. Bioact Mater. 2024; 37: 86–93.
20. Schinas G, Polyzou E, Dimakopoulou V, Tsoupra S, Gogos C, et al. Immune-mediated liver injury following COVID-19 vaccination. World J Virol. 2023; 12: 100–8.
21. Flanagan KL, Fink AL, Plebanski M, Klein SL. Sex and Gender Differences in the Outcomes of Vaccination over the Life Course. Annu Rev Cell Dev Biol. 2017; 33: 577–99.
22. Klein SL, Jedlicka A, Pekosz A. The Xs and Y of immune responses to viral vaccines. Lancet Infect Dis. 2010; 10: 338–49.
23. Bignucolo A, Scarabel L, Mezzalira S, Polesel J, Cecchin E, et al. Sex Disparities in Efficacy in COVID-19 Vaccines: A Systematic Review and Meta-Analysis. Vaccines (Basel). 2021; 9.

Литература

1. Matarazzo L, Bettencourt PJG. mRNA vaccines: a new opportunity for malaria, tuberculosis and HIV. Front Immunol. 2023;14: 1172691.
2. Kazakova A, Zhelnov P, Sidorov R, Rogova A, Vasileva O, et al. DNA and RNA vaccines against tuberculosis: a scoping review of human and animal studies Frontiers in Immunology. 2024; 15.
3. Ndeupen S, Qin Z, Jacobsen S, Bouteau A, Estanbouli H, et al. The mRNA-LNP platform's lipid nanoparticle component used in preclinical vaccine studies is highly inflammatory. iScience. 2021; 24: 103479.
4. Pateev I, Seregina K, Ivanov R, Reshetnikov V. Biodistribution of RNA Vaccines and of Their Products: Evidence from Human and Animal Studies. Biomedicines. 2023; 12.
5. Kirshina AKA, Kolosova E, Imasheva E, Vasileva O, Zaborova O, Terenin I, Muslimov A, Reshetnikov V. Effects of various mRNA-LNP vaccine doses on neuroinflammation in BALB/c mice. RSMU. 2022; 6.
6. van den Ouweland F, Charpentier N, Tureci O, Rizzi R, Mensa FJ, et al. Safety and reactogenicity of the BNT162b2 COVID-19 vaccine: Development, post-marketing surveillance, and real-world data. Hum Vaccin Immunother. 2024; 20: 2315659.
7. Pang APS, Higgins-Chen AT, Comite F, Raica I, Arboleda C, et al. Longitudinal Study of DNA Methylation and Epigenetic Clocks Prior to and Following Test-Confirmed COVID-19 and mRNA Vaccination. Front Genet. 2022; 13: 819749.
8. European Medicines Agency. Moderna Assessment Report COVID-19 Vaccine Moderna. 2021.
9. European Medicines Agency. Assessment report: Comirnaty. 2021.
10. Jin Z, Wu J, Wang Y, Huang T, Zhao K, et al. Safety and immunogenicity of the COVID-19 mRNA vaccine CS-2034: A randomized, double-blind, dose-exploration, placebo-controlled multicenter Phase I clinical trial in healthy Chinese adults. J Infect. 2023; 87: 556–70.
11. Jackson LA, Anderson EJ, Rouphael NG, Roberts PC, Makhene M, et al. An mRNA Vaccine against SARS-CoV-2 - Preliminary Report. N Engl J Med. 2020; 383: 1920–31.
12. Walsh EE, Frenck RW, Jr, Falsey AR, Kitchin N, Absalon J, et al. Safety and Immunogenicity of Two RNA-Based Covid-19 Vaccine Candidates. N Engl J Med. 2020; 383: 2439–50.
13. Reshetnikov V, Terenin I, Shepelkova G, Yeremeev V, Kolmykov S, et al. Untranslated Region Sequences and the Efficacy of mRNA Vaccines against Tuberculosis. Int J Mol Sci. 2024; 25.
14. Vasileva O, Krapivin B, Muslimov A, Kukushkin I, Pateev I, Rybtsov S, et al. Immunogenicity of full-length and multi-epitope mRNA vaccines for M. Tuberculosis as demonstrated by the intensity of T-cell response: a comparative study in mice. Bulletin of RSMU. 2023; 03: 42–48.
15. Teijaro JR, Farber DL. COVID-19 vaccines: modes of immune activation and future challenges. Nat Rev Immunol. 2021; 21: 195–7.
16. Verbeke R, Hogan MJ, Lore K, Pardi N. Innate immune mechanisms of mRNA vaccines. Immunity. 2022; 55: 1993–2005.
17. Muslimov A, Tereshchenko V, Shevyrev D, Rogova A, Lepik K, et al. The Dual Role of the Innate Immune System in the Effectiveness of mRNA Therapeutics. Int J Mol Sci. 2023; 24.
18. Zhuang CL, Lin ZJ, Bi ZF, Qiu LX, Hu FF, et al. Inflammation-related adverse reactions following vaccination potentially indicate a stronger immune response. Emerg Microbes Infect. 2021; 10: 365–75.
19. Kang DD, Hou X, Wang L, Xue Y, Li H, et al. Engineering LNPs with polysarcosine lipids for mRNA delivery. Bioact Mater. 2024; 37: 86–93.
20. Schinas G, Polyzou E, Dimakopoulou V, Tsoupra S, Gogos C, et al. Immune-mediated liver injury following COVID-19 vaccination. World J Virol. 2023; 12: 100–8.
21. Flanagan KL, Fink AL, Plebanski M, Klein SL. Sex and Gender Differences in the Outcomes of Vaccination over the Life Course. Annu Rev Cell Dev Biol. 2017; 33: 577–99.
22. Klein SL, Jedlicka A, Pekosz A. The Xs and Y of immune responses to viral vaccines. Lancet Infect Dis. 2010; 10: 338–49.
23. Bignucolo A, Scarabel L, Mezzalira S, Polesel J, Cecchin E, et al. Sex Disparities in Efficacy in COVID-19 Vaccines: A Systematic Review and Meta-Analysis. Vaccines (Basel). 2021; 9.

GENETIC PORTRAITS OF KHANTY AND MANSI BASED ON THE Y CHROMOSOME HAPLOGROUPS IN THE CONTEXT OF GENE POOLS OF RUSSIA

Ponomarev GYu ✉, Agdzhoyan AT, Potanina AYu, Adamov DS, Balanovska EV

Research Centre for Medical Genetics, Moscow, Russia

Khanty and Mansi are small indigenous peoples of Western Siberia with the unique cultural, anthropological, and linguistic characteristics. The study of their gene pool will make it possible to reconstruct the genetic structure of the Ugric-speaking population, of which in modern times only Khanty and Mansi remain, along with Hungarians, in whose gene pool there are traces of medieval migration of the Ugric-speaking Magyars. The detailed characterization of the gene pool of Khanty and Mansi is important for reconstruction of Ugric populations and genetic history of the region. The study was aimed to assess representative samples of Khants (n = 83) and Mansi (n = 74) based on the standard panel of 60 SNP markers and the extended panel of 74 Y-chromosomal SNP markers by statistical and cartographic methods in the context of indigenous population of Urals and Western Siberia. The differences between the gene pools of Khanty and Mansi have been revealed based on both standard panel of Y chromosome haplogroups and branches of haplogroups N2 and N3a4. Most of the Khanty gene pool is evenly distributed between N2-Y3195 (26%), N2-VL67 (23%), and N3a4-Z1936 (23%). The “Western” branch N2-Y3195 predominates in the Mansi gene pool (69%). Mansi gravitate towards populations of the Urals-Volga region in the multidimensional genetic space. Based on the standard panel of Y haplogroups, Khanty are close to the populations of Western and South Siberia. However, the analysis of branches N3a4 has shown that Khanty are intermediate between the “Uralic” and “Siberian” clusters: when the ancestors of Khanty moved from the Ural region to the northeast, these acquired both genetic components. The gene geographic maps of 10 haplogroup N3a4 branches in the populations of Urals and Western Siberia reflect the dynamic changes of the gene pool that took place 4–2 kya.

Keywords: Khanty, Mansi, gene pool, Y-chromosome, SNP, haplogroup, N3a4-Z1936, N2-Y3195, N2-VL67

Funding: State Assignment of the Ministry of Science and Higher Education of the Russian Federation for the Research Centre for Medical Genetics.

Acknowledgements: the authors would like to thank all participants of the expedition survey (donors of samples) and Biobank of North Eurasia for access to DNA collections.

Author contribution: Balanovska EV — management; Agdzhoyan AT — contribution to the expedition survey of Ob Ugrians; Ponomarev GYu — Y-SNP marker genotyping; Ponomarev GYu, Potanina AYu, Adamov DS — statistical and cartographic analysis, manuscript formatting; Balanovska EV, Ponomarev GYu — study design and manuscript writing.

Compliance with ethical standards: the study was approved by the Ethics Committee of the Research Centre for Medical Genetics (protocol No. 1 dated 29 June 2020).

✉ **Correspondence should be addressed:** Georgy Yu. Ponomarev
Moskvorechie, 1, 115522, Moscow, Russia; st26i900@gmail.com

Received: 09.09.2024 **Accepted:** 01.10.2024 **Published online:** 28.10.2024

DOI: 10.24075/brsmu.2024.044

ГЕНЕТИЧЕСКИЕ ПОРТРЕТЫ ХАНТОВ И МАНСИ ПО ГАПЛОГРУППАМ Y-ХРОМОСОМЫ В КОНТЕКСТЕ ГЕНОФОНДОВ РОССИИ

Г. Ю. Пономарёв ✉, А. Т. Агджоян, А. Ю. Потанина, Д. С. Адамов, Е. В. Балановская

Медико-генетический научный центр имени академика Н. П. Бочкова, Москва, Россия

Ханты и манси — коренные малочисленные народы Западной Сибири с уникальными культурными, антропологическими и лингвистическими особенностями. Изучение их генофонда позволяет реконструировать генетическую структуру населения, говорившего на угорских языках, от которого в современности сохранились только ханты, манси, а также венгры, в чьем генофонде присутствуют следы средневековой миграции угроязычных мадьяр. Детальная характеристика генофонда хантов и манси важна для реконструкции угорских популяций и генетической истории региона. Целью исследования было изучить репрезентативные выборки хантов (n = 83) и манси (n = 74) на основе базовой панели из 60 SNP-маркеров и углубленной панели 74 SNP-маркеров Y-хромосомы статистическими и картографическими методами в контексте коренного народонаселения Урала и Западной Сибири. Выявлены различия генофондов хантов и манси и по базовой панели гаплогрупп Y-хромосомы, и по ветвям гаплогрупп N2 и N3a4. Основная часть генофонда хантов равномерно распределена между N2-Y3195 (26%), N2-VL67 (23%) и N3a4-Z1936 (23%). В генофонде манси резко преобладает «западная» ветвь N2-Y3195 (69%). В многомерном генетическом пространстве манси тяготеют к популяциям Урало-Поволжья. Ханты по базовой панели Y-гаплогрупп сближаются с популяциями Западной и Южной Сибири. Анализ ветвей N3a4 показал, что ханты занимают промежуточное положение между «уральским» и «сибирским» кластерами: при движении предков хантов из Приуралья на северо-восток они включили оба генетических компонента. Геногеографические карты 10 ветвей гаплогруппы N3a4 в популяциях Урала и Западной Сибири отражают динамику генофонда в период от 4 до 2 тыс. лет назад.

Ключевые слова: ханты, манси, генофонд, Y-хромосома, SNP, гаплогруппа, N3a4-Z1936, N2-Y3195, N2-VL67

Финансирование: государственное задание Министерства науки и высшего образования РФ для Медико-генетического научного центра имени академика Н. П. Бочкова

Благодарности: авторы благодарят всех участников экспедиционного обследования (доноров образцов) и АНО «Биобанк Северной Евразии» (за предоставление коллекций ДНК).

Вклад авторов: Е. В. Балановская — руководство; А. Т. Агджоян — участник экспедиционного обследования обских угров; Г. Ю. Пономарёв — генотипирование Y-SNP маркеров; Г. Ю. Пономарёв, А. Ю. Потанина, Д. С. Адамов — статистический и картографический анализ, оформление статьи; Е. В. Балановская, Г. Ю. Пономарёв — дизайн исследования и написание статьи.

Соблюдение этических стандартов: исследование одобрено этическим комитетом Медико-генетического научного центра имени Н. П. Бочкова (протокол № 1 от 29 июня 2020 г.).

✉ **Для корреспонденции:** Георгий Юрьевич Пономарёв
ул. Москворечье, д. 1, 115522, г. Москва, Россия; st26i900@gmail.com

Статья получена: 09.09.2024 **Статья принята к печати:** 01.10.2024 **Опубликована онлайн:** 28.10.2024

DOI: 10.24075/vrgmu.2024.044

Most representatives of the Ob Ugrians, Khanty and Mansi, live in the Khanty-Mansi Autonomous Okrug – Yugra of the Tyumen Region (hereinafter, KhMAO). According to the 2010 census, the population of Mansi is 11,614 people, and the population of Khanty is 29,277 people. They speak languages of the Ugric branch of the Uralic language family. Among contemporary peoples, only Hungarians, who have inherited a negligible genetic trace from medieval Magyars, speak these languages [1]. The Ob Ugrians have a unique combination of anthropological traits distinguished as a distinct "Uralic race" [2], and their culture comprises two components: the ancient northern, hunter, taiga component (inherited from the indigenous population) and the southern pastoralist one (associated with migration of the Indo-Iranian-speaking population) [3]. The population structure of the Ob Ugrians took shape in the 1st millennium A. D. on both sides of the Ural Mountains: between the Kama region and the Ob River basin. Their range has been declining gradually and shifting to the northeast since 14th–15th century under the pressure of the Komi people, who migrated due to expansion of the Russian population.

Four ethnographic groups characterized by high endogamy levels were distinguished in Mansi: in the 18th–19th centuries, the average share of endogamous marriages in these groups exceeded 80%. Later, part of Southern Mansi was assimilated by Tatars and Russians, and the Western Mansi were absorbed into the northern and eastern groups of Mansi. The largest northern group of Mansi included the populations of Western and Southern Mansi, as well as Khanty; marriages with the Nenets people added some Mongoloid traits to their genetic portrait. The Eastern Mansi maintain the anthropological type close to that of the Finnish-speaking peoples of the Urals-Volga region [2].

In Khanty, the dialects of three ethnographic groups differed so much that these were considered as independent languages, and the average endogamy level reached 90% in the 18th–19th century [2]. The culture of Northern Khanty is most similar to that of Northern Mansi and the Nenets people, while the culture of Eastern Khanty is most close to that of the Selcup people. To date, the southern group has been lost, however, it is assumed that the "Ugric" substrate of the culture [4, 5] and gene pool [6] of the Zabolotny Siberian Tatars is inherited from the southern groups of Mansi and Khanty.

Both genetic components, the Western Eurasian and Eastern Eurasian, are found in the Y gene pool of the Ob Ugrians [1, 7–14]; the eastern component prevails (77% in Khanty, 89% in Mansi), the origin of which is considered to be associated with the Upper Paleolithic migration from South Siberia and Central Asia [10]. An opposite trend is reported based on the mtDNA data: the maximum share of the Eastern Eurasian component (59% in Khanty, 69% in Mansi) [10]. A genetic relationship between Khanty and the Komi-Zyrians, Samoyedic peoples (Enets, Tundra and Forest Nenets, Nganasans) against the background of genetic differences between the Ob Ugrians and the majority of peoples of Siberia (Altaians, Buryats, Kets, Selkup people, Evenki, Dolgans, Yakuts) and Central Asia was demonstrated [15].

In the study of the haplogroup N phylogeography and the model of expansion of the haplogroup N carriers, the data on the Ob Ugrians provided are based on the sum of haplogroups N2 and N3 [9] (according to the haplogroup N nomenclature introduced in the studies [12]). Later it was shown that the haplogroup N2 frequency decreased from north to south in the Western Siberia, while the haplogroup N3 frequency increased [12]. The analysis of the N3a4 sub-variants in the gene pool of Hungarians [1, 12] showed that the ancestors of the Ob Ugrians and Magyars split up about 2.7–2.9 kya.

In Khanty, significant genetic differences between the ethnographic groups are likely to persist: if in the northern group the frequencies of N2 and N3 are equal (38% each) [7], then in the southern group the frequency of N3 is almost twice higher (64%) [10], although the differences can be due to small samples: $n = 47$ in the northern and $n = 28$ in the southern group.

The recent study of the Khanty and Mansi gene pool using the standard panel of 60 Y-chromosomal markers suggests that there are three components in the gene pool of the Ob Ugrians: Siberian, Uralic, and Northern European [16]. The Siberian component predominates (80%), in which haplogroup N2 is dominant, and the second place is shared by N3a4 (Northern European component) and N3a1 (Uralic). The identified differences between the gene pools of Mansi and Khanty [16] can reflect various aspects of the genetic history of Ugrians and require a more thorough analysis.

In this study we considerably expanded the range of the studied populations and improved the genotyping level, and maximum attention was given to the gene geography of different haplogroup N2 and N3a4 variants. N2 dominating in the Ob Ugrians is spread from the Volga region to Far East, and assessment of the genetic landscape of various haplogroup branches can provide new information about the genetic history of Ugrians. Haplogroup N3a4 that is more frequent in the Ob Ugrians, than in the majority of other populations of Urals and Siberia, is no less important. Despite the fact that the today's N3a4 area is centered round the north of the East European Plain, it is considered to originate from Western Siberia [1, 11, 12]. Therefore, construction of the detailed genetic portraits of the Ob Ugrians in the context of the broad range of surrounding populations is essential for understanding the genetic history of a large number of indigenous peoples of Russia.

METHODS

The population-based samples of Khanty ($n = 83$) and Mansi ($n = 74$) were assessed within the framework of the expedition survey (RFBR project No. 16-06-00303a) with the help of the Biobank of North Eurasia; the samples covered a broad spectrum of local populations (Fig. 1). Despite the existing genetic differences between local groups of Khanty (Fig. 1), we combined these groups into a single sample based on the shared ethnicity and cultural identity for the purposes of this study. Such a combination made it possible to perform statistical analysis showing the genetic characteristics of Khanty as a single ethnic population. Only unrelated (at least to the third generation) males, whose fathers and grandfathers were born in the studied populations of this ethnic group, were included in the study. The data on the comparison groups were provided by the Biobank of North Eurasia.

The Qiagen QIASymphony SP automated nucleic acid isolation and purification system was used to extract DNA from the venous blood samples; genotyping was performed by the OpenArray method using the QuantStudio 12 Flex PCR system (Thermo Fisher Scientific; USA). The basic analysis involved 60 Y-chromosomal SNP markers most typical for the population of North Eurasia: D-M174, E-M35, E-M78, C-M217, C-F3791, C-F5481, C-F3918, C-M48, C-SK1066, C-M407, G-M201, G1-M285, G2-P15, G2-FGC595, G2-M406, G2-P303, H-M69, I-M170, I-M253, I-P37.2, I-M223, J1-M267, J1-P58, J2-M172, J2-M12, J2-M67, J2-M9, L-M20, L-M317, T-M70, N-M231, N-M128, N2-Y3205, N-M178, N3a1-B211, N3a2-M2118, N3a3-CTS10760, N3a4-Z1936, N3a5a-F4205, N-B202, N-B479, O-P186, O-M119, O-P31, O-M122, O-P201, O-M134, Q-M242, R1a-M198, R1a-PF6202, R1a-Y2395,

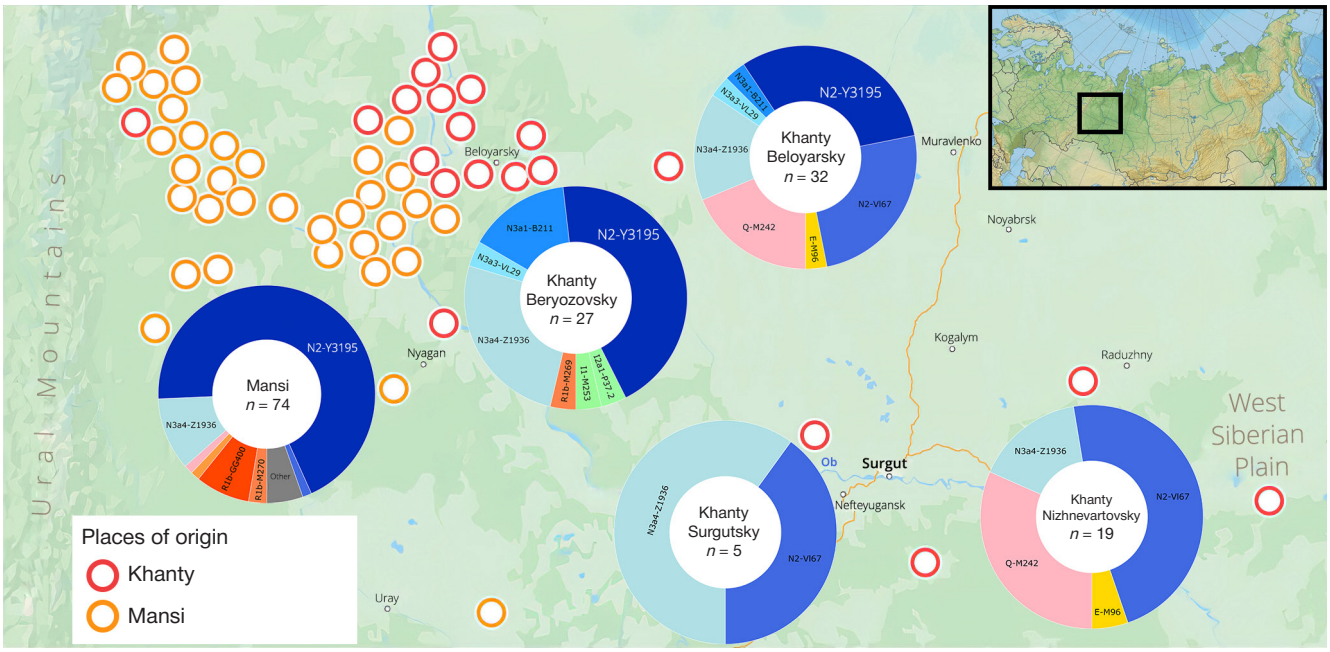

Fig. 1. Gene pool composition and the sites, where the samples of Mansi and various groups of Khanty were originate. Northern Mansi were surveyed in the Beryozovsky district of KhMAO and around, along the Sosva and Lyapin rivers (ancestors in the direct male line were born in villages of Beryozovo, Sosva, Vanzetur, Karym, Kimkyasui, Lombovozh, Verkhniye, Novinskaya, Nyaksimvol, Saranpaul, Khulimsunt, Patrasui, Rakhtynia, Sartynia, Khanglytur, Shhekurya, Yasunt, Unyugan, as well as the sites of Mansi settlements). Khanty were surveyed in the Beloyarsky (n = 32), Beryozovsky (n = 27), Surgutsky (n = 5), and Nizhnevartovsky (n = 19) districts of KhMAO

R1a-CTS1211, R1a-Z92, R1a-Z93, R1b-M343, R1b-Y13887, R1b-M269, R1b-L51, R1b-Z2105, R2-M124.

The samples were further genotyped by another 14 branches specifically for this study: haplogroups N2 (Y3195, VL67) and N3a4 (CTS1223, Y13850, Y24370, Y24360, L1034, L1442, Y28540, Y28544, Z1924, YP5259, Z35275, Z1928).

The genetic relationships and age to the origin of the haplogroups were obtained from the YFull Y-chromosome tree [17], unless otherwise specified. The evolutionary age of branches was based on the analysis of TMRCA (time to the most recent common ancestor) with the 95% confidence intervals (CI). Statistical analysis was performed using the Statistica 7.0 software (StatSoft; USA); the Nei's genetic distances were calculated in DJgenetic [18]. The gene geographic maps were created using the original GeneGeo software tool [19] by the Shepard's inverse distance weighting method with the weight function K = 2 and the radius of influence of 1100 km. Haplogroup N2 was mapped using the color chart with the frequency maximum of 60%, while N3a4 was mapped using the chart with the frequency maximum of 30%. Sampling for comparative analysis was performed based on the objectives of studying the genetic structure of Khanty and Mansi in Western Siberia and the Ural region on a large scale. In this regard, determination of grading for each population was driven by the combination of such factors, as the large population area and population heterogeneity, since it was necessary to ensure the widest possible geographical coverage to construct the detailed and reliable haplogroup distribution maps. The data of the Biobank of North Eurasia were complemented by the data of the earlier reported studies [1, 11–14, 20–23].

RESULTS

Genetic portraits of the Ob Ugrians in the context of surrounding peoples

A total of 13 Y chromosome haplogroup variants have been identified in the Ob Ugrian gene pools (Table 1, Fig. 1, 2) showing that the gene pools of Khanty and Mansi are dramatically different, despite their geographical and linguistic proximity. Despite the fact that haplogroup N2 predominates in both ethnic groups, its frequency is significantly higher in Mansi (70%), than in Khanty (49%); N3a4 is twice more common in Khanty (23%) compared to Mansi (11%). There are different proportions of rare haplogroups in Mansi and Khanty. Particularly noteworthy are the increased Q frequency in Khanty (14%) and the increased R1b frequency in Mansi (11%).

Haplogroups N2 and N3 that predominate in the genetic portraits of the Ob Ugrians are common in the indigenous populations of the Ural region and Western Siberia (Fig. 2): these predominate in many populations of the region suggesting similar historical processes and migration routes.

The pattern showing the haplogroup N2 predominance and a significant share of N3a4, that is typical for the Ob Ugrians and many indigenous peoples of the region suggests the importance of the Eastern Eurasian genetic component present

Table 1. Frequencies (%) of Y chromosome haplogroups in the gene pools of Khanty and Mansi

CORE	Размер выборки	C-M217 (xM48, M407)	E-M96	I1-M253	I2a1-P37.2	N2		N3a1-B211	N3a3-VL29	N3a4-Z1936	Q-M242	R1a-M198 (xM458, Z93)	R1b	
						Y3195	VI67						GG400	M269(xGG400)
Mansi	74	1.35	0	1.35	1.35	68.92	1.35	1.35	0	10.81	1.35	1.35	8.11	2.7
Khanty	83	0	2.38	1.19	1.19	26.19	22.62	5.95	2.38	22.62	14.29	0	1.19	0

Note: the gradient from minimum to maximum frequencies is highlighted in shades of *red and pink*: the more intense the cell color, the higher the frequency

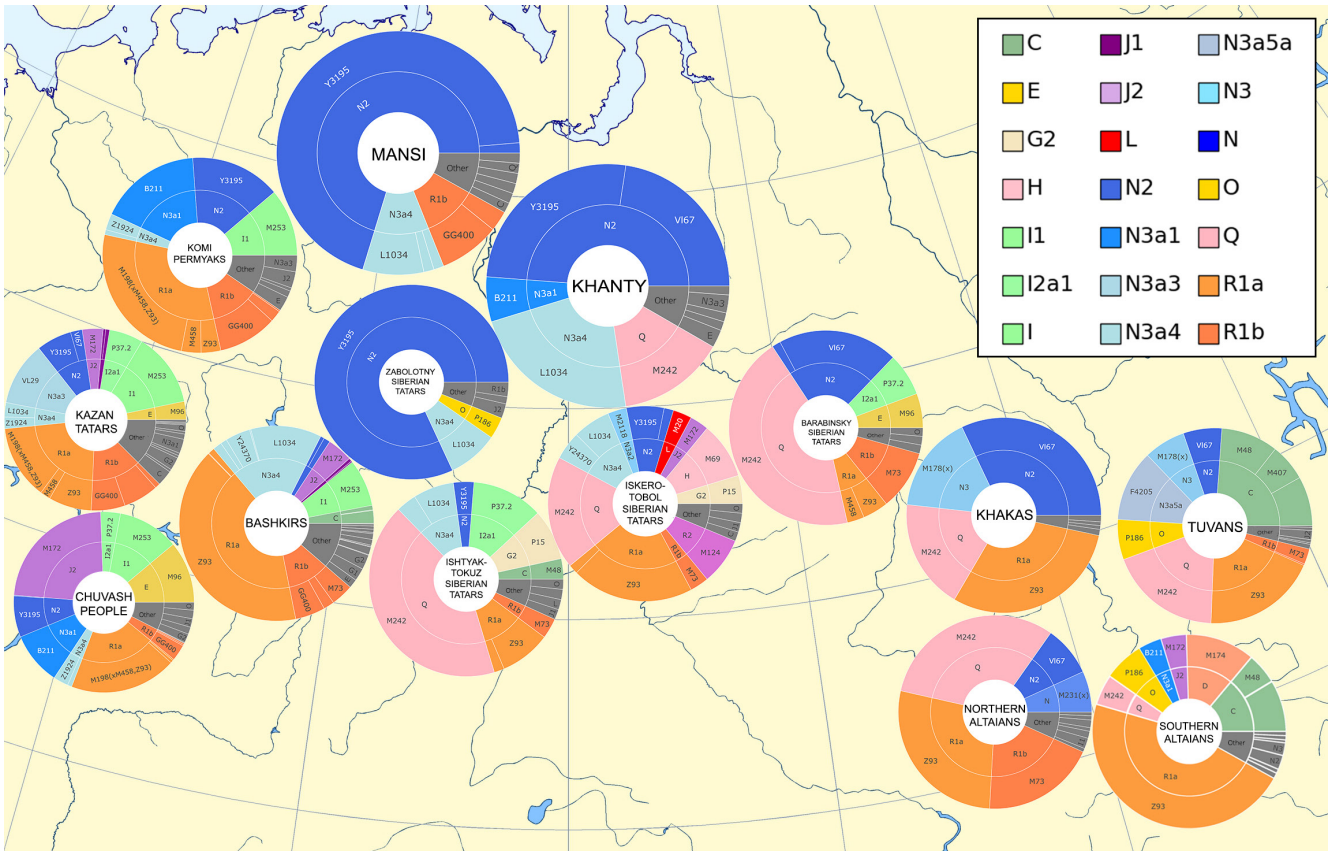

Fig. 2. Genetic portraits of the Ob Ugrians and surrounding indigenous peoples of the Ural region and Western Siberia. The haplogroup name is provided in the inner ring, while the outer ring provides markers determining the haplogroup; the outer ring division into sectors shows the sub-haplogroup frequency in the population. The color of each Y chromosome haplogroup is specified in the map key.

in their gene pools and possibly reflects ancient migration waves from Siberia and Central Asia.

The Mansi gene pool originality manifests itself in high frequency of haplogroup R1b (11%), specifically of its GG400 branch (8%). The Zabolotny Siberian Tatars, who are different from Mansi only by the fact of having the East Asian haplogroup O, are most close to the genetic portrait of Mansi. Among the populations of the Ural region, Komi Permyaks are most close to Mansi, however, in Komi Permyaks, the greater Western Eurasian influence is reflected in the increased frequency of R1a, N3a1, and I1.

Along with the large share of haplogroups N2 and N3a4, high frequency of the haplogroup Q reflecting great Eastern Eurasian influence is the feature of the Khanty gene pool. Haplogroup Q found in the Altaians, Khakas, Tuvans, most groups of Siberian Tatars can reflect the genetic relationships between the Ob Ugrians and the population, which has migrated from the Central and East Asia.

Gene geography of haplogroups N2 and N3a4

Cartographic analysis was performed for the branches of haplogroups N2 and N3a4 most typical for the Ob Ugrians (Fig. 3, 4). The analysis makes it possible to reveal spatial patterns even when the data on the Y chromosome frequencies in the surrounding populations are incomplete, which makes it

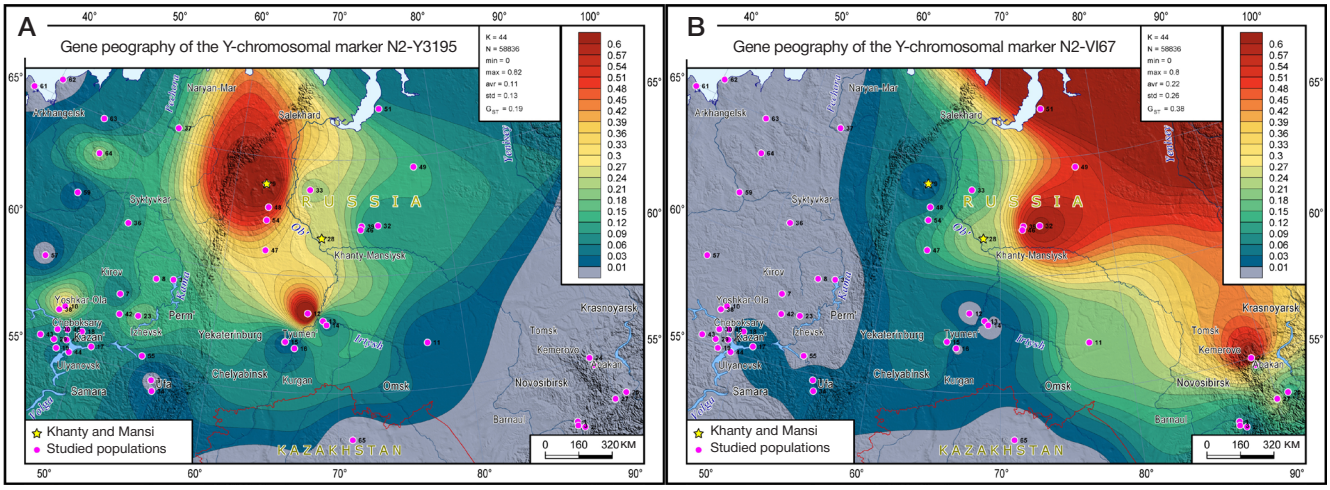

Fig. 3. Gene geography of the Y chromosome haplogroup N2 major branches: western branch Y3195 of the haplogroup N2 **(A)** and eastern branch VL67 of the haplogroup N2 **(B)**

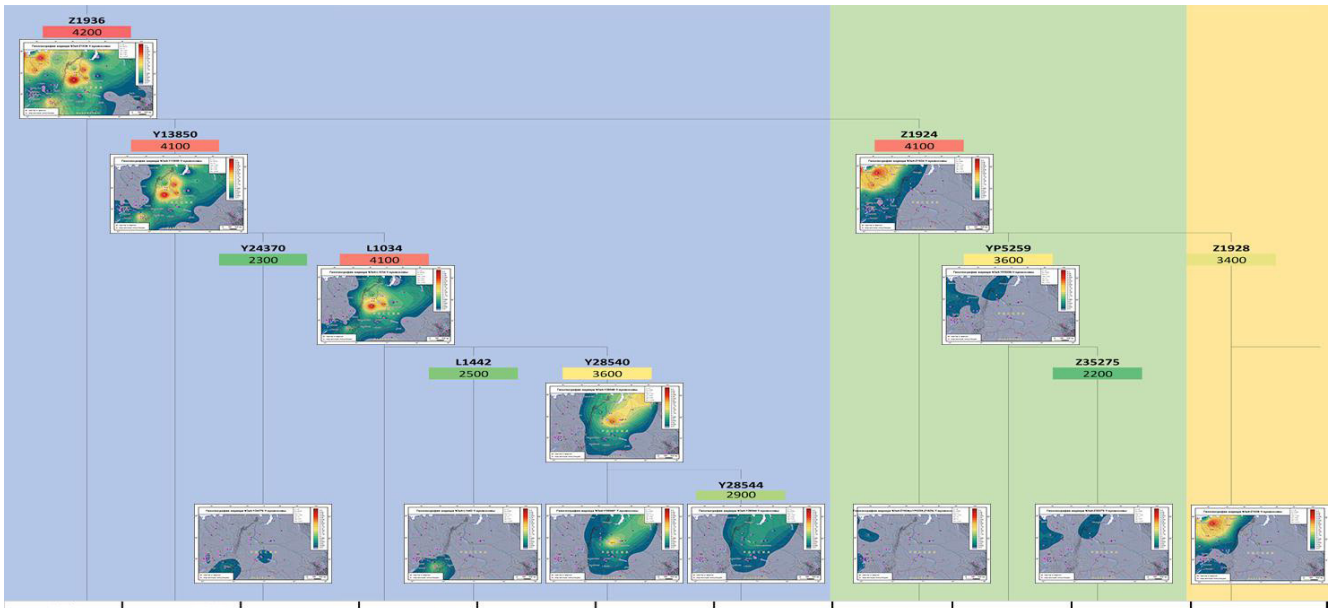

Population	Total frequency N3a4	CST1223*	Y13850*	L1034*	Y28540*	Y28544	Z1924*	YP5259*	Z35275	Z1928
Mansi	10.81	1.35	0	1.35	1.35	5.41	0	0	1.35	0
Khanty	22.62	0	0	0	15.48	7.14	0	0	0	0

Fig. 4. Phylogenetic structure of the Ural-Siberian cluster N3a4 and frequency of distinct lineages in the populations of Khanty and Mansi. The numbers provided under the names of the branches represent their age in thousands of years ago (kya); the 95% confidence intervals are provided in the text

possible to include the published data about haplogroups N2 and N3a4 in the analysis. Despite different provenance, these haplogroups are contemporaries: the haplogroups emerged about 4.5 kya (5.1–3.8 kya) and began growing phylogenetically.

Haplogroup N2 is divided into the western branch Y3195 (Fig. 3A) and the eastern branch VL67 (Fig. 3B). The eastern branch reaches high frequencies in the Eastern Khanty (60%) and the Gydan Nenets (72%) of the Tazovsky District (Yamalo-Nenets Autonomous Okrug), who maintain their traditional social framework [14]. Our findings suggest a different frequency range: the maximum frequency of VL67 (42%) is typical for Tofalars, the second place is shared by Khanty and Khakas (22%). However, when the Eastern Khanty (Surgutsky and Nizhnevartovsky districts) are specially highlighted, the VL67 frequency increases to 43%, reaching 61% in our small sample of the Forest Nenets.

In Mansi, on the contrary, the eastern branch N2 is the least frequent (1%), and the diversity of N2 is represented by the western branch Y3195 (69%). It reaches its maximum frequency in the Zabolotny Siberian Tatars (81%), while medium frequencies are found in Mari (32%), Khanty (26%), Udmurts (17%), and Komi Permyaks (14%).

The distribution of both branches shows a clear geographical correlation and a common area of overlap at the Ob and Irtysh river basins.

Haplogroup N3a4 is represented by two major branches, Y13850 and Z1924, in the area of Western Siberia and the Ural region most important for genetic history of Ugrians: in the tree of the haplogroup N3a4 (Fig. 4), the Y13850 branch is marked with the blue background, and the Z1924 branch is marked with the green background. Branch Y13850 emerged about 4.1 kya (4.8–3.4 kya) [1, 14, 23] and gave rise to the Ural-Siberian cluster of the Y-chromosomal lineages. The second branch, Z1924, emerged around that time (4.8–3.4 kya) and spread across the western regions of North Eurasia, showing low frequency in the Ural region, where the areas of both branches (Y13850 and Z1924) overlap. In the studied Ob Ugrian populations almost all samples belong to the large Ural-Siberian cluster Y13850. Exception is only one Mansi sample with the marker Z35275 belonging to the western cluster Z1924 (Fig. 4).

The main branch Y13850 (Fig. 5A) is important as a bridge between the Ugric-speaking peoples: the Ob Ugrians and medieval Magyars (who were among the ancestors of Hungarians) [11, 13]. In the gene pool of the Ob Ugrians, the frequency of the Y13850 lineage reaches 23% in Khanty and 8% in Mansi. It is divided into two sub-branches: Y24370 (not found in the Ob Ugrians) and L1034, to which almost all the studied samples of Khanty and Mansi with the haplogroup N3a4 belong (Fig. 5B). The sub-branch L1034 also gives rise to two descended lineages: L1442 (not found in the Ob Ugrians) and Y28540 that emerged 3.6 kya (4.5–2.7 kya) and included all carriers of N3a4 among Khanty (23%) and the majority of Mansi (7%). The branch Y28540, in turn, is divided into two variants (Fig. 4): the descended variant Y28544 (Fig. 5D) emerged 2.9 kya (3.9–2.1 kya), it is almost equally common in Khanty and Mansi; the root variant Y28540(xY28544) (Fig. 5C) predominates in Khanty (15%) and is rare in Mansi (1%).

Several descended lineages, which can be identified by whole genome sequencing, are likely to hide under high frequency of the root variant in Khanty. Maybe Khanty and Mansi have inherited both branches (Y28544 and basal Y28540(xY28544))

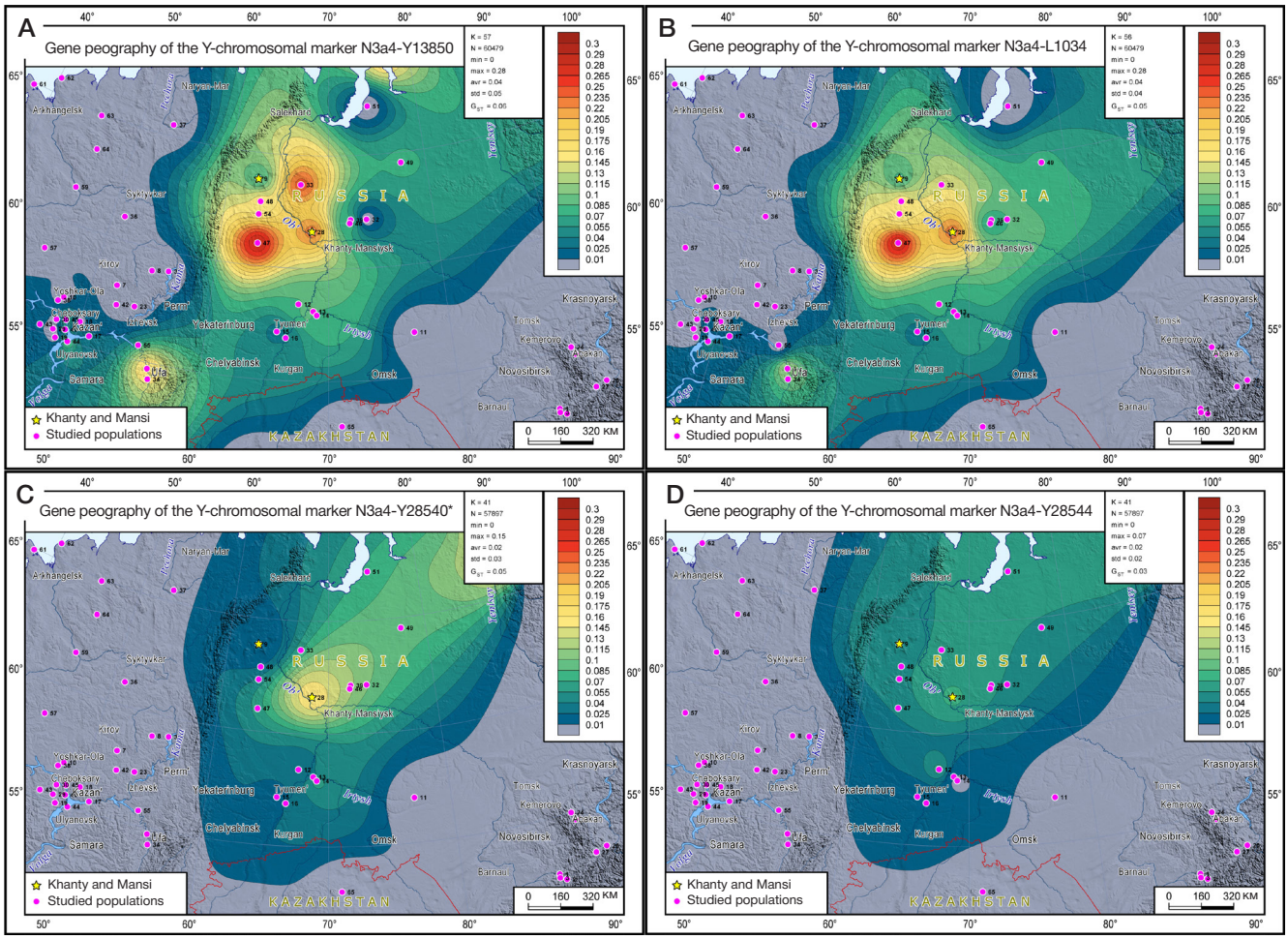

Fig. 5. Geographical distribution and frequency of the haplogroup N3a4 sub-branches. **A**. Gene geography of the haplogroup N3a4 branch Y13850. **B**. Gene geography of the haplogroup N3a4 branch L1034. **C**. Gene geography of the haplogroup N3a4 branch Y28540*. **D**. Gene geography of the haplogroup N3a4 branch Y28544

from their common ancestors, but Khanty maintained high frequency of the root variant due to larger population size and larger area of various endogamous ethnographic groups.

Mapping of the branch L1034 demonstrates that it's common in the Western Siberia and the Urals-Volga region, as well as that there are two frequency surges. The first L1034 maximum is observed in the Khanty included in this study (~23% of frequency), while the second was reported in the Southern Mansi (~27% of frequency), first described in the paper [13] and mentioned in other papers [1, 24]. Such high values of Southern Mansi are dramatically different from both our sample of Northern Mansi (8%) presented in this study and the sample [11] (15%). The differences in the branch L1034 frequency between the geographically distant subpopulations within Khanty and Mansi can be explained by the impact of genetic drift and small sample size, which have eventually shifted the haplogroup frequency ratios.

Position of the Ob Ugrians in the genetic space of indigenous peoples of Russia

The analysis of the position of Ob Ugrians in the genetic space by multidimensional scaling was performed twice: 1) based on the standard panel of 38 Y-SNP markers allowing us to include the literature data on the Nenets and Eastern Khanty [14, 23] (Table 2, Fig. 6A); 2) analysis of the populations of our team based on the extended panel of 48 Y-SNP markers (Table 2, Fig. 6B). The latter included 10 additional haplogroup N3a4 sub-branches, playing a key role in segregation of the genetic landscapes of Siberia and Europe. The analysis conducted in such a detailed manner for the first time makes it possible to trace the dynamic changes of the gene pool over time. The analysis based on the standard panel of 38 Y-SNP markers considers the pattern of genetic relationships that started to develop more than 4 kya (before the haplogroup N3a4 division into sub-branches). The analysis based on the panel of 48 Y-SNP markers extended through the haplogroup N3a4 subtyping reflects the features of the population of the studied territory in more recent times.

Analysis based on the standard panel of 38 Y-SNP markers. The multidimensional scaling plot based on the standard panel revealed two clusters of populations (Fig. 6A). The Uralic cluster included Finno-Ugric and Turkic populations of the Ural region; Mansi and Zabolotny Siberian Tatars are close to this cluster. The Siberian cluster included all populations of Khanty and Nenets, along with the Turkic-speaking peoples of Siberia. The populations of South Siberia (Todzhints, Tofalars, Tuvans, Khakas) are genetically close to Khanty, but dramatically different from Mansi (Fig. 6A, Table 2). The "geographical principle" is violated by the populations of the Yalutorovsky Siberian Tatars gravitating towards the Uralic cluster and the populations of Bashkirs that are most close to the Siberian cluster.

Analysis based on the extended panel of 48 Y-SNP markers. Position of the Ob Ugrians in the genetic space is clarified when comparing the multidimensional scaling plots (Fig. 6A and Fig. 6B) due to division of the taxonomically important haplogroup N3a4 into sub-branches. It is clear that the Siberian and Uralic clusters

Table 2. Pattern of genetic distances between the Ob Ugrians and surrounding peoples of Russia

Genotyping panel		Standard panel			Expanded panel		
Ethnic and sub-ethnic groups	Sample size (people)	38 SNP			48 SNP		
		Mansi	Khanty	Ob Ugrians	Mansi	Khanty	Ob Ugrians
Mansi	74	0.00	0.41	0.05	0.00	0.41	0.05
Zabolotny Siberian Tatars	83	0.01	0.45	0.07	0.01	0.43	0.06
Ob Ugrians	157	0.05	0.14	0.00	0.05	0.15	0.00
Mari	316	0.26	0.61	0.29	0.25	0.54	0.27
Khanty	84	0.41	0.00	0.14	0.41	0.00	0.15
Komi Permyaks	367	0.79	1.15	0.83	0.79	1.09	0.81
Kazan Tatars	432	1.20	1.24	1.13	1.25	1.35	1.20
Udmurts	260	1.22	1.23	1.14	1.22	1.17	1.12
Iskero-Tobol Siberian Tatars	64	1.47	0.74	1.04	1.58	0.95	1.21
Chuvash people of Tatarstan	80	1.47	1.57	1.42	1.49	1.50	1.41
Chuvash people of the Chuvash Republic	419	1.52	1.90	1.57	1.52	1.84	1.54
Mishar Tatars	158	1.84	2.03	1.82	1.85	1.97	1.81
Kryashen Tatars	66	1.91	2.06	1.88	1.91	2.00	1.85
Besermyan	49	2.00	1.53	1.70	1.99	1.47	1.68
Ishtyak–Tokuz Siberian Tatars	59	2.18	0.88	1.38	2.32	0.88	1.44
Bashkirs	943	2.57	1.54	1.95	3.31	3.20	3,18
Yalutorovsky Siberian Tatars	77	2.57	2.12	2.28	2.66	2.24	2,40
Barabinsky Siberian Tatars	70	2.90	0.68	1.38	2.90	0.62	1.36
Todzhints	69	3.88	1.16	1.92	3.87	1.10	1.90
Tyumen Siberian Tatars	59	3.90	1.97	2.62	4.21	2.04	2.76
Tofalars	42	3.91	0.89	1.68	3.91	0.83	1.65
Khakas	178	3.92	0.82	1.61	3.93	0.76	1.59
Tuvans	390	3.95	1.31	2.06	3.95	1.25	2.04
Northern Altaians	161	4.02	1.18	1.95	4.03	1.12	1.93
Southern Altaians	175	4.63	2.67	3.33	4.63	2.61	3.30
Kazym Khanty [14]	54	0.72	0.15	0.37	–	–	–
Russkinskaya Khanty [14]	64	1.85	0.56	1.06	–	–	–
Gydan Nenets [23]	322	2.23	0.43	1.06	–	–	–

become more distinct and drift further apart in the genetic space. Furthermore, Khanty come out of the Siberian cluster and get closer to the Uralic cluster. Bashkirs, on the contrary, move further away from both Uralic cluster and Khanty: after turning to the extended panel their genetic distances from Khanty increase 2-fold: from $d = 1.5$ to $d = 3.2$ (Table 2) due to significant contribution of haplogroup N3a4 to their gene pool. Mansi together with the Zabolotny Siberian Tatars, Khanty and Finnish-speaking populations of the Ural region (Mari, $d = 0.2$; Komi Permyaks, $d = 0.8$; Udmurts, $d = 1.2$) form the new Proto-Uralic cluster (Fig. 6B).

DISCUSSION

Continuing research on the Ugric peoples, we have significantly refined and expanded the conclusions drawn in the previous paper [16].

Further analysis of the sub-branches N2 and N3a4 and the position of the Ob Ugrians in the genetic space based on the extended panel of the Y-chromosomal markers confirmed the dominant influence of the Eastern Eurasian component on their gene pools. However, the N2 branch gene geography has revealed significant differences: in Khanty, the eastern Vl67 and the western Y3195 branches are almost equally frequent (about a quarter of the gene pool each); in Mansi, the western branch constitutes two thirds of the entire Mansi Y gene pool, while the eastern branch is almost absent. Considering migrations of the Mansi population, this can indicate that the Proto-Mansi populations lived far to the west of the current area during the period of the N2 sub-branch development, so the effect of the Eastern Eurasian component is small. This is also confirmed by the position of Mansi in the genetic space: the Finno-Ugric peoples of the Volga region are genetically most close to Mansi.

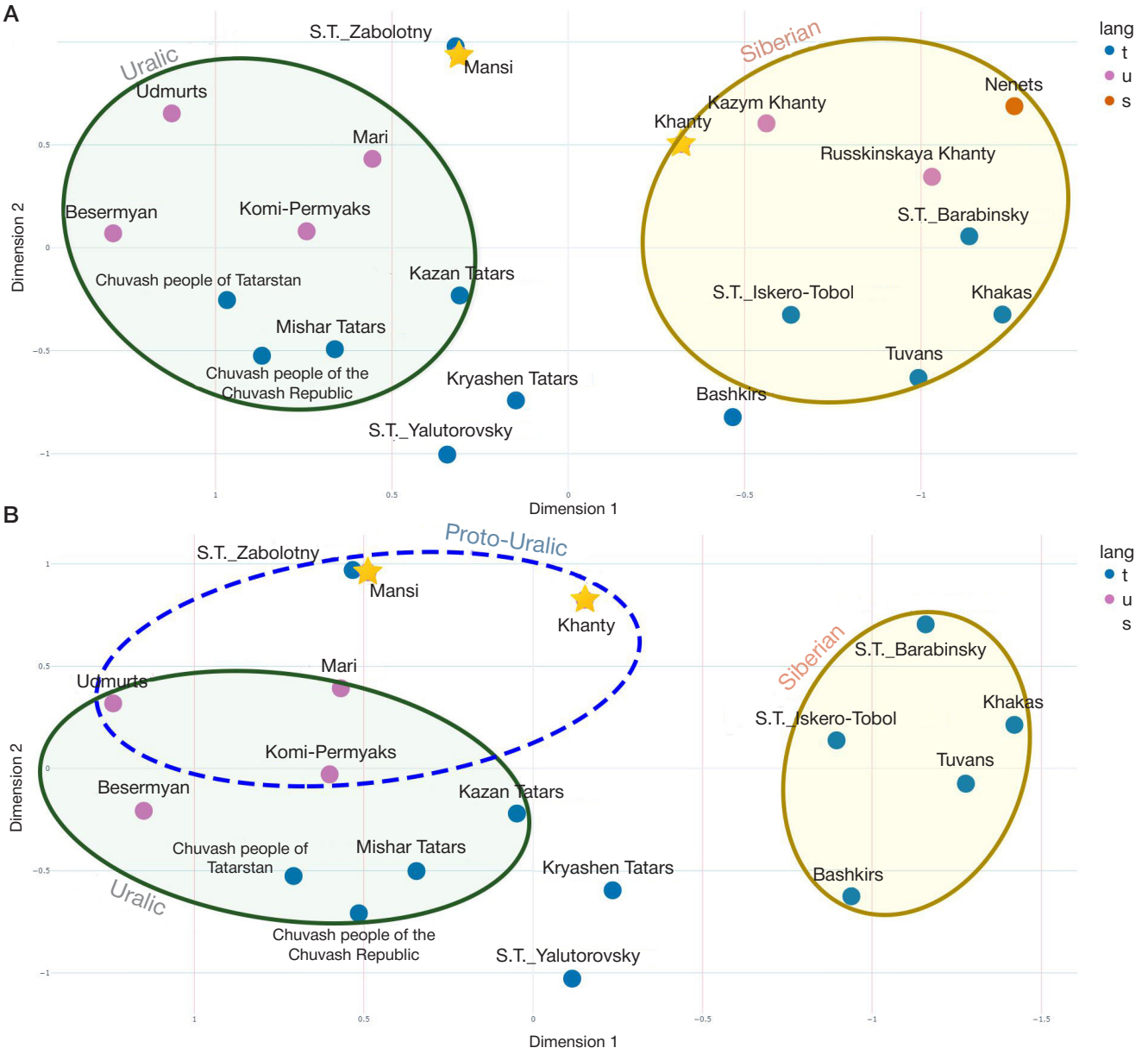

Fig. 6. Position of the Ob Ugrians in the genetic space of surrounding peoples of Russia. **A**. Multidimensional scaling plot based on the standard panel of 38 Y-chromosomal markers (stress coefficient = 0.14; alienation coefficient = 0.16). **B**. Multidimensional scaling plot based on the extended panel of 48 Y-chromosomal markers (stress coefficient = 0.16; alienation coefficient = 0.17). The peoples speaking languages of the Uralic linguistic family are highlighted in *pink*; those belonging to the Turkic branch of the Altaic language family are highlighted in *blue*

The Khanty genetic history reconstruction seems to be more challenging. Considering the large expanse of territory and equal contributions of the Eastern Eurasian and Uralic components, several hypotheses about the development of their gene pool can be proposed. Maybe the ancestors of Khanty originate from the territory of the Ural region; they assimilated local populations, in the gene pool of which the haplogroup Q was highly significant, when moving northeast. This hypothesis is based on the equal contribution of both N2 branches and high frequency of the eastern N2 branch in the Northern and Eastern Khanty, as well as on the increased frequency of N3a4. The multidimensional scaling plot confirms this hypothesis, showing that Khanty get closer to the peoples of the Finno-Ugric Volga region due to the haplogroup N3a4 contribution in Khanty. According to another hypothesis, the Proto-Khanty populations initially had both N2 branches, the Uralic cluster N3a4, and the Siberian haplogroup Q. This hypothesis is based on the fact that various groups have a similar spectrum of dominant haplogroups, despite broad ethnographic area of Khanty.

We can say unequivocally that the genetic relationships of the Ob Ugrians associated with the haplogroup N3a4 are ancient; these are important for the Ugrian gene pool reconstruction, along with the haplogroup N2 branches. Thus, our study is the first to demonstrate that the phylogenetic structure of haplogroups N3a4 and N2 clearly divides the gene pools of Siberia and Europe, which is an important step on the way to understanding the population history of the region.

CONCLUSIONS

We conducted a comprehensive analysis of the Khanty and Mansi gene pools based on the broad spectrum of the Y chromosome haplogroups in the context of indigenous populations of the Western Siberia and Urals. Thorough investigation of the haplogroup N3a4 eastern cluster phylogenetic structure has made it possible to clarify the time frame and the directions of migration in the region. Position of the Ob Ugrians among indigenous peoples of Siberia and Urals has been determined:

Mansi are genetically close to the populations of the Urals-Volga region; Khanty are intermediate between the Uralic and Siberian clusters, which reflects the complex historical interactions and mixing of genetic components. Thus, the aim of the study has been achieved; the findings extend understanding of the genetic history of the Ob Ugrians and emphasize the importance of the in-depth analysis of the Y chromosome haplogroup branches for reconstruction of historical processes in the region.

References

1. Post H, Németh E, Klima L, Flores R, Fehér T, Türk A, et al. Y-chromosomal connection between Hungarians and geographically distant populations of the Ural Mountain region and West Siberia. Scientific Reports. 2019; 9 (1): 7786.
2. Gemuev IN, i dr., redaktory. Narody Zapadnoj Sibiri: Hanty. Mansi. Sel'kupy. Nency. Jency. Nganasany. Kety. M.: Nauka, 2005; 804 s. Russian.
3. Sokolova ZP. Hanty i mansi. Vzgljad iz XXI veka. M.: Nauka, 2009; 755 s. Russian.
4. Tomilov NA. Tjurkojazychnoe naselenie Zapadno-Sibirskoj ravniny v konce XVI pervoj chetverti XIX vv. Izd-vo TGU. Tomsk, 1981; 276 s. Russian.
5. Bakieva GT, Kvashnin YuN. Tjurki, samodijcy i ugry v Tobol'skom Priirtysh'e (k voprosu ob jetnogeneze zabolotnyh tatar). Bol'she, chem jetnograf. Sbornik nauchnyh statej, posvjashhennyh pamjati professora V. V. Pimenova. M.: Izd-vo MGU, 2015. Russian.
6. Agdzhoyan AT, Balanovska EV, Padyukova AD, Dolinina DO, Kuznetsova MA, Zaporozhchenko VV, et al. Gene pool of Siberian Tatars: Five ways of origin for five subethnic groups. Molecular biology. 2016; 50: 860–73.
7. Karafet TM, Osipova LP, Gubina MA, Posukh OL, Zegura SL, Hammer MF. High Levels of Y-Chromosome Differentiation among Native Siberian Populations and the Genetic Signature of a Boreal Hunter-Gatherer Way of Life. Human Biology. 2002; 74 (6): 761–89.
8. Karafet TM, Osipova LP, Savina OV, Hallmark B, Hammer MF. Siberian genetic diversity reveals complex origins of the Samoyedic–speaking populations. American Journal of Human Biology. 2018; 30 (6): e23194.
9. Rootsi S, Zhivotovsky LA, Baldovič M, Kayser M, Kutuev IA, Khusainova R, et al. A counter-clockwise northern route of the Y-chromosome haplogroup N from Southeast Asia towards Europe. European Journal of Human Genetics. 2007; 15 (2): 204–11.
10. Pimenoff VN, Comas D, Palo JU, Vershubsky G, Kozlov A, Sajantila A. Northwest Siberian Khanty and Mansi in the junction of West and East Eurasian gene pools as revealed by uniparental markers. European Journal of Human Genetics. 2008; 16 (10): 1254–64.
11. Fehér T, Németh E, Vándor A, Kornienko IV, Csáji LK, Pamjav H. Y-SNP L1034: limited genetic link between Mansi and Hungarian-speaking populations. Molecular Genetics and Genomics. 2015; 290 (1): 377–86.
12. Ilumäe AM, Reidla M, Chukhryaeva M, Järve M, Post H, Karmin M, et al. Human Y Chromosome Haplogroup N: A Non-trivial Time-Resolved Phylogeography that Cuts across Language Families. The American Journal of Human Genetics. 2016; 99 (1): 163–73.
13. Dudás E, Vágó-Zalán A, Vándor A, Saypasheva A, Pomozi P, Pamjav H. Genetic history of Bashkirian Mari and Southern Mansi ethnic groups in the Ural region. Molecular Genetics and Genomics. 2019; 294 (4): 919–30.
14. Kharkov VN, Kolesnikov NA, Valikhova LV, Zarubin AA, Svarovskaya MG, Marusin AV, Khitrinskaya IY, Stepanov VA, i dr. Svjaz' genofonda hantov s narodami Zapadnoj Sibiri, Predural'ja i Altaja-Sajan po dannym o polimorfizme autosomnyh lokusov i Y-hromosomy. Vavilovskij zhurnal genetiki i selekcii. 2023; 27 (1): 46–54. Russian.
15. Karafet TM, Mendez FL, Meilerman MB, Underhill PA, Zegura SL, Hammer MF. New binary polymorphisms reshape and increase resolution of the human Y chromosomal haplogroup tree. Genome Research. 2008; 18 (5): 830–38.
16. Agdzhoyan AT, Ponomarev GYu, Salnikova AD, Lavryashina MB, Pylev VYu, Balanovskaya EV. Genofond obskih ugrov v kontekste narodonaselenija severnoj Evrazii: genogeografija vetvej gaplogruppy N Y-hromosomy. Kul'turnoe nasledie narodov Zapadnoj Sibiri: ugry. V sbornike: Materialy IX Vserossijskogo simpoziuma «Kul'turnoe nasledie narodov Zapadnoj Sibiri: ugry»; 8–9 dekabrja 2022 g.; Kirov: Izd-vo MCITO, 2023; s. 31–36. Russian.
17. Tree YTree v12.03.00 (cited 31 august 2024) Available from: https://www.yfull.com/sc/tree/
18. Balanovsky O, Rootsi S, Pshenichnov A, Kivisild T, Churnosov M, Evseeva I, et al. Two Sources of the Russian Patrilineal Heritage in Their Eurasian Context. The American Journal of Human Genetics. 2008; 82 (1): 236–50.
19. Koshel SM. Geoinformacionnye tehnologii v genogeografii. V knige: I. K. Lur'e, V. I. Kravcova, redaktory. Sovremennaja geograficheskaja kartografija. M.: Data+, 2012; s. 158–66. Russian.
20. Tambets K, Yunusbayev B, Hudjashov G, Ilumäe AM, Rootsi S, Honkola T, et al. Genes reveal traces of common recent demographic history for most of the Uralic-speaking populations. Genome Biology. 2018; 19 (1): 139.
21. Triska P, Chekanov N, Stepanov V, Khusnutdinova EK, Kumar GPA, Akhmetova V, et al. Between Lake Baikal and the Baltic Sea: genomic history of the gateway to Europe. BMC Genetics. 2017; 18 (S1): 110.
22. Wong EHM, Khrunin A, Nichols L, Pushkarev D, Khokhrin D, Verbenko D, et al. Reconstructing genetic history of Siberian and Northeastern European populations. Genome Research. 2017; 27 (1): 1–14.
23. Kharkov VN, Valihova LV, Yakovleva EL, Serebrova VN, Kolesnikov NA, Petelina TI, i dr. Rekonstrukcija proishozhdenija gydanskih nencev na osnove geneticheskogo analiza ih rodovoj struktury s pomoshh'ju novogo nabora YSTR-markerov. Genetika. 2021; 57 (12): 1403–14. Russian.
24. Pamjav H, Dudás E, Krizsán K, Galambos A. A Y-chromosomal study of mansi population from konda River Basin in Ural. Forensic Science International: Genetics Supplement Series. 2019; 7 (1): 602–03.

Литература

1. Post H, Németh E, Klima L, Flores R, Fehér T, Türk A, et al. Y-chromosomal connection between Hungarians and geographically distant populations of the Ural Mountain region and West Siberia. Scientific Reports. 2019; 9 (1): 7786.
2. Гемуев И. Н. и др., редакторы. Народы Западной Сибири: Ханты. Манси. Селькупы. Ненцы. Энцы. Нганасаны. Кеты. М.: Наука, 2005; 804 с.
3. Соколова З. П. Ханты и манси. Взгляд из XXI века. М.: Наука, 2009; 755 с.
4. Томилов Н. А. Тюркоязычное население Западно-Сибирской равнины в конце XVI первой четверти XIX вв. Изд-во ТГУ. Томск, 1981; 276 с.
5. Бакиева Г. Т., Квашнин Ю. Н. Тюрки, самодийцы и угры в Тобольском Прииртышье (к вопросу об этногенезе заболотных татар). Больше, чем этнограф. Сборник научных статей, посвященных памяти профессора В. В. Пименова. М.: Изд-во МГУ, 2015.
6. Агджоян А. Т., Балановская Е. В., Падюкова А. Д., Долинина Д. О., Кузнецова М. А., Запорожченко В. В. и др. Генофонд сибирских татар: пять субэтносов — пять путей этногенеза.

Молекулярная биология. 2016; 50 (6): 978–91.
7. Karafet TM, Osipova LP, Gubina MA, Posukh OL, Zegura SL, Hammer MF. High Levels of Y-Chromosome Differentiation among Native Siberian Populations and the Genetic Signature of a Boreal Hunter-Gatherer Way of Life. Human Biology. 2002; 74 (6): 761–89.
8. Karafet TM, Osipova LP, Savina OV, Hallmark B, Hammer MF. Siberian genetic diversity reveals complex origins of the Samoyedic–speaking populations. American Journal of Human Biology. 2018; 30 (6): e23194.
9. Rootsi S, Zhivotovsky LA, Baldovič M, Kayser M, Kutuev IA, Khusainova R, et al. A counter-clockwise northern route of the Y-chromosome haplogroup N from Southeast Asia towards Europe. European Journal of Human Genetics. 2007; 15 (2): 204–11.
10. Pimenoff VN, Comas D, Palo JU, Vershubsky G, Kozlov A, Sajantila A. Northwest Siberian Khanty and Mansi in the junction of West and East Eurasian gene pools as revealed by uniparental markers. European Journal of Human Genetics. 2008; 16 (10): 1254–64.
11. Fehér T, Németh E, Vándor A, Kornienko IV, Csáji LK, Pamjav H. Y-SNP L1034: limited genetic link between Mansi and Hungarian-speaking populations. Molecular Genetics and Genomics. 2015; 290 (1): 377–86.
12. Ilumäe AM, Reidla M, Chukhryaeva M, Järve M, Post H, Karmin M, et al. Human Y Chromosome Haplogroup N: A Non-trivial Time-Resolved Phylogeography that Cuts across Language Families. The American Journal of Human Genetics. 2016; 99 (1): 163–73.
13. Dudás E, Vágó-Zalán A, Vándor A, Saypasheva A, Pomozi P, Pamjav H. Genetic history of Bashkirian Mari and Southern Mansi ethnic groups in the Ural region. Molecular Genetics and Genomics. 2019; 294 (4): 919–30.
14. Харьков В. Н., Колесников Н. А., Валихова Л. В., Зарубин А. А., Сваровская М. Г., Марусин А. В. и др. Связь генофонда хантов с народами Западной Сибири, Предуралья и Алтая-Саян по данным о полиморфизме аутосомных локусов и Y-хромосомы. Вавиловский журнал генетики и селекции. 2023; 27 (1): 46–54.
15. Karafet TM, Mendez FL, Meilerman MB, Underhill PA, Zegura SL, Hammer MF. New binary polymorphisms reshape and increase resolution of the human Y chromosomal haplogroup tree. Genome Research. 2008; 18 (5): 830–38.
16. Агджоян А. Т., Пономарёв Г. Ю., Сальникова А. Д., Лавряшина М. Б., Пылёв В. Ю., Балановская Е. В. Генофонд обских угров в контексте народонаселения северной Евразии: геногеография ветвей гаплогруппы N Y-хромосомы. Культурное наследие народов Западной Сибири: угры. В сборнике: Материалы IX Всероссийского симпозиума «Культурное наследие народов Западной Сибири: угры»; 8–9 декабря 2022 г.; Киров: Изд-во МЦИТО, 2023; с. 31–36.
17. Tree YTree v12.03.00 (cited 31 august 2024) Available from: https://www.yfull.com/sc/tree/
18. Balanovsky O, Rootsi S, Pshenichnov A, Kivisild T, Churnosov M, Evseeva I, et al. Two Sources of the Russian Patrilineal Heritage in Their Eurasian Context. The American Journal of Human Genetics. 2008; 82 (1): 236–50.
19. Кошель С. М. Геоинформационные технологии в геногеографии. В книге: И. К. Лурье, В. И. Кравцова, редакторы. Современная географическая картография. М.: Дата+, 2012; с. 158–66.
20. Tambets K, Yunusbayev B, Hudjashov G, Ilumäe AM, Rootsi S, Honkola T, et al. Genes reveal traces of common recent demographic history for most of the Uralic-speaking populations. Genome Biology. 2018; 19 (1): 139.
21. Triska P, Chekanov N, Stepanov V, Khusnutdinova EK, Kumar GPA, Akhmetova V, et al. Between Lake Baikal and the Baltic Sea: genomic history of the gateway to Europe. BMC Genetics. 2017; 18 (S1): 110.
22. Wong EHM, Khrunin A, Nichols L, Pushkarev D, Khokhrin D, Verbenko D, et al. Reconstructing genetic history of Siberian and Northeastern European populations. Genome Research. 2017; 27 (1): 1–14.
23. Харьков В. Н., Валихова Л. В., Яковлева Е. Л., Сереброва В. Н., Колесников Н. А., Петелина Т. И. и др. Реконструкция происхождения гыданских ненцев на основе генетического анализа их родовой структуры с помощью нового набора YSTR-маркеров. Генетика. 2021; 57 (12): 1403–14.
24. Pamjav H, Dudás E, Krizsán K, Galambos A. A Y-chromosomal study of mansi population from konda River Basin in Ural. Forensic Science International: Genetics Supplement Series. 2019; 7 (1): 602–03.

DESIGNING OF CUSTOM BARCODES FOR SEQUENCING ON THE MGI PLATFORM

Shmitko AO✉, Bulusheva IA, Vasiliadis IA, Suchalko ON, Syrko DS, Belova VA, Pavlova AS, Korostin DO

Pirogov Russian National Research Medical University, Russia

The MGI (MGI Tech Co. Ltd., China) next-generation sequencing platform, including the DNBSEQ-G50, -G400, and -T7 sequencers, is being actively adopted in research. Despite its widespread adoption, challenges persist in the form of limitations associated with the manufacturer's provided barcode set for library preparation. These limitations include constraints on the number of samples that can be concurrently sequenced, compatibility issues with barcodes from diverse or incomplete sets, and restrictions on the sample ratio. Purpose: to develop a universal method that allows sequencing of up to 252 samples simultaneously on a single sequencer lane, while eliminating barcode-related limitations. We proposed a “quad method” that provides 4 or 4*n*+2 equilibration of barcodes. This paper also delves into its comprehensive analysis, verification procedures, seamless integration into the sequencing process and validation of the method on the DNBSEQ G-400 platform. The quad method showed efficiency and reliability, allowing sequencing of up to 252 samples simultaneously without compromising data quality. The proposed method optimizes library preparation and improves the flexibility of sequencing on the MGI platform.

Keywords: DNBSEQ, MGI, BGI, NGS, custom barcodes, custom indexes, custom adapters

Funding: this research was funded by the grant №075-15-2019-1789 from the Ministry of Science and Higher Education of the Russian Federation allocated to the Center for Precision Genome Editing and Genetic Technologies for Biomedicine.

Author contribution: Shmitko AO — study planning, data collection, writing Original Draft Preparation; Bulusheva IA — methodology, data analysis, writing Original Draft Preparation; Vasiliadis IA, Suchalko ON, Syrko DS — data analysis, software, visualization; Belova VA — study planning, manuscript review and editing; Pavlova AS — data curation, data analysis, software; Korostin DO — conceptualization, supervision, methodology, manuscript review and editing.

✉ **Correspondence should be addressed:** Anna O. Shmitko
Ostrovityanova, 1/1, Moscow, 117997, Russia; annashmi97@gmail.com

Received: 15.08.2024 **Accepted:** 17.09.2024 **Published online:** 10.10.2024

DOI: 10.24075/brsmu.2024.040

РАЗРАБОТКА КАСТОМНЫХ БАРКОДОВ ДЛЯ СЕКВЕНИРОВАНИЯ НА ПЛАТФОРМЕ MGI

А. О. Шмитко✉, И. А. Булушева, Ю. А. Василиадис, О. Н. Сучалко, Д. С. Сырко, В. А. Белова, А. С. Павлова, Д. О. Коростин

Российский национальный исследовательский медицинский университет имени Н. И. Пирогова, Москва

Платформа секвенирования следующего поколения MGI (MGI Tech Co. Ltd., Китай), включающая секвенаторы DNBSEQ-G50, -G400 и -T7, активно внедряется в научные исследования. Однако сохраняются ограничения, связанные с использованием стандартных баркодов, в частности, на количество одновременно секвенируемых образцов и на соотношение их количества, а также присутствует проблема совместимости баркодов из разных или неполных сетов. Целью работы было разработать универсальный метод, позволяющий секвенировать до 252 образцов одновременно на одной дорожке секвенатора, с устранением ограничений, связанных с баркодами. Мы предложили «метод четверок», обеспечивающий уравновешивание баркодов по принципу 4 или 4*n*+2. Проведена проверка метода на соответствие требованиям к баркодам для секвенирования, а также валидация метода на платформе DNBSEQ G-400. Метод четверок показал эффективность и надежность, позволяет секвенировать до 252 образцов одновременно без снижения качества данных, он оптимизирует процесс подготовки библиотек и повышает гибкость секвенирования на платформе MGI.

Ключевые слова: кастомные баркоды, кастомные индексы, кастомные адаптеры, DNBSEQ, MGI, BGI, NGS

Финансирование: соглашение о предоставлении из федерального бюджета грантов в форме субсидий в соответствии с пунктом 4 статьи 78.1 Бюджетного кодекса Российской Федерации на осуществление государственной поддержки создания и развития центра геномных исследований мирового уровня «Центр высокоточного редактирования и генетических технологий для биомедицины» No 075-15-2019-1789 от 22.11.2019.

Вклад авторов: А. О. Шмитко — планирование исследования, сбор данных, подготовка рукописи; И. А. Булушева — методология, анализ данных, подготовка рукописи; Ю. А. Василиадис, О. Н. Сучалко, Д. С. Сырко — анализ данных, программное обеспечение, визуализация; В. А. Белова — планирование исследования, рецензирование и редактирование рукописи; А. С. Павлова — курация данных, анализ данных, программное обеспечение; Д. О. Коростин — концептуализация, супервизия, методология, рецензирование и редактирование рукописи.

✉ **Для корреспонденции:** Анна Олеговна Шмитко
ул. Островитянова, д. 1, с. 1, г. Москва, 117997, Россия; annashmi97@gmail.com

Статья получена: 15.08.2024 **Статья принята к печати:** 17.09.2024 **Опубликована онлайн:** 10.10.2024

DOI: 10.24075/vrgmu.2024.040

MGI Tech is a relatively new player in the NGS market, founded in 2016 as a subsidiary of BGI Group [1–3]. The company's first sequencing platform, the MGISEQ-2000, was introduced in 2017, followed by the MGISEQ-200RS and MGISEQ-T7 platforms. MGI produces a range of sequencers based on the DNA nanoball technology and cPAS sequencing [4]. It allows for sequencing in single-end or paired-end mode using single or dual barcode conditions. The technology involves barcoding of samples during the ligation of adapters containing barcode sequences. DNA library barcoding is necessary for labeling sequences from different biological samples and read identification during the transformation of temporary sequencing files into the commonly used fastq format. The length of MGI barcodes is 10 bp.

The standard kits for library preparation and sequencing with the mid-throughput sequencer DNBSEQ G-400 are designed for single-indexed sequencing, whereas the dual barcoding mode is optional and requires purchasing additional kits. Currently, MGI provides a kit that includes 96 barcode adapters for the ligation step in DNA library preparation for single-end sequencing. In addition, MGI lists 32 barcode sequences for synthesis.

The G-400 system is sensitive to nucleotide balance at each cycle of barcode sequencing, as the quality drastically

drops if the same position in the barcode sequences from the same lane is occupied by the same nucleotide. This explains why the barcode set from the same lane should meet the criteria for combining their sequences and enable generating compatible sets. The set of 96 adapters provided by MGI allows for forming 11 balanced sets (2 of 4, 8 of 8, and 1 of 24). In practice, however, it is often necessary to combine the samples containing barcodes from different sets, change the number of the samples loaded on a lane, and vary their ratio. In the laboratory routine, it is not uncommon to encounter scenarios where one or several DNA libraries fail to meet the quality control standards in the final stage. To address this issue, a flexible approach to combining samples simplifies the task of pooling libraries for loading to the lane. Additionally, the task of combining samples with different required amounts of output data, such as exomes with different coverage of ×200, ×100, must also be considered. Therefore, the manufacturer imposes limitations on the users of this platform, providing a small number of barcodes and sets, which thus prevents uncovering its true potential for sequencing. This may prove critical when selecting a sequencing platform. Custom solutions for various applications have been developed for the Illumina platform [5–7], whereas for the MGI platform, such solutions have not yet been provided.

We previously developed software that allows choosing the optimal combination of provided barcodes at various ratios and sample numbers for MGI adapter sets [8]. The updated software, including custom barcodes, is available in the GitHub repository (https://github.com/genomecenter/BC-store/tree/custom-adapter-sets). Other software for selecting a balanced ratio of barcodes, depending on the sequencing tasks, has been developed earlier for Illumina NGS Instruments [9–11].

The purpose of this paper is to present the algorithm we have developed, that can generate the required number of barcode sequences for a given study. Using this algorithm, we designed 252 barcodes, forming 63 balanced sets, each comprising 4 barcodes, and allowing any set to be combined with the others.

METHODS

Method formulation and barcode selection

The sequencer has limits in terms of the intensity of the registered signal from the fluorophores corresponding to the nucleotides. If the same position of barcodes contains the same nucleotide, the read quality significantly drops, leading to errors in barcode identification and further assigning reads to the samples [8]. Therefore, we had to design barcodes to generate the most balanced combinations. The algorithm of sequence design is based on the "quad method," which involves adding three barcodes obtained by the consecutive substitutions of bases to each barcode from the MGI set (Fig. 1A, B).

Following this method, each of the 96 barcodes can serve as a root barcode for its quad, resulting in generating 96 * 4 = 384 unique barcodes.

As the percentage of each base at each position is 25%, the resulting combination is perfectly balanced and guarantees the highest quality of sequencing.

Verification of compliance with the criteria

Validation of the compatibility based on the balance

As each quad is perfectly balanced, any number of quads can be combined with each other. The ratio between the quads in a pool can vary; however, the ratios between barcodes in each quad should be equal.

Furthermore, we checked whether it was possible to generate pools containing $4n + 2$ barcodes, where n is the number of quads. We checked the compatibility using the BC-Store software by combining 10 barcodes (as shown in Fig. 2). The nucleotide fraction of each nucleotide at any position in a pool of 10 barcodes has the highest and lowest deviations equal to 0.2 and 0.3, respectively, and meets the criteria for a balanced combination. This is still valid when any of the two barcodes from the same quad are added to *n* quads at a ratio equal to or lower than in quads.

Verifying the compatibility of barcodes based on a mismatch number

At the next step, all quads were checked for compatibility by the number of mismatches. Each sample labeled by a barcode had to be uniquely identified, so the barcode sequences of a certain length should not overlap with others. We selected a threshold of 4 mismatches, as all 96 10 bp barcodes provided by the manufacturer differ by more than 4 bases. The analysis also included the 999 verification MGI barcode (a 10bp technical sequence present in the original software's demultiplexing file). We constructed a graph of incompatible quads (S1 Fig.) and, using an adjacency matrix (S2 Fig.), we selected 63 quads (252 barcodes) compatible with each other based on the number of permitted mismatches (Fig. 3). The sequences of all 252 barcodes are listed in S1 Table.

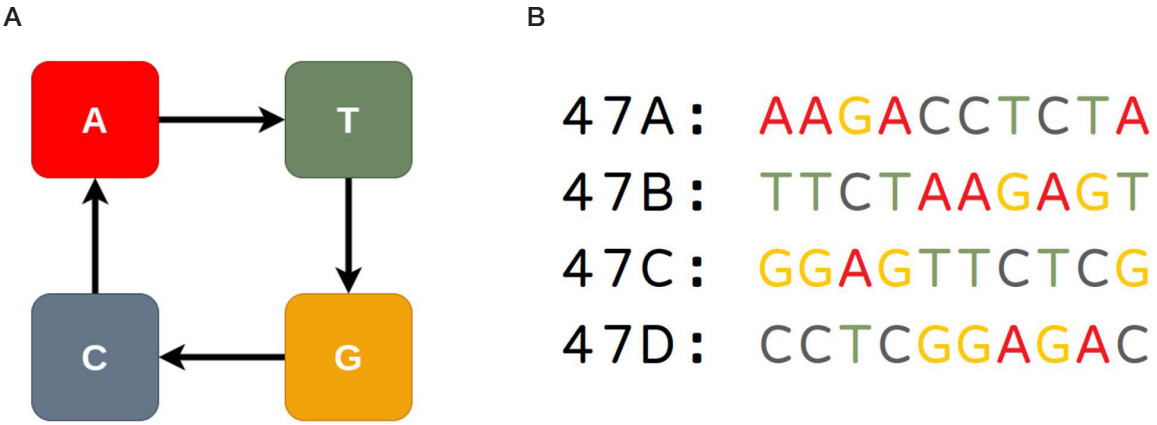

Fig. 1. A. The concept of the quad method. Each MGI barcode serves as a root for the quad, and custom barcodes are generated by sequential changes at each position of the original barcode: A→T, T→G, G→C, C→A. **B**. An example of a barcode quad. 47A is the original MGI barcode, and 47B, 47C, 47D are the custom barcodes generated using the quad method.

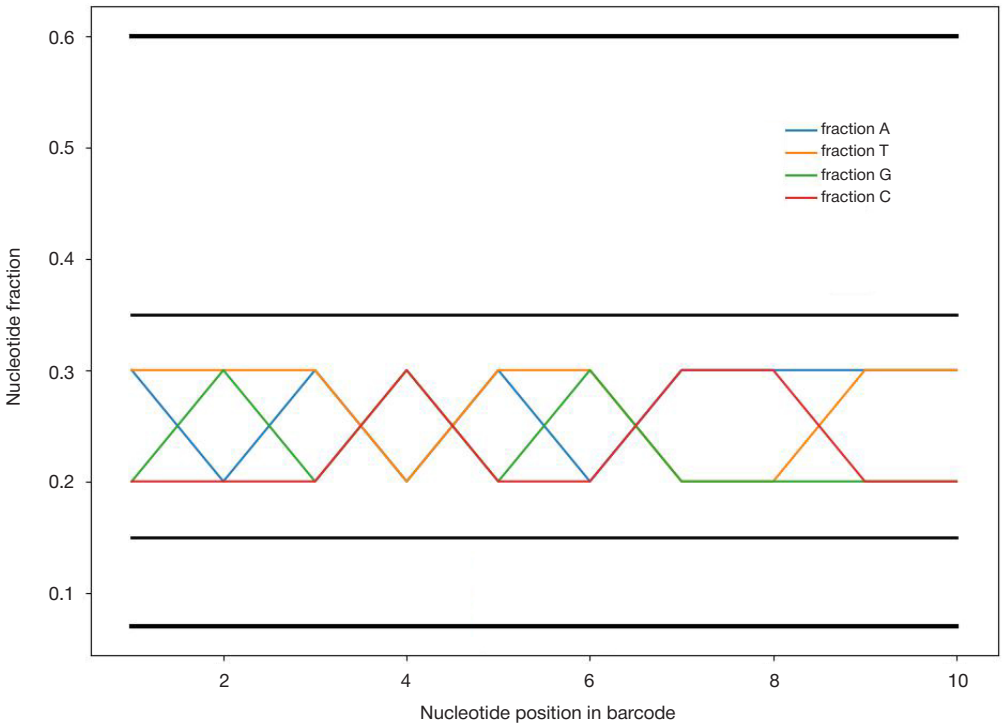

Fig. 2. The nucleotide balance in a pool of $4n + 2$ barcodes. The colored lines represent 295 the nucleotide fractions. The black strong lines represent the boundaries of the weak criterion. 296 The fine lines represent the boundaries of the strong criterion for barcode compatibility [8]

Validating the uniqueness

We checked if the sequences of the designed barcodes are present among the original MGI barcodes. This is necessary for generating the file containing barcodes for automatic demultiplexing. For this purpose, we created a Venn diagram showing the sets of custom and original MGI barcodes. We obtained 63 overlaps, where all 63 barcodes were original MGI barcodes, while the other 189 sequences were unique sequences not coinciding with the MGI barcodes from different kits (Fig. 4).

Preparation for sequencing

Adapter synthesis

According to the manufacturer's instructions, designing an individual adapter requires annealing two oligonucleotides.

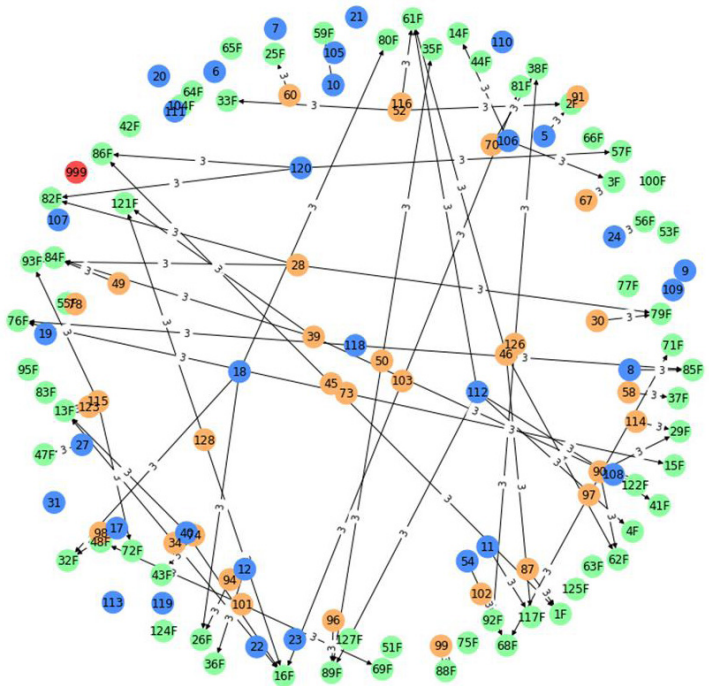

Fig. 3. The incompatibility graph showing 63 quads and MGI barcodes not included in 298 the quads. All quads that passed filtering based on the mismatch number are shown in green, 299 the barcodes from the set of 96 MGI barcodes not included in the quads are shown in orange, 300 the MGI barcodes from the set of 128 MGI barcodes are shown in blue, the 999- manufacturer 301 verification sequence is shown in red. The line connects the incompatible barcodes and quads; 302 the number above the line indicates the lowest number of mismatches between them

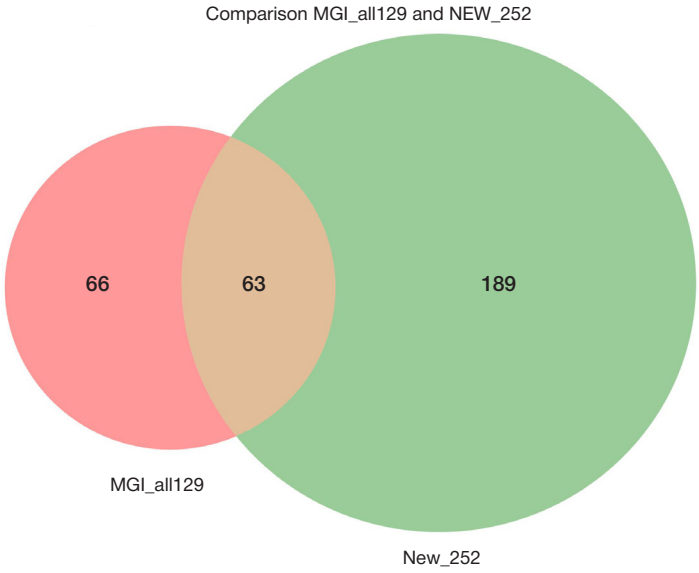

Fig. 4. Venn diagram for comparing the sequences of custom and original MGI barcodes from the 128 barcode set and 999 validation barcode provided by MGI. The custom barcodes are shown in green, the original MGI barcodes which do not overlap with quads are shown in red, and the MGI barcodes overlapping with quads (which were used as roots for the quads) are shown in orange

One of them (top oligonucleotide) contains the barcode sequence and a phosphate at the 5'-end (Ad153_5T_1-index # (1~128) according to the manufacturer), the sequence of bottom oligonucleotide is partially complementary to the top oligonucleotide (Ad153Ω_Bottom_2) (https://en.mgitech.cn/Download/download_file/id/71) [12].

The sequences of oligonucleotides containing the barcodes 1A-1D are shown in Table 1, all sequences containing 252 barcodes are listed in S1 Table.

The sequences of oligonucleotides containing the barcodes 1A-1D are shown in Table 1, all sequences containing 252 barcodes are listed in S1 Table.

To prepare the adapters, a mixture was created by adding 1 µL of 5M NaCl, 10 µL of 200 µM top oligonucleotide, and 10 µL of 200 µM bottom oligonucleotide to 79 µL of LowTE buffer. The mixture was then heated at 95 °C for 2 minutes and gradually cooled to 17°C at a rate of 0.5 °C every 30 seconds.

The algorithm of uploading new barcodes to a sequencer

To automatically demultiplex the sequenced libraries and following the MGI's recommendations, we created a .csv file (S2 Table) containing barcode sequences, including new custom barcodes, the original MGI barcodes, and 999-validation barcode. MGI barcodes that were included in the quads had an nA structure, where n is an adapter number in the original MGI kit, while custom barcodes had *n*B, *n*C, *n*D structure according to the order of quad formation. The format of the original MGI barcodes not included in quads remained unchanged. The barcode numbers were separated from the barcode sequences using commas without spaces.

RESULTS

To validate the designed barcodes, we prepared libraries with the synthesized custom adapters (Evrogen). The libraries, prepared following the standard MGI protocol, were pooled and enriched using the SureSelect Human All Exon v7 kit [13] and then sequenced in the PE100 mode using the DNBSEQ G-400 machine. Fastq demultiplexing was performed by the software built in G-400 provided by MGI basecalllite based on the uploaded file containing the barcode sequencing data. By default, the algorithm considers a read "undecoded" if there are two or more mismatches in a 10 bp barcode sequence. Therefore, the fraction of undecoded reads can be used as a quality metric for the performance of DIY barcode adapters. We compared the fraction of undecoded reads in the complete data from each lane with custom barcodes (44 lanes) and the data from previous runs (44 lanes) that employed MGI barcodes. On average (mean ± SD), the fractions of undecoded reads per lane were 1.08 ± 0.19% and 1.68 ± 0.22% for the MGI adapters and custom adapters, respectively (Fig. 5). Although the proportion of undecoded data increased when utilizing custom barcodes compared to the original barcodes (T = 13.5, df = 83, *p*-value = 1.17E-22), the absolute value relative to the total data output from a single lane is considered to be negligible. The values of undecoded and full data in GB are presented in S3 Table.

Thus, we have developed a viable approach for designing custom barcodes that allows for simultaneous sequencing of more than 96 samples on MGI called the 'quad method.' We obtained 189 custom barcodes that can be combined with the 63 MGI barcodes to generate 63 balanced quads. One barcode from each quad is an original MGI barcode (*n*A, where *n* is a number of an original barcode), and the other three are custom barcodes (*n*B, *n*C, *n*D) that complement it.

Table 1. The list of barcode sequences and full sequences of top and bottom oligonucleotides for adapter preparation. Ad_Bttm -bottom oligo

Name	Barcode/index sequence	Top oligo sequence
1A	TAGGTCCGAT	/5Phos/AGTCGGAGGCCAAGCGGTCTTAGGAAGACAATAGGTCCGATCAACTCCTTGGCTCACA
1B	GTCCGAACTG	/5Phos/AGTCGGAGGCCAAGCGGTCTTAGGAAGACAAGTCCGAACTGCAACTCCTTGGCTCACA
1C	CGAACTTAGC	/5Phos/AGTCGGAGGCCAAGCGGTCTTAGGAAGACAACGAACTTAGCCAACTCCTTGGCTCACA
1D	ACTTAGGTCA	/5Phos/AGTCGGAGGCCAAGCGGTCTTAGGAAGACAAACTTAGGTCACAACTCCTTGGCTCACA
Ad_Bttm		TTGTCTTCCTAAGGAACGACATGGCTACGATCCGACTT

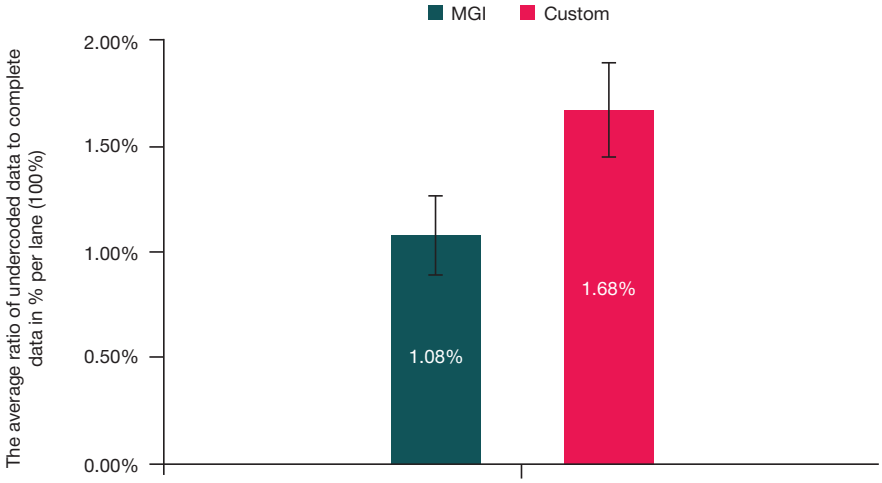

Fig. 5. The average ratio of undecoded reads (%) and complete data (Gb) per lane for 309 the libraries with MGI barcodes (in blue, data from 40 lanes) and with custom barcodes (red, 310 data from 7 lanes)

These quads can be combined with each other at any ratio and number as long as the ratio between the barcodes from the same quad remains equal. It is possible to create library pools with $4n + 2$ barcodes, where n is a number of quads, which can include any two barcodes from the other quad. In this case, the fraction of the last two barcodes should not exceed the fractions of the others.

DISCUSSION

The MGI platform is designed for fast, high-throughput sequencing, offering undeniable benefits yet prone to limitations. We attempted to overcome certain limits resulting from the solutions and kits provided by the manufacturer. Our approach allows for improving the efficiency of sequencing and expanding the possibilities of the MGI platform. However, it is important to bear in mind that the combinations of the quads with some original MGI adapters not included in the quads can fail to meet the compatibility criterion for the mismatch number. That is why we recommend checking whether they are balanced using the BC-Store software. We assume that a higher value of undecoded reads may be related to the insufficient purity of the synthesized oligonucleotides compared to MGI [14]. Previously, we ordered the synthesis of identical barcodes from two different manufacturers and observed that, in the case of one of them, the proportion of undecoded reads was elevated.

CONCLUSIONS

The custom barcodes we devised enable the alteration of the ratio and the number of libraries loaded to a lane depending on the purpose and required data amount. Using the BC-store software we had earlier developed, the libraries can be more easily and quickly pooled for sequencing on the MGI NGS instruments, both in paired-end or single-end modes. Therefore, given all the advantages and disadvantages of this method, it can be used as an additional or alternative solution to the solution provided by MGI.

References

1. Jeon SA, Park JL, Park SJ, Kim JH, Goh SH, Han JY, et al. Comparison between MGI and Illumina sequencing platforms for whole genome sequencing. Genes Genomics. 2021; 43: 713–24. DOI: 10.1007/s13258-021-01096-x.
2. Kim HM, Jeon S, Chung O, Jun JH, Kim HS, Blazyte A, et al. Comparative analysis of 7 short-read sequencing platforms using the Korean Reference Genome: MGI and Illumina sequencing benchmark for whole-genome sequencing. Gigascience. 2021; 10. DOI: 10.1093/gigascience/giab014.
3. Xu Y, Lin Z, Tang C, Tang Y, Cai Y, Zhong H, et al. A new massively parallel nanoball sequencing platform for whole exome research. BMC Bioinformatics. 2019; 20. DOI: 10.1186/s12859-019-2751-3.
4. Drmanac R, Sparks AB, Callow MJ, Halpern AL, Burns NL, Kermani BG, et al. Human genome sequencing using unchained base reads on self-assembling DNA nanoarrays. Science (1979). 2010; 327: 78–81. DOI: 10.1126/science.1181498.
5. Fadrosh DW, Ma B, Gajer P, Sengamalay N, Ott S, Brotman RM, et al. An improved dual-indexing approach for multiplexed 16S rRNA gene sequencing on the Illumina MiSeq platform. 2014. Available from: http://www.microbiomejournal.com/content/2/1/6.
6. Baym M, Kryazhimskiy S, Lieberman TD, Chung H, Desai MM, Kishony RK. Inexpensive multiplexed library preparation for megabase-sized genomes. PLoS One. 2015; 10. DOI: 10.1371/journal.pone.0128036.
7. Kozich JJ, Westcott SL, Baxter NT, Highlander SK, Schloss PD. Development of a dual-index sequencing strategy and curation pipeline for analyzing amplicon sequence data on the miseq illumina sequencing platform. Appl Environ Microbiol. 2013; 79: 5112–20. DOI: 10.1128/AEM.01043-13.
8. Bulusheva I, Belova V, Nikashin B, Korostin D. BC-store: A program for MGISEQ barcode sets analysis. PLoS One. 2021; 16. DOI: 10.1371/journal.pone.0247532.
9. Faircloth BC, Glenn TC. Not all sequence tags are created equal: Designing and validating sequence identification tags robust to indels. PLoS One. 2012; 7. DOI: 10.1371/journal.pone.0042543.
10. Trébeau C, De Monvel JB, Tai FWJ, Petit C, Etournay R. DNA Barcode Compatibility: An R-package for optimizing DNA-barcode combinations in multiplex sequencing experiments. Bioinformatics. 2019; 35: 2690–1. DOI: 10.1093/bioinformatics/bty1030.
11. Varet H, Coppée JY. CheckMyIndex: A web-based R/Shiny interface for choosing compatible sequencing indexes. Bioinformatics. 2019; 35: 901–2. DOI: 10.1093/bioinformatics/bty706.
12. Oligos and primers for BGISEQ/DNBSEQ/MGISEQ - MGI Tech. Available from: https://en.mgitech.cn/Download/download_file/id/71.
13. SureSelectXT HS Target Enrichment System For Illumina Multiplexed Sequencing Platforms, Version D1, July 2021. Available from: https://www.agilent.com/cs/library/usermanuals/public/G7530-90000.pdf.

14. Li Q, Zhao X, Zhang W, Wang L, Wang J, Xu D, et al. Reliable multiplex sequencing with rare index mis-assignment on DNB-based NGS platform. BMC Genomics. 2019; 20. DOI: 10.1186/s12864-019-5569-5.

Литература

1. Jeon SA, Park JL, Park SJ, Kim JH, Goh SH, Han JY, et al. Comparison between MGI and Illumina sequencing platforms for whole genome sequencing. Genes Genomics. 2021; 43: 713–24. DOI: 10.1007/s13258-021-01096-x.
2. Kim HM, Jeon S, Chung O, Jun JH, Kim HS, Blazyte A, et al. Comparative analysis of 7 short-read sequencing platforms using the Korean Reference Genome: MGI and Illumina sequencing benchmark for whole-genome sequencing. Gigascience. 2021; 10. DOI: 10.1093/gigascience/giab014.
3. Xu Y, Lin Z, Tang C, Tang Y, Cai Y, Zhong H, et al. A new massively parallel nanoball sequencing platform for whole exome research. BMC Bioinformatics. 2019; 20. DOI: 10.1186/s12859-019-2751-3.
4. Drmanac R, Sparks AB, Callow MJ, Halpern AL, Burns NL, Kermani BG, et al. Human genome sequencing using unchained base reads on self-assembling DNA nanoarrays. Science (1979). 2010; 327: 78–81. DOI: 10.1126/science.1181498.
5. Fadrosh DW, Ma B, Gajer P, Sengamalay N, Ott S, Brotman RM, et al. An improved dual-indexing approach for multiplexed 16S rRNA gene sequencing on the Illumina MiSeq platform. 2014. Available from: http://www.microbiomejournal.com/content/2/1/6.
6. Baym M, Kryazhimskiy S, Lieberman TD, Chung H, Desai MM, Kishony RK. Inexpensive multiplexed library preparation for megabase-sized genomes. PLoS One. 2015; 10. DOI: 10.1371/journal.pone.0128036.
7. Kozich JJ, Westcott SL, Baxter NT, Highlander SK, Schloss PD. Development of a dual-index sequencing strategy and curation pipeline for analyzing amplicon sequence data on the miseq illumina sequencing platform. Appl Environ Microbiol. 2013; 79: 5112–20. DOI: 10.1128/AEM.01043-13.
8. Bulusheva I, Belova V, Nikashin B, Korostin D. BC-store: A program for MGISEQ barcode sets analysis. PLoS One. 2021; 16. DOI: 10.1371/journal.pone.0247532.
9. Faircloth BC, Glenn TC. Not all sequence tags are created equal: Designing and validating sequence identification tags robust to indels. PLoS One. 2012; 7. DOI: 10.1371/journal.pone.0042543.
10. Trébeau C, De Monvel JB, Tai FWJ, Petit C, Etournay R. DNA Barcode Compatibility: An R-package for optimizing DNA-barcode combinations in multiplex sequencing experiments. Bioinformatics. 2019; 35: 2690–1. DOI: 10.1093/bioinformatics/bty1030.
11. Varet H, Coppée JY. CheckMyIndex: A web-based R/Shiny interface for choosing compatible sequencing indexes. Bioinformatics. 2019; 35: 901–2. DOI: 10.1093/bioinformatics/bty706.
12. Oligos and primers for BGISEQ/DNBSEQ/MGISEQ - MGI Tech. Available from: https://en.mgitech.cn/Download/download_file/id/71.
13. SureSelectXT HS Target Enrichment System For Illumina Multiplexed Sequencing Platforms, Version D1, July 2021. Available from: https://www.agilent.com/cs/library/usermanuals/public/G7530-90000.pdf.
14. Li Q, Zhao X, Zhang W, Wang L, Wang J, Xu D, et al. Reliable multiplex sequencing with rare index mis-assignment on DNB-based NGS platform. BMC Genomics. 2019; 20. DOI: 10.1186/s12864-019-5569-5.

CLINICAL POPULATION GENETIC STUDIES OF HEREDITARY DISEASES IN THE PEDIATRIC POPULATION OF NORTH OSSETIA – ALANIA

Zinchenko RA[1]✉, Tebieva IS[2,3], Kadyshev VV[1], Murtazina AF[1], Borovikov AO[1], Marakhonov AV[1], Perepelov AV[4], Getoeva ZK[5], Kutsev SI[1]

[1] Research Centre for Medical Genetics, Moscow, Russia
[2] North-Ossetian State Medical Academy, Vladikavkaz, Russia
[3] Republican Children's Clinical Hospital, Vladikavkaz, Russia
[4] Obninsk Institute for Nuclear Power Engineering, branch of the National Research Nuclear University (NRNU) MEPhI, Obninsk, Russia
[5] Center of Protection of Motherhood and Childhood of the City of Sochi of the Ministry of Health of Krasnodar Krai, Sochi, Russia

Currently, there is limited understanding about the cumulative prevalence, diversity, and frequency of distinct orphan hereditary diseases (OHDs) in the pediatric population, both within the Russian Federation and in the global literature. This gap exists despite a significant demand for such knowledge in healthcare and society. Variability and heterogeneity of the above indicators are common across different populations, reflecting significant genetic heterogeneity of OHDs. The study aimed to assess OHDs in the pediatric population of the Republic of North Ossetia – Alania (RNO-A). A total of 543,817 people were evaluated, including 145,560 children aged 0–18 years. The cumulative prevalence of autosomal recessive (AR), autosomal dominant (AD), and X-linked (XL) OHDs was determined. The findings indicate an overall prevalence of OHDs among children of the RNO-A of 1 : 119, meaning that approximately 1% of children are diagnosed with these conditions. Notably, the total burden in children of all types of OHDs in rural areas exceeds that in urban areas and district centers by more than twofold. We identified 1,241 patients from 1,037 families with 241 distinct OHDs (109 with AD inheritance, 102 with AR inheritance, and 30 with XL inheritance). Three diseases were particularly prevalent in this population and have not been documented in similar studies: congenital myasthenia type 12, a rare form of congenital adrenal cortex dysfunction (3-beta-hydroxysteroid dehydrogenase deficiency), and brachydactyly E — amelogenesis — mental retardation — nanism syndrome. Thus, the population of the RNO-A exhibits a unique spectrum of OHDs caused by rare mutations, some of which are infrequent in other populations of the world and the Russian Federation. The significantly higher prevalence of these disorders in rural populations is noteworthy, underscoring the need for tailored, region-specific programs aimed at preventing childhood disability and/or mortality.

Keywords: orphan hereditary diseases, cumulative prevalence of hereditary diseases among children, diversity of hereditary diseases common among children, Republic of North Ossetia–Alania, Russian Federation

Funding: the study was supported as part of the State Assignment of the Research Centre for Medical Genetics and the Ministry of Health of the Republic of North Ossetia–Alania.

Author contribution: Zinchenko RA, Tebieva IS, Kadyshev VV, Murtazina AF, Borovikov AO, Marakhonov AV, Getoeva ZK — patient examination, making the diagnosis, obtaining the informed consent, and biomaterial collection; Zinchenko RA, Tebieva IS — acquisition of data on the number of patients; Zinchenko RA, Tebieva IS, Kutsev SI — study planning, statistical analysis, manuscript writing; Marakhonov AV — analysis of molecular genetic tests; Tebieva IS, Marakhonov AV, Zinchenko RA — editing; Zinchenko RA, Kutsev SI — general management, editing.

Compliance with ethical standards: the study was approved by the Ethics Committee of the Research Centre for Medical Genetics (protocol No. 7 dated 20 December 2017), it was compliant with the standards of Good Clinical Practice and evidence-based medicine. All patients submitted informed consent to participate in the study.

✉ **Correspondence should be addressed:** Rena A. Zinchenko
Moskvorechie, 1, 115522, Moscow, Russia; renazinchenko@mail.ru

Received: 06.08.2024 **Accepted:** 20.09.2024 **Published online:** 17.10.2024

DOI: 10.24075/brsmu.2024.041

КЛИНИЧЕСКИЕ ПОПУЛЯЦИОННО-ГЕНЕТИЧЕСКИЕ ИССЛЕДОВАНИЯ НАСЛЕДСТВЕННЫХ БОЛЕЗНЕЙ СРЕДИ ДЕТСКОГО НАСЕЛЕНИЯ СЕВЕРНОЙ ОСЕТИИ – АЛАНИИ

Р. А. Зинченко[1] ✉, И. С. Тебиева[2,3], В. В. Кадышев[1], А. Ф. Муртазина[1], А. О. Боровиков[1], А. В. Марахонов[1], А. В. Перепелов[4], З. К. Гетоева[5], С. И. Куцев[1]

[1] Медико-генетический научный центр имени Н. П. Бочкова, Москва, Россия
[2] Северо-Осетинская государственная медицинская академия Министерства здравоохранения России, Владикавказ, Россия
[3] Республиканская детская клиническая больница, Владикавказ, Россия
[4] Обнинский институт атомной энергетики, филиал Федерального государственного автономного образовательного учреждения высшего образования «Национальный исследовательский ядерный университет «МИФИ», Обнинск, Россия
[5] Центр охраны материнства и детства г. Сочи Министерства здравоохранения Краснодарского края, Сочи, Россия

Современные знания о кумулятивной распространенности, разнообразии и частоте встречаемости отдельных орфанных наследственных болезней (ОНБ) среди детского населения ограничены в РФ и мировых исследованиях несмотря на широкую востребованность для здравоохранения и общества. Для ОНБ характерны изменчивость и неоднородность вышеперечисленных показателей для разных популяций, которая также проявляется в широкой генетической гетерогенности. Целью работы было изучение ОНБ среди детского населения Республики Северная Осетия – Алания (РСО-А). Обследовано 543 817 человек, в том числе 145560 детей (от 0 до 18 лет). Рассчитана кумулятивная распространенность аутосомно-рецессивной (АР), аутосомно-доминантной (АД) и Х-сцепленной (Х-сц.) наследуемой патологии. По полученным результатам, суммарная распространенность ОНБ среди детей РСО-А составляет 1 : 119, т. е. 1% детей имеет диагноз ОНБ. В сельской местности суммарная отягощенность детского населения всеми типами ОНБ более чем в 2 раза выше, чем в городах и районных центрах. Выявлен 1241 пациент (из 1037 семей) с 241 нозологической формой ОНБ (109 форм — с АД-наследованием, 102 — с АР и 30 — с Х-сц.). Особенностью обследованной популяции является высокая распространенность трех заболеваний, ранее не установленных в подобных исследованиях: врожденная миастения 12-го типа, редкая форма врожденной дисфункции коры надпочечников — дефицит 3-бета-гидроксистероиддегидрогеназы, синдром брахидактилии типа Е — амелогенеза — умственной отсталости — нанизма. Таким образом, население РСО-А характеризуется специфическим спектром ОНБ, обусловленных редкими мутациями, часть из которых редко встречается в других популяциях мира и РФ. Обращает на себя внимание более высокая распространенность данного спектра патологий в сельских популяциях. Выявленные показатели свидетельствуют о необходимости разработки специализированных регион-специфических программ для профилактики детской инвалидности и/или летальности.

Ключевые слова: орфанные наследственные заболевания, кумулятивная распространенность наследственных болезней среди детей, разнообразие частых наследственных болезней среди детей, Республика Северная Осетия – Алания, Российская Федерация

Финансирование: исследование выполнено при финансовой поддержке Государственного задания ФГБНУ «МГНЦ» Минобрнауки России и Минздрава РСОА.

Вклад авторов: Р. А. Зинченко, И. С. Тебиева, В. В. Кадышев, А. Ф. Муртазина, А. О. Боровиков, А. В. Перепелов, З. К. Гетоева — обследование пациентов, постановка диагноза, получение информированного согласия и забор биоматериала; Р. А. Зинченко, И. С. Тебиева — сбор данных о количестве пациентов; Р. А. Зинченко, И. С. Тебиева, С. И. Куцев — планирование исследования, выполнение статистического анализа, написание рукописи; А. В. Марахонов — анализ молекулярно-генетических исследований; И. С. Тебиева, А. В. Марахонов, Р. А. Зинченко — редактирование; Р. А. Зинченко, С. И. Куцев — общее руководство, редактирование.

Соблюдение этических стандартов: исследование одобрено этическим комитетом ФГБНУ Медико-генетический научный центр имени Н. П. Бочкова (протокол № 7 от 20 декабря 2017 г.), соответствует стандартам добросовестной клинической практики и доказательной медицины. Все пациенты подписали добровольное информированное согласие на участие в его проведении.

✉ **Для корреспонденции:** Рена Абульфазовна Зинченко
ул. Москворечье, д. 1, 115522, г. Москва, Россия; renazinchenko@mail.ru

Статья получена: 06.08.2024 **Статья принята к печати:** 20.09.2024 **Опубликована онлайн:** 17.10.2024

DOI: 10.24075/vrgmu.2024.041

According to the international OMIM database, the number of nosological forms of orphan hereditary diseases (OHDs) is about 7000–8000. The majority of these (more than 80%) are considered to be rare, i.e. the prevalence is less than 1 case per 1 million population [1]. A total of 10–20% of nosological forms fall on common OHDs, however, the number of patients with such disorders exceeds 60% [2, 3]. According to the research, the OHD burden on the population varies between 5–17 per 1000 people [4], and the pediatric population accounts for the major share (> 2%) due to the lower survival rate and adaptability of children with severe diseases. In 30% of cases, OHDs manifest at birth, while in 87% of cases these manifest by the end of puberty [5]. The issue of OHDs is very important for both healthcare and society in general since many cases of such disorders are characterized by high disability and mortality rates: at least 35% of childhood mortality in developed economies is associated with OHDs [2, 3].

Variability and heterogeneity of the OHD cumulative prevalence and diversity reported for various countries and populations, which are also manifested in genetic heterogeneity, are typical for OHDs [6]. Current knowledge about the genetic burden in human populations, diversity, prevalence, and heterogeneity of OHDs among children is scarce; the main reports issued both in Russia and abroad are focused on the analysis of data by hospitals or on certain ethnic populations [2, 7–16]. In the Russian Federation, the clinical population genetic studies of OHDs in the pediatric population involving recording of the maximum number of disorders in distinct federal entities are conducted only by the Research Centre for Medical Genetics and are under development. Differentiation of populations by both the prevalence of certain diseases and the cumulative prevalence of OHDs has been shown, which confirms the need to study each region in order to ensure the possibility of optimizing the region-specific care provided to patients [17–20].

The study aimed to assess OHDs in the pediatric population of the Republic of North Ossetia – Alania (RNO-A).

METHODS

We performed a medical genetic examination of the population of RNO-A. People of various age groups in all eight rural districts and the city of Vladikavkaz were examined in order to identify OHDs. The population survey was conducted in accordance with the examination protocol developed by the team of the Research Centre for Medical Genetics more than 40 years ago for small populations of the Russian Federation (populations of districts and towns) and tested in 15 Russian regions (110 rural districts) over this period. The protocol was published earlier [21–24]. Patients with congenital and presumably hereditary diseases were found via physicians and paramedical staff of medical institutions of the Republic using the questionnaire developed. The questionnaire represents the list of symptoms (neurological, ophthalmological, dermatological, skeletal, endocrinological, genetic, etc.) of various OHDs distributed across the main medical specialties. In addition to the lists obtained, we used the data from the medical and social examination service and from other medical and social sources. Given the fact that each symptom can be typical for more than one disease and is usually typical for a group of diseases, the entire clinical picture entails identifying the highest possible number of cases of OHDs (affecting both individual systems and multiple organs). Examination of families and patients of various age groups was performed during the meeting of experts in various medical specialties, which made it possible to identify a broad range of OHDs [20–24]. The diagnoses were verified by clinical, instrumental, and laboratory methods (biochemical, cytogenetic, molecular genetic, etc.).

The size of the actually examined population of the RNO-A (2017–2023) was 543,817 people, including 145,560 (26.77%) children aged 0–18 years (Table 1). Epidemiological analysis of OHDs in the pediatric population of the RNO-A was performed.

Considering the heterogeneity of many OHDs, we performed segregation analysis aimed to confirm certain inheritance types (autosomal dominant (AD), autosomal recessive (AR), or X-linked (XL)) showing that the resulting distribution was correct: $p = 0.27 \pm 0.06$ (expected value 0.25) for AR inheritance and $p = 0.49 \pm 0.04$ (expected value 0.5) for AD inheritance [25–26].

The cumulative prevalence, or genetic burden, of OHDs per 1000 examined individuals by populations was calculated using the following formula: $n / (N / 1000)$, where n was the number of affected individuals, and N was the number of children. The standard error of the OHD genetic burden values was calculated using the formula $((n / N) \times (1 - (n / N)) / N) / 0.5 \times 1000$, where n was the number of affected individuals, N was the number of children [25–26].

To analyze the OHD diversity, we compiled the list of diseases and calculated the disease prevalence (n / N) per 100,000 children. The genetic burden and prevalence of X-linked OHDs were calculated for boys. The genetic burden values were compared by the χ^2 method [17–26].

RESULTS

Cumulative prevalence of OHDs in pediatric population of the RNO-A

Comprehensive assessment of the population of the RNO-A resulted in the identification of 1241 patients (from 1037 families)

Table 1. Size of the population examined

№	District	Urban population		Rural population		Entire population	
		All	Children	All	Children	All	Children
1	Ardonsky	19 800	4296 (21.70%)	11 632	2700 (23.21%)	31 432	6996 (22.06%)
2	Pravoberezhny	37 029	13 147 (35.50%)	22 683	4224 (18.62%)	59 712	17 371 (29.09%)
3	Kirovsky	13 500	2374 (17.59%)	14 916	2655 (17.80%)	28 416	5029 (17.70%)
4	Alagirsky	20 950	5435 (25.94%)	16 577	2351 (14.18%)	37 527	7786 (20.75%)
5	Digorsky	11 072	2784 (25.14%)	9224	2200 (23.85%)	20 296	4984 (24.56%)
6	Irafsky	7700	2150 (27.92%)	7679	1650 (21.49%)	15 377	3800 (24.71%)
7	Prigorodny	10 067	2228 (22.13%)	43 361	9529 (21.98%)	53 428	11 757 (22.01%)
8	Mozdoksky	42 155	11 630 (27.59%)	48 089	10 469 (24.77%)	90 244	22 099 (24.49%)
9	City of Vladikavkaz	220 167	65 738 (29.86%)	–	–	220 167	65 738 (29.86%)
	total	378 873	114 782 (30.29%)	174 161	35 778 (19.08%)	543 817	145 560 (26.77%)

Table 2. Cumulative prevalence of hereditary diseases (per 1000 examined children) in pediatric populations of eight districts of the RNO-A and the city of Vladikavkaz

District/subpopulations	Population size	Genetic burden per 1000 children/boys*				Prevalence
		AD	AR	XL*	Total	
	Children from rural areas					
Ardonsky	2700	9.26 ± 1.84	6.30 ± 1.52	5.19 ± 1.96	20.37 ± 2.56	1 : 55
Pravoberezhny	4224	6.16 ± 1.20	6.16 ± 1.20	1.42 ± 0.82	13.73 ± 1.74	1 : 77
Kirovsky	2655	6.40 ± 1.55	6.40 ± 1.55	6.03 ± 2.12	18.83 ± 2.42	1 : 63
Alagirsky	2351	13.19 ± 2.35	7.23 ± 1.75	2.55 ± 1.47	22.97 ± 3.01	1 : 46
Digorsky	2200	10.00 ± 2.12	8.18 ± 1.92	1.82 ± 1.28	20.00 ± 2.92	1 : 52
Irafsky	1650	16.97 ± 3.18	10.30 ± 2.49	3.64 ± 2.09	30.91 ± 4.14	1 : 34
Prigorodny	9529	4.51 ± 0.69	4.41 ± 0.68	2.10 ± 0.66	11.02 ± 1.02	1 : 100
Mozdoksky	10469	7.55 ± 0.85	7.26 ± 0.83	2.29 ± 0.66	17.10 ± 1.23	1 : 63
Weighted average	35778	7.57 ± 0.46	6.43 ± 0.42	2.29 ± 0.66	16.69 ± 0.65	1 : 65
Pediatric populations of towns (district centers)						
Ardonsky (town of Ardon)	4296	7.22 ± 1.29	3.96 ± 0.96	1.86 ± 0.93	13.04 ± 1.68	1 : 83
Pravoberezhny (town of Beslan)	13147	2.36 ± 0.42	2.36 ± 0.42	0.76 ± 0.34	5.48 ± 0.62	1 : 196
Kirovsky (rural locality of Elkhotovo)	2374	5.05 ± 1.39	2.95 ± 1.11	2.53 ± 1.46	10.53 ± 1.97	1 : 108
Alagirsky (town of Alagir)	5435	4.42 ± 0.89	3.31 ± 0.78	2.58 ± 0.97	10.30 ± 1.28	1 : 111
Digorsky (town of Digora)	2784	5.39 ± 1.39	4.31 ± 1.24	1.44 ± 1.02	11.14 ± 1.92	1 : 96
Irafsky (rural locality of Chikola)	2150	4.65 ± 1.47	4.65 ± 1.47	0.93 ± 0.93	10.70 ± 2.17	1 : 102
Prigorodny	2228	3.14 ± 1.19	3.14 ± 1.19	2.10 ± 0.66	11.02 ± 1.02	1 : 149
Mozdoksky	11630	3.10 ± 0.52	2.32 ± 0.45	2.24 ± 0.62	7.65 ± 0.75	1 : 153
City of Vladikavkaz	65738	2.08 ± 0.18	2.49 ± 0.19	1.83 ± 0.24	6.40 ± 0.29	1 : 182
Weighted average	109782	2.76 ± 0.16	2.67 ± 0.16	1.75 ± 0.18	7.18 ± 0.24	1 : 159
Burden of the entire pediatric population of districts and towns						
Ardonsky	6996	8.00 ± 1.07	4.86 ± 0.83	3.14 ± 0.95	16.01 ± 1.43	2:09
Pravoberezhny	17371	3.28 ± 0.43	3.28 ± 0.43	0.92 ± 0.33	7.48 ± 0.63	3:22
Kirovsky	5029	5.57 ± 1.07	4.77 ± 0.97	4.37 ± 1.32	14.91 ± 1.58	2:19
Alagirsky	7786	7.06 ± 0.95	4.50 ± 0.76	2.57 ± 0.81	14.13 ± 1.28	1 : 78
Digorsky	4984	7.42 ± 1.22	6.02 ± 1.09	1.61 ± 0.80	15.05 ± 1.68	1 : 70
Irafsky	3800	10.00 ± 1.61	7.11 ± 1.36	2.11 ± 1.05	19.21 ± 2.10	1 : 55
Prigorodny	11757	4.25 ± 0.60	4.17 ± 0.59	1.87 ± 0.56	10.29 ± 0.89	1 : 107
Mozdoksky	22099	5.20 ± 0.48	4.66 ± 0.46	2.26 ± 0.45	12.13 ± 0.70	1 : 91
City of Vladikavkaz	65738	2.08 ± 0.18	2.49 ± 0.19	1.83 ± 0.24	6.40 ± 0.29	1 : 182
Weighted average	145560	3.94 ± 0.16	3.59 ± 0.16	1.98 ± 0.16	9.51 ± 0.24	1 : 117

with various nosological forms of OHDs, which accounted for 58.62% of the total number of affected individuals of various age groups identified in this region (2115 patients from 1489 families). We calculated the genetic burden of OHDs in the city of Vladikavkaz and eight rural districts of the RNO-A.

The cumulative prevalence (per 1000 children) of the main types of OHDs (AD, AR, and XL) in the pediatric population of the RNO-A (in the city of Vladikavkaz, Ardonsky, Pravoberezhny, Kirovsky, Alagirsky, Digorsky, Irafsky, Prigorodny, and Mozdoksky districts) was calculated (Table 2).

We revealed variability of cumulative prevalence by subpopulations between 5.48 ± 0.621 (1 : 196) in the town of Beslan and 30.91 ± 4.137 (1 : 34) in rural areas of the Irafsky District (Table 2). The analysis of 17 subpopulations showed that the cumulative prevalence of all types of OHDs in rural areas was more than twice higher compared to that in towns and district centers (χ^2AD = 54.35; χ^2AR = 48.89; χ^2XL = 29.46; χ^2Tot. = 136.18; d.f. = 16; $p < 0.05$), which is typical for populations of the Russian Federation [17–20].

The average prevalence in the surveyed sample was 1 : 117 children, i.e. about 1% of children were diagnosed with OHDs. This indicator varies widely: between 1 : 34 in rural areas of the Irafsky District (more than 2% of children) and 1 : 196 (0.5%) in the town of Beslan.

Comparative analysis of the cumulative prevalence of hereditary diseases among children in the surveyed pediatric populations of the Russian Federation

We conducted a comparative analysis of the cumulative prevalence of hereditary diseases among children in the surveyed pediatric populations of the Russian Federation, including the data reported for the RNO-A. It should be noted that the share of the total number of affected children among all the OHD patients identified was 58.62% (1241/2117, respectively), even though the share of the pediatric population in the Republic is 26.77%.

A comparison of the cumulative prevalence values reported for the AD, AR, and XL diseases in the pediatric population showed that the genetic burden of OHDs in children was higher in rural areas than in towns and district centers (Table 3). The analysis conducted showed differentiation and revealed

Table 3. Weighted average values of cumulative prevalence (genetic burden) of OHDs in pediatric populations of the rural areas, towns, and district centers by surveyed populations of Russia (per 1000 examined children) [17–20]

Subpopulations/regions	Population size	Genetic burden per 1000 children/boys*				Prevalence
		AD	AR	XL*	Total	
	Genetic burden in rural pediatric populations					
Kirov Region	17 032	6.22 ± 0.60	4.40 ± 0.51	2.35 ± 0.53	12.98 ± 0.83	1 : 85
Rostov Region	55 489	4.99 ± 0.29	3.78 ± 0.26	1.51 ± 0.23	10.29 ± 0.41	1 : 105
Karachay-Cherkessia	38 033	7.47 ± 0.44	5.52 ± 0.38	3.21 ± 0.41	16.20 ± 0.62	1 : 69
North Ossetia – Alania	35 778	7.57 ± 0.46	6.43 ± 0.42	2.29 ± 0.66	16.69 ± 0.65	1 : 65
Udmurt Republic	34 400	7.18 ± 0.46	4.24 ± 0.35	2.56 ± 0.39	13.98 ± 0.60	1 : 79
Republic of Bashkortostan	27 512	5.05 ± 0.43	2.51 ± 0.30	1.96 ± 0.38	9.52 ± 0.56	1 : 117
Republic of Tatarstan	49 612	4.37 ± 0.29	2.70 ± 0.23	1.09 ± 0.219	8.16 ± 0.39	1 : 131
Chuvash Republic	47 226	2.86 ± 0.25	2.22 ± 0.22	0.93 ± 0.19	6.01 ± 0.34	1 : 180
In all rural populations	305 082	5.49 ± 0.13	3.86 ± 0.11	1.91 ± 0.11	11.27 ± 0.18	1 : 97
Genetic burden in pediatric populations of towns and district centers						
Kirov Region	20 316	2.31 ± 0.34	1.58 ± 0.28	0.69 ± 0.26	4.58 ± 0.46	1 : 236
Rostov Region	46 356	1.68 ± 0.19	1.42 ± 0.16	0.43 ± 0.14	3.54 ± 0.27	1 : 301
Karachay-Cherkessia	52 706	3.57 ± 0.26	2.73 ± 0.23	1.25 ± 0.22	7.55 ± 0.36	1 : 144
North Ossetia – Alania	109 782	2.76 ± 0.16	2.67 ± 0.16	1.75 ± 0.18	7.18 ± 0.24	1 : 159
Udmurt Republic	23 248	2.84 ± 0.35	1.94 ± 0.29	1.20 ± 0.32	5.98 ± 0.48	1 : 186
Republic of Bashkortostan	32 685	1.90 ± 0.24	1.25 ± 0.19	1.16 ± 0.27	4.31 ± 0.34	1 : 268
Republic of Tatarstan	15 323	2.22 ± 0.38	1.89 ± 0.35	0.39 ± 0.23	4.50 ± 0.53	1 : 232
Chuvash Republic	20 637	1.45 ± 0.27	2.08 ± 0.32	0.48 ± 0.22	4.02 ± 0.43	1 : 265
In all urban populations	300 416	2.59 ± 0.09	2.16 ± 0.09	1.13 ± 0.08	5.89 ± 0.14	1 : 178
Genetic burden by regions						
Kirov Region	37 348	4.10 ± 0.33	2.86 ± 0.28	1.45 ± 0.28	8.41 ± 0.45	1 : 130
Rostov Region	101 845	3.49 ± 0.18	2.71 ± 0.16	1.02 ± 0.14	10.14 ± 0.73	1 : 149
KKarachay-Cherkessia	90 739	5.20 ± 0.23	3.90 ± 0.21	2.07 ± 0.21	11.17 ± 0.33	1 : 99
North Ossetia – Alania	145 560	3.94 ± 0.16	3.59 ± 0.16	1.98 ± 0.16	9.51 ± 0.24	1 : 117
Udmurt Republic	60 197	3.34 ± 0.23	1.83 ± 0.17	1.53 ± 0.23	6.69 ± 0.31	1 : 173
Republic of Bashkortostan	64 935	3.87 ± 0.24	2.51 ± 0.19	0.92 ± 0.17	7.30 ± 0.32	1 : 146
Republic of Tatarstan	57 648	5.43 ± 0.31	3.31 ± 0.24	2.01 ± 0.26	10.75 ± 0.4	1 : 103
Chuvash Republic	67 863	2.43 ± 0.19	2.18 ± 0.18	0.80 ± 0.15	5.41 ± 0.27	1 : 200
In all pediatric populations	626 135	3.97 ± 0.08	2.99 ± 0.07	1.53 ± 0.07	8.48 ± 0.11	1 : 130

the differences in this indicator between the rural and urban populations. In rural populations, the highest prevalence values were reported for the RNO-A (1 : 65), Karachay-Cherkessia (1 : 69), Udmurt Republic (1 : 79), Kirov Region (1 : 85), while the average value for rural areas was 1 : 97, i.e. more than 1% of children. As for towns and district centers, the prevalence ranged between 1 : 144 in Karachay-Cherkessia and 1 : 301 in the Rostov Region [17–20].

According to Table 3 and Figure, the average values of OHDs prevalence in the pediatric population of the RNO-A obtained in our study (1 : 117) are similar to the values reported for other regions of the Russian Federation we have assessed (1 : 103 for Tatarstan, 1 : 146 for Bashkortostan, 1 : 200 for the Chuvash Republic, 1 : 173 for the Udmurt Republic, 1 : 149 for the Rostov Region, 1 : 130 for the Kirov Region, 1 : 99 for the Republic of Karachay-Cherkessia). It is important that the average prevalence among children is 1 : 130, i.e. 1% of children are diagnosed with OHDs, which has to be taken into account when developing prevention programs and treatment programs for orphan diseases.

OHD diversity in pediatric population of the RNO-A

A total of 1241 patients with various OHD forms from 1037 families were identified in the pediatric population of the RNO-A. The diversity of OHDs is made up of 241 nosological forms: 109 ones with AD inheritance, 102 ones with AR inheritance, and 30 XL diseases. The largest number of affected individuals (n = 880, 70.91%) is reported for the group of 57 (23.65%) common OHD disease entities. In contrast, the smallest number (n = 87, 7.01%) is noted for the group of 87 (36.10%) rare diseases (Table 4).

The majority of diseases have been already found in the surveyed populations of the Russian Federation. Table 5 presents the diversity of common (with the prevalence exceeding 1 : 30 000) OHDs in the RNO-A, along with the average prevalence in seven previously assessed regions of European Russia (ER) and the disease prevalence according to the data of the international Orphanet database [6, 17–20].

High prevalence (per 100,000 children) of 11 diseases is the feature of the surveyed population: childhood myotonic

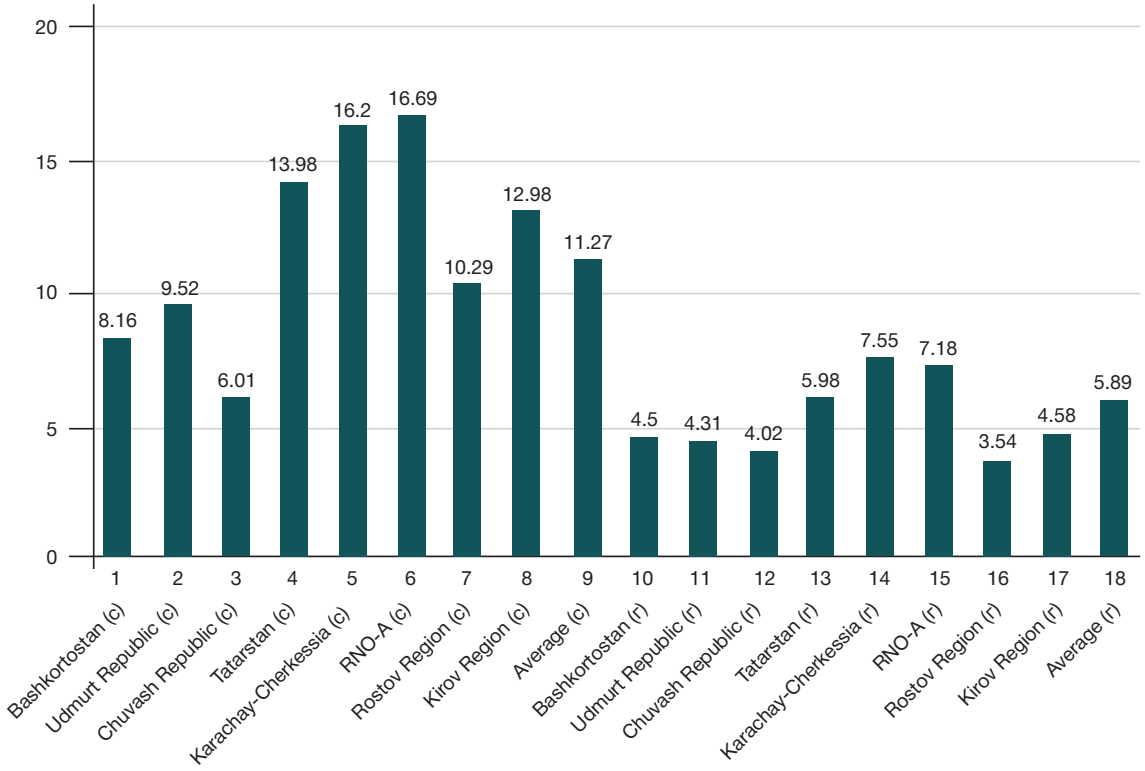

Fig. Cumulative prevalence of OHDs in urban and rural pediatric population of the surveyed regions of Russia

dystrophy — 6.87 (1 : 14.556), Duchenne muscular dystrophy — 37.10 (1 : 2696 boys), type I neurofibromatosis — 18.06 (1 : 7661), type 12 congenital myasthenia — 3.44 (1 : 29.112), congenital X-linked ichthyosis — 12.37 (1 : 8087 boys), fragile X syndrome — 9.62 (1 : 10,327 boys), Rett syndrome — 9.62 (1 : 12,130 boys), achondroplasia — 9.62 (1 : 10.397), AR deafness — 70.76 (1 : 1413), rare form of congenital adrenal hyperplasia due to 3-beta-hydroxysteroid dehydrogenase 2 deficiency — 6.18 (1 : 16.173). All patients with the above diseases were genotyped, and the locus and allelic heterogeneity were determined. The previously unreported brachydactyly E–amelogenesis–mental retardation–nanism syndrome showing high prevalence (11.28/100,000) was identified in four families. This syndrome was submitted to Orphanet, but it has not been mapped.

The prevalence of other diseases in the RNO-A was similar to that observed in other regions and aligned with the frequency reported in Europe as documented in Orphanet [6, 17–20]. However, we would like to note the high prevalence of undifferentiated intellectual developmental disorder with all types of inheritance (AD, AR, XL) in the RNO-A (13.74/100,000; 39.85/100,000 and 35.72/100,000 boys, respectively), the overall prevalence was 1 : 1400 children.

Thus, the OHD analysis conducted revealed regional specifics of the spectrum and showed the need to develop specific regional prevention programs.

DISCUSSION

In global practice, there is a limited number of studies focused on assessing the cumulative prevalence, diversity, and features of the spread of OHDs in pediatric populations [2, 7–16]. In the Russian Federation, such studies are conducted only by the team of the Research Centre for Medical Genetics. Assessment of the OHD cumulative prevalence in the pediatric population of the RNO-A revealed variability of this indicator in 17 subpopulations of the region: between 5.48 ± 0.621 (1 : 196) in the town of Beslan and 30.91 ± 4.137 (1 : 34) in rural areas of the Irafsky District. A more than 2-fold increase in genetic burden relative to the values reported for towns and district centers

Table 4. Distribution of patients and disease entities with OHDs depending on the disease prevalence

	Prevalence	Number (%) of affected individuals				Number (%) of diseases			
		AD	AR	XL	Σ	AD	AR	XL	Σ
1	1 : 30 000 and higher	379	388	113	880	23	23	11	57
		69.41%	70.93%	76.35%	70.91%	20.91%	22.33%	39.29%	23.65%
2	1 : 30 001 – 1 : 50 000	69	66	14	149	17	16	4	37
		12.64%	12.07%	9.46%	12.01%	15.45%	15.53%	14.29%	15.35%
3	1 : 50 001 – 1 : 100 000	52	52	21	125	24	23	13	60
		9.52%	9.51%	14.19%	10.07%	21.82%	22.33%	46.43%	24.90%
4	1 : 100 001 – and lower	46	41		87	46	41		87
		8.42%	7.50%		7.01%	41.82%	39.81%		36.10%
	TOTAL	546	547	148	1241	110	103	28	241

Table 5. Nosological spectrum and prevalence (per 100,000 children) of common hereditary diseases (with the prevalence exceeding 1 : 30,000) identified in the pediatric population of the RNO-A

№	№ OMIM	Diagnosis	I/T	N/P	Prevalence		
					RNO-A	ER	Orphanet
Hereditary neurological diseases							
1	162200	Neurofibromatosis, type I	AD	29	18.06	13.58	10–15
2	PS308350	Epileptic encephalopathy, early infantile	AD	8	5.5	2.56	n/d
3	PS191100	Tuberous sclerosis	AD	7	4.81	5.75	1–4
4	160900	Myotonic dystrophy	AD	10	6.87	2.4	1–9
5	PS156200	Intellectual developmental disorder, AD	AD	20	13.74	13.42	n/d
6	PS249500	Intellectual developmental disorder, AR	AR	58	39.85	39.45	n/d
7	PS309530	Intellectual developmental disorder, X-linked	XL	26	35.72	37.69	n/d
8	PS251200	Microcephaly, primary	AR	23	15.8	17.25	n/d
9	PS251280	Microcephaly, seizures with spastic quadriplegia	AR	7	4.81	4.95	n/d
10	610542	Myasthenia, congenital, 12	AR	5	3.44	н/д	0.1–0.9
11	PS117000	Congenital myopathy	AR	8	5.5	2.56	n/d
12	310200	Duchenne muscular dystrophy	XL	27	37.1	17.25	1–9
13	310376	Becker muscular dystrophy	XL	3	4.12	2.24	5.4–6
Hereditary eye diseases							
14 15	PS116200	Congenital hereditary cataract	AD, AR	15 11	10.31 7.56	10.54 8.15	n/d
16	231300	Glaucoma, primary open angle, congenital	AR	7	4.81	3.83	1–9
17	PS310700	Nystagmus, congenital, X-linked	XL	8	10.99	11.82	n/d
18	120200	Coloboma, ocular	AD	6	4.12	4.47	n/d
19	PS148300	Keratoconus	AD	5	3.44	1.12	n/d
20	PS268000	Retinitis pigmentosa	AR	5	3.44	2.4	10–50
Hereditary genodermatoses							
21	148700	Keratosis palmoplantaris	AD	15	11.68	13.89	2.5–50
22	146700	Ichthyosis vulgaris	AD	5	3.44	26.99	20–25
23	308100	Ichthyosis, X-linked	XL	9	12.37	15.01	10–50
24	PS305100	Ectodermal dysplasia	XL	3	4.12	2.24	0.1–1
Hereditary skeletal disorders							
25	100800	Achondroplasia	AD	14	9.62	5.43	
26	146000	Hypochondroplasia	AD	6	4.12	3.35	
27	185900	Syndactyly 1	AD	5	3.44	6.55	10–50
28	PS166200	Osteogenesis imperfecta	AD	9	6.18	7.51	10–50
29	181800	Scoliosis, idiopathic	AD	22	15.11	7.35	10–25
30	PS136760	Frontonasal dysplasia	AD	7	4.81	3.35	n/d
31	226900	Epiphyseal dysplasia, multiple, 4	AR	5	3.44	0.8	n/d
Hereditary syndromes							
32 33	PS130000	Ehlers–Danlos syndrome	AD AR	145 5	99.62 3.44	44.56 2.56	52
34	PS309510	Intellectual developmental disorder, X-linked syndromic	XL	12	16.49	3.83	n/d
35	PS119530	Orofacial cleft syndrome	AD	6	4.12	1.6	10–50
36	300624	Fragile X syndrome	XL	7	9.62	5.43	10–50
37	113477	Brachydactyly E syndrome, amelogenesis, growth retardation, intellectual developmental disorder (BOD syndrome)	AD	9	6.18	n/d	n/d
38	143500	Gilbert syndrome	AR	9	6.18	3.03	n/d
39	PS118100	Klippel–Feil syndrome	AD	6	4.12	2.4	
40	PS163950	Noonan syndrome	AD	5	3.44	4.95	10–50
41	PS180849	Rubinstein–Taybi syndrome	AD	5	3.44	1.92	
42	185300	Sturge–Weber syndrome	AD	5	3.44	4.31	1–9
43	312750	Rett syndrome	XL	6	8.24	4.15	1–9

Table 5. Ending

Other hereditary diseases							
44	PS220290	Deafness, autosomal recessive	AR	103	70.76	61.97	20–50
45	274400	Thyroid dyshormonogenesis 1	AR	25	17.18	11.34	
46	261600	Phenylketonuria	AR	40	24.94	22.02	
47	PS173900	Polycystic kidney disease 1	AD	20	13.74	4.63	10–50
48	PS262400	Growth hormone deficiency, isolated	AR	10	6.87	5.91	1–9
49	230400	Galactosemia	AR	12	8.24	2.56	n/d
50	219700	Cystic fibrosis	AR	12	8.24	7.35	10–50
51	201910	Adrenal hyperplasia, congenital, due to 21-hydroxylase deficiency	AR	11	7.56	3.51	1–9
52	201810	Adrenal hyperplasia, congenital, due to 3-beta-hydroxysteroid dehydrogenase 2 deficiency	AR	9	6.18	n/d	< 0.1
53	PS203200	Albinism, oculocutaneous, type II	AR	6	4.12	2.4	1–9
54	PS203100	Albinism, oculocutaneous, type IA	AR	5	3.44	5.59	1–9
55	608644	Thalassemia, beta	AR	5	3.44	0.8	n/d
56	306700	Hemophilia A	XL	9	12.37	12.14	1–9
57	306900	Hemophilia B	XL	3	4.12	1.92	1–9

Note: No. OMIM — numbers of diseases according to the international OMIM catalog by Dr. Victor A. McKusick; PS — phenotypic series of the diseases of heterogeneous group according to OMIM; I/T — inheritance type; N/P — number of patients; RNO-A — Republic of North Ossetia–Alania; ER — average disease prevalence values according to the genetic and epidemiological studies of pediatric population in European Russia; n/d — no data; the prevalence of X-linked diseases is represented by the number of boys.

was found in children living in rural areas of 17 subpopulations. Such a situation is observed in all seven pediatric populations previously surveyed in the Russian Federation [17–20].

The average OHD prevalence (1 : 117) in children of the RNO-A (Table 3 and Figure) obtained in this study is similar to the data on cumulative prevalence in the previously assessed regions of the Russian Federation (the values range between 1 : 200 in the Chuvash Republic and 1 : 99 in Karachay-Cherkessia). It is important to note that the average prevalence among children is 1 : 130, i.e. 1% of children are diagnosed with OHDs, which is consistent with the data provided in the reports of foreign colleagues [2, 3]. It is important for scientists, practical healthcare, and the society to emphasize that it is children, who constitute the share of the total number of patients with OHDs in the population: 58.62% of all patients identified in the Republic. The same situation is observed in other regions. The average share of pediatric patients with OHDs among all the patients identified in eight surveyed constituent territories of the Russian Federation was 43.5% (from 35% in the Kirov Region to 58% in the RNO-A), although the share of children in the surveyed regions varies between 17.80% in the Kirov Region and 26.77% in the RNO-A. Such a situation is due to the high mortality rate and decreased genotype fitness associated with a number of common OHDs [2, 3, 17–20].

The diversity of OHDs is made up of 241 diseases (109 AD, 102 AR, and 30 XL ones). The largest number of affected individuals (n = 880, 70.91%) is reported for the group of common (with the prevalence exceeding 1 : 30.000) OHD disease entities: 57 (23.65%). We have analyzed the spectrum of common OHDs and their prevalence in the RNO-A (Table 5); a comparison with the prevalence in seven previously surveyed regions of European Russia (ER) and the data deposited in the international Orphanet database has been conducted [6, 17–20].

High prevalence (per 100,000 children) of 11 diseases, three of which have not been previously reported in our studies (type 12 congenital myasthenia (GFPT1 gene) — 3.44 (1 : 29,112); the rare form found globally in 1% of patients with congenital adrenal cortex dysfunction (3-beta-hydroxysteroid dehydrogenase 2 deficiency — HSD3B2 gene) — 6.18 (1 : 16,173); brachydactyly E–amelogenesis–mental retardation–nanism syndrome — 11.28 (has not been mapped)), is the feature of the surveyed population.

We identified type 1 congenital myotonic dystrophy — 6.87 (1 : 14.556), associated with the trinucleotide repeat expansion in the DMPK gene, Duchenne muscular dystrophy — 37.10 (1 : 2696 boys), type I neurofibromatosis — 18.06 (1 : 7661), congenital X-linked ichthyosis — 12.37 (1 : 8087 boys), fragile X syndrome — 9.62 (1 : 10,327 boys), Rett syndrome — 9.62 (1 : 12,130 boys), achondroplasia — 9.62 (1 : 10,397), AR deafness — 70.76/100,000 (1 : 1413) showing high prevalence among children. All patients with the above diseases have been genotyped, the locus and allelic heterogeneity have been determined.

CONCLUSIONS

The population of the Republic of North Ossetia–Alania (RNO-A) is characterized by a specific spectrum of OHDs caused by rare mutations, some of which do not occur or are significantly less common in other populations of the world and the Russian Federation. The higher prevalence of this spectrum of diseases in rural populations attracts attention. The findings suggest the need to develop customized region-specific programs for the prevention of childhood disability. Given the fact that hereditary diseases in children are characterized by severe course and often lead to premature death, the development of methods to prevent such diseases constitutes the obligatory direction of reducing child mortality. In general, the data obtained during this study are important in practical terms; these also contribute to global science and fundamental epidemiological studies of OHDs.

References

1. Online Mendelian Inheritance in Man. Available from: http://www.ncbi.nlm.nih.gov/OMIM (data obrashhenija 31.07.2024)
2. Ferreira CR. The burden of rare diseases. Am J Med Genet. 2019; 179 (A): 885–92. DOI: 10.1002/ajmg.a.61124.
3. Wakap SN, Lambert DM, Olry A, et al. Estimating cumulative point prevalence of rare diseases: analysis of the Orphanet database. European Journal of Human Genetics. 2020; 28: 165–73. https://doi.org/10.1038/s41431-019-0508-0.
4. Passarge E. Color Atlas of Genetics. George Thieme Verlag Stuttgart. 5rd ed. New York, USA, 2017; 474 p.
5. Bochkov NP. Genetika v praktike pediatra. Pediatrija. 2004; 5: 13–18. Russian.
6. Orphanet Reports Series. Available from: http://www.orpha.net/ (data obrashhenija 31.07.2024).
7. McKusick VA. Ethnic distribution of disease in non-Jews. Israel J Med Sci. 1973; 9: 1375–82.
8. Dong-Dong Wu and Ya-Ping Zhang. Different level of population differentiation among human genes. BMC Evolutionary Biology. 2011; 11 (16). DOI: 10.1186/1471-2148-11–16.
9. Goodman RM. Genetic disorders among the Jewish people. Baltimor: The Gohn Hopkins Univ Press. 1980; p. 965–970.
10. Norio R. Finnish Disease Heritage I: characteristics, causes, background. Hum Genet. 2003; 112: 441–56.
11. Laberge Anne-Marie. Prevalence and distribution of genetic diseases in Quebec: impact of the past on the present. Medicine sciences. 2007; 23: 997–1001.
12. De Braekeleer M, Dao T-N. Hereditary disorders in the French Canadian population of Quebec. I. In search of founders. Hum Biol. 1994; 66: 205–24.
13. De Braekeleer M, Dao T-N. Hereditary disorders in the French Canadian population of Quebec. II. Contribution of Perche. Hum Biol. 1994; 66: 225–50.
14. Verheij JB, ten Kate LP. Mendelian phenotypes in the Netherlands. Hum Hered. 1993; 43: 223–31.
15. Zlotogora J, Patrinos GP. The Israeli National Genetic Database: a 10-year experience. Hum Genomics. 2017; 11: 5. DOI: 10.1186/s40246-017-0100-z.
16. Zlotogora J, Patrinos GP, Meiner V. Ashkenazi Jewish genomic variants: integrating data from the Israeli National Genetic Database and gnomAD. Genet Med. 2018; 20 (8): 867–71. DOI: 10.1038/gim.2017.193.
17. Bessonova LA, Elchinova GI, Zinchenko RA. Populjacionnaja genetika nasledstvennyh boleznej sredi detskogo naselenija Respublik Bashkortostan, Respublik Chuvashija i Udmurtija. Genetika. 2012; 48 (5): 644–54. Russian.
18. Zinchenko RA, Elchinova GI, Vetrova NV, Amelina MA, Petrin AN, Amelina SS. Jepidemiologija nasledstvennyh boleznej sredi detskogo naselenija 12 rajonov Rostovskoj oblasti. Otjagoshhennost' nasledstvennyh boleznej i geneticheskaja struktura populjacii. Medicinskaja genetika. 2013; 12 (5): 21–28. Russian.
19. Zinchenko RA, Vasileva TA, Elchinova GI, Petrova NV, Petrin AN, Ginter EK. Jepidemiologija nasledstvennyh boleznej sredi detskogo naselenija 8 rajonov Respubliki Tatarstan. Jakutskij medicinskij zhurnal. 2014; 2: 17–19. Russian.
20. Zinchenko RA, Kadyshev VV, Galkina VA, Dadali EL, Mihajlova LK, Marakhonov AV, i dr. Klinicheskaja populjacionnaja genetika nasledstvennyh boleznej sredi detskogo naselenija Karachaevo-Cherkesskoj Respubliki. Genetika. 2019; 55 (8): 964–71. DOI: 10.1134/S0016758190801860. Russian.
21. Zinchenko RA, Ginter EK, Marakhonov AV, et al. Epidemiology of rare hereditary diseases in European part of Russia: point and cumulative prevalence. Frontiers in Genetics. 2021; 12: 678957. Available from: https://doi.org/10.3389/fgene.2021.678957.
22. Ginter EK, Revazov AA, Talanov MI, i dr. Mediko-geneticheskoe izuchenie naselenija Kostromskoj oblasti: 2. Raznoobrazie nasledstvennoj patologii v pjati rajonah oblasti. Genetika. 1985; 21 (8): 1294–301. Russian.
23. Petrin AN, Ginter EK, Rudenskaja GI, i dr. Mediko-geneticheskoe izuchenie naselenija Kostromskoj oblasti. Soobshhenie 4. Otjagoshhennost' i raznoobrazie nasledstvennoj patologii v 5 rajonah oblasti. Genetika. 1988; 24 (1): 151–55. Russian.
24. Zinchenko RA, Makaov AKh, Marakhonov AV, et al. Epidemiology of hereditary diseases in Karachay-Cherkess Republic. International Journal of Molecular Sciences. 2020; 21 (1): 325. Available from: https://doi.org/10.3390/ijms21010325.
25. Cavalli-Sforza LL, Bodmer WF. The Genetics of Human populations. San Francisco, Freeman WH and Company, 1971; 965 p.
26. Morton NE. Genetic tests under incomplete ascertainment. Am J Hum Genet. 1959; 11: 1–16.

Литература

1. Online Mendelian Inheritance in Man. Available from: http://www.ncbi.nlm.nih.gov/OMIM (дата обращения 31.07.2024)
2. Ferreira CR. The burden of rare diseases. Am J Med Genet. 2019; 179 (A): 885–92. DOI: 10.1002/ajmg.a.61124.
3. Wakap SN, Lambert DM, Olry A, et al. Estimating cumulative point prevalence of rare diseases: analysis of the Orphanet database. European Journal of Human Genetics. 2020; 28: 165–73. https://doi.org/10.1038/s41431-019-0508-0.
4. Passarge E. Color Atlas of Genetics. George Thieme Verlag Stuttgart. 5rd ed. New York, USA, 2017; 474 p.
5. Бочков Н. П. Генетика в практике педиатра. Педиатрия. 2004; 5: 13–18.
6. Orphanet Reports Series. Available from: http://www.orpha.net/ (дата обращения 31.07.2024).
7. McKusick VA. Ethnic distribution of disease in non-Jews. Israel J Med Sci. 1973; 9: 1375–82.
8. Dong-Dong Wu and Ya-Ping Zhang. Different level of population differentiation among human genes. BMC Evolutionary Biology. 2011; 11 (16). DOI: 10.1186/1471-2148-11–16.
9. Goodman RM. Genetic disorders among the Jewish people. Baltimor: The Gohn Hopkins Univ Press. 1980; p. 965–970.
10. Norio R. Finnish Disease Heritage I: characteristics, causes, background. Hum Genet. 2003; 112: 441–56.
11. Laberge Anne-Marie. Prevalence and distribution of genetic diseases in Quebec: impact of the past on the present. Medicine sciences. 2007; 23: 997–1001.
12. De Braekeleer M, Dao T-N. Hereditary disorders in the French Canadian population of Quebec. I. In search of founders. Hum Biol. 1994; 66: 205–24.
13. De Braekeleer M, Dao T-N. Hereditary disorders in the French Canadian population of Quebec. II. Contribution of Perche. Hum Biol. 1994; 66: 225–50.
14. Verheij JB, ten Kate LP. Mendelian phenotypes in the Netherlands. Hum Hered. 1993; 43: 223–31.
15. Zlotogora J, Patrinos GP. The Israeli National Genetic Database: a 10-year experience. Hum Genomics. 2017; 11: 5. DOI: 10.1186/s40246-017-0100-z.
16. Zlotogora J, Patrinos GP, Meiner V. Ashkenazi Jewish genomic variants: integrating data from the Israeli National Genetic Database and gnomAD. Genet Med. 2018; 20 (8): 867–71. DOI: 10.1038/gim.2017.193.
17. Бессонова Л. А., Ельчинова Г. И., Зинченко Р. А. Популяционная генетика наследственных болезней среди детского населения Республик Башкортостан, Республик Чувашия и Удмуртия. Генетика. 2012; 48 (5): 644–54.
18. Зинченко Р. А., Ельчинова Г. И., Ветрова Н. В., Амелина М. А., Петрин А. Н., Амелина С. С. Эпидемиология наследственных болезней среди детского населения 12 районов Ростовской области. Отягощенность наследственных болезней и генетическая структура популяции. Медицинская генетика. 2013; 12 (5): 21–28.
19. Зинченко Р. А., Васильева Т. А., Ельчинова Г. И., Петрова Н. В.,

Петрин А. Н., Гинтер Е. К. Эпидемиология наследственных болезней среди детского населения 8 районов Республики Татарстан. Якутский медицинский журнал. 2014; 2: 17–19.
20. Зинченко Р. А., Кадышев В. В., Галкина В. А., Дадали Е. Л., Михайлова Л. К., Марахонов А. В., и др. Клиническая популяционная генетика наследственных болезней среди детского населения Карачаево-Черкесской Республики. Генетика. 2019; 55 (8): 964–71. DOI: 10.1134/S0016675819080186O.
21. Zinchenko RA, Ginter EK, Marakhonov AV, et al. Epidemiology of rare hereditary diseases in European part of Russia: point and cumulative prevalence. Frontiers in Genetics. 2021; 12: 678957. Available from: https://doi.org/10.3389/fgene.2021.678957.
22. Гинтер Е. К., Ревазов А. А., Таланов М. И. и др. Медико-генетическое изучение населения Костромской области: 2. Разнообразие наследственной патологии в пяти районах области. Генетика. 1985; 21 (8): 1294–301.
23. Петрин А. Н., Гинтер Е. К., Руденская Г. И. и др. Медико-генетическое изучение населения Костромской области. Сообщение 4. Отягощенность и разнообразие наследственной патологии в 5 районах области. Генетика. 1988; 24 (1): 151–55.
24. Zinchenko RA, Makaov AKh, Marakhonov AV, et al. Epidemiology of hereditary diseases in Karachay-Cherkess Republic. International Journal of Molecular Sciences. 2020; 21 (1): 325. Available from: https://doi.org/10.3390/ijms21010325.
25. Cavalli-Sforza LL, Bodmer WF. The Genetics of Human populations. San Francisco, Freeman WH and Company, 1971; 965 p.
26. Morton NE. Genetic tests under incomplete ascertainment. Am J Hum Genet. 1959; 11: 1–16.

LORI, A NEW RECOMBINANT RNase INHIBITOR FOR *IN VITRO* APPLICATIONS

Sukhov DA[1,2,3], Kholoshenko IV[1,4], Petrova TV[1], Romanenko GA[1,2], Myshkin MYu[3], Kost VYu[3], Trofimov DYu[1], Usman NYu[5] ✉, Barsova EV[3,5]

[1] DNA-Technology LLC, 117587, Moscow, Russia

[2] MIREA — Russian Technological University, Moscow, Russia

[3] Shemyakin-Ovchinnikov Institute of Bioorganic Chemistry RAS, Moscow, Russia

[4] Bauman Moscow State Technical University, Moscow, Russia

[5] Pirogov Russian National Research Medical University, Moscow, Russia

The novel ribonuclease inhibitor LoRI is a 63 kDa recombinant protein optimized for high-throughput expression in *E. coli* and purification by metal chelate affinity chromatography (IMAC). The product was obtained by N-terminal fusion of mouse placental RNase inhibitor polypeptide to a thioredoxin module. Advantage of the engineering strategy in terms of protein structure and function was predicted in silico. Under laboratory settings, the yield of purified soluble recombinant product was about 12 mg per 1 L of expression bacterial culture. By RNase inhibition capacity *in vitro*, the product is comparable or superior to a commercial reference. The kinetic data comply with Lineweaver-Burk model.

Keywords: ribonuclease inhibitor, thioredoxin, immobilized metal chelate affinity chromatography, Lineweaver–Burk model

Funding: The study was funded by DNA-Technology LLC.

Author contribution: Sukhov DA, Romanenko GA — protein engineering, expression and purification; Kholoshenko IV, Petrova TV — product characterization, writing; Myshkin MYu — protein structure analysis; Kost VYu — study design; Trofimov DYu — project supervision; Usman NYu — writing; Barsova EV — project coordination, writing.

✉ **Correspondence should be addressed:** Natalia Yu. Usman
Ostrovityanova 1/1, Moscow, 117997, Russia; n_usman@rambler.ru

Received: 02.09.2024 **Accepted:** 09.10.2024 **Published online:** 28.10.2024

DOI: 10.24075/brsmu.2024.043

НОВЫЙ РЕКОМБИНАНТНЫЙ ИНГИБИТОР РНКаз LORI ДЛЯ ПРИМЕНЕНИЯ *IN VITRO*

Д. А. Сухов[1,2,3], И. В. Холошенко[1,4], Т. В. Петрова[1], Г. А. Романенко[1,2], М. Ю. Мышкин[3], В. Ю. Кост[3], Д. Ю. Трофимов[1], Н. Ю. Усман[5] ✉, Е. В. Барсова[3,5]

[1] ООО «ДНК-Технология», Москва, Россия

[2] МИРЭА — Российский технологический университет, Москва, Россия

[3] Институт биоорганической химии имени М. М. Шемякина и Ю. А. Овчинникова, Москва, Россия

[4] Московский государственный технический университет имени Н. Э. Баумана, Москва, Россия

[5] Российский национальный исследовательский медицинский университет имени Н. И. Пирогова, Москва, Россия

Ингибиторы РНКазы давно используют в биотехнологии и лабораторной диагностике. Целью работы было получить и охарактеризовать новый рекомбинантный ингибитор РНКаз LoRI. Полученный новый ингибитор рибонуклеаз LoRI представляет собой рекомбинантный белок массой 63 кДа, оптимизированный для высокопроизводительной экспрессии в *E. coli* и очистки с помощью металлохелатной аффинной хроматографии (IMAC). Продукт получен за счет *N*-концевого слияния полипептидной последовательности плацентарного ингибитора РНКаз мыши с тиоредоксиновым модулем. Целесообразность данной модификации с точки зрения структуры и функции белка подтверждена *in silico*. Выход очищенного растворимого рекомбинантного продукта в лабораторных условиях составил около 12 мг на 1 л экспрессионной бактериальной культуры. По активности *in vitro* продукт сопоставим с коммерческим аналогом или превосходит его. Кинетические данные соответствуют модели Лайнуивера–Берка.

Ключевые слова: ингибитор рибонуклеаз, тиоредоксин, металлохелатная аффинная хроматография (IMAC), модель Лайнуивера–Берка

Финансирование: исследование выполнено при финансовой поддержке ООО «ДНК-Технология».

Вклад авторов: Д. А. Сухов, Г. А. Романенко — инженерия, экспрессия и очистка белков; И. В. Холошенко, Т. В. Петрова — характеризация продукта, написание статьи; М. Ю. Мышкин — анализ структуры белка; В. Ю. Кост — дизайн исследования; Д. Ю. Трофимов — руководство проектом; Н. Ю. Усман — написание статьи; Е. В. Барсова — координация проекта, написание статьи.

✉ **Для корреспонденции:** Наталья Юрьевна Усман
ул. Островитянова, д. 1/1, г. Москва, 117997, Россия; n_usman@rambler.ru

Статья получена: 02.09.2024 **Статья принята к печати:** 09.10.2024 **Опубликована онлайн:** 28.10.2024

DOI: 10.24075/vrgmu.2024.043

Specific proteins that directly inhibit cellular and extracellular ribonucleases (RNases) are expressed by various cell types and their overall physiological effect is cytoprotective [1]. Kinetic studies on RNase inhibition by these proteins used several model targets, notably RNase A and angiogenin — a secreted RNase with low catalytic activity, promoting vascularization [2]. Experiments with angiogenin and placental RNase inhibitor revealed a two-step binding mechanism, with rapidly formed loose complex of the two proteins E·I eventually tightened into stable E·I* complex by slow isomerization (k_2 = 97 s^{-1}) [3].

RNase inhibitors have long been used in biotechnology and laboratory diagnostics. The highly efficient RNase inhibition is essential for the accuracy of reverse transcription-based analytical methods, as underscored by the diagnostic experience during SARS-CoV2 pandemic [4]. Large-scale production of recombinant RNase inhibitors in bacterial systems is complicated due to redox sensitivity of these proteins [5] which may also impair their stability at storage.

Thioredoxins (Trx), small proteins found in all living cells, participate in redox control, which involves the electron retention capacity of cysteine residues in the active site of Trx. By sponging the electron flux from NADPH (catalyzed by Trx reductase) Trx stabilize activated thiolate groups in miscellaneous cellular proteins thereby protecting their

native, active state [6]. In protein engineering, the use of Trx as a covalently linked chaperone can substantively improve the yields of a redox-sensitive recombinant product without compromising its properties; the overall benefit will depend on details of both the expression system and the target product. In *E. coli*-based systems, a Trx fusion module may effectively prevent the product from being misfolded and sequestered to inclusion bodies. *E. coli* Trx transcripts are highly translated in authentic media thus supporting high yields of the chimeric protein; in addition, Trx has a robust tertiary structure and can be further modified for metal chelate purification [7].

This article describes production and characterization of a novel recombinant RNase inhibitor LoRI, constructed from the mouse placental RNase inhibitor polypeptide, supplemented with a thioredoxin module to enhance redox stability and a His tag for advanced purification by metal affinity chromatography (IMAC).

METHODS

Protein engineering

Murine ribonuclease inhibitor sequence retrieved from UniProt database (*M. musculus* Rnh1; Uniprot Q91VI7) was fused at the N-terminus to thioredoxin module (*E. coli* trxA; Uniprot P0AA25) via a linker comprising hexahistidine tag (6H), thrombin recognition site (LVPRGS), S-Tag (KETAAAKFERQH), and enterokinase recognition site (DDDDK):

MNHKVHMNSDKIIHLTDDSFDTDVLKADGAILVDFWAEWC
GPCKMIAPILDEIADEYQGKLTVAKLNIDQNPGTAPKYGIRGIPT
LLLFKNGEVAATKVGALSKGQLKEFLDANLAGSGSGHMHHH
HHHSSGLVPRGSGMKETAAAKFERQHMDSPDLGTDDDDKA
MSLDIQCEQLSDARWTELLPLIQQYEVVRLDDCGLTEVRCKDI
SSAVQANPALTELSLRTNELGDGGVGLVLQGLQNPTCKIQKLS
LQNCGLTEAGCGILPGMLRSLSTLRELHLNDNPMGDAGLKLL
CEGLQDPQCRLEKLQLEYCNLTATSCEPLASVLRVKADFKELV
LSNNDLHEPGVRILCQGLKDSACQLESLKLENCGITAANCKDL
CDVVASKASLQELDLSSNKLGNAGIAALCPGLLLPSCKLRTLW
LWECDITAEGCKDLCRVLRAKQSLKELSLASNELKDEGARLLC
ESLLEPGCQLESLWIKTCSLTAASCPYFCSVLTKSRSLLELQMS
SNPLGDEGVQELCKALSQPDTVLRELWLGDCDVTNSGCSSL
ANVLLANRSLRELDLSNNCMGGPGVLQLLESLKQPSCTLQQL
VLYDIYWTNEVEEQLRALEEERPSLRIIS*

In silico study used the AlphaFold 3 protein structure prediction model [8].

Molecular cloning and bacterial expression system

Codon optimization for *E. coli* was based on codon usage data retrieved from public sources (NCBI GenBank, Codon Usage Database). The nucleotide sequence was further adjusted manually to minimize the prevalence of GC-rich regions while preserving the encoded amino acid identity. De novo synthesis of the nucleotide sequence by assembly with partially overlapping oligonucleotides and subsequent amplification was ordered as a service from Evrogen JSC (Moscow, Russia) and performed according to original protocol by Dr. A. F. Fradkov in 2021.

The codon-optimized trxA-6H-Rnh1 DNA template was cloned into pET32 plasmid (Pharmacia). The construct was verified by Sanger sequencing. To potentiate expression of the active recombinant protein in *E. coli* system, electrocompetent *E. coli* BL21(DE3) (Novagen) were transformed with pGro7 chaperone plasmid (Takara Bio) to enable GroEL-ES assisted folding advisable for cysteine-rich recombinant products [9]. The obtained producer strain *E. coli* BL21(DE3)-pGro7 was transformed with the pET32-trxA-6H-Rnh1 construct.

Bacterial culture

The *BL21(DE3)-pGro7* producer strain transformed with the pET32-trxA-6H-Rnh1 expression plasmid was grown overnight at 37 °C in LB broth containing 10 g/L NaCl, 10 g/L tryptone and 5 g/L yeast extract, with ampicillin and chloramphenicol added to final concentrations of 100 μg/mL and 30 μg/mL, respectively. The culture was subsequently re-inoculated to a fresh flask with antibiotic-supplemented LB and incubated overnight at 37 °C/225 rpm. Next day, the pre-culture was diluted in LB supplemented with 2.5 mM $MgCl_2$ and grown in a F25L bioreactor (BioTechno Group; Russia) at 37 °C, 400 rpm, 0.6 bar and 0.25 m^3/h to exponential phase defined as OD_{600} = 0.5. At this point, the culture was induced with 1 g/L arabinose to activate the chaperone genes and allowed to grow at 37 °C to OD_{600} = 0.9. The temperature was subsequently reduced to 20 °C and the culture was induced with isopropyl β-d-1-thiogalactopyranoside (IPTG) at a final concentration of 1 mM. Twenty hours post-induction the cells were collected at 4,500 rpm in a Beckman Coulter Avanti™ J-15R centrifuge equipped with Beckman Coulter Avanti™ JS-4.750 rotor (Beckman Coulter; USA).

Protein extraction

A 50 g total yield of bacterial cells expressing Trx-RI fusion protein was resuspended in 10 v/v of Ni-A buffer solution (500 mM NaCl, 20 mM Tris-Cl, 10 mM Imidazole (ImH), 0.1% Tween 20, 10 mM 2-mercaptoethanol (2-bme); pH 7.6) with 1 mM PMSF and lysed with Q500 ultrasonic homogenizer (Qsonica, USA) set at amplitude 60, pulse on/off 05/05 s for 10 min on ice. The lysate was clarified by centrifugation in HERMLE Z-36HK equipped with HERMLE 12/035 rotor (HERMLE Labortechnik GmbH, Germany) at 21,000 rpm for 40 min. To precipitate soluble proteins, the clarified lysate was supplemented with 15% w/w $(NH_4)_2SO_4$ and centrifuged in HERMLE Z-36HK with HERMLE 12/035 rotor at 21,000 rpm for 10 min, then supplemented with 10% w/w $(NH_4)_2SO_4$ and centrifuged identically. The supernatant was discarded and the pellet was dissolved in 5 v/v of Ni-A. The purified protein solution was passed through a 0.22 μm polyethersulfone filter membrane (Vacuum Filtration „rapid"-Filtermax; TPP, Switzerland).

Chromatography

The filtered product was loaded onto an XK 26/20 chromatography column (Cytiva, USA) filled with Ni-INDIGO resin (Cube Biotech GmbH; Germany). The column volume (CV, 20 mL) was pre-equilibrated with 15 CV of Ni-A buffer at a rate of 5 mL/min. The loading proceeded at a rate of 4 mL/min. The loaded column was washed with 10 CV of Ni-A buffer. The elution used 5 CV of 0.5X Ni-B buffer and 5 CV of 1X Ni-B buffer (500 mM NaCl, 20 mM Tris-Cl, 500 mM ImH, 0.1% Tween 20, 10 mM 2-bme; pH 7.6) (Fig. 1).

The eluate was analyzed by 10% SDS–PAGE (Figure 2). Fractions containing the recombinant target product were pooled and dialyzed in Q-A buffer (20 mM Tris-Cl, 120 mM KCl, 0.1 % Tween 20, 10 mM 2-bme; pH 7.2) at 1:40 v/v for 12 h.

High-performance anion exchange chromatography II used a HiScale™ 16/10 column filled with Q Sepharose Fast Flow (CV=10 mL; Cytiva) pre-equilibrated with 15 CV of Q-A buffer.

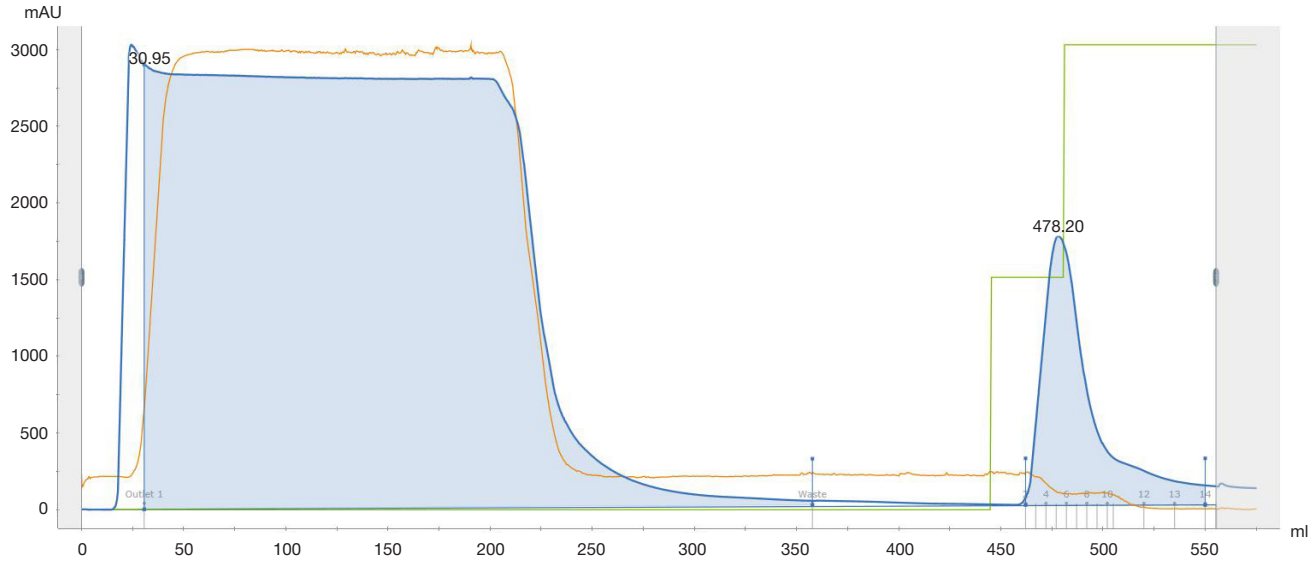

Fig. 1. Chromatography I profile (IMAC on Ni-INDIGO, Cube Biotech)

The filtered dialysate was loaded onto the column at a rate of 3 mL/min (Supplementary Fig. S1). The loaded column was washed with 10 CV of Q-A buffer. The elution used 20 CV of 0–15% Q-B buffer (20 mM Tris-Cl, 1 M KCl, 0.1% Tween 20, 10 mM 2-bme; pH 7.2).

Fractions of interest containing the recombinant product were determined by SDS–PAGE (7–26; Supplementary Fig. S2), pooled and dialyzed in storage buffer (50 mM KCl, 20 mM Hepes-K, 0.1 % Tween 20, 8 mM DTT, 50% Glycerol; pH 7.2) at 1:40 v/v for 12 h. After dialysis, concentration and purity of the product were assessed by spectrophotometry using Bradford method and by SDS–PAGE with bovine serum albumin as a standard (Supplementary Fig. S3). The stock was diluted to 1 mg/mL (15.75 μM) with storage buffer (pH = 7.0), aliquoted and stored at –25…–18 °C.

Commercial reference

Thermo Scientific™ RiboLock RNase Inhibitor 40 U/μL (#EO0381) was chosen as RNasin activity reference. Molecular weight of the protein, 49.6 kDa, was provided in the manufacturer's data. Concentration of the protein in supplied aliquots, 1 mg/mL (20.16 μM), was determined using Bradford method.

RNA substrates

Two types of RNA prep were used as substrates: (1) human total RNA isolated from HEK 293 cell cultures using ExtractRNA reagent (Evrogen; Russia); and (2) synthetic single-stranded RNA, 1.7 kb, obtained by transcription in vitro using HiScribe T7 High Yield RNA Synthesis Kit (NEB #E2040S). RNA concentrations were measured in NanoDrop™ 2000/2000c at 260/280 and 260/230 absorbance ratios; the integrity was verified by electrophoresis.

RNA stability assay

The ribonuclease inhibitor (RNasin) activity was assessed through extent of RNA degradation in the presence of RNase A.

Monarch® RNase A 20 mg/mL (NEB #T3018L) was selected as a model partner for the inhibitory binding. Working solution of the target was obtained by dilution of the stock with pure deionized water to 5 ng/μL. The RNase inhibition activity is

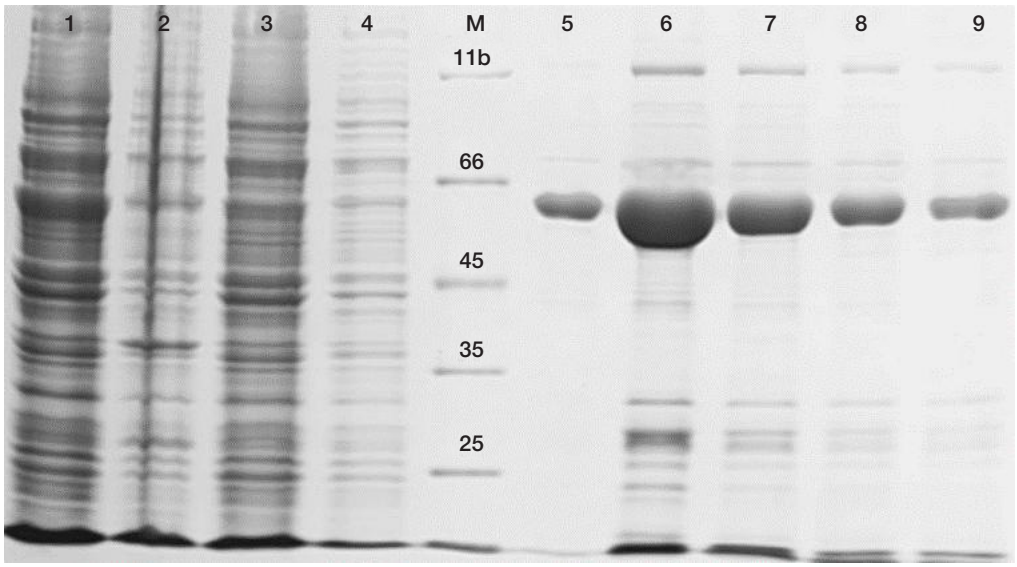

Fig. 2. Chromatography I samples, 10% SDS–PAGE. Lanes: 1 — supernatant; 2 — insoluble residue; 3 — flow-through; 4 — wash; M — protein molecular weight marker with band values, kDa, indicated in the image; 5–9 — eluted fractions 2, 5, 8, 10 and 11, respectively

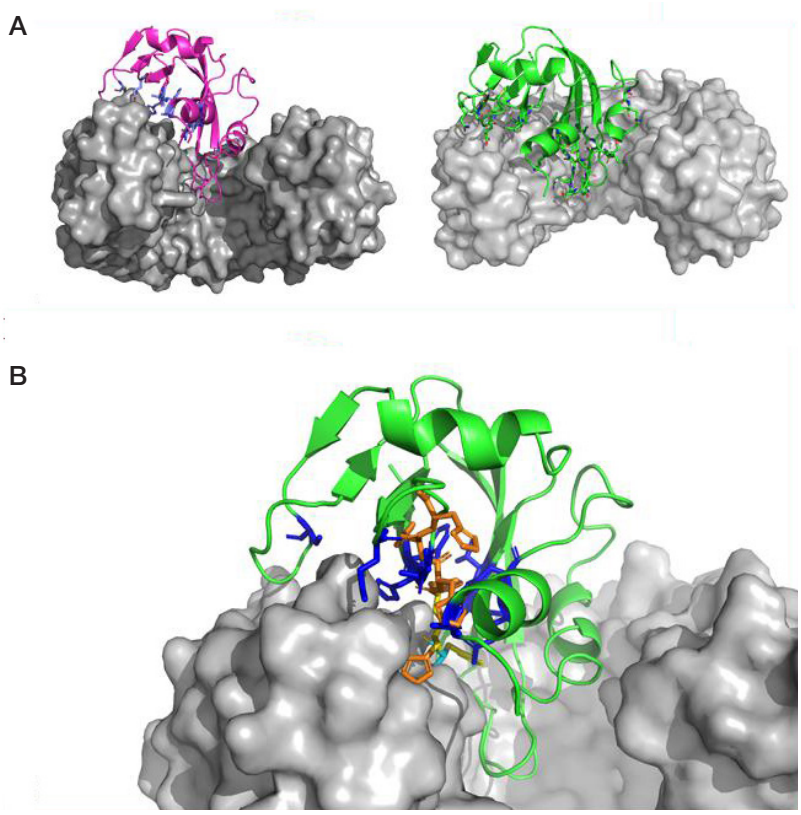

Fig. 3. Ribonuclease A (RibA) interacts with core inhibitor Rnh1 (grey surface). **A**. The enzyme contacts the inhibitor with its ligand-binding groove; the residues forming the active center are highlighted (PDB id: 1DFJ) [10]. **B**. Enlarged image of the C-terminus in close contact with residues of the active site in ribonuclease (blue) which sterically hinders the RNA binding. The histidine tag at the C-terminus (orange) disrupts the interaction by 'protruding' into RibA; overlay of AlphaFold3 model of Rnh1 with C-terminal His tag and crystal structure of Rnh1/RibA complex (PDB id: 1DFJ).

conventionally measured in units, with single unit corresponding to the amount of agent capable of reducing the activity of 5 ng of RNase A to 50% of initial value.

The reactions were set up in buffer (10 mM TrisHCl, 2 mM $MgCl_2$, 10 mM KCl, pH 8.0 at 25 °C) with 0.3–1.0 μg human total RNA, 2.5–5.0 ng RNase A and 0.0–4.0 μg inhibitor (LoRI or RiboLock). The inhibitor and the RNase were premixed and added to RNA. The 10 μL reaction mixtures were incubated under varying conditions, basically at 37 °C for 30 min, and analyzed by 1.2% agarose gel electrophoresis. The RNase A reaction was terminated by addition of 2-bme to 0.5 M and the mixtures were placed on ice or frozen. Before electrophoresis, the samples were mixed with gel loading buffer (#PB020; Evrogen). For reverse transcription, the aliquots were sampled before the addition of 2-bme and analyzed immediately.

Fluorimetry

The RNA stability was monitored by fluorimetry with Ribo488 RNA Quantification Reagent (product code 11510, Lumiprobe, Russia). Kinetic curves of RNA degradation were built using CLARIOstar® Plus microplate reader (BMG LABTECH, Germany) in AMC enzyme kinetics mode.

Specific activity assay used Lumiprobe QuDye ssDNA Reagent (product code 17102, Lumiprobe) with synthetic single-stranded RNA combined to 2.5 ng RNase A and 0.5–4.0 μg inhibitor in 40 μL reaction volume. The binding proceeded at 37 °C for 1 hour. The measurements were made in a Hidex Sense 425-311 microplate reader (HIDEX; Finland).

Kinetic study used human total RNA and Lumiprobe QuDye ssDNA Reagent. The mixtures were set up using 10X Reaction Buffer (300 mM TrisHCl, 50 mM $MgCl_2$, 500 mM KCl; pH 7.9-8.0 at 25 °C) with varying amounts of RNA (150, 300, 600 ng) and LoRI (1, 0.9, 0.8 μg — respectively, 197, 177, 157 nM in 80 μL reaction volume); the measurements were made in CLARIOstar® Plus. The reference Thermo Fisher™ RiboLock inhibitor was used in a final concentration of 252 nM. RNase A (5 ng per reaction) was used as a target; the RNase-free and inhibitor-free controls were included in the series, representing the intact substrate and the uninhibited enzymatic degradation samples, respectively.

PCR tests

RNA quantification by reverse transcription PCR used OneTube RT-PCR TaqMan setup (# SK031; Evrogen, Russia) with primers flanking a 130 bp fragment of *B2M* cDNA (5'-ATTATAACCCTA CATTTTGTG, 5'-TGTAAGCAGCATCATGGAGGTT, 0.2 μM each) and a TaqMan probe covering exon junction to exclude noise from residual genomic DNA (5'-FAM-GCCGCATTTGGATTGGATGAATTCCA-BHQ1, 0.1 μM).

PCR (non)inhibition tests used 5X qPCRmix-HS PCR setup (# PK145; Evrogen) with a FAM-BHQ1 TaqMan system. A 90 bp fragment of *GAPDH* was amplified from 100 pg of human genomic DNA in 25 μL reaction volume. All tests were run in 5 technical replicates in a BioRad CFX 96 real-time amplification instrument (BioRad; USA).

RESULTS

In silico structural study

The prototypical ribonuclease inhibitor Rnh1 has multiple leucine-rich repeat motifs and its overall folded shape resembles a horseshoe lined with negatively charged residues. Fig. 3A shows Rnh1 binding ribonuclease A (RibA), a small

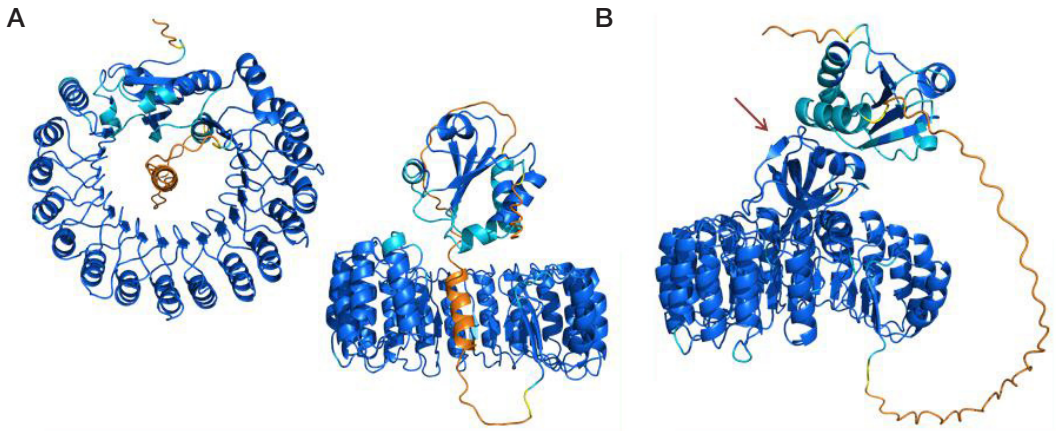

Fig. 4. AlphaFold3 models of Trx::Rnh1 fusion product. **A**. The product, native and unbound, comprising the horseshoe-shaped core inhibitor connected via linker to the compact Trx. The color scheme reflects predicted local distance difference test (pLDDT), a per-residue model confidence score provided by AlphaFold3, with pLDDT > 90, *blue*, high-confidence model; pLDDT 70–90, *light-blue*, high confidence for the backbone; pLDDT 50–70, *yellow* (low-confidence representation of a volatile structure); and pLDDT < 50, *orange*, region unstructured in isolation. Accordingly, the Rnh1 and Trx functional modules are imaged with high accuracy, whereas representation of the linker is conditional: it can be oriented and located differently e.g. outside the horseshoe. **B**. RibA (*arrow*) appears sandwiched between Trx and Rnh1 modules of the fusion product

protein of ~120 amino acids stabilized by four disulfide bonds. The binding involves C-terminal region of the inhibitor, notably positions V405, V428, Y430, D431, Y433 and E436 [10]. The inhibition mechanism is based on steric hindrance of the active site in RibA. Importantly, N-terminal region of the inhibitor does not participate in the interaction, which makes it a preferable location for a fusion point (especially since fusing Trx at the C-terminus would have excluded it as a cis chaperone module that should be already in place by the time of Rnh1 synthesis). Moreover, a His tag at the C-terminus was predicted to interfere with the ligand binding (Fig. 3B) which ultimately determined the engineering strategy.

Fig. 4A shows the Trx::Rnh1 fusion protein, with two compact functional modules of high prediction accuracy connected by loose, disordered linker. AlphaFold3 images of the Trx::Rnh1/RibA complex show close juxtaposition of Trx and RibA moieties during the interaction (Fig. 4B).

Thus, Trx module may stabilize the complex by 'pressing' RibA to the inhibitor. Electrostatically, the 'pressure' is favored by a negative surface potential on Trx. The estimated total charge of Trx module is –4, whereas the ribonuclease molecule has a total charge of +4 and electrostatically positive surface (to attract RNA) apart from a single cluster of negatively charged residues. In addition, Trx may act as an enzyme itself, opening the exposed disulfides in RibA and thereby disrupting its structure while bound to the inhibitor (Supplementary Fig. S4).

Yields

The design afforded a 3–5-fold increase in yields of soluble recombinant protein compared with unmodified Rnh1 sequence. The raw yields were estimated 2.7–3 mg of recombinant target per 1 g of E. coli biomass. The cumulative losses at all purification steps amounted to 25–30%. The yield

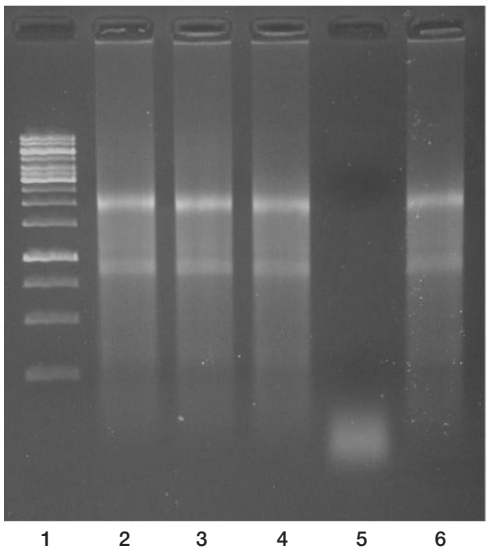

	2	3	4	5	6
RNase A	–	–	5 ng	5 ng	5 ng
LoRI		1 µg	1 µg	–	–
Thermo Scientific™ RiboLock	–	–	–	–	1 µg

Fig. 5. RNA stability assay, pilot series. Lane 1: Thermo Scientific™ GeneRuler 1kb DNA Ladder. Lanes 2–6: 1 µg RNA +. The treatment proceeded at 37 °C for 30 min.

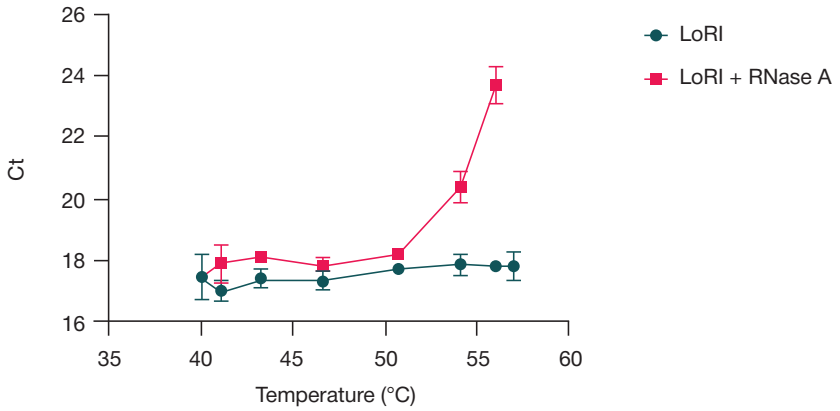

Fig. 6. Reverse transcription PCR data for RNA stability assay at 40–57 °C using 1 µg RNA + 2 µg LoRI with or without RNase A (2.5 ng), treatment time — 30 min

of purified active product under laboratory conditions was 2 mg per 1 g of *E. coli* biomass, or about 12 mg per 1 L of expression culture.

RNA stability assay

Pilot tests using 1 µg of human total RNA combined to 5 ng RNase A and 1 µg LoRI in 10 µL reaction volume revealed excellent protective properties of the product towards RNA (Fig. 5).

The effective temperature range of inhibition was determined using a 40–57 °C temperature gradient programmed in a thermal block. The setup used 1 µg of human total RNA combined to 2.5 ng RNase A and 2 µg LoRI in 10 µL reaction volume. For comparison, identical samples of total RNA + LoRI were incubated for 30 minutes at the same range of fixed temperatures without added RNase. The 30 min incubations were followed by collection of 1 µL aliquots for PCR tests of RNA integrity run immediately; the data are shown in Fig. 6. The remaining portions were 2-bme-treated and analyzed by electrophoresis (Fig. 7, Supplementary Fig. S5).

Alternative setups varying the reaction parameters are shown in Supplementary Figs. S6–S14. The data show that LoRI fully preserves RNA at temperatures up to 46.6 °C with further increase leading to partial RNA degradation. At 54.1 °C electropherograms show a diffuse smear shifted to a low-molecular-weight region (Fig. 7, lane 4), while Ct increases by 3 cycles corresponding to a one-order decrease in effective concentration of the 130 b template (Fig. 6). At 57.0 °C, the protective properties of LoRI are residual: electropherograms shows full degradation of the sample with ΔCt reaching 7 cycles compared with the initial value.

PCR (non)inhibition tests

The data indicate no change in PCR efficiency in the presence of up to 4.0 µg of LoRI in a 25 µl reaction volume (Supplementary Fig. S15).

Specific activity assay

Calibration curve for the assay is shown in Supplementary Fig. S16. Considering the linear response range of 0.1–0.6 µg, all measurements were performed with 1.0 µg RNA in order to improve the inhibition kinetics plot accuracy against Thermo Fisher™ RiboLock RNase Inhibitor (40 U/µL ~ 1 µg/µL) as a reference activity. Fluorescence measurements for excess of an inhibitor were accepted as 100%. Based on the data, 1 µg of LoRI was found to correspond to 50 U (Supplementary Fig. S17).

Comparative kinetic study

The Lineweaver-Burk graphical model assuming a mixed ribonuclease inhibition mechanism is shown in Supplementary Fig. S18.

The inhibition constant value, Ki, determined by the graphical representation approach was consistent with computational

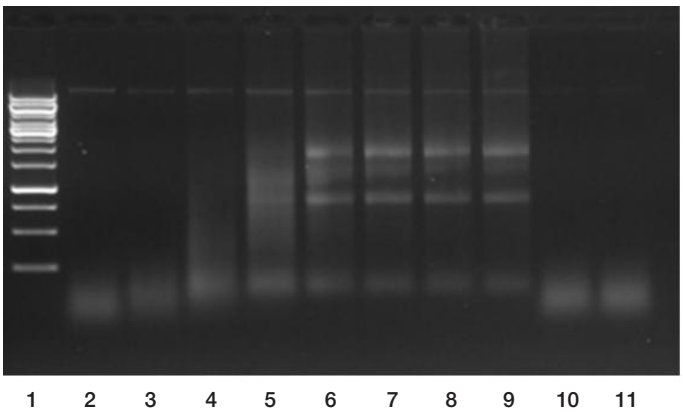

Fig. 7. RNA stability assay at 40–57 °C, treatment time— 30 min. Lane 1: Thermo Scientific™ GeneRuler 1kb DNA Ladder Lanes 2–9: 1 µg RNA + 2.5 ng RNase A + 2 µg LoRI at

2	3	4	5	6	7	8	9
57.0 °C	56.0 °C	54.1 °C	50.7 °C	46.6 °C	43.3 °C	41.1 °C	40.0 °C

Lanes 10–11: 1 µg RNA + 2.5 ng RNase A, no inhibitor added, incubated at 57.0 and 40.0 °C, respectively.

findings for the mixed inhibition model [11]. The calculated inhibition constant for LoRI towards RNase A constituted 0.825 pM. The approach was further applied to calculate the inhibition constant for Thermo Fisher™ RiboLock, which constituted 1.199 pM. According to the data, LoRI outperformed the reference activity in terms of inhibitory capacity associated with the formation of a low-dissociation enzyme-inhibitor complex.

DISCUSSION

The study was aimed at developing an RNase inhibitor for use in precision molecular medicine, in particular in diagnostic test systems based on reverse transcription PCR and library preparation for RNA sequencing. The proposed strategy of Trx fusion in combination with His-tagging was successful. The product is intended for a wide scope of research and diagnostic applications.

The growing demand for effective RNase inhibitors of molecular biological quality is related to the current interest in RNA as a key information carrier in molecular medicine and related medical biotechnology; the latest products include diagnostic kits, RNA vaccines, etc. The placental RNase inhibitor Rnh1 is an ideal prototype agent for preserving RNA isolated from cell cultures or tissues. A major obstacle to its industrial-scale production is redox-sensitivity: this leucine-rich repeat protein contains about 30 cysteine residues per molecule, all of which must be reduced to form SH groups and prevented from intramolecular disulfide bonding [12]. Overexpression of unmodified Rnh1 in *E. coli* is undermined by foreign redox environment, suboptimal synthesis rates and missing chaperone apparatus. The misfolded recombinant protein tends to irretrievably precipitate in the form of inclusion bodies. Klink et al (2001) overexpressed porcine inhibitor in *E. coli* using *trp* promoter and minimal growth medium to isolate ~10 mg of purified active product per liter of culture; typically for the time, purification used affinity chromatography with immobilized RNase A [13]. Another (historical) alternative was to isolate the inhibitor from fresh animal tissues; the approach yielded ~6 mg of inhibitor per kg of wet liver tissue using ribonuclease affinity chromatography followed by anion-exchange chromatography, and a similar amount from the placenta [14]. In modern realities, the RNase affinity chromatography is disadvantageous in terms of versatility and costs, especially concerning the risks of downstream trace contamination with RNase.

CONCLUSIONS

The use of Trx module as intramolecular chaperone in bacterial expression system afforded high yields of the mammalian prototype-based recombinant ribonuclease inhibitor in soluble active form after purification by IMAC. The product shows excellent RNA preservation properties under a broad range of conditions relevant to molecular research and laboratory diagnostics.

References

1. Thomas SP, Kim E, Kim JS, Raines RT. Knockout of the ribonuclease inhibitorgGene leaves human cells vulnerable to secretory ribonucleases. Biochemistry. 2016; 55 (46): 6359–62. DOI: 10.1021/acs.biochem.6b01003.
2. Abel RL, Haigis MC, Park C, Raines RT. Fluorescence assay for the binding of ribonuclease A to the ribonuclease inhibitor protein. Anal Biochem. 2002; 306 (1): 100–07. DOI: 10.1006/abio.2002.5678.
3. Lee FS, Shapiro R, Vallee BL. Tight-binding inhibition of angiogenin and ribonuclease A by placental ribonuclease inhibitor [published correction appears in Biochemistry 1989 Mar 7; 28 (5): 2354]. Biochemistry. 1989; 28 (1): 225–30. DOI: 10.1021/bi00427a031.
4. Nishibata Y, Koshimoto S, Ogaki K, Ishikawa E, Wada K, Yoshinari M, Ishizu A. RNase in the saliva can affect the detection of severe acute respiratory syndrome coronavirus 2 by real-time one-step polymerase chain reaction using saliva samples. Pathol Res Pract. 2021; 220: 153381. DOI: 10.1016/j.prp.2021.153381.
5. Šiurkus J, Neubauer P. Heterologous production of active ribonuclease inhibitor in Escherichia coli by redox state control and chaperonin coexpression. Microb Cell Fact. 2011; 10: 65. DOI: 10.1186/1475-2859-10-65.
6. Lee S, Kim SM, Lee RT. Thioredoxin and thioredoxin target proteins: from molecular mechanisms to functional significance. Antioxid Redox Signal. 2013; 18 (10): 1165–207. DOI: 10.1089/ars.2011.4322.
7. LaVallie ER, Lu Z, Diblasio-Smith EA, Collins-Racie LA, McCoy JM. Thioredoxin as a fusion partner for production of soluble recombinant proteins in Escherichia coli. Methods Enzymol. 2000; 326: 322–40. DOI: 10.1016/s0076-6879(00)26063-1.
8. Abramson J, Adler J, Dunger J, et al. Accurate structure prediction of biomolecular interactions with AlphaFold 3. Nature. 2024; 630: 493–500 DOI: 10.1038/s41586-024-07487-w.
9. Kyratsous CA, Silverstein SJ, DeLong CR, Panagiotidis CA. Chaperone-fusion expression plasmid vectors for improved solubility of recombinant proteins in Escherichia coli. Gene. 2009; 440 (1–2): 9–15. DOI: 10.1016/j.gene.2009.03.011.
10. Kobe B, Deisenhofer J. A structural basis of the interactions between leucine-rich repeats and protein ligands. Nature. 1995; 374 (6518): 183–6. DOI: 10.1038/374183a0.
11. Dixon M, Webb EC. Enzymes. 2nd Edition. New York: Academic Press, 1964.
12. Fominaya JM, Hofsteenge J. Inactivation of ribonuclease inhibitor by thiol-disulfide exchange. J Biol Chem. 1992; 267 (34): 24655–60.
13. Klink TA, Vicentini AM, Hofsteenge J, Raines RT. High-level soluble production and characterization of porcine ribonuclease inhibitor. Protein Expr Purif. 2001; 22 (2): 174–9. DOI: 10.1006/prep.2001.1422.
14. Dickson KA, Haigis MC, Raines RT. Ribonuclease inhibitor: structure and function. Prog Nucleic Acid Res Mol Biol. 2005; 80: 349–74. DOI: 10.1016/S0079-6603(05)80009-1.

Литература

1. Thomas SP, Kim E, Kim JS, Raines RT. Knockout of the ribonuclease inhibitorgGene leaves human cells vulnerable to secretory ribonucleases. Biochemistry. 2016; 55 (46): 6359–62. DOI: 10.1021/acs.biochem.6b01003.
2. Abel RL, Haigis MC, Park C, Raines RT. Fluorescence assay for the binding of ribonuclease A to the ribonuclease inhibitor protein. Anal Biochem. 2002; 306 (1): 100–07. DOI: 10.1006/abio.2002.5678.
3. Lee FS, Shapiro R, Vallee BL. Tight-binding inhibition of angiogenin and ribonuclease A by placental ribonuclease inhibitor [published correction appears in Biochemistry 1989 Mar 7; 28 (5): 2354]. Biochemistry. 1989; 28 (1): 225–30. DOI: 10.1021/bi00427a031.
4. Nishibata Y, Koshimoto S, Ogaki K, Ishikawa E, Wada K, Yoshinari M, Ishizu A. RNase in the saliva can affect the detection of severe acute respiratory syndrome coronavirus 2 by real-time one-step

polymerase chain reaction using saliva samples. Pathol Res Pract. 2021; 220: 153381. DOI: 10.1016/j.prp.2021.153381.
5. Šiurkus J, Neubauer P. Heterologous production of active ribonuclease inhibitor in Escherichia coli by redox state control and chaperonin coexpression. Microb Cell Fact. 2011; 10: 65. DOI: 10.1186/1475-2859-10-65.
6. Lee S, Kim SM, Lee RT. Thioredoxin and thioredoxin target proteins: from molecular mechanisms to functional significance. Antioxid Redox Signal. 2013; 18 (10): 1165–207. DOI: 10.1089/ars.2011.4322.
7. LaVallie ER, Lu Z, Diblasio-Smith EA, Collins-Racie LA, McCoy JM. Thioredoxin as a fusion partner for production of soluble recombinant proteins in Escherichia coli. Methods Enzymol. 2000; 326: 322–40. DOI: 10.1016/s0076-6879(00)26063-1.
8. Abramson J, Adler J, Dunger J, et al. Accurate structure prediction of biomolecular interactions with AlphaFold 3. Nature. 2024; 630: 493–500 DOI: 10.1038/s41586-024-07487-w.
9. Kyratsous CA, Silverstein SJ, DeLong CR, Panagiotidis CA. Chaperone-fusion expression plasmid vectors for improved solubility of recombinant proteins in Escherichia coli. Gene. 2009; 440 (1–2): 9–15. DOI: 10.1016/j.gene.2009.03.011.
10. Kobe B, Deisenhofer J. A structural basis of the interactions between leucine-rich repeats and protein ligands. Nature. 1995; 374 (6518): 183–6. DOI: 10.1038/374183a0.
11. Dixon M, Webb EC. Enzymes. 2nd Edition. New York: Academic Press, 1964.
12. Fominaya JM, Hofsteenge J. Inactivation of ribonuclease inhibitor by thiol-disulfide exchange. J Biol Chem. 1992; 267 (34): 24655–60.
13. Klink TA, Vicentini AM, Hofsteenge J, Raines RT. High-level soluble production and characterization of porcine ribonuclease inhibitor. Protein Expr Purif. 2001; 22 (2): 174–9. DOI: 10.1006/prep.2001.1422.
14. Dickson KA, Haigis MC, Raines RT. Ribonuclease inhibitor: structure and function. Prog Nucleic Acid Res Mol Biol. 2005; 80: 349–74. DOI: 10.1016/S0079-6603(05)80009-1.

NEUROIMAGING APPROACH TO IDENTIFICATION OF WORKING MEMORY BIOMARKERS IN PATIENTS WITH CHRONIC CEREBRAL ISCHEMIA

Fokin VF ✉, Ponomareva NV, Konovalov RN, Medvedev RB, Boravova AI, Lagoda OV, Krotenkova MV, Tanashyan MM

Research Center of Neurology, Moscow, Russia

Verbal working memory (VWM) is a fundamental function responsible for temporary storage and short-term handling of verbal information. The study was aimed to determine the working memory biomarker associated with imaging of the source of infra-slow electrical activity in patients with chronic cerebral ischemia (CCI). A total of 50 patients with CCI took part in the study: 16 males and 34 females aged 50–85 years. VWM was evaluated by the Luria test. The subjects were divided into two groups matched by age with the VWM below and above the average level for the studied sample. The infra-slow, below 0.1 Hz, electrical activity, otherwise known as the DC potentials (DCPs) of the brain, was recorded with five monopolar leads: frontal, central, occipital, right and left temporal. The resting state fMRI was used to analyze brain regions with the activated BOLD (blood-oxygen-level-dependent) signal that were associated with the brain regions responsible for VWM and the DCP generation sources recorded with the non-polarizable electrodes. The differences in BOLD signal activation and infra-slow activity amplitude were found in two VWM groups. These resting-state neural networks, VWM and the neural network responsible for DCP generation, overlapped in frontal regions. There were significant differences in DCP recorded with the frontal lead in two VWM groups (p = 0.00004). In patients with CCI, infra-slow activity, recorded with the frontal lead that is generated by the neural network fragment representing an intersection of the VWM network and the part of the brain responsible for DCP generation in the frontal region, is a VWM biomarker.

Keywords: chronic cerebral ischemia, verbal working memory, resting fMRI, infra-slow electrical activity, DC potential, overlapping resting neural networks

Funding: the study was supported by the RSF grant (No. 22-15-00448).

Author contribution: Fokin VF — manuscript writing; Ponomareva NV — design of physiological and neuropsychological tests, general study design; Konovalov RN — neuroimaging test design; Medvedev RB — Doppler tests; Boravova AI — psychophysiological tests; Lagoda OV — clinical tests; Krotenkova MV — neuroimaging test management; Tanashyan MM — clinical test management, general study design.

Compliance with ethical standards: the study was approved by the Ethics Committee of the Research Center of Neurology (protocol No. 5-6/22 dated 1 June 2022). The informed consent was submitted by all study participants.

✉ **Correspondence should be addressed:** Vitaly F. Fokin
Volokolamskoye shosse 80, Moscow, 125367, Russia; fvf@mail.ru

Received: 29.08.2024 **Accepted:** 16.09.2024 **Published online:** 30.09.2024

DOI: 10.24075/brsmu.2024.039

НЕЙРОВИЗУАЛИЗАЦИОННЫЙ ПОДХОД ДЛЯ ВЫЯВЛЕНИЯ БИОМАРКЕРОВ РАБОЧЕЙ ПАМЯТИ У БОЛЬНЫХ С ХРОНИЧЕСКОЙ ИШЕМИЕЙ МОЗГА

В. Ф. Фокин ✉, Н. В. Пономарева, Р. Н. Коновалов, Р. Б. Медведев, А. И. Боравова, О. В. Лагода, М. В. Кротенкова, М. М. Танашян

Научный центр неврологии, Москва, Россия

Вербальная рабочая память (ВРП) — фундаментальная функция, ответственная за временное хранение и краткосрочную работу с вербальной информацией. Целью работы было определить биомаркер рабочей памяти, связанный с нейровизуализацией источника сверхмедленной электрической активности у больных с хронической ишемией мозга (ХИМ). В исследовании приняли участие 50 пациентов с ХИМ: 16 мужчин и 34 женщины в возрасте 50–85 лет. ВРП оценивали по тесту Лурия. Испытуемые были разделены на две группы, не различающиеся по возрасту, с ВРП ниже и выше среднего уровня в исследованной выборке. Регистрировалась сверхмедленная, менее 0,1 Гц, электрическая активность, иначе называемая уровнем постоянного потенциала (УПП) головного мозга в пяти монополярных отведениях: лобном, центральном, затылочном, правом и левом височных. С помощью фМРТ покоя анализировали области мозга с активированным BOLD (blood-oxygen-level-dependent) сигналом и связанные с областями мозга, ответственными за ВРП и за источники генерации УПП, регистрируемые неполяризуемыми электродами. В двух группах ВРП найдены различия в активации BOLD-сигнала и амплитуде сверхмедленной активности. Эти нейросети покоя, ВРП и нейросеть, ответственная за генерацию УПП, пересекаются в лобных областях. УПП в лобном отведении достоверно различался в двух группах ВРП (p = 0,00004). Биомаркером ВРП у больных ХИМ является сверхмедленная активность, регистрируемая в лобном отведении и генерируемая тем участком нейросети, который является пересечением сети ВРП и участка мозга, ответственного за генерацию УПП в лобной области.

Ключевые слова: хроническая ишемия мозга; вербальная рабочая память, фМРТ покоя, сверхмедленная электрическая активность, уровень постоянного потенциала, пересекающиеся нейросети покоя

Финансирование: работа поддержана грантом РНФ №22-15-00448.

Вклад авторов: В. Ф. Фокин — написание статьи; Н. В. Пономарева — дизайн физиологических и нейропсихологических исследований, общий дизайн работы; Р. Н. Коновалов — дизайн нейровизуализационных исследований; Р. Б. Медведев — допплерографические исследования; А. И. Боравова — психофизиологические исследования; О. В. Лагода — клинические исследования; М. В. Кротенкова — руководство нейровизуализационными исследованиями; М. М. Танашян — руководство клиническими исследованиями, общий дизайн работы.

Соблюдение этических стандартов: исследование одобрено локальным этическим комитетом Научного центра неврологии (протокол №5-6/22 от 1 июня 2022 г.). Получено информированное согласие всех участников исследования.

✉ **Для корреспонденции:** Виталий Федорович Фокин
Волоколамское шоссе, д. 80, г. Москва, 125367, Россия; fvf@mail.ru

Статья получена: 29.08.2024 **Статья принята к печати:** 16.09.2024 **Опубликована онлайн:** 30.09.2024

DOI: 10.24075/vrgmu.2024.039

Verbal working memory (VWM) is a fundamental function responsible for temporary storage and short-term handling of verbal information that is necessary to solve a number of problems: reasoning, understanding, learning. Identification of VWM biomarkers can help us understand individual differences in cognitive ability, as well as diagnose and treat memory disorders [1]. The working memory deficit can also serve as an indicator of the cerebral disease process development. Functional magnetic resonance imaging (fMRI) studies revealed certain brain regions and networks involved in the VWM functioning, such as prefrontal cortex, parietal cortex, anterior cingulate cortex, hippocampus, etc., which can vary depending on the VWM assessment conditions, individual psychophysiological characteristics, and the disease type [2, 3]. In the prefrontal cortex, neurotransmitters dopamine and norepinephrine are involved in the VWM processes; these depend on the genes associated with dopamine receptors (for example, *DRD2*, *COMT*) and determine the working memory capacity and effectiveness [4]. fMRI and electrophysiological measurement, for example, performed when conducting the P300, N-back and other tests, provided valuable insights into neuronal activity associated with working memory and its capacity. Structural characteristics of the brain, such as grey matter volume and white matter integrity in the regions that support working memory (in the dorsolateral prefrontal cortex, anterior cingulate gyrus, etc.) can be correlated to the working memory indicators [5–6]. The VWM capacity decreases with aging; it is also reduced in individuals with neurodegenerative and vascular disorders, such as chronic cerebral ischemia (CCI) [2].

The widespread use of fMRI provided a separate source for the development of ideas about the neurovascular unit (NVU), the cellular complex ensuring interaction between the BOLD signal and the neuronal activity. NVU consists of neurons, glia, endothelial cells, and some other components [7–8]. The processes that ensure working memory result in the NVU activation, due to which increased activity of BOLD signals, neuronal responses, and infra-slow activity shifts are observed. In the Russian literature, the term “infra-slow activity” is used along with the term “DC potential (DCP)”. Active functioning of neurons associated with working memory activation can lead to changes in the NVU pH and, as a result, to the dynamics of potential difference between blood and cerebrospinal fluid. The normal resting state pH of cerebrospinal fluid is 7.31–7.34, while that of arterial blood is slightly more alkaline, 7.35–7.45. According to the calculations based on the Nernst equation due to differences in hydrogen ion concentration (https://www.physiologyweb.com/calculators/nernst_potential_calculator.html), the BBB membrane steady potential shift of up to 9 mV can be normally observed. Additional shift is possible due to differences in concentrations of other ions (potassium, sodium, chloride). The dynamic changes in acidity change the hemoglobin's affinity for oxygen, thereby affecting the BOLD signal (Bohr effect) and cellular acidosis [9]. Thus, infra-slow activity in the millivolt range reflects primarily complex energy processes occurring in the NVU and can serve as an indicator of the state of VWM and other cerebral functions, since disturbances of the acid base balance on both sides of the BBB are associated with changes in the functioning of neurons. The dynamics of infra-slow oscillations of potentials in the millivolt range reflecting the energy characteristics of metabolism could potentially play a role of the energy process biomarker [10–14]. The association of DC potential with neuronal activity is ambiguous. Higher neuronal activity normally corresponds to higher DCP values. In case of disorder, for example neurodegenerative or cardiovascular disease, DCP tends to rise due to the brain acidity increase resulting from neurodegenerative and atrophic processes, as well as vascular incompetence, as it happens in Alzheimer's disease [15].

Conventional VWM biomarkers, such as the previously mentioned P300 and N-back tests, are often correlated to various fMRI characteristics in the paradigm of tasks, when the subjects execute certain cognitive tasks. These tasks ensure direct activation of the working memory networks and direct measurement of cognitive functions and related brain activity indicators. At the same time, the resting state fMRI records spontaneous brain activity fluctuations, when the subjects are in the resting state and do not execute any specific tasks, however, these rather accurately reflect the VWM state. The resting-state neural networks represent brain regions exerting synchronized activity in the relaxed wakefulness state. Obviously, the state preceding the cognitive task has a decisive influence on the cognitive test performance. In the resting state, neural networks can overlap with the networks associated with the tasks; such a relationship is likely to be important for assessment of cognitive function using the resting-state networks, as well as for the search for biomarkers. The evidence, that regions of the brain functionally connected in the resting state facilitate transmission of information related to cognitive tasks between these brain regions, is provided [16]. The authors of this paper have developed an approach for demonstration of the relationship between the network topology in the resting state and transmission of information in the networks during execution of tasks. The resting-state neural networks also can overlap with each other, which reflects some fundamental pattern of internal organization of the brain. Correlations between brain regions measure statistical relationships (correlations) between the neuronal activity in various brain structures and show the degree, to which two brain regions are synchronized (in-phase or out-of-phase) in these areas in different states of the brain. The brain regions, for which strong correlations are reported, are inherent to the same resting-state neural network. It is theoretically possible that neural networks can exist in two different states and their size would be different in these two states. It is also possible that neural networks can be correlated to several neural networks due to their multilayered structure. Significant overlapping of some neural networks with each other suggest that there are strong functional relationships between the networks reflecting their common functional roles and coordinated models of activity in the brain [17–18].

The study was aimed to search for a biomarker being a component of the VWM neural network in patients with chronic cerebral ischemia. This biomarker must be inherently involved in the working memory process, which makes it a useful tool for solving the research and applied problems. The currently known working memory biomarkers are compared with the fMRI data in the paradigm of tasks. To date, no biomarker has been found that could be considered within the resting fMRI paradigm. This approach is aimed to fill the gap.

METHODS

A total of 50 patients with chronic cerebral ischemia (CCI) took part in the study: 16 males and 34 females aged 50–85 years. There were no significant differences in the average age between the samples of males (64.3 ± 2.7) and females (66.2 ± 1.5); significance levels were as follows: $p = 0.78$ for differences between males; $p = 0.42$ for differences between females. All patients were right-handed.

In CCI, cerebral blood flow through the main and small arteries of the head is disturbed, which can result in various functional disorders of the brain. The disorder often occurs

in elderly and senile individuals. This is usually accompanied by atherosclerosis, hypertension, diabetic angiopathy, and other diseases. Inclusion criteria: initial manifestations and subcompensated CCI; no need for permanent care from others in patients' daily life [19–21]. Exclusion criteria: dementia severity score 1 or more (Clinical Dementia Rating) [22], history of acute cerebrovascular accident, traumatic brain injury, severe heart or renal failure, uncompensated thyroid dysfunction.

Cognitive function assessment

Verbal working memory (VWM) was evaluated by the Luria test. The test was modified taking into account the capabilities of patients with CCI. The subjects were offered to memorize 10 unrelated words repeated five times and immediately reproduce them. The final fifth value for the correctly reproduced words was counted.

Infra-slow electrical activity was recorded: DC potential of the brain. DCPs of patients with CCI were measured with the 5-channel Neuroenergokartograf unit (Statokyn; Russia) using the non-polarizable silver chloride electrodes. Active electrodes were placed on the head, and the reference electrode was placed on the right wrist. The electrode placement scheme was as follows: along the sagittal plane — inferior frontal (F), hereinafter frontal, central (C), occipital (O) leads; parasagittal plane — right and left temporal leads (Td) and (Ts). Recording was performed after applying the measures aimed to control and radical reduction of electrode artifacts with virtual elimination of the skin potentials. The electrode placement matched the international 10–20 scheme, standard topographic symbols are provided in parentheses. The details of DCP recording were reported earlier [11].

Resting state functional magnetic resonance imaging (fMRI)

The subjects underwent T2* weighted fMRI to obtain the BOLD signal in the Magnetom Verio magnetic resonance imaging scanner (Siemens; Germany) with the magnetic field strength of 3.0 Tesla. The subjects were offered to relax as much as possible, lay still with the eyes closed (to avoid stimulation of visual sensory system) and not to think about anything in particular. The MRI data were processed using the SPM12 software (UK) in the MATLAB computing environment (USA). The MAGNETOM Verio magnetic resonance imaging unit (Siemens; Germany) had the magnetic field strength of 3.0 Tesla. Functional scans were acquired in the resting state using the T2* weighted EPI sequence: TR — 1500 ms, TE — 30 ms, flip angle — 70°, slice thickness — 2 mm, FOV — 190 mm, FoV phase — 100.0%.

The resting state fMRI was used to assess brain areas showing the BOLD signal activation and intersecting with the sources generating infra-slow brain activity recorded by the non-polarizable electrodes in the inferior frontal lead.

Additional Doppler tests were performed in order to exclude abnormal circulation asymmetry.

Statistical processing of the data obtained was performed using the Statistica-12 software package (Dell; USA). The Kolmogorov–Smirnov test was used to test the distribution for normality. We calculated mean values, standard deviations, standard errors, and variance, conducted one-way analysis of variance and correlation analysis.

RESULTS

The average number of words reproduced by 50 patients with CCU after five repeats of 10 words was 7.6 words (standard error ± 0.2 words). The subjects were organized into two groups: group 1 (25 individuals) reproduced seven words or less after five repeats, subjects of group 2 (25 individuals) reproduced eight words or more, respectively. The average number of words memorized in the first group was 6.4 ± 0.2 words; in the second group it was 8.9 ± 0.2 words. The groups were matched by age (significance of differences in age $p = 0.91$). The average age of group 1 was 66.7 ± 2.0 years, while that of group 2 was 64.4 ± 1.8 years.

Fig. 1 shows brain regions, in which the BOLD signal values are higher in the second group of subjects.

When assessing the BOLD signal difference, the regions with high T-value are highlighted. Then MNI (Montreal Neurological Institute) brain coordinates are provided in parentheses, followed by the anatomy name and in some cases network name. The most activated region with the MNI coordinates (–27 –67 6) corresponds to the left lingual gyrus — Visual network, *L. lingual gyrus*, which in this situation is activated primarily as a working memory structure. In Fig. 1 this region is located at the coordinate axes intersection. Among other the following should be noted: left postcentral gyrus — Somatomotor network, *L. postcentral gyrus* (–28 –26 60), left cingulate gyrus — Default mode network, *L. cingulate gyrus* (–28 –51 38), and left inferior frontal gyrus — Language network, *L. inferior frontal gyrus* (–28 25 8).

In the group of patients with good working memory, the fMRI BOLD signal activation was significantly higher, than in patients with poor working memory, which is due to higher neuronal activity in the regions shown in Fig. 1. This is also associated with higher energy exchange in these areas and adjacent regions, which suggests the pH change and, therefore, differences in DCP. However, cerebral circulation is often disturbed in patients with CCI. Therefore, neurodegenerative processes resulting in higher DCP in individuals with poor memory are activated. Individuals with high VWM have no acidosis, so DCP is lower. ANOVA revealed significant differences in DCP recorded with the frontal lead in individuals with high and low VWM values reported in the resting state and when performing cognitive tests (Fig. 2A, B).

What's interesting is that the differences between two groups are more significant in the resting state, than during execution of a cognitive task (Fig. 2A, B). This supports the idea that neural networks in the resting state and during execution of cognitive tests largely overlap, especially those implementing similar tasks related to solving verbal problems and concentration, as in this case.

The intergroup differences in DCP recorded with other leads are less pronounced (see Table).

Consider fMRI differences in the subjects differing in DCP recorded with the frontal lead. The first group included the subjects with the DCP recorded with the frontal lead below 6.5 mV, the second group included those, whose DCP recorded with the frontal lead exceeded 6.5 mV (Fig. 3).

Fig. 3 shows distribution of the difference of activated voxels associated with the groups of patients differing in DCP recorded with the frontal lead.

Comparison of fMRI in two groups of patients different in terms of VWM indicators and with two groups with low and high DCP is used. This makes it possible to identify the areas of activation caused simultaneous by these two factors, since overlapping of the regions associated with both working memory and generation of DCP recorded with the frontal lead is one of possible reasons for the relationship between DCP and cognitive functions. We have found such areas (Fig. 4).

Thus, we can understand, which regions are responsible for DCP generation and why DCP is a working memory marker in this situation.

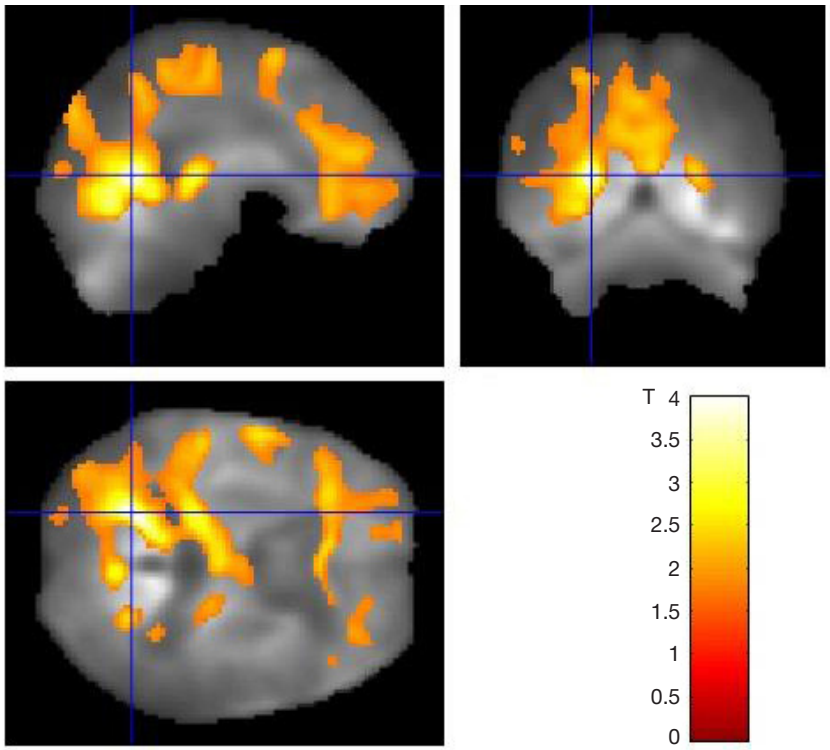

Fig. 1. Brain regions corresponding to the activated voxel difference in patients with high and low working memory indicators based on fMRI data. Lower right — T-value scale. The activated voxel difference at the significance level below 0.05 corresponds to the T-value exceeding 1.68

DISCUSSION

In our sample, the patients included in group 2 having higher VWM showed almost normal indicators. This resonates with the data provided by other authors about the fact that there is often no objective evidence of cognitive decline in patients with the early stage vascular disorders, even if the patients have subjective complaints [23]. In patients with CCI included in the first group with lower VWM, the VWM indicators were typical for patients with vascular or neurodegenerative disorders showing no signs of dementia [23]. In individuals having higher VWM, the voxels activated were located primarily in the left hemispheric structures, while the regions of visuospatial working memory are located primarily in the right hemisphere [2, 3]. Certain parallel between the fMRI activated voxel difference in two groups and DCPs in patients with good and poor working memory was found. The ideas about the association of infra-slow activity in the millivolt range with the resting-state neural networks have been discussed in the literature for a long time and have been confirmed by the study [24]. The authors of the paper do not preclude the relationship between these potentials and the BBB potentials. This study shows a particular mechanism underlying such interaction that is associated with the presence of common fragment in the VWM and DCP

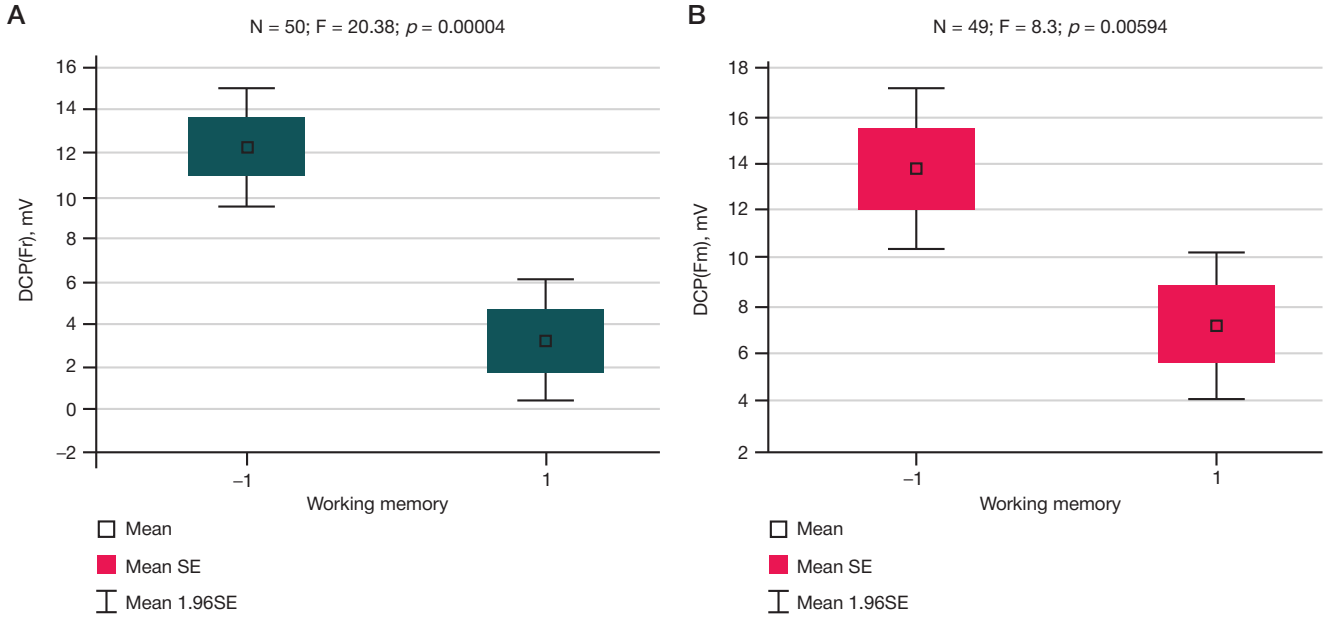

Fig. 2. DCP recorded with the frontal lead in two groups of patients with CCI having low (–1) and high (1) VWM values reported in the resting state **(A)** and when performing the Luria test **(B)**. Statistical characteristics of differences are shown at the top of the figure. DCP values in mV are along the vertical axis. F — Fisher's exact test; N — number of subjects; *p* — significance level

Table. Significance of differences in two VWM groups of patients with CCI for various DCP leads

DCP leads	Significance of differences in DCP in two groups (*p*)
F (Frontal)	0.000041
C (Central)	0.015256
O (Occipital)	0.007895
Td (Right temporal	0.010093
Ts (Left temporal)	0.085361

neural networks. Apparently, this VWM fragment consists of neurons synergistic with the infra-slow electrical activity generation processes. Other fragments of the VWM network and DCP are generated by the non-overlapping neural network fragments. In the active wakefulness state, for example, during execution of the tasks, the resting-state neural networks cease to execute old tasks, while the anatomically close fragments of these networks and most likely the same networks possessing multimodal neurons switch to solving other problems that meet the new conditions [16]. Furthermore, the VWM capacity can be predicted based on the resting-state networks [25]. A similar pattern was observed in our studies, when the differences of infra-slow activity at rest and during execution of a cognitive task corresponded to the differences in VWM of patients with CCI. This can be exemplified by the fact that two groups of subjects demonstrate stable, unchanging differences in the infra-slow activity characteristics in the resting wakefulness state and during execution of cognitive tasks. Since the ratio of DCP (Fig. 2) in the resting state and during execution of tasks in two groups of patients was almost the same, it can be assumed that the ratio of activated (functioning) neurons remains the same in both groups in these two states.

The use of resting state fMRI opens new avenues for identification of biomarkers; for this it is enough to assess overlapping of two resting-state neural networks. The first resting-state network is the network of the main process (in this paper it is the VWM neural network), while the second neural network is the network of biomarker itself, i.e. of specific synchronized group of neurons responsible not only for genesis of the main process, but also for the specific type of electrical processes that can be recorded by non-invasive methods. This approach to the use of resting state fMRI eliminates the main question of biomarker specificity, since specificity is determined by overlapping between the VWM network and another neural network, functioning of which can be recorded by a convenient method, for example by non-invasive electrophysiological method, like in this situation.

CONCLUSIONS

Working memory is a fundamental function responsible for temporary storage and processing of information that is necessary to solve various cognitive problems. The working memory biomarkers can help understand individual differences in cognitive ability, as well as improve the diagnosis and treatment of cognitive impairment. The fact that working memory was considered in terms of the neurovascular unit functioning resulted in the fact that the dynamics of infra-slow potentials as

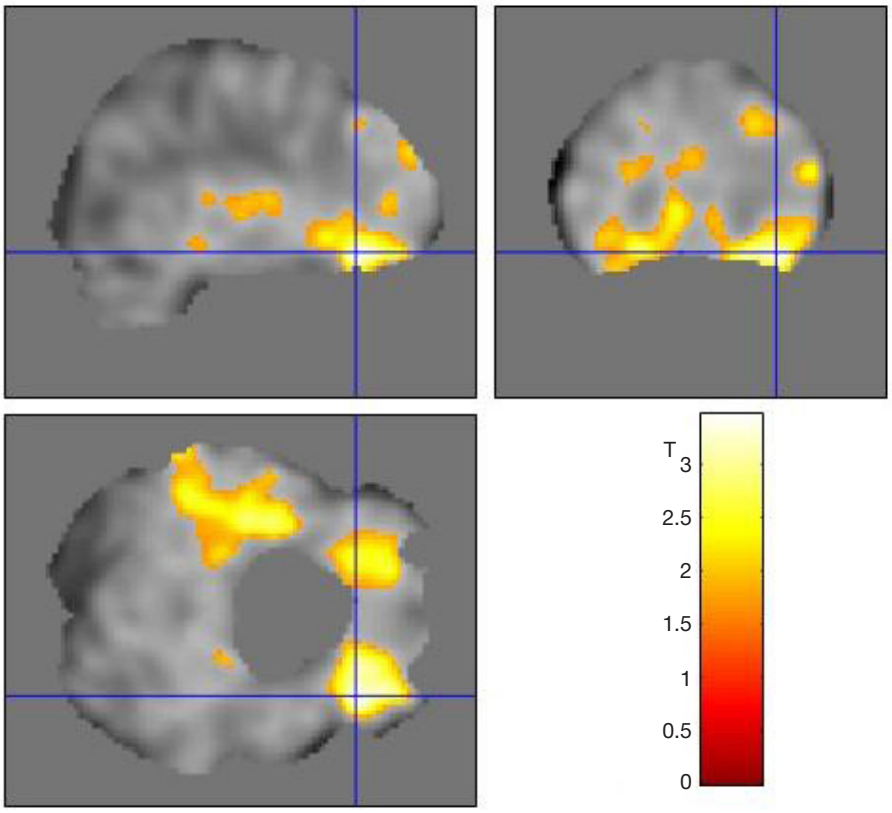

Fig. 3. Brain regions corresponding to the activated voxel difference in CCI patients with low and high DCP in the frontal region. The activated voxels in the right and left lateral fronto-orbital gyri (28 36 –16) and (–28 36 –16), as well as in the left superior temporal gyrus (–40 –17 –7) are highlighted in Fig. 3. Other designations are the same, as in Fig. 1

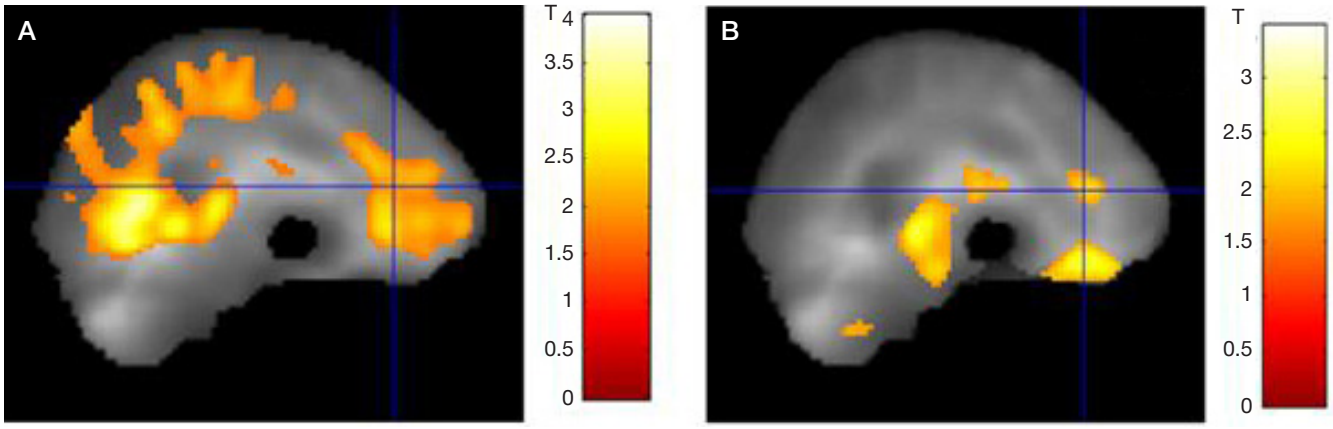

Fig. 4. Brain regions corresponding to the working memory overlap with the areas that generate infra-slow activity. Intersection of the coordinate axes corresponds to the MNI coordinates –28 32 18 — middle frontal gyrus, to the DMN networks and Salience Network. The activated voxel difference in patients with good and worse working memory **(A)** and with low and high DCPs recorded in the frontal lead of infra-slow potentials **(B)** is observed in these regions. This area is marked with the coordinate axes intersection on both figures, A and B

possible working memory biomarkers was studied. The resting state fMRI studies revealed brain regions and networks involved in the working memory functioning. Some of these overlap with the brain regions generating infra-slow activity that can be recorded with the frontal lead. Such infra-slow potentials can be considered as the VWM biomarkers due to overlapping of the brain regions involved in the working memory processes and generation of infra-slow electrical activity.

References

1. Miller EK, Lundqvist M, Bastos AM. Working Memory 2.0. Neuron. 2018; 100 (2): 463–75. Available from: http://doi:10.1016/j.neuron.2018.09.023.
2. Goethals I, Audenaert K, Jacobs F, Van De Wiele C, Vermeir G, et al. Toward clinical application of neuropsychological activation probes with SPECT: a spatial working memory task. J Nucl Med. 2002; 43 (11): 1426–31. PMID: 12411543.
3. Kotyusov AI, Kasanov D, Kosachenko AI, Gashkova AS, Pavlov YG, Malykh S. Working memory capacity depends on attention control, but not selective attention. Behav Sci (Basel). 2023; 13 (2): 92. Available from: http://doi:10.3390/bs13020092. PMID: 36829321; PMCID: PMC9952259.
4. Klaus K, Pennington K. Dopamine and working memory: genetic variation, stress and implications for mental health. Curr Top Behav Neurosci. 2019; 41: 369–91. Available from: http://doi:10.1007/7854_2019_113. PMID: 31502081.
5. Olesen PJ, Westerberg H, Klingberg T. Increased prefrontal and parietal activity after training of working memory. Nat Neurosci. 2004; 7: 75–79. Available from: http://doi:10.1038/nn1165.
6. Owen AM, McMillan KM, Laird AR, Bullmore E. N-back working memory paradigm: a meta-analysis of normative functional neuroimaging studies. Hum Brain Mapp. 2005; 25 (1): 46–59. Available from: http://doi:10.1002/hbm.20131. PMID: 15846822; PMCID: PMC6871745.
7. Muoio V, Persson PB, Sendeski MM. Neurovascular unit — an overview of the concept. Acta Physiol (Oxf). 2014; 210 (4): 790–8. Available from: http://doi:10.1111/apha.12250. PMID: 24629161.
8. Schaeffer S, Iadecola C. Revisiting the neurovascular unit. Nat Neurosci. 2021; 24: 1198–209. Available from: https://doi.org/10.1038/s41593-021-00904-7.
9. Ho C, Russu IM. How much do we know about the Bohr effect of hemoglobin? Biochemistry. 1987; 26 (20): 6299–305. Available from: http://doi:10.1021/bi00394a001. PMID: 3322377.
10. Abbott NJ, Rönnbäck L, Hansson E. Astrocyte-endothelial interactions at the blood-brain barrier. Nat Rev Neurosci. 2006; 7 (1): 41–53. Available from: http://doi:10.1038/nrn1824. PMID: 16371949.
11. Fokin VF, Ponomareva NV. Jenergeticheskaja fiziologija mozga. M.: Antidor, 2003; 288 s. Russian.
12. Drew PJ, Mateo C, Turner KL, Yu Xin, Kleinfeld D. Ultra-slow oscillations in fMRI and resting-state connectivity: neuronal and vascular contributions and technical confounds. Neuron. 2020; 107 (5): 782–804. ISSN 0896-6273. Available from: https://doi.org/10.1016/j.neuron.2020.07.020.
13. Nita DA, Vanhatalo S, Lafortune F-D, Voipio J, Kaila K, Amzica F: Nonneuronal origin of CO2-related DC EEG shifts: an in vivo study in the cat. Journal of Neurophysiology. 2004; 92: 1011–22. Available from: https://doi:10.1152/jn.00110.2004. Epub 2004 Mar 31. PMID: 15056689.
14. Voipio J, Tallgren P, Heinonen E, Vanhatalo S, Kaila K: Millivolt-scale DC shifts in the human scalp EEG: evidence for a nonneuronal generator. Journal of neurophysiology. 2003, 89: 2208–14. Available from: https://doi:10.1152/jn.00915.2002. Epub 2002 Dec 11. PMID: 12612037.
15. Ponomareva NV, Selezneva ND, Kolyhalov IV. Nejrofiziologicheskie mehanizmy dejatel'nosti mozga pri bolezni Al'cgejmera. Voprosy gerontopsihiatrii.1991: 107–12. Russian.
16. Ito T, Kulkarni KR, Schultz DH, et al. Cognitive task information is transferred between brain regions via resting-state network topology. Nat Commun. 2017; 8 (1): 1027. Available from: https://https://doi.org/10.1038/s41467-017-01000-w.
17. Biswal BB, Mennes M, Zuo XN, Gohel S, Kelly C, Smith SM, et al. Toward discovery science of human brain function. Proc Natl Acad Sci USA. 2010; 107 (10): 4734–9. Available from: https://doi:10.1073/pnas.0911855107. Epub 2010 Feb 22. PMID: 20176931; PMCID: PMC2842060.
18. Jian Li, Yijun Liu, Jessica L. Wisnowski, Richard M. Leahy. Identification of overlapping and interacting networks reveals intrinsic spatiotemporal organization of the human brain. NeuroImage. 2023; 270. Available from: https://doi.org/10.1016/j.neuroimage.2023.119944.
19. Tanashjan MM, Maksimova MYu, Domashenko MA. Discirkuljatornaja jencefalopatija. Putevoditel' vrachebnyh naznachenij. 2015; 2: 1–25. Russian.
20. Batysheva TT, Artemova IYu, Vdovichenko TV. Hronicheskaja ishemija mozga: mehanizmy razvitija i sovremennoe kompleksnoe lechenie. Consilium medicum. 2004; 3 (4). Russian.
21. Zaharov VV, Lokshina AB. Kognitivnye narushenija pri discirkuljatornoj jencefalopatii. RMZh. 2009; 20: 1325–31. Russian.
22. Morris JC. Clinical dementia rating: a reliable and valid diagnostic and staging measure for dementia of the Alzheimer type. Int Psychogeriatric. 1997; (9 Suppl 1): 173–6.
23. Blom K, Koek HL, Zwartbol MHT, van der Graaf Y, Kesseler L, Biessels GJ, et al. SMART Study Group. Subjective cognitive decline, brain imaging biomarkers, and cognitive functioning in

patients with a history of vascular disease: the SMART-Medea study. Neurobiol Aging. 2019; 84: 33–40. Available from: https://doi:10.1016/j.neurobiolaging.2019.07.011. Epub 2019 Jul 24. PMID: 31479862.
24. Hiltunen T, Kantola J, Abou Elseoud A, Lepola P, Suominen K, Starck T, et al. Infra-slow EEG fluctuations are correlated with resting-state network dynamics in fMRI. J Neurosci. 2014; 34 (2): 356–62. Available from: https://doi:10.1523/JNEUROSCI.0276-13.2014. PMID: 24403137; PMCID: PMC6608153.
25. Osaka M, Kaneda M, Azuma M, et al. Capacity differences in working memory based on resting state brain networks. Sci Rep. 2021; 11 (19502). Available from: https://doi.org/10.1038/s41598-021-98848-2.

Литература

1. Miller EK, Lundqvist M, Bastos AM. Working Memory 2.0. Neuron. 2018; 100 (2): 463–75. Available from: http://doi:10.1016/j.neuron.2018.09.023.
2. Goethals I, Audenaert K, Jacobs F, Van De Wiele C, Vermeir G, et al. Toward clinical application of neuropsychological activation probes with SPECT: a spatial working memory task. J Nucl Med. 2002; 43 (11): 1426–31. PMID: 12411543.
3. Kotyusov AI, Kasanov D, Kosachenko AI, Gashkova AS, Pavlov YG, Malykh S. Working memory capacity depends on attention control, but not selective attention. Behav Sci (Basel). 2023; 13 (2): 92. Available from: http://doi:10.3390/bs13020092. PMID: 36829321; PMCID: PMC9952259.
4. Klaus K, Pennington K. Dopamine and working memory: genetic variation, stress and implications for mental health. Curr Top Behav Neurosci. 2019; 41: 369–91. Available from: http://doi:10.1007/7854_2019_113. PMID: 31502081.
5. Olesen PJ, Westerberg H, Klingberg T. Increased prefrontal and parietal activity after training of working memory. Nat Neurosci. 2004; 7: 75–79. Available from: http://doi:10.1038/nn1165.
6. Owen AM, McMillan KM, Laird AR, Bullmore E. N-back working memory paradigm: a meta-analysis of normative functional neuroimaging studies. Hum Brain Mapp. 2005; 25 (1): 46–59. Available from: http://doi:10.1002/hbm.20131. PMID: 15846822; PMCID: PMC6871745.
7. Muoio V, Persson PB, Sendeski MM. Neurovascular unit — an overview of the concept. Acta Physiol (Oxf). 2014; 210 (4): 790–8. Available from: http://doi:10.1111/apha.12250. PMID: 24629161.
8. Schaeffer S, Iadecola C. Revisiting the neurovascular unit. Nat Neurosci. 2021; 24: 1198–209. Available from: https://doi.org/10.1038/s41593-021-00904-7.
9. Ho C, Russu IM. How much do we know about the Bohr effect of hemoglobin? Biochemistry. 1987; 26 (20): 6299–305. Available from: http://doi:10.1021/bi00394a001. PMID: 3322377.
10. Abbott NJ, Rönnbäck L, Hansson E. Astrocyte-endothelial interactions at the blood-brain barrier. Nat Rev Neurosci. 2006; 7 (1): 41–53. Available from: http://doi:10.1038/nrn1824. PMID: 16371949.
11. Фокин В. Ф., Пономарева Н. В. Энергетическая физиология мозга. М.: Антидор, 2003; 288 с.
12. Drew PJ, Mateo C, Turner KL, Yu Xin, Kleinfeld D. Ultra-slow oscillations in fMRI and resting-state connectivity: neuronal and vascular contributions and technical confounds. Neuron. 2020; 107 (5): 782–804. ISSN 0896-6273. Available from: https://doi.org/10.1016/j.neuron.2020.07.020.
13. Nita DA, Vanhatalo S, Lafortune F-D, Voipio J, Kaila K, Amzica F: Nonneuronal origin of CO2-related DC EEG shifts: an in vivo study in the cat. Journal of Neurophysiology. 2004; 92: 1011–22. Available from: https://doi:10.1152/jn.00110.2004. Epub 2004 Mar 31. PMID: 15056689.
14. Voipio J, Tallgren P, Heinonen E, Vanhatalo S, Kaila K: Millivolt-scale DC shifts in the human scalp EEG: evidence for a nonneuronal generator. Journal of neurophysiology. 2003, 89: 2208–14. Available from: https://doi:10.1152/jn.00915.2002. Epub 2002 Dec 11. PMID: 12612037.
15. Пономарева Н. В., Селезнева Н. Д., Колыхалов И. В. Нейрофизиологические механизмы деятельности мозга при болезни Альцгеймера. Вопросы геронтопсихиатрии.1991: 107–12.
16. Ito T, Kulkarni KR, Schultz DH, et al. Cognitive task information is transferred between brain regions via resting-state network topology. Nat Commun. 2017; 8 (1): 1027. Available from: https://https://doi.org/10.1038/s41467-017-01000-w.
17. Biswal BB, Mennes M, Zuo XN, Gohel S, Kelly C, Smith SM, et al. Toward discovery science of human brain function. Proc Natl Acad Sci USA. 2010; 107 (10): 4734–9. Available from: https://doi:10.1073/pnas.0911855107. Epub 2010 Feb 22. PMID: 20176931; PMCID: PMC2842060.
18. Jian Li, Yijun Liu, Jessica L. Wisnowski, Richard M. Leahy. Identification of overlapping and interacting networks reveals intrinsic spatiotemporal organization of the human brain. NeuroImage. 2023; 270. Available from: https://doi.org/10.1016/j.neuroimage.2023.119944.
19. Танашян М. М., Максимова М. Ю., Домашенко М. А. Дисциркуляторная энцефалопатия. Путеводитель врачебных назначений. 2015; 2: 1–25.
20. Батышева Т. Т., Артемова И. Ю., Вдовиченко Т. В. Хроническая ишемия мозга: механизмы развития и современное комплексное лечение. Consilium medicum. 2004; 3 (4).
21. Захаров В. В., Локшина А. Б. Когнитивные нарушения при дисциркуляторной энцефалопатии. РМЖ. 2009; 20: 1325–31.
22. Morris JC. Clinical dementia rating: a reliable and valid diagnostic and staging measure for dementia of the Alzheimer type. Int Psychogeriatric. 1997; (9 Suppl 1): 173–6.
23. Blom K, Koek HL, Zwartbol MHT, van der Graaf Y, Kesseler L, Biessels GJ, et al. SMART Study Group. Subjective cognitive decline, brain imaging biomarkers, and cognitive functioning in patients with a history of vascular disease: the SMART-Medea study. Neurobiol Aging. 2019; 84: 33–40. Available from: https://doi:10.1016/j.neurobiolaging.2019.07.011. Epub 2019 Jul 24. PMID: 31479862.
24. Hiltunen T, Kantola J, Abou Elseoud A, Lepola P, Suominen K, Starck T, et al. Infra-slow EEG fluctuations are correlated with resting-state network dynamics in fMRI. J Neurosci. 2014; 34 (2): 356–62. Available from: https://doi:10.1523/JNEUROSCI.0276-13.2014. PMID: 24403137; PMCID: PMC6608153.
25. Osaka M, Kaneda M, Azuma M, et al. Capacity differences in working memory based on resting state brain networks. Sci Rep. 2021; 11 (19502). Available from: https://doi.org/10.1038/s41598-021-98848-2.

MORPHOFUNCTIONAL STATE OF CRYOPRESERVED BLOOD CELLS AT MODERATE LOW TEMPERATURE

Vlasov AA[1] ✉, Andrusenko SF[1], Denisova EV[1], Elkanova AB[1], Kadanova AA[1], Melchenko EA[1], Sokulskaya NN[1], Domenyuk DA[2]

[1] North Caucasus Federal University, Stavropol, Russia

[2] Stavropol State Medical University, Stavropol, Russia

Cryoprotectants enable the long-term storage of biomaterials. Despite progress in cryopreservation, there are a number of problems associated with damage to the cell membranes that result from insufficient efficacy and toxicity of some components. In this regard, it is important to develop non-toxic cryopreservation agents performing well at low temperature. The study was aimed to assess morphofunctional features of blood cells in the lactulose-based cryopreservation agent considering the effects of moderate low temperature (–40 °C). Blood cells (leukocytes, erythrocytes, platelets) collected from 30 conditionally healthy female voluntary donors aged 18–23 years were assessed. The complete blood count test was performed using the Gemalight 1270 automated hematology analyzer. Computerized cytomorphometric assessement was performed using the MECOS-C2 hardware and software complex. The study results showed morphological and functional integrity of blood cells after the 24 h storage at the temperature of–40 °C when added the lactulose-based cryopreservation agent developed: erythrocytes — 85.3 ± 0.30% ($p < 0.05$), platelets – 75 ± 0.71% ($p < 0.05$), leukocytes – 90.1 ± 0.91% ($p < 0.05$) of the values reported before freezing. The findings demonstrate the potential of using lactulose as a non-toxic component of cryopreservation systems, which will expand the range of cryopreservation agents used and make it possible to analyze morphofunctional parameters of frozen whole blood samples when conducting large-scale studies.

Keywords: cryopreservation, erythrocytes, leukocytes, platelets, lactulose, moderate low temperature

Author contribution: Vlasov AA — study concept, procedure, interpretation of the results; Andrusenko SF — study design, literature review, manuscript writing; Denisova EV, Kadanova AA, Sokulskaya NN — data acquisition; Elkanova AB, Melchenko EA — data processing; Domenyuk DA — manuscript editing.

Compliance with ethical standards: the study was approved by the Ethics Committee of the North Caucasus Federal University (protocol No. 002 dated 11 July 2024); all subjects submitted the informed concent to participation in the study.

✉ **Correspondence should be addressed:** Alexander A. Vlasov
Pushkina, 1, Stavropol, 355017, Russia; avlasov@ncfu.ru

Received: 17.07.2024 **Accepted:** 25.08.2024 **Published online:** 17.09.2024

DOI: 10.24075/brsmu.2024.038

МОРФОФУНКЦИОНАЛЬНОЕ СОСТОЯНИЕ КРИОКОНСЕРВИРОВАННЫХ ФОРМЕННЫХ ЭЛЕМЕНТОВ КРОВИ ПРИ УМЕРЕННО НИЗКИХ ТЕМПЕРАТУРАХ

А. А. Власов[1] ✉, С. Ф. Андрусенко[1], Е. В. Денисова[1], А. Б. Эльканова[1], А. А. Каданова[1], Е. А. Мельченко[1], Н. Н. Сокульская[1], Д. А. Доменюк[2]

[1] Северо-Кавказский федеральный университет, Ставрополь, Россия

[2] Ставропольский государственный медицинский университет, Ставрополь, Россия

Криопротекторы позволяют долгосрочно хранить биоматериалы. Несмотря на имеющиеся успехи в криоконсервации, существует ряд проблем, связанных с разрушением клеточных оболочек, из-за недостаточной эффективности и токсичности некоторых компонентов. В связи с этим, важное значение имеет разработка нетоксичных криоконсервантов, эффективно работающих при низких температурах. Целью работы было оценить морфофункциональные особенности форменных элементов крови в криоконсерванте с лактулозой с учетом воздействия умеренно низкой температуры (–40 °C). Были исследованы форменные элементы крови (лейкоциты, эритроциты, тромбоциты), полученные от 30 условно здоровых добровольцев-доноров женского пола в возрасте 18–23 лет. Общий анализ крови выполняли на автоматическом гематологическом анализаторе «Гемалайт 1270». Компьютерное цитоморфометрическое исследование проводили на аппаратно-программном комплексе «МЕКОС-Ц2». По результатам исследования установлена морфологическая и функциональная сохранность форменных элементов крови после одних суток хранения при температуре –40 °C при добавлении разработанного криоконсерванта с лактулозой: для эритроцитов — 85,3 ± 0,30% ($p < 0,05$), для тромбоцитов — 75 ± 0,71% ($p < 0,05$), для лейкоцитов — 90,1 ± 0,91% ($p < 0,05$) от значений, зарегистрированных до замораживания. Результаты демонстрируют потенциал использования лактулозы в качестве нетоксичного компонента для криоконсервирующих систем, что расширит спектр применяемых криоконсервантов и позволит проводить анализ морфофункциональных параметров образцов замороженной цельной крови при крупномасштабных исследованиях.

Ключевые слова: криоконсервирование, эритроциты, лейкоциты, тромбоциты, лактулоза, умеренно низкая температура

Вклад авторов: А. А. Власов — концепция исследования, проведение и интерпретация результатов; С. Ф. Андрусенко — дизайн исследования, анализ литературы, написание статьи; Е. В. Денисова, А. А. Каданова, Н. Н. Сокульская — сбор информации; А. Б. Эльканова, Е. А. Мельченко — обработка данных; Д. А. Доменюк — редактирование статьи.

Соблюдение этических стандартов: исследование одобрено этическим комитетом Северо-Кавказского федерального университета (протокол № 002 от 11 июля 2024 г.); все участники подписали добровольное информированное согласие на участие в исследовании.

✉ **Для корреспонденции:** Александр Александрович Власов
ул. Пушкина, д. 1, г. Ставрополь, 355017, Россия; avlasov@ncfu.ru

Статья получена: 17.07.2024 **Статья принята к печати:** 25.08.2024 **Опубликована онлайн:** 17.09.2024

DOI: 10.24075/vrgmu.2024.038

Optimization of biomaterial cryopreservation methods enabling the prolonged preservation of their functional and phenotypic features is one of the priorities and promising directions of modern biology, as well as experimental and clinical medicine. Biomaterial cryopreservation methods should have low toxicity and support the cellular homeostatic mechanisms. A significant slowdown in cell metabolism begins at the temperature of –70 °C, therefore, the liquid nitrogen cryopreservation is used. However, this requires bulky, expensive equipment, regular liquid nitrogen supply, which affects the material storage cost. Furthermore, such preservation type contributes to the thrombogenicity changes [1], therefore, effective cryopreservation agents ensuring maximum integrity of the preserved biological entity biological properties are in demand.

The best results are achieved when using the combined cryopreservation agents containing both penetrating and non-penetrating cryoprotectants. However, despite progress in cryopreservation, there are a number of problems associated with damage to the cell membranes that result from insufficient efficacy [2] and toxicity of some components [3–5]. It is reasonable to add lipids, proteins and carbohydrates as the components of natural origin [6–10], as well as polyhydric alcohols [11] in order to reduce toxic effects of the cryopreservation agent components, including when freezing human venous blood [12]. Trehalose has a pronounced protective effect on the cell membranes [13–16]; a synergistic effect has been confirmed for trehalose used in combination with dimethyl sulfoxide (DMSO) [17].

The search for new non-toxic components, such as lactulose, represents one of the cryopreservation improvement directions. No data on the toxic, teratogenic or mutagenic effects were obtained when conducting animal experiments and human clinical trials [18]. Furthermore, protective effects of lactulose improving the lactic acid bacterial culture survival rate during freezing have been reported. Adding up to 3% lactulose to the mixture containing the lactic acid bacteria contributed to the increase in the number of viable bacterial cells when freezing the products to the temperature of –18 °C [19]. There is evidence that lactulose used in combination with lecithin has a cryoprotective effect on probiotics at the temperature of –20 °C [20]. Thus, lactulose can be used in practice as a non-toxic cryopreservation agent component to preserve biological entities during freezing.

Fresh whole blood samples are most preferable for analysis, however, the disadvantages of handling whole blood include the need for rapid analysis after biosample collection and the limited number of the repeated tests that can be conducted without collecting extra blood [21]. The experience of capillary blood cryopreservation in the field with subsequent cytometry analysis due to the need for immediate sample testing have been reported [22], however, there are no similar data on cryopreservation of venous blood. Moreover, preservation of the peripheral blood hematopoietic stem cells as a procedure for treatment of hematological, oncological and autoimmune diseases is relevant [23].

The study was aimed to assess morphofunctional features of blood cells in the lactulose-based cryopreservation agent considering the effects of moderate low temperature (–40 °C).

METHODS

Inclusion criteria: conditionally healthy female donors aged 18–23 years in the first phase of their menstrual cycle, a total of 30 individuals with no exacerbation of chronic disorders. The research object was peripheral venous blood stabilized with K3 EDTA (ethylenediaminetetraacetic acid) in vitro.

Samples of peripheral venous blood collected from voluntary donors were divided into three groups. The control group included 10 blood samples, in which blood cell characteristics and parameters were assessed at the temperature of +20 ± 1.0 °C. Experimental group 1 included 10 blood samples supplemented with the cryopreservation agent. These samples were assessed after 4 h at the temperature of +20 ± 1.0 °C. Experimental group 2 included 10 blood samples supplemented with the cryopreservation agent; the samples were put into a state of cold anabiosis for 24 h at the temperature of–40 °C. Then the samples were thawed to assess blood cell characteristics and parameters at the temperature of +20 ± 1.0 °C.

Isotonic salines were used to prepare the model cryopreservation agent. Glycerin and DMSO were used as the cryocomponents penetrating into the cell, while the non-penetrating component was represented by the lactulose disaccharide. The ultimate composition of the model cryopreservation agent had the following component ratios (% v/v): glycerin (AR, Russia) — 20, DMSO (CP, Russia) — 10, lactulose (Lactisan manufactured according to TU 9229-004-53757476–04; Russia) — 2.5, sodium chloride (AR, Russia) — 0.25, sodium phosphate, dibasic (AR, Russia) — 0.25, water for injection (Dalhimfarm; Russia) — to 100%.

The cryopreservation agent solution was autoclaved (without DMSO) at 1.2 atm for 30 min. The resulting solution was stored in a refrigerator at +2 – +4 °C. DMSO was sterilized using the sterilizing filtration unit and stored in the sterile tubes at the temperature of –10 °C. The DMSO solution was added to the ready-made sterile cryopreservation agent immediately before freezing blood samples.

Cryopreservation agent was added to the samples of the experimental groups 1 and 2 to the blood : cryopreservation agent ratio of 2 : 1 (v/v) using a dispenser. The tubes were sealed with plugs, and the content was mixed for 10 min. Later (after 4 h) samples of the experimental group 1 were assessed at the temperature of +20 ± 1.0 °C. Samples of the experimental group 2 were put in the freezer of the electric deep-freeze refrigerator with the temperature of –20 ± 1.0 °C into the refrigerant in the form of solution (38–45% v/v of 96% (v/v) ethanol) with the cold adaptation temperature of –26 — –30 °C; the volume of sample to be frozen was 10% of the refrigerant volume, the samples were kept in it for 30 min and transferred to the electric deep-freeze refrigerator chamber with the temperature of –40 ± 1.0 °C for 24 h for final freezing and storage. After that the samples were thawed in the UT-4334 water bath (ULAB; Russia) while rocking (2–3 times/s) in the manual mode at the temperature of +40 ± 1 °C for 1 min. Then blood cell characteristics and parameters were assessed at the temperature of +20 ± 1.0 °C. The computerized cytomorphometric assessement of blood cells was performed using the MECOS-C2 hardware and software complex (Medical Computer Systems; Russia). The Gemalight 1270 automated hematology analyzer (Dixion; Russia) was used to conduct in vitro diagnostic testing of blood in laboratory settings. To determine red blood counts (RBC), cells were enumerated in the blood cell suspension with the sample diluted to the ratio of 1 : 40,000. The hematology analyzer was used to determine 21 laboratory indicators reflecting the state of the white blood cell, red blood cell, and platelet components.

The results obtained were processed using the IBM SPSS Statistic 23.0 software package (IBM Corp., Armonk, NY; USA). Distributions of the studied indicator values were assessed using the Shapiro–Wilk test. When the indicator value distribution was normal, significance of intergroup differences was assessed using the nonparametric Student's t-test for independent samples; the Mann–Whitney U test was used when the distribution of indicator values was non-normal. The mean (X), error of the mean (м), and standard deviation (δ) were calculated for the normally distributed indicators. The intergroup differences were considered significant at the error probability (p) ≤ 0.05 (5% probability).

RESULTS

The analysis of white blood cell indicators of blood in the control group was performed before adding the cryopreservation agent. In the experimental group 1, it was conducted 4 h after adding

Table 1. White blood cell indicators of CBC in the studied groups (X ± м; *p*)

CBC indicators	Control group (*n* = 10)	Experimental group 1 +20 ± 1.0 °C (*n* = 10)	Experimental group 2 –40 ± 1.0 °C (*n* = 10)	Significance of differences, *p*
WBC, ×10⁹/l	5.60 ± 0.92	4.55 ± 0.74*	4.14 ± 0.85**	*p* < 0.01
Lym, %	38.31 ± 1.35	25.70 ± 1.87*	11.9 ± 1.10**	*p* < 0.01
Gran, %	56.20 ± 3.67	51.10 ± 2.05*	45.3 ± 2.71**	*p* < 0.01
Mid, %	6.20 ± 0.32	10.20 ± 1.21	10.32 ± 1.27	*p* ≥ 0.2
Integrity, %	100	81 ± 0.89*	90.1 ± 0.91**	*p* < 0.01

Note: * — a significant difference between the control group and the experimental group 1 (*p* < 0.01); ** — a significant difference between the control group and the experimental group 2 (*p* < 0.01)

the cryopreservation agent at the temperature of +20 ± 1.0 °C. In the experimental group 2, it was performed after thawing blood samples with the cryopreservation agent following the 24 h incubation at the temperature of –40 ± 1.0 °C (Table 1).

The analysis of white blood cell indicators in the experimental groups 1 and 2 revealed a downward trend of these indicators, however, the proportion and percentage were still within the reference ranges.

The white blood cell computerized cytomorphometry data analysis was performed before adding the cryopreservation agent in the control group, after adding the cryopreservation agent and 4 h incubation in the experimental group 1 at the temperature of +20 ± 1.0 °C, and after thawing blood samples with the cryopreservation agent with the 24 h incubation in the experimental group 2 at the temperature of –40 ± 1.0 °C (Table 2).

The data obtained show a downward trend of the indicators, however, the values are within the reference range of changes. Furthermore, in the experimental groups 1 and 2, where the cryopreservation agent was added, the indicator values are stable: the total number of nuclei is 1, the total number of nuclear segments is 1, the number of inclusion bodies/holes in the nucleus is 0, and the number of nuclear "tails" is 2.

The analysis of red blood cell indicators was performed before adding the cryopreservation agent in the control group, after adding the cryopreservation agent and 4 h incubation in the experimental group 1 at the temperature of +20 ± 1.0 °C, and after thawing blood samples with the cryopreservation agent with the 24 h incubation in the experimental group 2 at the temperature of –40 ± 1.0 °C (Table 3).

Comparative analysis of complete blood counts in the control group, experimental groups 1 and 2 under exposure to moderate low temperature has revealed a downward trend of the indicators, however, the proportion and percentage are still within the reference ranges of blood cell characteristics.

The red blood cell computerized cytomorphometry data analysis was performed before adding the cryopreservation agent in the control group, after adding the cryopreservation agent and 4 h incubation in the experimental group 1 at the temperature of +20 ± 1.0 °C, and after thawing blood samples with the cryopreservation agent with the 24 h incubation in the experimental group 2 at the temperature of –40 ± 1.0 °C (Table 4).

The results of comparative analysis of the control group and experimental group 1 demonstrate a downward trend of the majority of indicators, however, the values obtained are within the reference ranges of blood cell characteristics. The data obtained by comparative analysis in the experimental group 2 demonstrate a downward trend of all the indicators. Furthermore, the values obtained are within the reference ranges of blood cell characteristics and suggest stability of the samples amidst crioprotectant load.

The analysis of red blood cell indicators was performed before adding the cryopreservation agent in the control group, after adding the cryopreservation agent and 4 h incubation in the experimental group 1 at the temperature of +20 ± 1.0 °C, and after thawing blood samples with the cryopreservation agent with the 24 h incubation in the experimental group 2 at the temperature of –40 ± 1.0 °C (Table 5).

Comparative analysis of complete blood counts in the control group and experimental group 1 at the temperature of +20 ± 1.0 °C has revealed a downward trend of a number of indicators, however, all the values are at the boundary of reference range. The analysis of platelet indicators in the experimental group 2 has revealed a downward trend of the values, however, the proportion and percentage are still within the reference ranges of blood cell characteristics.

The platelet computerized cytomorphometry data analysis was performed before adding the cryopreservation agent in the control group, after adding the cryopreservation agent and 2 h incubation in the experimental group 1 at the temperature

Table 2. Differences in the computerized cytomorphometry data in the studied groups (X ± м; *p*)

Entity properties	Control group (*n* = 10)	Experimental group 1 +20 ± 1.0 °C (*n* = 10)	Experimental group 2 –40 ± 1.0 °C (*n* = 10)	Significance of differences, *p*
Cell area, μm²	70 ± 4.19	59 ± 4.75	70 ± 3.98	*p* ≥ 0.1
Cell shape factor	14.11 ± 1.62	18.01 ± 1.23	17.2 ± 1.45	*p* ≥ 0.1
Cell polarization index	0.16 ± 0.01	0.31 ± 0.01	0.11 ± 0.01	*p* ≥ 0.1
Optical density of cytoplasm	0.66 ± 0.01	0.50 ± 0.01	0.63 ± 0.01	*p* ≥ 0.1
Area of the nucleus, μm²	52 ± 3.85	40 ± 3.21*	32 ± 2.24**	*p* < 0.01
Nucleus shape factor	14.3 ± 2.1	13.1 ± 2.88	13.9 ± 2.88	*p* ≥ 0.05
Polarization of the nucleus	0.06 ± 0.001	0.02 ± 0.001*	0.16 ± 0.01**	*p* < 0.01
Nuclear–cytoplasmic ratio	0.74 ± 0.01	0.68 ± 0.01	0.45 ± 0.01	*p* ≥ 0.1
Nuclear complement share	0.04 ± 0.001	0.02 ± 0.001	0.04 ± 0.001	*p* ≥ 0.1

Note: * — a significant difference between the control group and the experimental group 1 (*p* < 0.01); ** — a significant difference between the control group and the experimental group 2 (*p* < 0.01)

Table 3. Red blood cell indicators of CBC in the studied groups (X ± м; *p*)

CBC indicators	Control group (*n* = 10)	Experimental group 1 +20 ± 1,0 °C (*n* = 10)	Experimental group 2 –40 ± 1,0 °C (*n* = 10)	Significance of differences, *p*
RBC, ×10^{12}/l	4.62 ± 0.23	4.08 ± 0.21	3.5 ± 0.55	$p \geq 0.05$
HGB, g/l	131 ± 5.27	119.25 ± 5.48*	101.3 ± 4.73**	$p \geq 0.1$
MCV, fl	86.3 ± 4.32	84.3 ± 4.14	80.6 ± 3.38	$p \geq 0.1$
HCT, %	39.3 ± 1.58	35.4 ± 1.49	30.4 ± 1.63	$p \geq 0.2$
MCH, pg	28.5 ± 1.37	26.2 ± 1.45	21.1 ± 1.52	$p \geq 0.05$
MCHC, g/l	336 ± 29.72	311 ± 23.46	266 ± 14.42	$p \geq 0.5$
RDW, %	12.2 ± 1.67	11.7 ± 1.48	10.3 ± 1.25	$p \geq 0.5$
Integrity, %	100	89 ± 0.20*	85.3 ± 0.30**	$p < 0.01$

Note: * — a significant difference between the control group and the experimental group 1 ($p < 0.01$); ** — a significant difference between the control group and the experimental group 2 ($p < 0.01$)

of +20 ± 1.0 °C, and after thawing blood samples with the cryopreservation agent with the 24 h incubation in the experimental group 2 at the temperature of –40 ± 1.0 °C (Table 6).

The analysis of data of the control group and experimental group 1 at the temperature of +20 ± 1.0 °C demonstrates a downward trend of the majority of indicators, however, the values obtained are within the reference ranges of blood cell characteristics. The data of comparative analysis in the experimental group 2 demonstrate a downward trend of the indicators, being within the reference ranges of blood cell characteristics.

DISCUSSION

The results of comparative analysis of the white blood cell indicators in the control group and experimental group 1, where the cryopreservation agent was added, showed a downward trend of the majority of indicators, however, all values were within the reference ranges. Such indicators, as the "total number of nuclei — 1", "total number of nuclear segments — 1", "number of inclusion bodies/holes in the nucleus — 0", "number of nuclear "tails" — 2" were the same in the control group and the experimental group 1. The values obtained were used as a reference for the indicators of frozen samples. The analysis of white blood cell computerized cytomorphometry data before and after adding the cryopreservation agent with freezing to –40 °C showed that the indicators of the experimental group 2 were the same as in the control group: the total number of nuclei was 1, the total number of nuclear segments was 1, the number of inclusion bodies/holes in the nucleus was 0, and the number of nuclear "tails" was 2. The analysis of complete blood count indicators and the whole blood leukocyte morphometry characteristics in the control group and experimental groups revealed a downward trend of the indicator values, however, the data obtained were within the permissible range of blood cell characteristics. Thus, in the control group WBC × 10^9/L were 5.60 ± 0.92 ($p < 0.01$), in the experimental group 1 these were 4.55 ± 0.74 ($p < 0.01$), and in the experimental group 2 these were 4.14 ± 0.85 ($p < 0.01$). The leukocyte morphometry indicators, such as the cell area measured in μm^2, were 70 ± 4.19 ($p \geq 0.1$) in the control group, 59 ± 4.75 ($p \geq 0.1$) in the experimental group 1, and 70 ± 3.98 ($p \geq 0.1$) in the experimental group 2.

The results of comparative analysis of the red blood cell computerized cytomorphometry data in the control group and the experimental groups 1 and 2, where the cryopreservation agent was added, showed a downward trend of indicators, however, all the values were within the reference ranges. The analysis of the red blood cell computerized cytomorphometry data in the experimental group 2 with the cryopreservation agent added at the freezing temperature of –40 °C showed a downward trend, however, the results obtained suggested stability of samples and were within the reference ranges of blood cell characteristics. Thus, in the control group RBC × 10^{12}/L were 4.62 ± 0.23 ($p \geq 0.05$), in the experimental group 1 these were 4.08 ± 0.21 ($p \geq 0.05$), and in the experimental group 2 these were 3.5 ± 0.55 ($p \geq 0.05$). The erythrocyte morphometry indicators, such as the cell area measured in μm^2, were 46.6 ± 4.12 ($p < 0.01$) in the control group, 53.3 ± 4.68 ($p < 0.01$) in the experimental group 1, and 41.1 ± 2.42 ($p < 0.01$) in the experimental group 2, respectively.

According to the comparative analysis results, the majority of platelet indicators in the control group and the experimental group 1, where the cryopreservation agent was added,

Table 4. Differences in the erythrocyte computerized cytomorphometry data in the studied groups (X ± м; *p*)

Entity properties	Control group (*n* = 10)	Experimental group 1 +20 ± 1,0 °C (*n* = 10)	Experimental group 2 –40 ± 1,0 °C (*n* = 10)	Significance of differences, *p*
Cell area, μm^2	46.6 ± 4.12	53.3 ± 4.68*	41.1 ± 2.42**	$p < 0.01$
Average diameter, μm	6.4 ± 1.14	7.8 ± 1.17	6.85 ± 1.16	$p \geq 0.1$
Shape factor	13.5 ± 1.2	13.6 ± 1.2	12.7 ± 1.2	$p \geq 0.1$
Polarization	0.096 ± 1.001	0.083 ± 0.001*	0.048 ± 0.001**	$p < 0.01$
Integrated optical density (Red), μm^2	16.4 ± 2.78	18.1 ± 2.91	16.2 ± 2.74	$p \geq 0.05$
Integrated optical density (Green), μm^2	20.3 ± 2.24	21.3 ± 2.31	19.8 ± 2.13	$p \geq 0.1$
Integrated optical density (Blue), μm^2	11.28 ± 2.11	12.95 ± 2.17	11.75 ± 2.15	$p \geq 0.1$

Note: * — a significant difference between the control group and the experimental group 1 ($p < 0.01$); ** — a significant difference between the control group and the experimental group 2 ($p < 0.01$)

Table 5. Platelet indicators of CBC in the studied groups (X ± м; *p*)

CBC indicators	Control group (*n* = 10)	Experimental group 1 +20 ± 1,0 °C (*n* = 10)	Experimental group 2 –40 ± 1,0 °C (*n* = 10)	Significance of differences, *p*
PLT, ×10^9/l	230.8 ± 5.78	198.6 ± 5.36*	150.1 ± 4.71**	$p < 0.01$
MPV, fl	8.24 ± 1.22	7.56 ± 1.24	7.04 ± 1.17	$p \geq 0.1$
PCT, %	2.23 ± 0.31	2.1 ± 0.24	1.97 ± 0.71	$p \geq 0.1$
P-LCR, %	17.38 ± 2.72	21.24 ± 2.61	19.17 ± 2.45	$p \geq 0.05$
P-LCC, ×10^9/l	41.61 ± 3.12	50.8 ± 3.32	46.14 ± 3.74	$p \geq 0.05$
Integrity, %	100	86.2 ± 0.31*	75 ± 0.71**	$p < 0.01$

Note: * — a significant difference between the control group and the experimental group 1 ($p < 0.01$); ** — a significant difference between the control group and the experimental group 2 ($p < 0.01$)

Table 6. Platelet computerized cytomorphometry indicators in the studied groups (X ± м; *p*)

Entity properties	Control group (*n* = 10)	Experimental group 1 +20 ± 1,0 °C (*n* = 10)	Experimental group 2 –40 ± 1,0 °C (*n* = 10)	Significance of differences, *p*
Area, μm^2	7.7 ± 0.21	7.5 ± 0.36	7.2 ± 0.31	$p \geq 0.1$
Min. diameter, μm	2.85 ± 0.14	2.63 ± 0.16	2.31 ± 0.24	$p \geq 0.1$
Max. diameter, μm	4.03 ± 0.24	3.94 ± 0.32	3.74 ± 0.36	$p \geq 0.1$
Average diameter, μm	3.44 ± 0.13	3.29 ± 0.16*	3.03 ± 0.21**	$p < 0.01$
Shape factor	12.9 ± 2.18	12.3 ± 1.21	12.1 ± 1.74	$p \geq 0.05$

Note: * — a significant difference between the control group and the experimental group 1 ($p < 0.01$); ** — a significant difference between the control group and the experimental group 2 ($p < 0.01$)

showed a downward trend at room temperature, however, all the values were were within the reference ranges of blood cell characteristics. The analysis of platelet indicators in the experimental group 2, where the cryopreservation agent was added, with incubation at the temperature of –40 °C showed a downward trend of the proportion and percentage of indicators, however, the values obtained were within the reference ranges of blood cell characteristics. Thus, in the control group PLT × 10^9/L were 230.8 ± 5.78 ($p < 0.01$), in the experimental group 1 these were 198.6 ± 5.36 ($p < 0.01$), and in the experimental group 2 these were 150.1 ± 4.71 ($p < 0.01$). The platelet morphometry indicators, such as the cell area measured in μm^2, were 7.7 ± 0.21 ($p \geq 0.1$) in the control group, 7.5 ± 0.36 ($p \geq 0.1$) in the experimental group 1, and 7.2 ± 0.31 ($p \geq 0.1$) in the experimental group 2, respectively.

The analysis of studies focused on the search for new effective cryopreservation agents has shown that there are a large number of studies focused on cryopreservation of erythrocytes rather than platelets or leukocytes. When the Cryosin solution was used as a cryopreservation agent, the erythrocyte integrity rate was 83.8 ± 4.09% [24]. The following data were obtained when assessing viability of the nucleated cells contained in the leukocyte concentrates in the phases of cell acquisition, freezing and thawing: much more cells remained viable after washing off DMSO than without washing — 94.4% vs. 86.7% [25]. When the donor blood platelets protected with the combined cryopreservation agent were frozen, their functional activity was maintained within the range of 63.5–88.8% [26]. Thus, the data obtained during our study are comparable with the literature data on the analysis of integrity of certain blood cells in the course of cryopreservation.

The lactulose-based cryopreservation agent developed is effective under conditions of freezing to –40 °C and affordable (all the components are produced in the Russian Federation), which expands the range of the cryopreservation agents used and enables the analysis of morphofunctional parameters of frozen whole blood samples within the framework of large-scale studies conducted in emergency situations, in the aftermath of accidents of natural and human-induced origin, under conditions of terrorist attacks, armed conflicts, biomaterial storage in the long expeditions and remote areas. Moreover, the personalized approach to blood component transfusion in the cases of emergency need for transfusion of one's own cryopreserved whole blood aimed to reduce the risk of the influence of foreign complexes on the recipient's body is promising. The data provided suggest the need for further investigation of the effects of lactulose used as the cryocomponent on the integrity of biological entities.

CONCLUSIONS

Processing of the data obtained revealed morphological and functional integrity of blood cells in the lactulose-based cryopreservation agent developed after freezing for 24 h at the temperature of –40 °C: erythrocytes — 85.3 ± 0.30% ($p < 0.05$), platelets — 75 ± 0.71% ($p < 0.05$), leukocytes — 90.1 ± 0.91% ($p < 0.05$) of the values reported before freezing. In the light of current studies focused on the search for new effective cryopreservation agents, lactulose can be used as a non-toxic component when developing cryocompositions for preservation of biological entities during freezing.

References

1. Hidi L, Komorowicz E, Kovács GI, Szeberin Z, Garbaisz D, Nikolova N, et al. Cryopreservation moderates the thrombogenicity of arterial allografts during storage. PLoS One. 2021; 16 (7): e0255114. Available from: https://doi.org/10.1371/journal.pone.0255114.
2. Bojic S, Murray A, Bentley BL, Spindler R, Pawlik P, Cordeiro JL, et al. Winter is coming: the future of cryopreservation. BMC Biol 19. 2021; 56. Available from: https://doi.org/10.1186/s12915-021-00976-8.
3. Awan M, Buriak I, Fleck R, Fuller B, Goltsev A, Kerby J, at al. Dimethyl sulfoxide: a central player since the dawn of cryobiology, is efficacy balanced by toxicity? Regenerative medicine. 2020; 15 (3): 1463–91. DOI: 10.2217/rme-2019-0145.
4. Liu X, Pan Y, Liu F, He Y, Zhu Q, Liu Z, at al. A review of the material characteristics, antifreeze mechanisms, and applications of cryoprotectants (CPAs). Journal of Nanomaterials. 2021; 2021. Available from: doi.org/10.1155/2021/9990709.
5. Zaikina EV, Goncharova AS, Pozdnyakova VV, Pandova OV, Przhedeckij YuV, Volovik V. G, i dr. Obzor sovremennyh metodov kriokonservacii razlichnyh vidov biologicheskogo materiala. Sovremennye problemy nauki i obrazovanija. 2022; 4. Доступно по ссылке: https://science-education.ru/ru/article/view?id=31790. Russian.
6. Silyukova YuL, Stanishevskaja OI, Pleshanov NV, Kurochkin AA. Jeffektivnost' ispol'zovanija kombinacij saharidov v sredah dlja kriokonservacii spermy petuhov. Sel'skohozjajstvennaja biologija. 2020; 55 (6): 1148–58. DOI: 10.15389/agrobiology.2020.6.1148rus. Russian.
7. Jahan S, Kaushal R, Pasha R, Pineault N. Current and future perspectives for the cryopreservation of cord blood stem cells. Transfus Med Rev. 2021; 35 (2): 95–102. DOI: 10.1016/j.tmrv.2021.01.003. PMID: 33640254.
8. Tas RP, Sampaio-Pinto V, Wennekes T, van Laake LW, Voets IK. From the freezer to the clinic: Antifreeze proteins in the preservation of cells, tissues, and organs. 2021; 22 (3): 52162. DOI: 10.15252/embr.202052162. PMID: 33586846; PMCID: PMC7926221.
9. Whaley D, Damyar K, Witek RP, Mendoza A, Alexander M, Lakey JR. Cryopreservation: an overview of principles and cell-specific considerations. Cell Transplant. 2021; 30: 963689721999617. DOI: 10.1177/0963689721999617. PMID: 33757335; PMCID: PMC7995302.
10. Li J, Wang H, Wang L, et al. Stabilization effects of saccharides in protein formulations: A review of sucrose, trehalose, cyclodextrins and dextrans. Eur J Pharm Sci. 2024; 192: 106625. DOI: 10.1016/j.ejps.2023.106625. Epub 2023 Nov 2. PMID: 37918545.
11. Zhong Y, McGrath JK, Gong B. Dipropinonates of sugar alcohols as water-soluble, nontoxic CPAs for DMSO-Free cell cryopreservation. ACS Biomater Sci Eng. 2021; 7 (10): 4757–62. DOI: 10.1021/acsbiomaterials.1c00995. PMID: 34587440.
12. Shirokih IG, Polezhaeva TV, Shirokih AA, Hudyakov AN, Sergushkina MI, Nazarova YaI, i dr. Kriozashhitnye svojstva polisaharidsoderzhashhej frakcii Hericium erinaceus BP 16. Izvestija RAN. Serija biologicheskaja. 2020; 1: 5–11. DOI: 10.31857/S0002332920010129. Russian.
13. Olsson C, Swenson J. Structural comparison between sucrose and trehalose in aqueous solution. J Phys Chem B. 2020; 124 (15): 3074–82. DOI: 10.1021/acs.jpcb.9b09701. PMID: 32223195; PMCID: PMC7311057.
14. Janis BR, Priddy MC, Otto MR, Kopechek JA, Menze MA. Sonoporation enables high-throughput loading of trehalose into red blood cells. Cryobiology. 2021; 98: 73–79. DOI: 10.1016/j.cryobiol.2020.12.005. PMID: 33359645.
15. Xu B, Wang Z, Wang R, Song G, Zhang Y, Su R, at al. Metabolomics analysis of buck semen cryopreserved with trehalose. Front Genet. 2022; 13: 938622. DOI: 10.3389/fgene.2022.938622. PMID: 35991557; PMCID: PMC9386307.
16. Yao J, Shen L, Chen Z, Zhang B, Zhao G. Hydrogel microencapsulation enhances cryopreservation of red blood cells with trehalose. ACS Biomater Sci Eng. 2022; 8 (5): 2066–75. DOI: 10.1021/acsbiomaterials.2c00051. PMID: 35394755.
17. Murray A, Congdon TR, Tomás RMF, Kilbride P, Gibson MI. Red blood cell cryopreservation with minimal post-thaw lysis enabled by a synergistic combination of a cryoprotecting polyampholyte with DMSO/Trehalose. Biomacromolecules. 2022; 23 (2): 467–77. DOI: 10.1021/acs.biomac.1c00599. PMID: 34097399; PMCID: PMC7612374.
18. Ryabceva SA, Hramcov AG, Budkevich RO, Anisimov GS, Chuklo AO, Shpak MA. Fiziologicheskie jeffekty, mehanizmy dejstvija i primenenie laktulozy. Voprosy pitanija. 2020; 89 (2): 5–20. DOI: 10.24411/0042-8833-2020-10012. Russian.
19. Shpak M, Ryabtseva S, Bratsikhin A. Lactulose effect on viability of starter cultures. Journal of Hygienic Engineering and Design. 2019; 27: 162–7.
20. Killer J, Bunešová VN, Modráčková N, Vlková E, Pechar R, Šplíchal I. Lactulose in combination with soybean lecithin has a cryoprotective effect on probiotic taxa of bifidobacteria and Lactobacillaceae. Lett Appl Microbiol. 2023; 76 (2): ovad008. DOI: 10.1093/lambio/ovad008. PMID: 36657381.
21. Dayal R, Beyls E, Vral A, et al. The micronucleus assay on cryopreserved whole blood. J Vis Exp. 2024; 204. DOI: 10.3791/65855. PMID: 38465937.
22. Blackwell AD, Garcia AR, Keivanfar RL, et al. A field method for cryopreservation of whole blood from a finger prick for later analysis with flow cytometry. Am J Phys Anthropol. 2021; 174 (4): 670–85. DOI: 10.1002/ajpa.24251. Epub 2021 Feb 17. PMID: 33595836.
23. Kit OI, Gnennaya NV, Filippova SYu, Chembarova TV, Lysenko IB, Novikova IA, i dr. Kriokonservacija gemopojeticheskih stvolovyh kletok perifericheskoj krovi v transplantologii: sovremennoe sostojanie i perspektivy. Kardiovaskuljarnaja terapija i profilaktika. 2023; 22 (11): 3691. DOI: 10.15829/1728-8800-2023-3691. EDN YTCTTM. Russian.
24. Kiryanova GYu, Volkova SD, Kasyanov AD, Grishina GV, Golovanova IS, Chechetkin AV. Kriokonservirovanie jeritrocitov pri temperaturah –40 S i –80 S. Vestnik mezhdunarodnoj akademii holoda. 2017; 1: 72–78. DOI: 10.21047/1606-4313-2017-16-1-72-78. Russian.
25. Isaeva NV, Minaeva NV, Utemov SV, Sherstnev FS, Zorina NA, Zmeeva YuS, i dr. Zhiznesposobnost' jadrosoderzhashhih kletok v lejkokoncentratah na jetapah ih poluchenija, zamorazhivanija i dekriokonservirovanija. Bjulleten' sibirskoj mediciny. 2023; 22 (2): 46–52. Available from: https://doi. org/10.20538/1682-0363-2023-2-46-52. Russian.
26. Vetoshkin KA, Utemov SV, Sherstnev FS, Knyazev MG, Kostjaev AA. Rezul'taty kriokonservirovanija donorskih trombocitnyh koncentratov pri nizkih i ul'tranizkih temperaturah. Transfuziologija. 2015. 2 (16): 22–27. Russian.

Литература

1. Hidi L, Komorowicz E, Kovács GI, Szeberin Z, Garbaisz D, Nikolova N, et al. Cryopreservation moderates the thrombogenicity of arterial allografts during storage. PLoS One. 2021; 16 (7): e0255114. Available from: https://doi.org/10.1371/journal.pone.0255114.
2. Bojic S, Murray A, Bentley BL, Spindler R, Pawlik P, Cordeiro JL, et al. Winter is coming: the future of cryopreservation. BMC Biol 19. 2021; 56. Available from: https://doi.org/10.1186/s12915-021-00976-8.
3. Awan M, Buriak I, Fleck R, Fuller B, Goltsev A, Kerby J, at al. Dimethyl sulfoxide: a central player since the dawn of cryobiology, is efficacy balanced by toxicity? Regenerative medicine. 2020; 15 (3): 1463–91. DOI: 10.2217/rme-2019-0145.
4. Liu X, Pan Y, Liu F, He Y, Zhu Q, Liu Z, at al. A review of the material characteristics, antifreeze mechanisms, and applications of cryoprotectants (CPAs). Journal of Nanomaterials. 2021; 2021. Available from: doi.org/10.1155/2021/9990709.
5. Заикина Е. В., Гончарова А. С., Позднякова В. В., Пандова О. В., Пржедецкий Ю. В., Воловик В. Г и др. Обзор современных методов криоконсервации различных видов биологического материала. Современные проблемы науки и образования. 2022; 4. Доступно по ссылке:

https://science-education.ru/ru/article/view?id=31790.
6. Силюкова Ю. Л., Станишевская О. И., Плешанов Н. В., Курочкин А. А. Эффективность использования комбинаций сахаридов в средах для криоконсервации спермы петухов. Сельскохозяйственная биология. 2020; 55 (6): 1148–58. DOI: 10.15389/agrobiology.2020.6.1148rus.
7. Jahan S, Kaushal R, Pasha R, Pineault N. Current and future perspectives for the cryopreservation of cord blood stem cells. Transfus Med Rev. 2021; 35 (2): 95–102. DOI: 10.1016/j.tmrv.2021.01.003. PMID: 33640254.
8. Tas RP, Sampaio-Pinto V, Wennekes T, van Laake LW, Voets IK. From the freezer to the clinic: Antifreeze proteins in the preservation of cells, tissues, and organs. 2021; 22 (3): 52162. DOI: 10.15252/embr.202052162. PMID: 33586846; PMCID: PMC7926221.
9. Whaley D, Damyar K, Witek RP, Mendoza A, Alexander M, Lakey JR. Cryopreservation: an overview of principles and cell-specific considerations. Cell Transplant. 2021; 30: 963689721999617. DOI: 10.1177/0963689721999617. PMID: 33757335; PMCID: PMC7995302.
10. Li J, Wang H, Wang L, et al. Stabilization effects of saccharides in protein formulations: A review of sucrose, trehalose, cyclodextrins and dextrans. Eur J Pharm Sci. 2024; 192: 106625. DOI: 10.1016/j.ejps.2023.106625. Epub 2023 Nov 2. PMID: 37918545.
11. Zhong Y, McGrath JK, Gong B. Dipropinonates of sugar alcohols as water-soluble, nontoxic CPAs for DMSO-Free cell cryopreservation. ACS Biomater Sci Eng. 2021; 7 (10): 4757–62. DOI: 10.1021/acsbiomaterials.1c00995. PMID: 34587440.
12. Широких И. Г., Полежаева Т. В., Широких А. А., Худяков А. Н., Сергушкина М. И., Назарова Я. И. и др. Криозащитные свойства полисахаридсодержащей фракции Hericium erinaceus БП 16. Известия РАН. Серия биологическая. 2020; 1: 5–11. DOI: 10.31857/S0002332920010129.
13. Olsson C, Swenson J. Structural comparison between sucrose and trehalose in aqueous solution. J Phys Chem B. 2020; 124 (15): 3074–82. DOI: 10.1021/acs.jpcb.9b09701. PMID: 32223195; PMCID: PMC7311057.
14. Janis BR, Priddy MC, Otto MR, Kopechek JA, Menze MA. Sonoporation enables high-throughput loading of trehalose into red blood cells. Cryobiology. 2021; 98: 73–79. DOI: 10.1016/j.cryobiol.2020.12.005. PMID: 33359645.
15. Xu B, Wang Z, Wang R, Song G, Zhang Y, Su R, at al. Metabolomics analysis of buck semen cryopreserved with trehalose. Front Genet. 2022; 13: 938622. DOI: 10.3389/fgene.2022.938622. PMID: 35991557; PMCID: PMC9386307.
16. Yao J, Shen L, Chen Z, Zhang B, Zhao G. Hydrogel microencapsulation enhances cryopreservation of red blood cells with trehalose. ACS Biomater Sci Eng. 2022; 8 (5): 2066–75. DOI: 10.1021/acsbiomaterials.2c00051. PMID: 35394755.
17. Murray A, Congdon TR, Tomás RMF, Kilbride P, Gibson MI. Red blood cell cryopreservation with minimal post-thaw lysis enabled by a synergistic combination of a cryoprotecting polyampholyte with DMSO/Trehalose. Biomacromolecules. 2022; 23 (2): 467–77. DOI: 10.1021/acs.biomac.1c00599. PMID: 34097399; PMCID: PMC7612374.
18. Рябцева С. А., Храмцов А. Г., Будкевич Р. О., Анисимов Г. С., Чукло А. О., Шпак М. А. Физиологические эффекты, механизмы действия и применение лактулозы. Вопросы питания. 2020; 89 (2): 5–20. DOI: 10.24411/0042-8833-2020-10012.
19. Shpak M, Ryabtseva S, Bratsikhin A. Lactulose effect on viability of starter cultures. Journal of Hygienic Engineering and Design. 2019; 27: 162–7.
20. Killer J, Bunešová VN, Modráčková N, Vlková E, Pechar R, Šplíchal I. Lactulose in combination with soybean lecithin has a cryoprotective effect on probiotic taxa of bifidobacteria and Lactobacillaceae. Lett Appl Microbiol. 2023; 76 (2): ovad008. DOI: 10.1093/lambio/ovad008. PMID: 36657381.
21. Dayal R, Beyls E, Vral A, et al. The micronucleus assay on cryopreserved whole blood. J Vis Exp. 2024; 204. DOI: 10.3791/65855. PMID: 38465937.
22. Blackwell AD, Garcia AR, Keivanfar RL, et al. A field method for cryopreservation of whole blood from a finger prick for later analysis with flow cytometry. Am J Phys Anthropol. 2021; 174 (4): 670–85. DOI: 10.1002/ajpa.24251. Epub 2021 Feb 17. PMID: 33595836.
23. Кит О. И., Гненная Н. В., Филиппова С. Ю., Чембарова Т. В., Лысенко И. Б., Новикова И. А. и др. Криоконсервация гемопоэтических стволовых клеток периферической крови в трансплантологии: современное состояние и перспективы. Кардиоваскулярная терапия и профилактика. 2023; 22 (11): 3691. DOI: 10.15829/1728-8800-2023-3691. EDN YTCTTM.
24. Кирьянова Г. Ю., Волкова С. Д., Касьянов А. Д., Гришина Г. В., Голованова И. С., Чечеткин А. В. Криоконсервирование эритроцитов при температурах –40 °С и –80 °С. Вестник международной академии холода. 2017; 1: 72–78. DOI: 10.21047/1606-4313-2017-16-1-72-78.
25. Исаева Н. В., Минаева Н. В., Утемов С. В., Шерстнев Ф. С., Зорина Н. А., Змеева Ю. С. и др. Жизнеспособность ядросодержащих клеток в лейкоконцентратах на этапах их получения, замораживания и декриоконсервирования. Бюллетень сибирской медицины. 2023; 22 (2): 46–52. Available from: https://doi. org/10.20538/1682-0363-2023-2-46-52.
26. Ветошкин К. А., Утемов С. В., Шерстнев Ф. С., Князев М. Г., Костяев А. А. Результаты криоконсервирования донорских тромбоцитных концентратов при низких и ультранизких температурах. Трансфузиология. 2015. 2 (16): 22–27.